JSCSEN 75(2)157–295(2010)

Journal of the Serbian Chemical Society

VOLUME 75

No 2

BELGRADE 2010

Available on line at

www.shd.org.rs/JSCS/

The full search of JSCS is available through

DOAJ DIRECTORY OF OPEN ACCESS JOURNALS

www.doaj.org

Journal of the Serbian Chemical Society
JSCS@tmf.bg.ac.rs • www.shd.org.rs/JSCS

J. Serb. Chem. Soc. Vol. 75, No. 2 (2010)

CONTENTS

Published by the Serbian Chemical Society
Karnegijeva 4/III, 11000 Belgrade, Serbia
Printed by the Faculty of Technology and Metallurgy
Karnegijeva 4, P.O. Box 35-03, 11120 Belgrade, Serbia

Journal of the Serbian Chemical Society
JSCS@tmf.bg.ac.rs • www.shd.org.rs/JSCS

J. Serb. Chem. Soc. *75* (2) 157–163 (2010) UDC 547.11:541.57+547.37+547.211–327:539.2
JSCS–3948 *Original scientific paper*

N–H···O hydrogen bonding. An FT-IR, NIR study of *N*-methylformamide–ether systems

BRANISLAV JOVIĆ[1]*, ALEKSANDAR NIKOLIĆ[1], ERNA DAVIDOVIĆ[2] and SLOBODAN PETROVIĆ[3#]

[1]*Department of Chemistry, Faculty of Sciences, University of Novi Sad, 21000 Novi Sad, Serbia,* [2]*"Lavoslav Ružička" Polytehnic of Vukovar, 32000 Vukovar, Croatia and* [3]*Faculty of Technology and Metallurgy, University of Belgrade, 11000 Belgrade, Serbia*

(Received 7 March, revised 3 September 2009)

Abstract: This paper reports the results of an FT-IR and NIR study of *N*-methylformamide in carbon tetrachloride solution in presence of ethers as the O--electron donors, *i.e.*, diethyl ether (DEE), diisopropyl ether (DiPE), methyl *t*--butyl ether (M*t*BE), dibutyl ether (DBE), dipentyl ether (DPE), tetrahydrofuran (THF) and tetrahydropyran (THP). The spectroscopic characteristics of the N–H···O hydrogen bonded complexes are given. In addition, the equilibrium constants for 1:1 complex formation were determined at 25 °C using Mid-IR and NIR measurements.

Keywords: hydrogen bonding; *N*-methylformamide; ethers molecular complex.

INTRODUCTION

This paper is a part of continuing and systematic investigations of secondary amides in solution from both spectroscopic[1–6] and thermodynamic[7–9] points of view. In the case of ethers, numerous measurements of the hydrogen bond formation constants have been reported.[10–13] This study should contribute to a better understanding of N-H···O hydrogen bonding of *N*-methylformamide (NMF) with ethers. It seemed interesting to perform experiments using two different spectroscopic techniques: Mid-IR and NIR.

EXPERIMENTAL

N-Methylformamide (Frinton, >99 %), and carbon tetrachloride (J. T. Baker, >99.9 %) were used without further purification. Diethyl ether, dibutyl ether, dipentyl ether, tetrahydrofuran, tetrahydropyran (Fluka, >98 %), diisopropyl ether (Carlo Erba >98 %) and methyl *t*--butyl ether (Riedel-de Haën >99 %) were redistilled and dried prior to use.

* Corresponding author. E-mail: jovicb@ih.ns.ac.rs
# Serbian Chemical Society member.
doi: 10.2298/JSC1002157J

In order to avoid self-association, the amide concentration in the carbon tetrachloride solutions was below 0.0030 mol dm^{-3}. The concentration of the ethers was varied between 0.20 and 1.0 mol dm^{-3}.

The Mid IR and NIR spectra were obtained using a Thermo-Nicolet Nexus 670 instrument. A DTGS detector was employed in the Mid-IR measurements and a MCTA detector cooled with liquid nitrogen was used for the NIR measurements. The samples were placed in 1–5 cm (IR) and 10 cm (NIR) UVIRSIL cells and the spectra were recorded at 298 K. The reported frequencies and half-widths were reproducible to within 0.2 and 1 cm^{-1}, respectively. The integrated molar absorption coefficients were obtained within ±5 %. The equilibrium constants were determined with an average relative standard deviation of 6 %.

RESULTS AND DISCUSSION

The hydrogen bonding between *N*-methylformamide and ethers can be represented by the scheme given in Fig. 1.

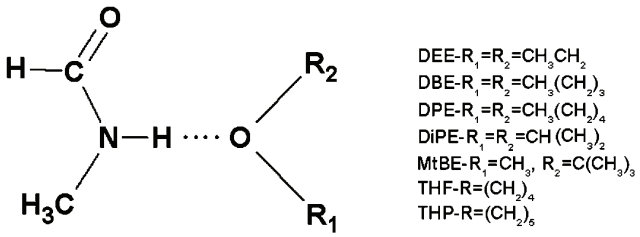

Fig. 1. Hydrogen bonded complexes between NMF and dialkyl ethers.

The equilibrium of NMF–ether hydrogen bond formation can be represented as:

$$\text{M–H} + \text{A} \rightarrow \text{M–H}\cdots\text{A} \quad (1)$$

where M–H is NMF monomer, A is an O-electron donor (ether) and M–H···A is the molecular complex. In the case when the electron donor is present in excess over the amide concentration, then:

$$K = \frac{c_{\text{M}}^0 - c_{\text{M}}}{c_{\text{M}} c_{\text{A}}^0} \quad (2)$$

Using the Becker procedure,[14] the formation constant was determined from the absorbance of the monomer band:

$$K = \frac{A^0 - A}{A c_{\text{A}}^0} \quad (3)$$

where A^0 is the monomer absorbance for a carbon tetrachloride solution containing c_{M}^0, mol dm^{-3}, of NMF and A is the absorbance of the same band for a solution with both NMF (c_{M}^0) and ether donor (c_{A}^0). The spectroscopic characteristics of the monomer (free) ν(NH) band of *N*-methylformamide are given in Table I. ν(NH) and $\nu_{1/2}$ are the wavenumber and halfwidth of the band, respect-

tively, ε and B^0 represent the molar absorption coefficient and the integrated absorption coefficient, respectively. The characteristics for the band of the corresponding first overtone are also given in Table I. In addition, the, IR and NIR spectra of NMF monomer are given in Fig. 2.

TABLE I. Spectroscopic characteristics for the monomer (free) ν(NH) band and the corresponding first overtone of *N*-methylformamide

ν_0(NH) /cm^{-1}	$\nu_{1/2}$ / cm^{-1}	$\varepsilon\times10^{-3}$ / cm^2 mol^{-1}	$B^0\times10^{-6}$/ cm mol^{-1}
3466.1	12	74.9	3.3
6792.8	32	17.2	0.6

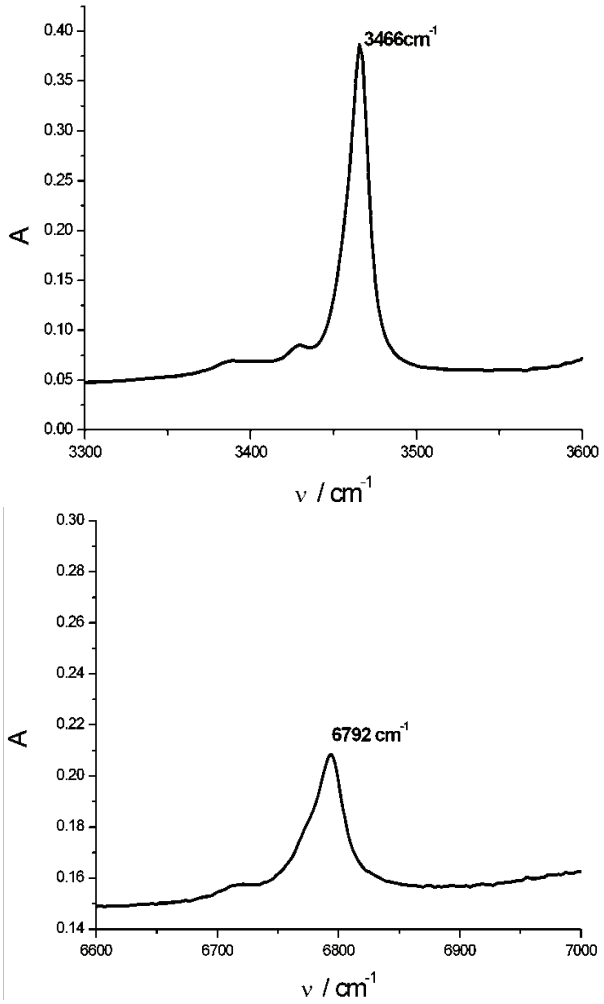

Fig. 2. IR and NIR spectra of *N*-methylformamide monomer in CCl_4 solution, in the regions of the N–H stretching vibration band and the first overtone, at 298.15 K.

The IR spectra and the first derivative NIR spectra of NMF in the presence of different ethers are shown in Figs. 3 and 4, respectively. The spectroscopic parameters for the N–H···O molecular complexes obtained in the IR and NIR measurements are summarized in Table II. The equilibrium constants from both IR and NIR experiments are given in Table III.

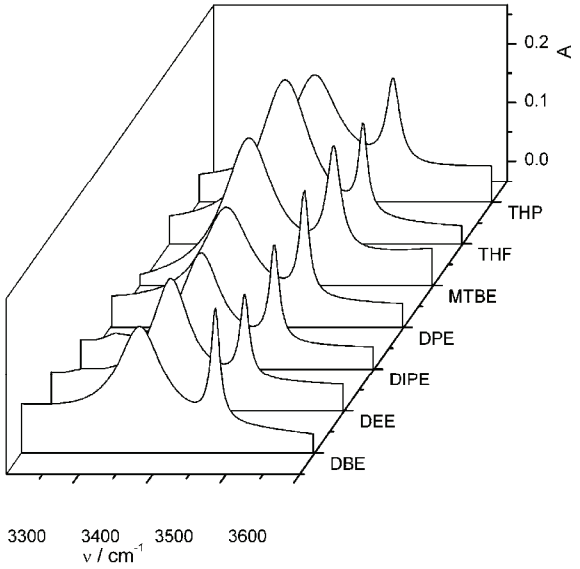

Fig. 3. IR spectra of *N*-methylformamide in the presence of seven different ethers at the same concentration.

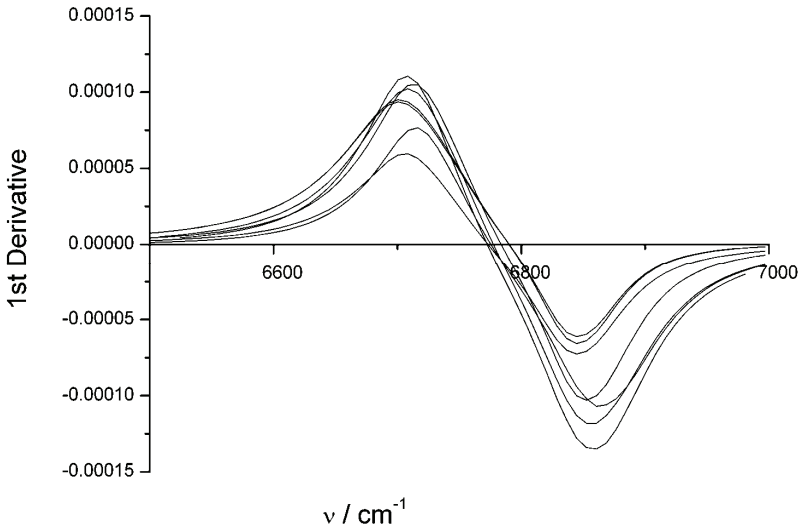

Fig. 4. First derivative NIR spectra of NMF in the presence of different ethers.

TABLE II. Spectroscopic parameters for the N–H···O hydrogen bonded complexes obtained in IR spectroscopy

O-electron donor	$\Delta\nu$ / cm^{-1}	$\nu_{1/2}$ / cm^{-1}	$\varepsilon\times10^{-3}$ / cm^2 mol^{-1}	$B^0\times10^{-6}$ / cm mol^{-1}
Dibutyl ether	101.3	83	73.3	8.2
Diethyl ether	99.0	71	88.5	8.5
Diisopropyl ether	106.5	92	202.8	23.4
Dipentyl ether	102.6	77	62.3	6.7
Methyl *t*-butyl ether	113.5	71	116.8	11.5
Tetrahydrofuran	101.8	75	97.2	9.9
Tetrahydropyran	102.9	75	96.6	10.7

TABLE III. The equilibrium constants from both IR and NIR measurements

O-electron donor	K / dm^3 mol^{-1}	
	IR	NIR
Dibutyl ether	0.84	0.76
Diethyl ether	1.23	1.11
Diisopropyl ether	0.85	0.97
Dipentyl ether	0.92	0.79
Methyl *t*-butyl ether	0.72	0.99
Tetrahydrofuran	1.44	1.56
Tetrahydropyran	1.22	1.27

The obtained IR spectroscopic parameters clearly indicate N–H···O hydrogen bonding between NMF and the ethers.

The stability of molecular complexes increases in the order: M*t*BE < DBE DiPE < DPE <THP < DEE < THF. The differences in the stability of the N–H···O complexes for the five studied dialkyl ethers can be interpreted using the Taft equation:[15]

$$\log K_{298} = \log K^0_{298} + \rho\sigma^* + \delta E_S \quad (6)$$

where K^0_{298} represents the formation constant of the complex with dimethyl ether and σ^* and E_S represent the inductive and steric factors for the alkyl groups, respectively. If $\log K_{298}$ is correlated with both σ^* and E_S, a good correlation is obtained:

$$\log K_{298} = 0.2 + 0.280\sigma^* - 0.182E_S\,,\ R = 0.95 \quad (7)$$

Several investigators[10–13] obtained equilibrium constants for hydrogen bonding between phenols and various (cyclic and aliphatic) ethers and they established that donor-acceptor interactions are sensitive to both steric and inductive effects.

In order to determine the possible contribution of the charge transfer mechanism to the associations in this study, the correlation between donor ionization potential, I_D, and the function of the frequency shift, $(\nu_0/\Delta\nu)^{1/2}$, was examined.

Puranik and Kumar,[16] based on the Mulliken perturbation theory,[17] proposed a relationship between I_D and $(\nu_0/\Delta\nu)^{1/2}$. For the same acceptor and a series of electron donors, the relationship has a simple form:

$$I_D = C_1\left(\frac{\nu_0}{\Delta\nu}\right)^{1/2} + C_2 \quad (8)$$

where ν_0 is the frequency of the NH monomer band; C_1 and C_2 are constants for a given acceptor. The plot of I_D *vs.* the experimental $(\nu_0/\Delta\nu)^{1/2}$ for *N*-methylformamide–electron donors (except MTBE and DPE) is given in Fig 5.

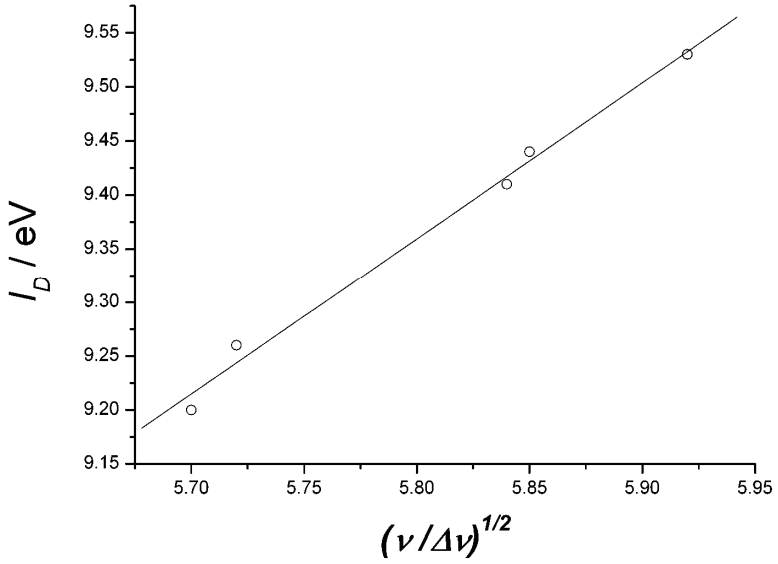

Fig. 5. Plot of I_D *vs.* experimental $(\nu_0/\Delta\nu)^{1/2}$ for *N*-methylformamide–electron donors.

The following equation was obtained based on the least-squares treatment of the data in Table II.

$$I_D = 1.444\left(\frac{\nu_0}{\Delta\nu}\right)^{1/2} + 0.98\,,\ R = 0.99 \quad (9)$$

The linear relationship between the donor ionization potential (I_D) and the function, $(\nu_0/\Delta\nu)^{1/2}$, indicates that the charge transfer mechanism significantly contributes to the hydrogen bonding in the studied systems.

A comparison of the equilibrium constants obtained in this study with those obtained for *N*-methylpropionamide–ether complexes[5,6] showed that the constants for N–H···O hydrogen bonding in NMF–ether complexes are significantly higher. The difference in the stability of NMF and *N*-methylpropionamide complexes with ethers can be attributed to the more expressed steric hindrance in the latter complexes.

An attempt was made to estimate the equilibrium constant using Eq. (3) applied to the monomer first overtone. The equilibrium constants from the IR and NIR measurements agreed quite well.

ИЗВОД

N-H···O ВОДОНИЧНА ВЕЗА. FT-IR И NIR СПЕКТРОСКОПСКО ИСПИТИВАЊЕ СИСТЕМА *N*-МЕТИЛФОРМАМИД–ЕТРИ

БРАНИСЛАВ ЈОВИЋ[1], АЛЕКСАНДАР НИКОЛИЋ [1], ERNA DAVIDOVIĆ[2] и СЛОБОДАН ПЕТРОВИЋ[3]

[1]*Природно–математички факултет, 21000 Нови Сад,* [2]*"Lavoslav Ružička" Polytehnic of Vukovar, 32000 Vukovar, Croatia и* [3]*Технолошко–металуршки факултет, 11000 Београд*

За карактеризацију особина молекулских комплекса *N*-метилформамида са седам различитих етара праћене су промене на основној валентној (истежућој) траци NH вибрације и траци првог вишег тона. Одређене су спектроскопске карактеристике и константе формирања 1:1 молекулских комплекса на 25 °C коришћењем FT-IR и NIR техника.

(Примљено 7. марта, ревидирано 3. септембра 2009)

REFERENCES

1. A. D. Nikolić, N. L. Kobilarov, A. N. Brzić, *J. Mol. Struct*. **99** (1983) 179
2. A. Nikolić, S. Petrović, D. Antonović, L. Gobor, *J. Mol. Struct*. **408** (1997) 355
3. A. D. Nikolić, M. Tarjani-Rozsa, N. U. Perišić-Janjić, A. Petrik, D. G. Antonović, *J. Mol. Struct*. **219** (1990) 245
4. A. D. Nikolić, M. Tarjani-Rozsa, A. Komaromi, J. Csanadi, S. D. Petrović, *J. Mol. Struct*. **219** (1990) 245
5. A. Nikolić, B. Jović, S. Csanady, S. Petrović, *J. Mol. Struct.* **834** (2007) 249
6. A. Nikolić, B. Jović , V. Krstić , J. Tricković, *J. Mol. Struct.* **889** (2008) 328
7. A. Nikolić, Dj. Vaštag, M. Tarjani-Rozsa, S. Petrović, *J. Chem. Eng. Data* **39** (1994) 618
8. A. Nikolić, L. Gobor, V. Krstić, S. Petrović, *J. Mol. Liq.* **121** (2005) 139
9. A. Nikolić, B. Jović, V. Krstić, J. Tričković, *J. Mol. Liq.* **133** (2007) 39
10. M. Berthelot, F. Besseau, C. Laurence, *Eur. J. Org. Chem.* (1998) 925
11. T. Iijima, H. Kakiuchi, *Tetrahedron* **35** (1979) 2992
12. L. Bellon, R. W. Taft, J.-L. M. Abboud, *J. Org. Chem.* **45** (1980) 1166
13. R. West, D. L. Powell, M. K. T. Lee, L. S. Whatley, *J. Am. Chem. Soc*. **86** (1964) 3227
14. E. D. Becker, *Spectrochim. Acta* **17** (1961) 436
15. R. W. Taft, *Steric Effects in Organic Chemistry*, Wiley, New York, 1956, p. 586
16. P. G. Puranik, V. Kumar, *Proc. Indian Acad. Sci*. **58** (1963) 29
17. R. S. Mulliken, *J. Am. Chem. Soc*. **74** (1952) 811.

Journal of the Serbian Chemical Society
JSCS@tmf.bg.ac.rs • www.shd.org.rs/JSCS

J. Serb. Chem. Soc. 75 (2) 165–173 (2010)
JSCS–3949

UDC 547.458.6+66.095.11+547.292–312
Original scientific paper

An efficient acetylation of dextran using *in situ* activated acetic anhydride with iodine

MUHAMMAD A. HUSSAIN[1]*, DURE SHAHWAR[1], MUHAMMAD N. TAHIR[2], MUHAMMAD SHER[1], MUHAMMAD N. HASSAN[1] and ZAKIA AFZAL[1]

[1]*Department of Chemistry, University of Sargodha, Sargodha 40100, Pakistan and* [2]*Institute of Inorganic and Analytical Chemistry, Johannes Guttenberg University, Duesbergweg 10–14, 55099, Mainz, Germany*

(Received 7 April, revised 2 June 2009)

Abstract: A facile, efficient, cost-effective and solvent-free acetylation method has been developed for the acetylation of dextran. Dextran acetates were successfully synthesized using different molar ratios of acetic anhydride in the presence of iodine as a catalyst without the use of any solvent. The reactions were realized at 50 °C for 3 h under stirring and nitrogen. This efficient method yielded highly pure and organosoluble dextran esters. The reaction appears highly effective for obtaining higher degrees of substitution (*DS*) with great efficiency. Under solvent-free conditions, dextran triacetates were efficiently synthesized. It was also observed that the molar ratio can easily control the DS of pendant groups onto the polymer backbone. Hence, a range of products with varying *DS* were successfully designed, purified and characterized. Covalent attachment of the pendant groups onto the polymer backbone was verified by spectroscopic techniques. Thermogravimetric analysis indicated that the obtained dextran esters were thermally as stable as dextran. The *DS* of the pendant groups onto the polymer backbone was calculated using standard acid base titration after saponification. Furthermore, all products were thoroughly characterized by thermal analysis (TG and DTG), and FTIR and ^{1}H-NMR spectroscopic analysis.

Keywords: acetic anhydride; acetylation; dextran; iodine; polysaccharide.

INTRODUCTION

Dextran[1,2] is a very important polysaccharide commonly used in routine medical, microsurgical and laboratory procedures.[3,4] Dextran derivatives are used for reducing platelet adhesiveness,[5,6] wound healing,[7] tumor targeting of gene expression[8] and osmotic pressure control in biological molecules[9] and human enzyme regulation.[10] Dextran derivatives have well reported antiprolife-

* Corresponding author. E-mail: majaz172@yahoo.com
doi: 10.2298/JSC1002165H

rative and anti-tumor properties.[11] Dextran is receiving attention in the formulation of macromolecular prodrugs of acid sensitive drugs to target them to the colon and in this way, highly sensitive anticancer drugs, such as mitomycin C, can be safely targeted to its site of action.[12] Nowadays, dextran is being used for sustained release studies of several sensitive drug molecules after their covalent attachment (mostly esters) onto polymer backbone.[13] From these research areas, it is clear that esterification of dextran is a very important reaction in drug design. Hence, it is of high importance to develop highly efficient and soft esterification methods.

Regarding the esterification of polysaccharides, a few methods are reported in the literature, such as using acetyl chloride with pyridine,[14] acetic anhydride with pyridine and 4-(dimethylamino)pyridine,[15,16] carboxylic acids *in situ* activated with tosyl chloride,[17–19] iminium chloride[20] and 1,1'-carbonyldiimidazole[17,21,22] and acetic anhydride activated with strong acids or metal catalysts.

In present study, our interests were focused on the search for efficient reaction methodologies for the esterification of the biologically important polysaccharide dextran. Hence, the value of the conventional reagent acetic anhydride was explored using iodine as the catalyst.[23] This esterification method appeared more advantageous regarding cost effectiveness because the other esterification methods available until now need expensive acylation reagents, *i.e.*, *p*-toluenesulfonyl chloride,[19] 1,1'-carbonyldiimidazole,[20] *etc*. Secondly, the esterification of polysaccharides under homogeneous reaction conditions is a current area of research. However, the fact that solvent systems used to dissolve polysaccharides are quite expensive cannot be neglected; therefore, such methods cannot be readily commercialized. Another important aspect of commercial synthesis of polysaccharide acetates is that an acidic catalyst is employed, which significantly destroys glycosidic linkages of polysaccharides. Hence, the aim of this study was to exploit the use of a mild catalyst, *i.e.*, iodine. Being a cheap, commercially available, environment friendly and most importantly powerful reagent, iodine is currently being extensively explored regarding its catalytic properties on various substrates in different low molecular weight organic transformations.[24,25] Likewise, the focus of this investigation was to examine the possibility of employing the acid anhydride/iodine system for the acetylation of dextran.

EXPERIMENTAL

Reagents and chemicals

Dextran (M_w 40000, Fluka) was dried under vacuum at 110 °C for 8 h prior to use. Analytical grade organic solvents and other reagents obtained from Fluka were used without further purification.

Measurements

The FTIR spectra were recorded on an IRPrestige-21 instrument (Shimadzu, Japan) using the KBr pellet technique. The ^{1}H-NMR spectra of the products were acquired on a

Bruker 400 MHz instrument in suitable deuterated solvents. Thermogravimetric (TG) analysis and derivative thermogravimetric (DTG) analysis were realized on a SDT Q600 (USA) thermal analyzer. Thermal decomposition temperatures (t_d) of the dextran esters were determined from the DTG curves. The t_d is reported as the onset of significant weight loss from a heated sample. Samples (10 mg) were measured under air at heating rate of 10 °C/min from 35 up to 600 °C.

*Esterification of dextran using acetic anhydride and iodine under solvent-free conditions, a typical example (sample **4**)*

Iodine (0.50 g, 0.0041 mol) was filled into a pre-dried round bottom flask. Acetic anhydride (4.0 mL, 0.038 mol) was added and the reaction mixture was kept under stirring for 15 min. Pre-dried dextran (1.0 g, 0.0062 mol) was added and the resulting mixture was refluxed for 4 h. The excess of iodine (catalyst) was removed by adding a saturated aqueous sodium thiosulfate solution to the reaction mixture. The thus formed white precipitates of dextran acetate were filtered off, washed thrice with cold water and then reprecipitated from acetone into cold water. The precipitate of sample **4** was then dried under vacuum at 50 °C for 24 h.

Yield: 77 %; *DS* (degree of substitution): 2.90 (the *DS* was calculated by acid base titration after saponification). FTIR (KBr, cm^{-1}): 2931 (C–H stretching of sugar units), 1751 (C=O stretching ester), 1246 (C–O–C stretching of ester), 1431 (CH_2 stretching of sugar units). ^{1}H--NMR (400 MHz, acetone-d_6, δ / ppm): 3.15–4.93 (anhydroglucose unit–H), 2.02 (acetyl–H).

Calculation of degree of substitution, a typical procedure

For the purpose of *DS* calculation, 100 mg of sample was dissolved in 50 mL aqueous 1.0 M NaOH solution , stirred overnight and its pH was registered using a pH meter. HCl (0.010 M) was added to achieve pH 7, followed by a known quantity (20 mL) of 1.0 M NaOH solution. The excess base was finally titrated with 0.10 M HCl until neutralization. The *DS* of the free acid moieties was then calculated. The *DS* of acetyl moiety was calculated by ^{1}H-NMR spectrum[15] from spectral integral ratios of the protons of the AGU and methyl of the acetyl moiety.

RESULTS AND DISCUSSION

An acid anhydride and an alcohol react together in the presence of iodine as a catalyst. The general mechanism is outlined in Fig. 1 using acetic anhydride as the example.[24,25] Iodine first activates acetic anhydride in the presence of alcoholic groups, as the oxygen of R–OH attacks the carbonyl carbon resulting in sp^3 hybridization. The acetic ester of the respective alcohol is formed by reaction of the iodide ion with the iodine atom that was attached to the oxygen of the carbonyl group, resulting in free iodine. Acetic acid is formed as a by-product. At the end of the reaction, addition of a saturated aqueous solution of sodium thiosulfate removes all the free iodine.

Bearing in mind the immense importance and proved efficiency of iodine as a catalyst for acetylation of alcohols under solvent-free conditions, the aim was to explore its potential for employment in the acetylation of polysaccharides such as dextran. Dextran was reacted with acetic anhydride under solvent-free conditions using different mole ratios of acetic anhydride (see Fig. 1). All the reactions

were performed at 50 °C for 3 h under a nitrogen atmosphere. The reaction conditions and the results of dextran acetylation are summarized in Table I.

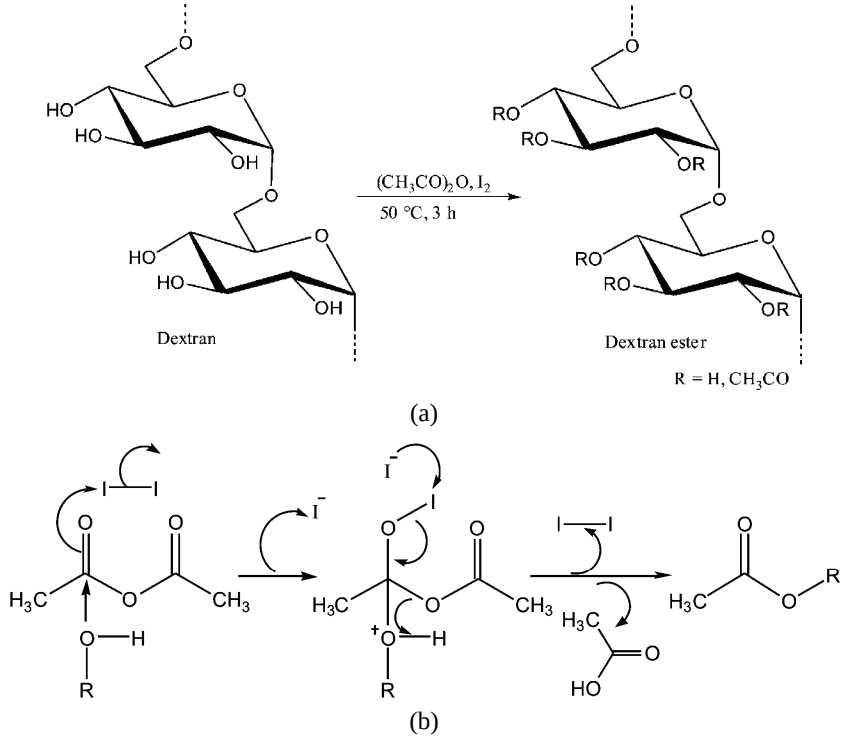

Fig. 1. a) Dextran acetylation with acetic anhydride catalyzed by iodine under solvent-free conditions and b) the generalized mechanism for alcohol (dextran) acetylation.

TABLE I. Conditions and results of acetylation of dextran with acetic anhydride *in situ* activated with iodine under solvent-free conditions

Sample	Mole ratio[a]	Yield, %	*DS*[b]	*DS*[c]
1	1:3	50	1.75	1.72
2	1:4	53	1.88	1.83
3	1:5	70	2.69	2.71
4	1:6	77	2.90	2.85
5	1:8	83	3.00	2.98
6	1:10	85	3.00	2.99

[a]Anhydroglucose unit (AGU):acetic anhydride; [b]*DS* calculated by acid-base titration after saponification; [c]*DS* calculated by ^{1}H-NMR spectroscopy

All the obtained dextran acetates (**1**–**6**) were of high purity and soluble in organic media, *e.g.*, dimethyl sulfoxide (DMSO), *N*,*N*-dimethylacetamide (DMA) and dimethylformamide (DMF). Samples **4**–**6** were additionally soluble in chloroform. All samples were insoluble in aqueous media. The dextran acetates were

purified by re-precipitation and their purity was verified by spectroscopic techniques. It was found that on increasing the molar ratio of acetic anhydride to dextran, the degree of substitution (*DS*) also increased, which means that in this way, the *DS* can be controlled. This observation is obvious from the results given in Table I. The products were obtained with excellent yields.

The results significantly indicated that this method is highly efficient for the synthesis of dextran acetates as samples **4**–**6** were obtained with almost complete substitution under solvent free-conditions. As dextran is a 1–6-linked polymer, a primary hydroxyl, which is generally more reactive toward acetylation, is absent in dextran. In addition, even dextran triacetate was achieved by using less than 1:8 anhydroglucose unit, AGU:acetic anhydride. Therefore, this method has the potential to be exploited for acetylation of polysaccharides in industry. All dextran acetates were thoroughly characterized by means of thermal analyses, and FTIR and ^{1}H-NMR spectroscopy.

FTIR spectroscopic studies were performed using the KBr pellet technique to observe the ester peaks and hydroxyl group absorptions. A distinct ester peak appeared at 1747 cm^{-1} for sample **5** (Fig. 2). The spectrum did not display hydroxyl group absorption at about 3500 cm^{-1}, which is indicative of complete substitution of the hydroxyl functions with acetate moieties. This shows the purity of the product and the success of the reaction. No peak was observed for any kind of possible impurity. For reference, the spectrum of the unsubstituted dextran polymer is being also provided in Fig. 2.

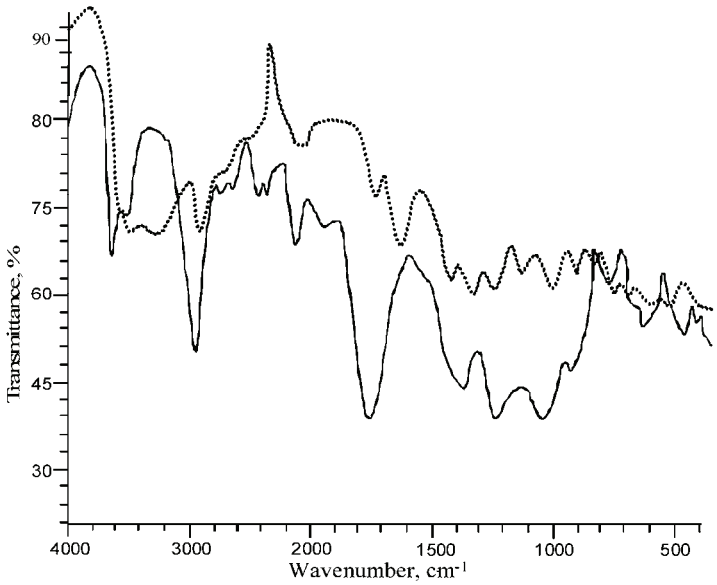

Fig. 2. FTIR (KBr) spectra of unsubstituted dextran polymer (▪▪▪) and dextran acetate **5** (—).

From DTG analysis, a thermal decomposition temperature (t_d) of 385.5 °C was obtained for dextran acetate **5**. Typical TG and DTG curves of sample **5** are shown in Fig. 3. Dextran acetate **5** showed increased stability when compared to the unsubstituted dextran polymer (t_d = 315.35 °C, Fig. 4).

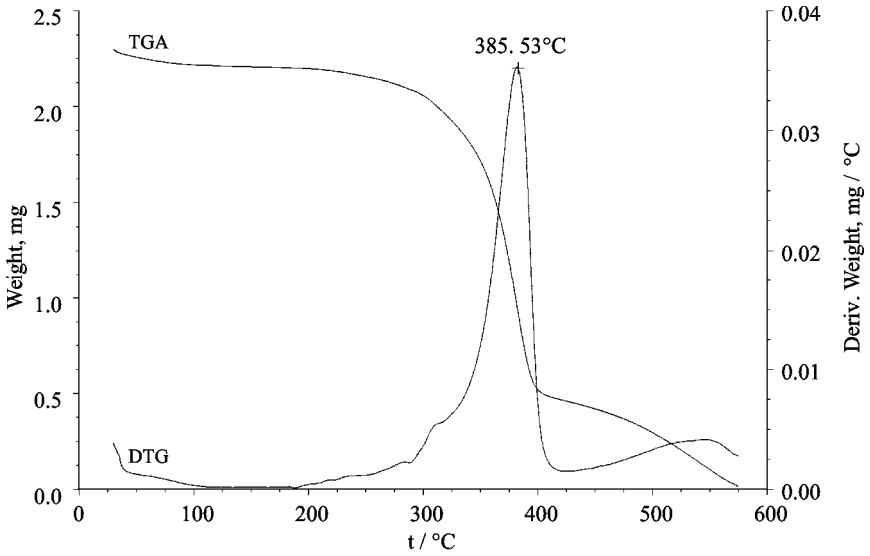

Fig. 3. Simultaneous DTG and TG curves of dextran acetate **5**.

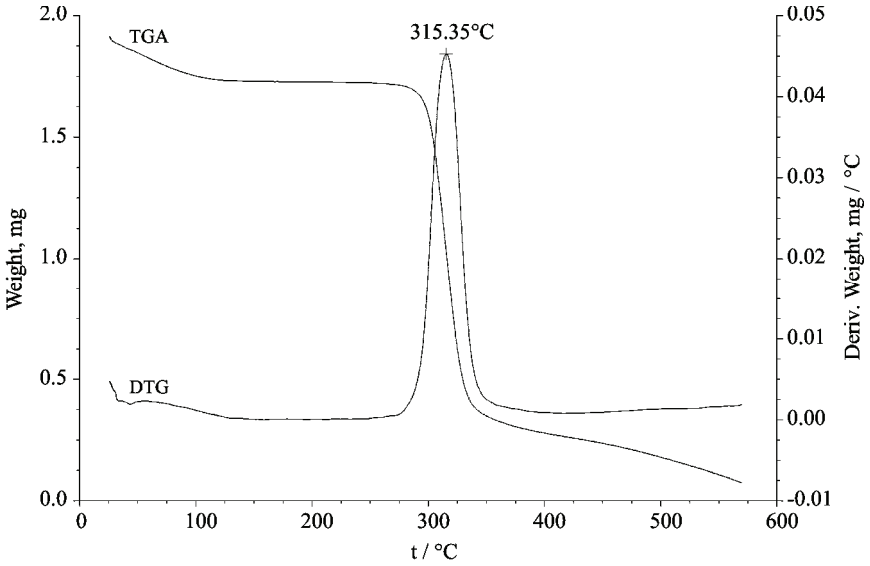

Fig. 4. Simultaneous DTG and TGA curves of unsubstituted dextran polymer.

^{1}H-NMR spectroscopy was thoroughly performed to check the success of the reaction and purity of the samples. A typical ^{1}H-NMR spectrum of dextran acetate **1** recorded in $CDCl_3$ is shown in Fig. 5. The spectrum revealed the success of the reaction as methyl protons of the acetyl moiety appeared at 2.05 ppm. The signals of AGU-H appeared well resolved at about 3.15–4.90 ppm. ^{1}H-NMR spectroscopy was also performed to calculate the *DS* of pendant acetyl groups onto dextran. The *DS* was successfully calculated from the ratios of the integrated peak areas. The results of the *DS* calculated from the ^{1}H-NMR results were found to be comparable with the *DS* values obtained by acid base titration after saponification (see Table I).

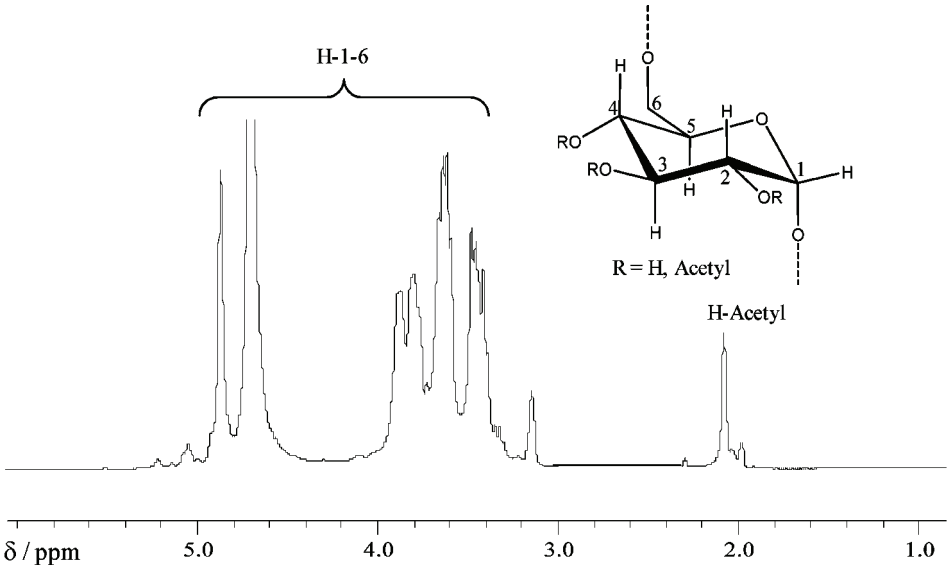

Fig. 5. 400 MHz ^{1}H-NMR spectrum ($CDCl_3$) of dextran acetate **1**.

CONCLUSIONS

In the present research work, a new method for the esterification of dextran was successfully designed, in which dextran was allowed to react with acetic anhydride *in situ* activated by the versatile reagent iodine. Highly pure and organosoluble dextran acetates were successfully synthesized, purified and characterized. This easily applicable method appeared highly efficient for the acetylation of dextran. As all reactions were performed at 50 °C for only 3 h, the reaction was highly efficient, fast, time saving and energy effective. Dextran acetylation up to complete substitution of free hydroxyl by acetyl moieties was successfully achieved under solvent-free conditions. As iodine is a cheap, commercially available and environment-friendly reagent, this reaction methodology could be adopted on a commercial scale for the acetylation of polysaccharides.

Acknowledgement. Financial support of the Higher Education Commission of Pakistan under the scheme entitled “International linkages of Pakistani Universities with Foreign Universities” is greatly acknowledged.

ИЗВОД

ЕФИКАСАНО АЦЕТИЛОВАЊЕ ДЕКСТРАНА У МАСИ АКТИВИРАЊЕМ АНХИДРИДА СИРЋЕТНЕ КИСЕЛИНЕ ЈОДОМ

MUHAMMAD A. HUSSAIN[1], DURE SHAHWAR[1], MUHAMMAD N. TAHIR[2], MUHAMMAD SHER[1], MUHAMMAD N. HASSAN[1] и ZAKIA AFZAL[1]

[1]*Department of Chemistry, University of Sargodha, Sargodha 40100, Pakistan и* [2]*Institute of Inorganic and Analytical Chemistry, Johannes Guttenberg University, Duesbergweg 10–14, 55099, Mainz, Germany*

У раду је приказан једноставан, ефикасан и јефтин поступак ацетиловања декстрана у маси тј. без присуства растварача. Ацетати декстрана су успешно синтетисани коришћењем различитих молских односа анхидрида сирћетне киселине и анхидроглукозне јединице из полимерног ланца и у присуству јода као катализатора. Реакције ацетиловања декстрана су извођене на температури 50 °C током 3 h уз мешање у инертној атмосфери азота. Добијени естри декстрана су били високе чистоће и растворни у органским растварачима. Реакција ацетиловања је врло ефикасна и добијени су производи високог степена супституције као и триацетати декстрана. Такође је уочено да се помоћу молског односа анхидрида сирећетне киселине и анхидроглукозне јединице декстрана може лако контролисати степен супституције (*DS*) хидроксилних група у полимерном ланцу. Дакле, серија узорака декстрана различитог степена супституције је дизајнирана, синтетисана, пречишћена и окарактерисана. Ковалентни карактер веза супституисаних група и молекула декстрана је потврђен спектроскопским техникама. Термогравиметрија је показала да су синтетисани естри декстрана сличне термичке стабилности као и полазни полимер, односно декстран. Степен супституције хидроксилних група на полимерном ланцу је одређиван користећи стандардни поступак титрације киселином након сапонификације. Сви узорци ацетилованог декстрана су у потпуности окарактерисани термичком анализом (TGA и DTG), FTIR и ^{1}H-NMR спектроскопијом.

(Примљено 7. априла, ревидирано 2. јуна 2009)

REFERENCES

1. E. Khalikova, P. Susi, T. Korpela, *Microb. Mol. Biol. Rev.* **69** (2005) 306
2. S. S. Dhaneshwar, M. Kandpal, N. Gairola, S. S. Kadam, *Indian J. Pharm. Sci.* **68** (2006) 705
3. E. Rotureau, M. Leonard, E. Dellacherie, A. Durand, *J. Colloid Interface Sci.* **279** (2004) 68
4. D. Carvalho, H. Dorigo, D. Bouskela, *Shock* **15** (2001) 157
5. N. Siddika, E. Mbemba, D. Letourneur, L. Ylisastigui, A. Benjouad, L. Saffar, J. C. Gluckman, J. Jozefonvicz, L. Gattegno. *Biochim. Biophys. Acta* **1362** (1997) 47
6. R. Huynh, F. Chaubet, J. Jozefonvicz, *Carbohydr. Res.* **332** (2001) 75
7. D. L. Avramoglou, R. Huynh, F. Chaubet, L. Sedel, A. Meunier, *Biochem. Pharmacol.* **63** (2002) 129
8. H. Hosseinkhani, T. Aoyama, O. Ogawa, Y. Tabata, *J. Controlled Release* **88** (2003) 297
9. E. Rotureau, M. Leonard, E. Marie, D. Dellacherie, T. A. Camesano, A. Durand, *Colloids Surf., A.* **288** (2006) 131
10. D. Ledoux, D. L. Merciris, D. Barritault, J. P. Caruelle, *FEBS Lett.* **537** (2003) 23

11. P. Bittoun, T. Avramoglou, J. Vassy, M. Crepin, F. Chaubet, S. Fermandjian, *Carbohydr. Res* **322** (1999) 247
12. R. Y. Cheung, Y. Ying, M. Andrew, A. M. Rauth, N. Marcon, X. Y. Wu, *Biomaterials* **26** (2005) 5375
13. Y. Miyazaki, K. Ogihara, S. Yakou, T. Nagai, K. Takayama, *Int. J. Pharm.* **258** (2003) 21
14. N. Teramoto, M. Shibata, *Carbohydr. Polym.* **63** (2006) 476
15. T. F. Liebert, M. A. Hussain, T. Heinze, *Macromol. Symp.* **223** (2005) 79
16. Y. Tezuka, *Carbohydr. Res*. **305** (1998) 155
17. M. A. Hussain, *J. Polym. Sci., Part A: Polym. Chem.* **46** (2008) 747
18. T. F. Liebert, M. A. Hussain, M. N. Tahir, T. Heinze, *Polym. Bull.* **57** (2006) 857
19. T. Heinze, T. F. Liebert, K. S. Pfeiffer, M. A. Hussain, *Cellulose* **10** (2003) 283
20. M. A. Hussain, T. F. Liebert, T. Heinze, *Macromol. Rapid Commun.* **25** (2004) 916
21. M. A. Hussain, T. F. Liebert, T. Heinze, *Polym. News* **29** (2004) 14
22. M. A. Hussain, T. Heinze, *Polym. Bull.* **60** (2008) 775
23. A. Memmi, R. Granet, Y. Champavier, P. Krausz, *E-Polym.* **83** (2005) 401
24. M. Adinolfi, G. Barone, A. Iadonisi, M. Schiattarella, *Tetrahedron Lett.* **44** (2003) 4661
25. P. Phukan, *Tetrahedron Lett.* **45** (2003) 4785.

Journal of the Serbian Chemical Society
JSCS@tmf.bg.ac.rs • www.shd.org.rs/JSCS
J. Serb. Chem. Soc. *75* (2) 175–183 (2010) UDC 54.05+547.495.2/.9:664.644.7:678.061
JSCS–3950 *Original scientific paper*

Immobilization of urease in alginate, paraffin and lac

KESPI PITHAWALA[2], NEELAM MISHRA[1] and ANITA BAHADUR[1]*

[1]*Department of Zoology, P. T. Sarvajanik College of Science, Surat, 395001 and*
[2]*Department of Biology Gujarat college, Ahmedabad-15, India*

(Received 14 May, revised 16 July 2009)

Abstract: The enzyme urease (EC.3.5.1.5) from jack bean meal was immobilized by various techniques, such as entrapment in calcium alginate gel spheres in aqueous suspension, lac impregnated muslin cloth as dry films and by embedding in paraffin wax impregnated muslin cloth. The activity of the free and immobilized enzymes as a function of pH, temperature, storage stability, kinetic parameters and periodic use were compared. The immobilized enzyme showed good storage stability. After repeated use, the alginate beads turned brown and deteriorated, hence the storage stability was not good. The paraffin films were preserved dry because during wet preservation, the film slightly softened and the protein leached out slightly. The alginate beads had moderate mechanical stability. The lac films were tougher than the paraffin wax films in terms of mechanical stability. The K_m and V_{max} values were altered after immobilization. The K_m values for calcium alginate and lac were low, while it was larger in paraffin film as compared to the free enzyme. This may be due to the fact that immobilization on calcium alginate and lac in presence of $CaCl_2$ and methanol exposed certain active sites of the urease. While immobilization on paraffin masks the active sites and may lead to reduced binding of the substrate.

Keywords: enzyme; immobilization; urease; calcium alginate; paraffin wax; lac.

INTRODUCTION

Immobilized enzymes are rooted deeply in the field of biotechnology due to their inherent properties, such as specificity, stability and reusability. The storage stability of free enzymes in solution is poor. Recovery from solution with their activity retained is not possible. Amongst supports used for immobilization, biological macromolecules (such as cellulose, chitin and chitosan) and their derivatives have been studied the most extensively through physical adsorption or chemical linkages.[1–4] A few reports have appeared on the immobilization of enzymes on cellulosic supports, calcium alginate gel-spheres and paraffin wax.[4–7] Studies are reported on the use of polymeric supports in the form of granules,

* Corresponding author. E-mail: anita26p@gmail.com
doi: 10.2298/JSC1002175P

powder, membrane, fibers and tubes.[7–12] Immobilization of chymotrypsin and trypsin on spherical particles of an anionic polymeric latex were also reported previously.[13,14] Urease was immobilized earlier on many supports, such as PVC, cellulose, alginate[15–18] and some natural seed coats.[19] The present investigation was undertaken with the view of studying the retention of urease activity, reusability, storage stability, changes in kinetic parameters and also superiority of the matrices, *viz.*, calcium alginate beads, paraffin film and reinforced lac film for immobilization. Paraffin wax (m.p. 58–60 °C) is non-toxic and therefore finds diverse uses, including medication, *etc*.[20,21]

Hitherto, there have been no reports of immobilization of enzymes on biomaterials such as natural lac (shellac). It is a naturally occurring resinous substance (chiefly derived from polysaccharides) and is a mixture of resin 60 %, coloring matter 10 %, wax 6 %, gum 5.5 %, sugar 4 % and remaining mud and dirt. Lac being non-toxic was tried for immobilizing enzymes. In this paper, the results of a systematic study of native and immobilized urease on different matrices and the effects of various factors, such as pH, temperature, storage stability and reusability on enzyme activity, are reported.

EXPERIMENTAL

Materials and methods

The enzyme urease from jackbean meal and its substrate urea (Loba Chem. Pvt. Ltd. India.) were used. Sodium alginate, Nessler's reagent, tris buffer (0.20 M) and all other employed chemicals were of Analar grade. Paraffin wax (m.p. 58–60 °C) was a Ranbaxy product and lac was obtained from a lac infected tree belonging to the genera *Albizzia lebbeck* and was used after purification by solvent extraction in methanol. Muslin cloth (Tata fabric pure cotton) was used for reinforcing.

Preparation of urease immobilized in calcium alginate gel spheres

Sodium alginate (200 mg) with 10 mg of urease in 10 ml aqueous medium was thoroughly mixed until a honey-like consistency was attained. The mixture was then filled in a syringe and allowed to drop into 50 ml of $CaCl_2$ solution (2 % w/v) from a constant height to form beads.[7] The beads were then stirred slowly for 20 min and then removed from the solution and subsequently washed with buffer before use.

Preparation of immobilized enzyme in reinforced paraffin film

To 4.0 g of molten paraffin wax in a thermostated water bath (at 65 °C), 1.0 g of enzyme powder was added under continuous stirring at a low speed. Sun dried muslin cloth previously washed in distilled water was cut into 1 cm^2 pieces which were added to the continuously stirred molten wax at 65 °C. After 3–5 s, these pieces were removed using pointed B. B. forceps, slightly shaken to remove dripping wax and allowed to dry at room temperature. In this way, 1 cm^2 reinforced films of paraffin wax with enzyme were made.

Procuring lac

Lac is produced by non-motile females of tiny insects belonging to the genera *Tracchardia* or *Laccifier lacca* to protect themselves against adverse conditions of weather, especially winter. Lac insects are parasites on trees, *e.g.*, *Albizzia lebbeck*, *Schleicheia oleosa*, *S.*

trijuga, Acacia catechu, A. arabica, Zizyphus jujuba, Z.mauritiana, Grewia sp., etc. Albizzia lebbeck, Schleicheia oleosa, S. trijuga, Accacia catechu, A. arabica, Zizyphus jujuba, Z. mauritiana, Grewia sp., Ficus religiosa, Shorea talura, Butea monosperma, B. frondosa, etc.

Natural lac, procured by scrapping infected twigs, was melted, squeezed through a cloth to obtain buttons. These was then dissolved in methanol and kept for 2 days. The thus obtained clear solution was centrifuged at high speed for 20 min to allow settling of impurities, if any. The clear supernatant was then poured into a porcelain evaporating dish and the methanol was allowed to evaporate in open air for 2 days, whereby a crust of pure crystalline lac was obtained on the evaporating dish. This was scrapped and used for the experiments.

Preparation of immobilized enzyme in reinforced lac

Purified lac (2.0 g) was dissolved in 5 ml of methanol. To this was added 1.0 g of urease powder and the mixture was stirred continuously on a magnetic stirrer. Cloths squares (as previously treated) were dipped into this mixture for 3–5 s and then allowed to dry and harden for a day at room temperature. These films were then weighed to find the amount of trapped enzyme. The enzyme in the washing was measured colorimetrically using the Lowry method[22] to obtain the amount of bound enzyme using BSA as the standard.

Assay of native urease

For measurement of the urease activity, the ammonia liberated on incubating the enzyme with urea for a fixed time was determined using Nessler's reagent.[19] One unit of urease activity liberates 1.0 mol of ammonia per min from 0.10 M urea under standard assay conditions.

Assay of immobilized urease

The alginate beads (17 beads) with urease entrapped were taken in 1 ml phosphate buffer (0.20 M, pH 7) solution and reacted with 1.0 ml of a 3 % urea solution for 15 min. The same procedure was used to follow the reaction and the measurements were performed in the same manner as for the native enzymes studies. Here the beads were removed before chilling the solution and adding H_2SO_4 to stop the reaction.

One film of paraffin wax and lac were each taken in 1 ml phosphate buffer (0.20 M, pH 7) and reacted with 1.0 ml of a 3 % urea solution for 30 min. The same procedure was used to follow the reaction and the measurements were performed as in the above-described experiment. The films were taken out from the reaction mixture to stop the reaction. The experiments were conducted in triplicate to confirm the reproducibility of the results.

Storage stability

For storage stability studies, the immobilized enzyme was kept at room temperature. The activity was measured for a month. Fresh preparations of immobilized enzymes were taken as controls for each assay. The enzyme immobilized on paraffin wax films was preserved in buffer, distilled water and under dry condition while the enzyme entrapped in beads was preserved in $CaCl_2$ solution because wet beads gave better result than dry beads.

Thermal stability

To determine the optimal temperature up to which the immobilized enzyme can withstand thermal stress, free and immobilized enzyme were suspended in phosphate buffer (0.20 M, pH 7) and incubated at different temperatures (30 to 80 °C) for 30 min before the activity was measured.

Determination of the kinetic parameters

For the determination of the kinetic parameters, the substrate concentration was varied and the optimum pH for native and immobilized enzyme was determined by varying the pH of the assay buffer. The relative enzyme activity was determined for each pH by the method described above for the assay of the enzyme. The absorbance was read at 500 nm. The rate of the reaction was measured as mmoles of ammonia produced / min / mg enzyme. The values of K_m and V_{max} were determined using Lineweaver–Burke plots.

RESULTS AND DISCUSSION

The structural integrity and activity of the urease were retained due to mild and precise physical condition during the immobilization procedure. The calcium alginate beads were chemically inert to the entrapped enzyme. The porosity of the gel was such that it allowed easy movement of the substrate molecules through the beads. The beads were quite stable in tris buffer (pH 7) and in phosphate buffer with pH > 7.8. However at higher pH values, the beads showed softening and stickiness of the surface. The entrapment of urease in alginate gel was approximately 60 %. The immobilized enzyme retained 41 % of its activity. Urease is a thermostable enzyme that is denatured at/above 80 °C[23] and, therefore, it could be easily immobilized on paraffin wax. Alginate beads are hydrophilic in nature while paraffin and lac are hydrophobic so only the surface molecules react. The reinforced films of paraffin were durable; the enzyme embedded could catalyze and retained 45–50 % of its activity.[24,25]

As the above immobilization procedures were not applicable for thermolabile enzymes, immobilization on lac films was a step refinement as it involved extremely mild physical conditions. The lac films were tougher, thermostable and the enzyme could easily catalyze and retained 28–30 % of its activity.

The results of the studies performed with these preparations were compared with those of native enzymes to determine the utility of immobilized urease in the hydrolysis of urea.

Storage stability and reusability

The native enzyme retained the same activity for about seven days, after which it slowly decreased and was lost completely after a month. The enzyme immobilized on calcium alginate retained the same activity for a fortnight, then decreased and was lost in 30 days. The beads darkened (slightly brown) and deteriorated (beads were stored at room temperature in $CaCl_2$ solution).

The enzyme immobilized on paraffin wax films preserved in buffer retained the same activity for a week and had retained about 73 % of its activity after a month. When the films were preserved in distilled water, 70 % activity of the immobilized enzyme was observed even after a month. When preserved under dry condition, the enzyme retained 88 % of its activity. During wet preservation, the film softened somewhat and the protein leached out slightly (Fig. 1).

The storage stability of the enzyme immobilized on lac films when preserved in dry condition was the greatest and the immobilized enzyme had retained 98 % of its activity even after a month.

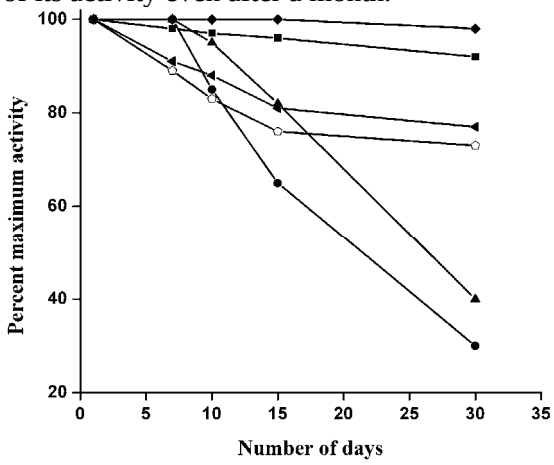

Fig. 1. Plot of the percentage of the maximum activity *vs.* time (days) for estimating the storage stability of urease on paraffin wax as dry films (■), films kept in buffer (◄) and films kept in distilled water; (⌂), native enzyme (●), Ca-alginate (▲), lac as a dry film (♦).

The immobilized enzyme lost activity after every use. The urease entrapped in alginate could be reused at the most five times, while the enzyme immobilized on paraffin and lac could be reused more than eight or nine times with less than 40 % activity. The native enzyme, being water soluble, could not be recovered and reused (Fig. 2).

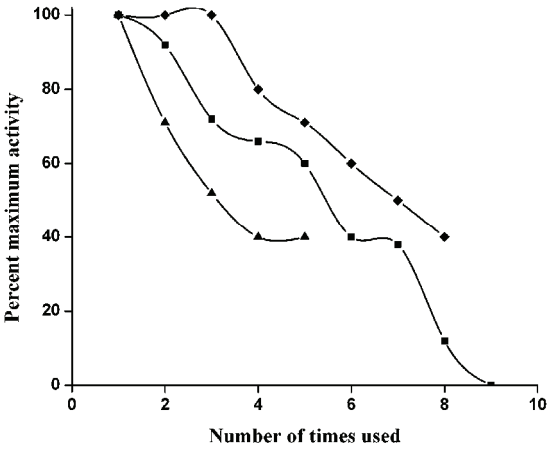

Fig. 2. Plot of the percentage of the maximum activity *vs.* the number of times used for reusability studies of urease immobilized on calcium alginate (▲), paraffin wax (■) and lac (♦).

Thermal stability

The temperature dependence of the relative activity of the enzyme is shown in Fig. 3. When kept for 30 min, the optimum temperature was found to be 55 °C for both the immobilized and native enzymes at pH 7, while the enzyme immo-

bilized on lac showed a comparatively higher relative activity up to 60 °C. Both the native and the immobilized enzyme were stable up to 70 °C, although a remarkable drop in percent maximum activity from 97 to 50 % was observed for the immobilized and native enzyme. Thermostability studies could not be realized for the enzyme immobilized on paraffin films (melting point 58–60 °C).

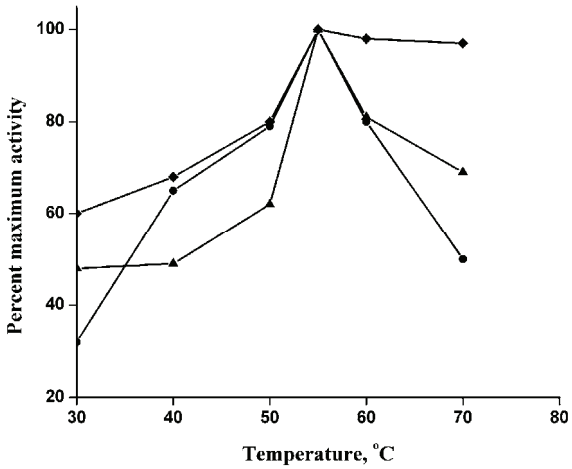

Fig. 3. Plot of the percentage of the maximum activity *vs.* temperature for temperature stability of free (●) and urease immobilized on calcium alginate (▲) and lac (♦).

Mechanical stability

Five to six beads of calcium alginate were centrifuged at 1200 rpm for 2–5 min. All the beads remained intact and none were broke or adhered. In addition, beads subjected to stirring for 5–10 min at slow speeds showed no breakage; similarly five to six films of paraffin wax were resistant to breakage when centrifuged but broke when subjected to stirring using a magnetic stirrer. The lac films were very tough, durable and highly resistant to mechanical wear when centrifuged as well as when stirred vigorously.

pH activity profile

The pH dependence of the relative activity of the enzyme was compared with that of the enzyme immobilized on the different supports. The reaction was performed in the pH range 5.6–7.8. The optimum pH for the native and the enzyme immobilized on calcium alginate, paraffin and lac were 6.8, 7.0, 7.0 and 7.2, respectively. This showed that immobilization shifted the optimum pH range in the basic direction by 0.2 units for calcium alginate and paraffin and 0.4 units for lac. Thus, there was an increased possibility of using urease over a broader range of pH (6.8–7.2) compared to native urease (Fig. 4).

Kinetic parameters

The kinetic behavior of native and the immobilized enzyme is shown in (Fig. 5). The values of K_m and V_{max} are given in Table I. They are in accordance with the Michaelis–Menten rate equation.

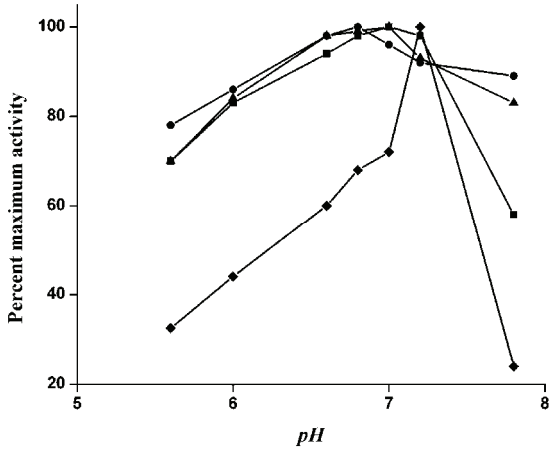

Fig. 4. Plot of the percentage of the maximum activity *vs*. pH, for the pH profile of free (●) and urease immobilized on calcium alginate (▲), paraffin, wax (■) and lac (♦).

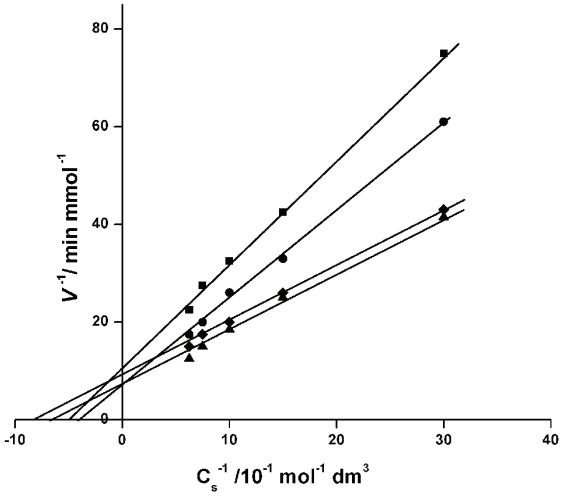

Fig. 5. Double reciprocal plot of rate V (mmol of NH_3 produced per min and mg of enzyme) *vs*. the concentration of urea for free (●) and urease immobilized on calcium alginate (▲), paraffin wax (■) and lac (♦).

TABLE I. Kinetic parameters of free and enzymes immobilized on calcium alginate, paraffin wax and lac

Support material	K_m / mol dm^{-3}	V_{max} / mmol min^{-1} mg^{-1}
Native enzyme	0.25	0.154
Ca alginate	0.18	0.154
Paraffin wax	0.20	0.100
Lac	0.13	0.125

It can be seen that the K_m values for the immobilized enzyme decreased, which shows that immobilization led to a masking of certain active sites of enzymes in all cases. The K_m values in the case of calcium alginate and lac as support materials were low compared when paraffin wax was used as the support. This might be attributed to the use of chemicals, *viz.* $CaCl_2$ and methanol, respectively, during the immobilization procedure.

Acknowledgement. A. B. thanks U.G.C. Major Research Project F. No.33-347/2007 (SR) for financial assistance.

ИЗВОД

ИМОБИЛИЗАЦИЈА УРЕАЗЕ У АЛГИНАТУ, ПАРАФИНУ И ЛАКУ

KESPI PITHAWALA[2], NEELAM MISHRA[1] и ANITA BAHADUR[1]

[1]*Department of Zoology, P. T. Sarvajanik College of Science, Surat, 395001 и* [2]*Department of Biology Gujarat college, Ahmedabad-15, India*

Ензим уреаза (EC.3.5.1.5) из пасуља је имобилизован различитим техникама: у сферном гелу калцијум-алгината у воденој суспензији, у лаку којим је у виду танког филма импрегнирано платно и у парафинском воску за импрегнацију платна. Упоређивана је активност слободног и имобилизованог ензима у функцији pH, температуре, стабилности при чувању, кинетичких параметара и учесталости употребе. Имобилизован ензим је био стабилан током чувања. После вишеструке употребе, зрна алгината су променила боју у браон и распала су се, што се одразило на стабилност овог матрикса. Парафински филм треба да се чува сув, пошто чување у влажним условима омекшава филм и доводи до губитка протеина. Зрна алгината су имала задовољавајућу механичку стабилност. Лак се показао механички чвршћим од парафинског воска. K_m и V_{max} вредности за ензим су се промениле после имобилизације. K_m вредност у калцијум-алгинату и лаку је била ниска, док је у парафинском филму била слична као код слободног ензима. Ово се може објаснити присуством $CaCl_2$ и метанола, који олакшавају излагање активних места уреазе. Имобилизација у парафину маскира активна места, што може довести до смањеног везивања супстрата.

(Примљено 14. маја, ревидирано 16. јула 2009)

REFERENCES

1. J. M. Guisan, *Immobilization of enzymes and cells*, Humana Press, Totowa, New Jersey, 2006
2. *Enzyme biocatalysis; principles and application*, F. A. Illanes, Ed., Springer, Valparaiso, 2008
3. R. C. Reddy, P. K. Srivastava, P. M. Dey, M. Kayastha, *Biotechnol. Appl. Biochem.* **39** (2004) 323
4. G. Yong, W. Jie, S. Xijin, *J. Zhejiang Univ. Sci.* **5** (2004) 1608
5. V. A. Savangikar, R. N. Joshi, *J. Food Sci.* **43** (1978) 1616
6. E. Hearn, R. J. Neufeld, *Process Biochem.* **35** (2000) 1253
7. K. Won, S. Kim, K. J. Kim, H. W. Park, S. J. Moon, *Process Biochem.* **40** (2005) 2149
8. Y. F. Li, F. Y. Jia, J. R. Li, G. Liu, Y. Z. Li, *Biotechnol. Appl. Biochem.* **33** (2001) 29
9. K. Kang, C. Kan, A. Yeung, D. Liu, *Mat. Sci. Eng. C* **26** (2006) 664
10. Q. Xing, S. R. Eadula, Y. M. Lvov, *Biomacromolecules* **8** (2007) 1987

11. T. Godjevargova, K. Gabrovska, *J. Biotechnol.* **103** (2003) 107
12. S. Mulagalapalli, S. Kumar, R. C. Reddy, A. M. Kayastha, *Appl. Biochem. Biotechnol.* **142** (2007) 2917
13. A. Bahadur, P. Bahadur, G. Riess, *Makromol. Chem*. **186** (1985) 1387
14. A. Bahadur, P. Bahadur, *Indian J. Biochem. Biophys.* **22** (1985) 107
15. C. Tyagi, L. K. Tomar, H. Singh, *J. Appl. Polym. Sci.* **111** (2009) 1381
16. P. V. Sundaram, *Biochim. Biophys. Acta* **321** (1973) 319
17. S. Rejikumar, S. Devi, *J. Mol. Catal. B* **4** (1998) 61
18. H. Hatayama, T. Swabe, Y. Kurokawa, *J. Sol-Gel Sci. Tech.* **7** (1996) 13
19. Y. Kulshrestha, Q. Husain, *Enzyme Microb. Technol*. **38** (2006) 470
20. K. Pithawala, A. Bahadur, *Nat. Acad. Sci. Lett.* **27** (2004) 53
21. H. Ertesvag, G. Skjak-Braek, *Methods Biotechnol.* **10** (1999) 71
22. O. H. Lowry, N. J. Rosebrough, A. L. Farr, *J. Biol.Chem.* **193** (1951) 265
23. B. Krajewska, *J. Mol. Catal. B: Enzym.***59** (2009) 22
24. A. Bahadur, Y. K. Rao, S. Ghosh, *Indian J. Biochem. Biophys.* **25** (1988) 273
25. C. D. Paul, A. Bahadur, B. A. Shah, *Cellulose Chem. Technol.* **31** (1997) 315.

Journal of the Serbian Chemical Society
JSCS@tmf.bg.ac.rs • www.shd.org.rs/JSCS

J. Serb. Chem. Soc. *75* (2) 185–194 (2010)
JSCS–3951

UDC 577.152:663.12:577.152.1+663.51
Original scientific paper

Binding of coenzymes to yeast alcohol dehydrogenase

VLADIMIR LESKOVAC[1*#], SVETLANA TRIVIĆ[2#], DRAGINJA PERIČIN[1#], MIRA POPOVIĆ[2#] and JULIJAN KANDRAČ[3#]

[1]*Faculty of Technology, University of Novi Sad, Bulevar Cara Lazara 1, Novi Sad,* [2]*Faculty of Science, University of Novi Sad, Novi Sad and* [3]*Faculty of Agriculture, University of Novi Sad, Novi Sad, Serbia*

(Received 26 May, revised 23 July 2009)

Abstract: In this work, the binding of coenzymes to yeast alcohol dehydrogenase (EC 1.1.1.1) were investigated. The main criterions were the change in the standard free energies for individual reaction steps, the internal equilibrium constants and the overall changes in the reaction free energies. The calculations were performed for the wild type enzyme at pH 6–9 and for 15 different mutant type enzymes, with single or double point mutations, at pH 7.3. The abundance of theoretical and experimental data enabled the binding of coenzymes to enzyme to be assessed in depth.

Keywords: coenzyme binding; Gibbs free energy; yeast alcohol dehydrogenase.

INTRODUCTION

Yeast alcohol dehydrogenase (EC 1.1.1.1, isoenzyme I) catalyzes the oxidation of primary and secondary alcohols (B) by NAD^+ (A) into the corresponding aldehydes or ketones (P) and NADH (Q):

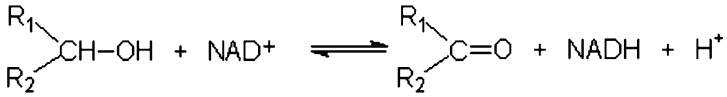

(1)

Reaction (1) is fully reversible and the equilibrium is shifted far to the left at neutral pH.[1]

In this paper, the investigation of coenzyme binding in the above reactions is reported, using the changes in the standard free energies as the main criterion of enzyme thermodynamics. The change in the standard free energies was calculated for individual reaction steps, the internal equilibrium constants in the reaction and the overall changes in the reaction free energies. The calculations were performed for the wild type enzyme at different pH values, mostly from pH 6–9,

* Corresponding author. E-mail: jkandrac@polj.ns.ac.rs
# Serbian Chemical Society member.
doi: 10.2298/JSC1002185L

and for mutant enzymes at pH 7.3. An abundance of theoretical and experimental data enabled the coenzyme binding to be investigated in depth.

In addition, the changes in the standard enthalpies and standard entropies of the reaction were calculated for the binding of coenzymes to the free enzyme.

METHODS

The standard transformed Gibbs energies of enzyme-catalyzed reactions, $\Delta_r G°'$, are connected with apparent equilibrium constants of reactions, K', at any specified pH and ionic strength, by the relationship:

$$\Delta_r G°'(\mathrm{pH},I) = -RT\ln K' \tag{2}$$

From Eq. (2), the apparent equilibrium constants may be easily calculated from the $\Delta_r G°'$ values, and *vice versa*.

The Gibbs free energies of the activated states, $\Delta G^{\ddagger}$, are connected with kinetic constants, k, by the relationship:

$$\Delta G^{\ddagger} = -RT\ln k \tag{3}$$

By subtracting the sum of the standard transformed Gibbs energies of formation of the reactants, $\Delta_f G°'$, from the sum of the standard transformed Gibbs energies of formation of the products, it is possible to determine the standard transformed reaction Gibbs energy, $\Delta_r G°'$, of any enzymatic reaction for which the free standard transformed Gibbs energy of formation of all reactants and products are known.[2–4]

$$\Delta_r G°'(\mathrm{pH},I) = \Sigma\Delta_f G°'(\mathrm{products}) - \Delta_f G°'(\mathrm{reactants}) \tag{4}$$

The influence of ionic strength is calculated from:[5,6]

$$\mathrm{p}K_1(I) = \mathrm{p}K_1(I=0) + 0.510651\frac{\sqrt{I}}{1+1.6\sqrt{I}}\Sigma\nu_i z_i^2 \tag{5}$$

where K_1 is the dissociation constant of the reactant at a given ionic strength, ν_i is the stoichiometric number of species i. $\Delta_f G_1°'$ is related to the most basic species of the reactant. From $\Delta_f G_1°'(I)$, the value of $\Delta_f G_1°'(I = 0)$ can be calculated and from this further $\Delta_f G_2°'(I = 0)$, from:

$$\Delta_f G_2°'(I=0) = \Delta_f G_1°'(I) - RT\ln 10p\mathrm{K}_1(I=0) \tag{6}$$

Then the standard transformed Gibbs energy of formation of the mixture of both ionic species is calculated at a given pH and ionic strength:[5,6]

$$\Delta_f G^{\circ,} = -RT\ln\left(\exp\left(-\frac{\Delta_f G_1^{\circ,}}{RT}\right) - \exp\left(-\frac{\Delta_f G_2^{\circ,}}{RT}\right)\right) \tag{7}$$

An expanded form of Eq. (7) is:

$$\begin{aligned}\Delta_f G^{\circ,} = -2.47897\ln\Big(&\exp\Big(-0.403393\big(\Delta_f G_1'^{\circ}(I=0,\mathrm{pH}\,0) - 2.91482\big(z_1^2 - N_{\mathrm{H}(1)}\big)\frac{\sqrt{I}}{1+1.6\sqrt{I}} + \\ &+ N_{\mathrm{H}(1)}RT\ln 10\mathrm{pH}\big) + \exp\Big(-0.403393\big(\Delta_f G_2'^{\circ}(I=0,\mathrm{pH}\,0) - \\ &-2.91482\big(z_2^2 - N_{\mathrm{H}(2)}\big)\frac{\sqrt{I}}{1+1.6\sqrt{I}} + N_{\mathrm{H}(2)}RT\ln 10\mathrm{pH}\big)\Big)\end{aligned} \tag{8}$$

Most experimental data reported in this work were conducted in aqueous buffers of ionic strength around 0.10 mol dm^{-3}. Since small changes in ionic strength make little contribution to thermodynamic parameters, specification of the ionic strength in the experiments reported was omitted throughout this work.

RESULTS AND DISCUSSION

Binding energies for the coenzymes

Yeast alcohol dehydrogenase, at neutral pH values, operates by an ordered addition of reactants on the aldehyde and a preferred order of addition of reactants on the alcohol side of the reaction, with some dissociation of coenzyme from the central complex EAB.[7] A kinetically detectable isomerization of the enzyme–NAD^+ binary complex occurs on the alcohol side of the reaction (Scheme 1).[1]

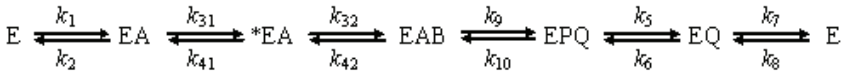

Scheme 1.

The standard free energy of binding for NAD^+ to the free enzyme may be calculated from the equilibrium constant k_1/k_2 using Eq. (2). In the same way, the standard free energy of binding for NADH may be calculated from the equilibrium constant k_8/k_7 using the same equation.[7,8] In an Ordered Bi-Bi mechanism, it may be expected that the binding energies for coenzymes to enzyme are independent of the nature of substrates. Table I shows that this indeed is true in most cases. The maximal difference in the binding energies for NAD^+ with widely different substrates is less then 3.7 kJ mol^{-1}, and for NADH less than 2.3 kJ mol^{-1}.

TABLE I. Binding energies for coenzymes operating with different substrates (collected at pH 7.0 and 25 °C, and calculated from the literature[1])

Alcohol	$\Delta G°'$[a] / kJ mol^{-1}	Aldehyde	$\Delta G°'$[b] / kJ mol^{-1}
Ethanol	19.91	Acetaldehyde	28.00
Propan-1-ol	20.72	Butyraldehyde	29.44
Butan-1-ol	21.67	Acetone	27.16
Propan-2-ol	19.54	Butan-2-one	27.51
Butan-2-ol	19.42	DACA[c]	29.23
Allyl alcohol	18.61		
Ethylene glycol	17.91		

[a]Values of $\Delta G°'$ for the binding of NAD^+ calculated from the relationship: $\Delta G°' = -RT \ln (k_1/k_2)$; [b]values of $\Delta G°'$ for the binding of NADH calculated from the relationship: $\Delta G°' = -RT \ln (k_8/k_7)$; [c]dimethylamino-cinnamaldehyde

pH-Dependence of the binding energies for the coenzymes

The binding energies for the coenzymes, NAD^+ and NADH, were calculated for the oxidation of propan-1-ol with the oxidized coenzyme.[9] The binding ener-

gies for NAD^+ were calculated from the equilibrium constant k_1/k_2 (in Scheme 1) with the aid of Eq. (2) (Fig. 1, bottom). The binding energies for NADH were calculated from the equilibrium constant k_8/k_7, again with the aid of Eq. (2) (Fig. 1, top). It is obvious from Fig. 1 that the equilibrium binding energy for NADH changes linearly with pH, with a slope of 2.25 kJ mol^{-1} per pH unit.

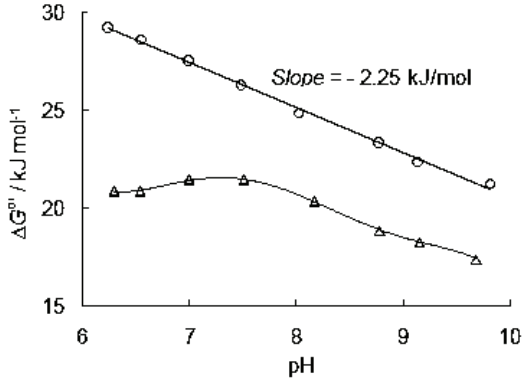

Fig. 1. pH-Dependence of the binding energies for coenzymes. Top: Free energy change for the binding of NADH to the free enzyme. Bottom: Free energy change for the binding of NAD^+ to the free enzyme.

On the other hand, the pH-dependence for the equilibrium binding energy for NAD^+ is a complex function, suggesting that several amino acid side chains on the enzyme participate in the binding of the oxidized coenzyme. In order to analyze this function in detail, the equilibrium constant k_1/k_2 was split into two functions, the second order rate constant k_1, and the first order rate constant k_2. The former was calculated from the initial rate kinetics, from the relationship ln (k_1) = = ln (V_1/K_A), while the latter was calculated from ln (k_2) = ln (k_1) – ln (k_1/k_2).

The pH dependences of the free energy changes associated with both rate constants are shown in Fig. 2. The activation energy, $\Delta G^{\ddagger}$, calculated from k_1

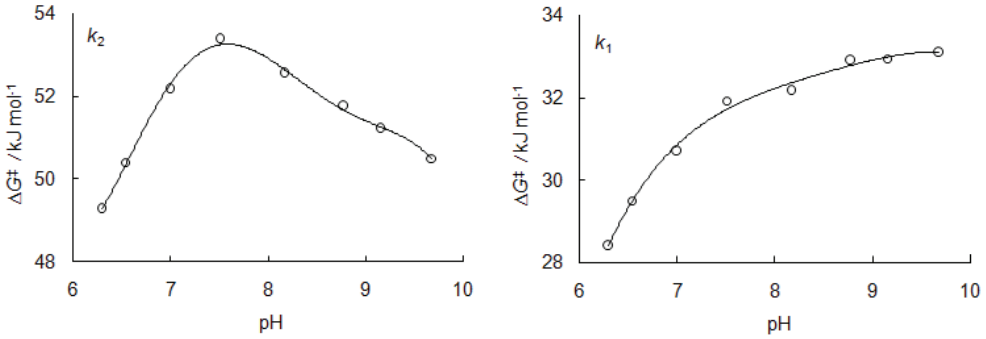

Fig. 2. pH-Dependence of the binding of the oxidized coenzyme. Left: free energy change of activation associated with the rate constant k_2 (s^{-1}) for the dissociation of the enzyme–NAD^+ complex. Right: free energy change of activation associated with the rate constant k_1 (mol^{-1} dm^3 s^{-1}) for the association of NAD^+ with the free enzyme.

(Eq. (3)), follows a complex titration curve governed by the dissociation of at least two amino acid side chains on the protein. The activation energy, $\Delta G^{\ddagger}$, calculated from k_2 (Eq. (3)), also follows a complex titration curve governed by the dissociation of at least two amino acid side chains. Thus, the association of NAD^+ with the free enzyme and dissociation of the enzyme–NAD^+ complex appear to be regulated by the dissociation of 2–4 amino acid side chains on the enzyme.

Temperature dependence of the equilibrium constants for coenzymes

The temperature dependence of the binding energies for the coenzymes was calculated from the initial rate data with the aid of the van't Hoff relationship:

$$\ln K_{eq} = \frac{\Delta S^{\circ}}{R} - \frac{\Delta H^{\circ}}{RT} \quad (9)$$

The K_{eq} values for the k_1/k_2 function were calculated for the oxidation of ethanol and propan-1-ol, while the K_{eq} values for the k_8/k_7 function were calculated only for the reduction of acetaldehyde; both constants may be formally regarded as equilibrium association constants with dimensions mol^{-1} dm^3.

From the straight line in Fig. 3 (bottom), the standard enthalpy, $\Delta H°'$, for the binding of NAD^+ (67.4 kJ mol^{-1}) and the standard entropy, $\Delta S°'$, for the same reaction (158.1 entropy units) can be calculated. Similarly, from the straight line in Fig. 3 (top), the standard enthalpy, $\Delta H°'$, for the binding of NADH (46.1 kJ mol^{-1}), and the standard entropy, $\Delta S°'$, for the same reaction (60.9 entropy units) were calculated.

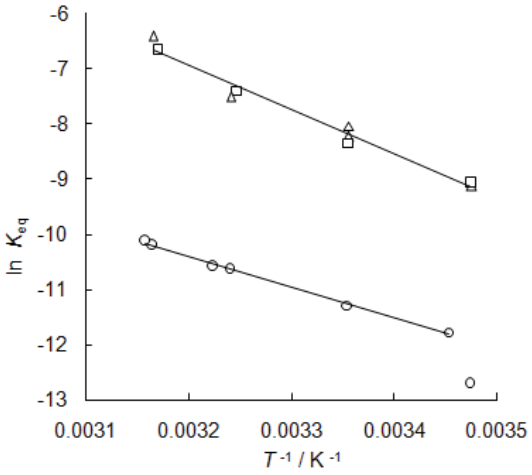

Fig. 3. Temperature dependence of the equilibrium constants for the binding of coenzymes at pH 7.05, calculated from the data of Dickenson and Dickinson.[10,11] Top: binding of NADH to the free enzyme. Bottom: binding of NAD^+ to the free enzyme.

Theoretical data are available in the literature that permit the estimation of the pH-dependence of standard enthalpy of the reaction, $\Delta_r H°'$, and of the standard entropy of the reaction, $\Delta_r S°'$; theoretically, the $\Delta_r H°'$ function is a constant

value for pH 5–9 (45.8 kJ mol^{-1}), while the $\Delta_r S°'$ function increases linearly from 41.1 e.u. at pH 5 to 117.7 e.u. at pH 9.[6] Unfortunately, there are not enough high quality experimental data available for the $\Delta_r H°'$ and $\Delta_r S°'$ values to permit direct comparison between theoretical and experimental results.

Reaction rates in the mechanism of the YADH reaction

The individual rate constants in the overall mechanism of the action of yeast enzyme for the oxidation of ethanol to acetaldehyde were estimated by a combination of the initial rate kinetics and the fitting of the rate constants to the reaction progress curves by appropriate computer fitting programs.[12] The values of these constants and the corresponding changes in the Gibbs free energies are given in Table II.

TABLE II. Thermodynamic properties of yeast alcohol dehydrogenase reaction at pH 7.0 and 25 °C, in the alcohol to aldehyde direction (adapted from the literature[12])

Constant type	Constant	$\Delta G^{\ddagger}$ / kJ mol^{-1}	$\Delta G°'$ / kJ mol^{-1}
Reaction rate	$k_1 = 7\times10^3$ mol^{-1} dm^3 s^{-1}	33.95	–
	$k_2 = 2.1\times10^3$ s^{-1}	54.05	–
Dissociation	$k_2/k_1 = 0.3\times10^3$ mol^{-1} dm^3	–	–20.08
Reaction rate	$k_{31} = 0.39\times10^3$ s^{-1}	58.22	–
	$k_{41} = 2.925\times10^4$ s^{-1}	47.52	–
Dissociation	$k_{41}/k_{31} = 75$	–	10.70
Reaction rate	$k_{32} = 1\times10^3$ mol^{-1} dm^3 s^{-1}	38.77	–
	$k_{42} = 2.11\times10^3$ s^{-1}	54.04	–
Dissociation	$k_{42}/k_{32} = 2.11$ mol^{-1} dm^3	–	–15.26
Reaction rate	$k_9 = 4.0\times10^3$ s^{-1}	52.45	–
	$k_{10} = 3.5\times10^4$ s^{-1}	47.08	–
Dissociation	$k_{10}/k_9 = 8.8$	–	5.37
Reaction rate	$k_5 = 1.09\times10^5$ s^{-1}	49.97	–
	$k_6 = 5\times10^3$ mol^{-1} dm^3 s^{-1}	34.78	–
Dissociation	$k_5/k_6 = 2.2\times10^3$ mol^{-1} dm^3	–	15.18
Reaction rate	$k_7 = 0.39\times10^3$ s^{-1}	58.23	–
	$k_8 = 2.81\times10^4$ mol^{-1} dm^3 s^{-1}	30.51	–
Dissociation	$k_7/k_8 = 14$ mol^{-1} dm^3	–	27.73
			Total: 23.64
	K_{eq}[a] $= 6.8\times10^{-5}$		23.7

[a]Calculated from the steady-state kinetic constants with the aid of the Haldane relationship[7]

From the changes in the standard free energies, a complete energy profile of yeast alcohol dehydrogenase reaction was constructed, which is shown in Fig. 4. There are six forms of enzyme including the free enzyme, with six equilibriums between them. If the complete reaction is followed in the alcohol to aldehyde direction, negative free energy changes are found for the association constant of NAD^+ to free enzyme, E+A $\rightleftarrows$ EA, and for the internal equilibrium *EA +

+ B ⟷ EAB. Positive free energy changes are found for the dissociation constant of the enzyme–NADH complex, EQ ⟷ E+Q, and for the two internal equilibriums, EA ⟷ *EA and EAB ⟷ EPQ. The entire reaction proceeds endothermally in the alcohol to aldehyde direction, with a positive change in the Gibbs free energy of 23.6 kJ mol^{-1}.

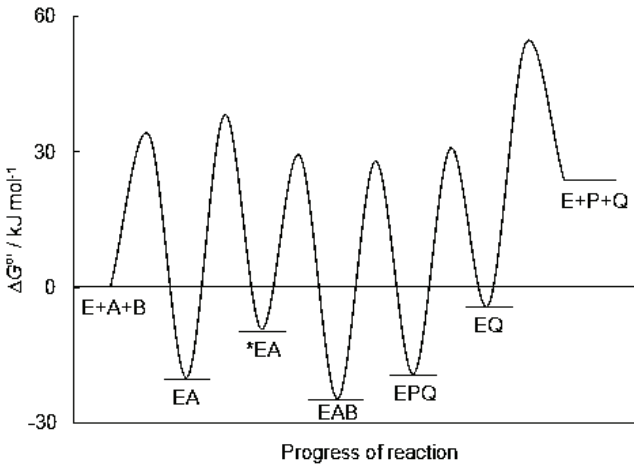

Fig. 4. Thermodynamic energy profile of yeast alcohol dehydrogenase reaction for the oxidation of ethanol to acetaldehyde, at pH 7.0, 25 °C, calculated from the data in Table II.

Binding of oxidized coenzyme to mutant enzymes

The active site of yeast alcohol dehydrogenase is drawn schematically in Fig. 5. The substrate binding pocket is lined with bulky amino acid side chains of Met294, Trp57 and Trp93. A proton relay system is formed by the hydrogen-bonded triad His67···Asp49···Thr84. The pyrophosphate binding region has His47 and Arg369, while the adenine binding pocket is lined with the amino acids Gly224, Phe243, and Ser198.[1]

In the 1990-es, a number of site-directed mutants of yeast alcohol dehydrogenase were constructed, purified, and kinetically characterized in the laboratory of B. V. Plapp.[13–18] The thermodynamic properties of these mutants are summarized in Table III. The standard reaction free energy change for all mutants, $\Delta_r G°'$, differs by less than 10 % from that of the wild type enzyme; this is in accordance with the notion that a catalyst can accelerate a reaction but cannot change its equilibrium. A different situation occurs when the free energy of coenzyme binding is examined. A difference in free energy of binding for both forms of coenzyme between a mutant and a wild type exceeds 50 % when Ser176, Gly183, Asp223, and in the double mutant Asp201 and Gly203 are replaced by another amino acid. This is interesting, since none of these amino acids appears to be directly involved in the binding of coenzymes, except

Asp223; replacement of this amino acid by Gly and the loss of charge, decreases the binding energy by approximately 50 %.

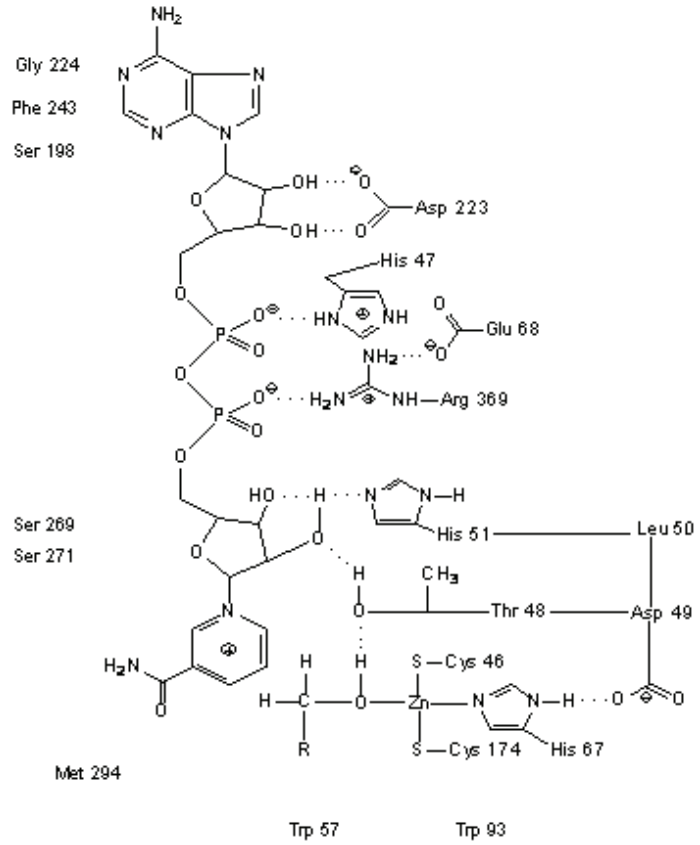

Fig. 5. The active site of yeast alcohol dehydrogenase.
The numeration of the amino acids from the literature.[1]

TABLE III. Thermodynamic properties of mutant enzymes catalyzing the oxidation of ethanol to acetaldehyde, at pH 7.3, 25 °C, calculated from the initial rate kinetic data

No.	Mutant[a]	$\Delta G^{o,b}$ kJ mol^{-1}	$\Delta G^{o,c}$ kJ mol^{-1}	$\Delta_r G^{o,d}$ kJ mol^{-1}	Numeration[e]	Source
1	Wild type	17.34	25.75	20.16	–	13
2	His47Arg	20.47	27.39	18.48	47	14
3	Thr48Ser	16.68	25.31	21.36	48	15
4	Asp49Asn	12.77	20.67	19.96	49	16
5	Trp57Met	14.58	23.99	20.89	57	15
6	Glu68Gln	20.67	25.91	21.68	68	16
7	Trp93Ala	18.70	24.11	—	93	15
8	Ser176Phe	8.78[f]	11.97[f]	18.73	198	17

TABLE III. Continued

No.	Mutant[a]	$\Delta G°'$[b] kJ mol^{-1}	$\Delta G°'$[c] kJ mol^{-1}	$\Delta_r G°'$[d] kJ mol^{-1}	Numeration (as in Fig. 8[e])	Source
9	Gly183Ala	9.55[f]	14.41[f]	18.19	205	17
10	Gly202Ile	13.46	20.29	18.75	224	17
11	Gly203Arg	16.89	27.09	21.28	225	17
12	Asp223Gly	10.255[f]	15.41[f]	19.96	243	18
13	Ser246Ile	15.54	20.67	16.515	269	17
14	Thr48Ser:Trp93Ala	19.96	25.83	18.69	48,93	15
15	Asp201Gly:Gly203Arg	10.255[f]	15.41[f]	17.87	223,225	17

[a]Numeration of amino acids as given by the authors; [b]calculated from the relationship $\Delta G'° = RT\ln(k_1/k_2)$; [c]calculated from the relationship $\Delta G'° = -RT\ln(k_8/k_7)$; [d]calculated from the Haldane relationship; [e]numeration of the amino acids as given in Fig. 5 by Leskovac *et al*;[1] [f]values that are different from the wild type enzyme by more than 50 %

On the other hand, mutation of His47 into Arg does not affect the binding of coenzymes, probably because both amino acids are charged.

CONCLUSIONS

From the evidence summarized in Table I, the ratios of rate constants k_1/k_2 and the rate constants k_8/k_7 may be identified with the equilibrium association constant for the binding of NAD^+ or NADH to the free enzyme, respectively.

From the evidence presented in Figs. 1 and 2, it appears that the association free energy for the binding for NADH to the free enzyme decreases linearly from pH 6–10. On the other hand, the association free energy for the binding for NAD^+ is a complex function, and 2–4 amino acid side chains are involved in the binding of NAD^+. The temperature dependences of the equilibrium constants for the binding of NAD^+ or NADH to the free enzyme are shown in Fig. 3. From the appropriate plots, the enthalpy and entropy for both reactions were calculated.

The energy profile of the entire yeast alcohol dehydrogenase reaction when ethanol is oxidized to acetaldehyde, constructed from the detailed thermodynamic data in Table II, is shown in Fig. 4.

Finally, Table III shows the association free energy for the binding of NAD^+ or NADH to the free enzyme, for 15 single or double mutants of the yeast enzyme, revealing the amino acid side chains important for the binding of the coenzyme.

In conclusion, this communication presents a complete and comprehensive survey of binding data for the enzyme, based only on thermodynamic data. This is the first survey of this kind reported so far in the literature.

Acknowledgement. The Ministry of Science and Technological Development of the Republic of Serbia financially supported this work under Grant No. 142046.

ИЗВОД

ВЕЗИВАЊЕ КОЕНЗИМА НА АЛКОХОЛ-ДЕХИДРОГЕНАЗУ ИЗ КВАСЦА

ВЛАДИМИР ЛЕСКОВАЦ[1], СВЕТЛАНА ТРИВИЋ[2], ДРАГИЊА ПЕРИЧИН[1], МИРА ПОПОВИЋ[2] и ЈУЛИЈАН КАНДРАЧ[3]

[1]Технолошки факултет, [2]Природно-математички факултет и [3]Пољопривредни факултет, Универзитет у Новом Саду, Република Србија

У овом раду је истраживано везивање коензима на алкохол-дехидрогеназу из квасца (EC 1.1.1.1). Главни критеријуми су били промене у стандардним слободним енергијама за поједине реакционе ступњеве, унутрашње константе равнотеже и промена слободне енергије укупне реакције. Израчунавања су спроведена за нативну врсту ензима при pH 6–9, и за 15 врста различитих мутантних ензима, са једном или две мутације, при pH 7,3. Обиље теоријских и експерименталних података омогућило је да се детаљно истражи везивање коензима на ензим.

(Примљено 26. маја, ревидирано 23. јула 2009)

REFERENCES

1. V. Leskovac, S. Trivić, D. Peričin, *FEMS Yeast Res.* **2** (2002) 481
2. L. Stryer, *Biochemistry*, 3rd ed., W. H. Freeman, New York, USA, 1988
3. D. Voet, J. G. Voet, *Biochemistry*, 3rd ed., Wiley, Hoboken, NJ, USA, 2004
4. D. L. Nelson, M. M. Cox, *Principles of biochemistry*, W. H. Freeman, New York, 2005
5. R. A. Alberty, *Thermodynamics of biochemical reactions*, Wiley-Interscience, Hoboken, NJ, 2003
6. R. A. Alberty, *Biochemical thermodynamics*, Wiley-Interscience, Hoboken, NJ, 2006
7. V. Leskovac, *Comprehensive enzyme kinetics*, Kluwer Academic/Plenum Publishers, New York, 2003
8. K. Dalziel, *Acta Chem. Scand.* **17** (1963) 27
9. V. Leskovac, S. Trivić, B. M. Anderson, *Indian J. Biochem. Biophys.* **33** (1996) 177
10. C. J. Dickenson, M. F. Dickinson, *Biochem. J.* **147** (1975) 303
11. C. J. Dickenson, M. F. Dickinson, *Biochem. J.* **147** (1975) 541
12. V. Leskovac, S. Trivić, D. Peričin, *J. Serb. Chem. Soc.* **68** (2003) 77
13. A. J. Ganzhorn, D. W. Green, A. D. Hershey, R. M. Gould, B. V. Plapp, *J. Biol. Chem.* **262** (1987) 3754
14. R. M. Gould, B. V. Plapp, *Biochemistry* **29** (1990) 5463
15. D. W. Green, H.-W. Sun, B. V. Plapp, *J. Biol. Chem.* **268** (1993) 7792
16. A. J. Ganzhorn, B. V. Plapp, *J. Biol. Chem.* **263** (1988) 5446
17. F. Fan, B. V. Plapp, *Arch. Biochem. Biophys.* **367 (**1999) 240
18. F. Fan, J. A. Lorenzen, B. V. Plapp, *Biochemistry* **30** (1991) 6397.

Journal of the Serbian Chemical Society
JSCS@tmf.bg.ac.rs • www.shd.org.rs/JSCS
J. Serb. Chem. Soc. 75 (2) 195–207 (2010) UDC 677.1/.5:677.017.4:541.12.03:547.455.65
JSCS–3952 *Original scientific paper*

The effects of commercial fibres on frozen bread dough

JELENA FILIPOVIĆ[1]*, NADA FILIPOVIĆ[2] and VLADIMIR FILIPOVIĆ[3]

[1]*Institute for Food Technology, Bul. Cara Lazara 1, 21000 Novi Sad,* [2]*Faculty of Technology, University of Novi Sad, Bul Cara Lazara 1, 21000 Novi Sad and* [3]*Mlinpek Institute, Bul. Oslobodjenja 66b, Novi Sad, Serbia*

(Received 25 May, revised 26 August 2009)

Abstract: The daily intake of dietary fibres in highly industrialized countries is at a low level and, therefore, adversely affecting human health. The objective of this research was to analyze the influence of different commercial fibres (originating from sugar beet pulp fibrex, and Jerusalem artichoke inulin HPX and GR) in yeast dough at a level of 5 %, on the rheological properties of dough and the quality of bread during frozen storage. Frozen dough characteristics were determined using a Brabender maturograph and test baking was followed according the AACC procedure. The dough was frozen at –18 °C and stored over a period of 60 days. The results concerning the dough (proving time and stability) and bread quality (volume and crumb quality) were statistically analyzed by multivariance Manova and discriminative analysis, which indicated that there was a significant difference between dough without fibres and dough with different fibres (fibrex, inulin HPX and GR). The discrimination coefficient points that the greatest influence of fibres on the final proof and proving stability is after 30 days (6.250) and after 0 days (6.158), respectively, but the greatest influence of fibres on bread volume and bread crumb quality (15.488 and 3.638, respectively) can be expected on non frozen dough, due to above mention their adverse the effect on gluten network.

Keywords: fibrex; inulin; frozen dough; bread quality.

INTRODUCTION

Bread has always been one of the most popular and appealing food products due to its superior nutritional, sensorial and textural characteristics. Bakery products, particularly bread, take a significant share in the food guide pyramid for daily food choices recommended by US Department of Health and Human Services,[1–3] and therefore can be a convenient food for adjusting the daily food intake according to specific needs. Dietary fibres in bread are a versatile functional food ingredients giving many benefits to human health [4–6] and playing a

* Corresponding author. E-mail: jelena.filipovic@fins.uns.ac.rs
doi: 10.2298/JSC1002195F

very important role in the human diet, helping in solving some digestive problems and also positively contributing to a long list of non infectious diseases.[3,7,8] The social and scientific modernization for the development of alternative or novel methods for the production and preservation of bakery products is freezing.[9]

Fresh bread is a product with a short shelf life and during its storage, a number of chemical and physical alterations occur, known as staling. Due to these changes, its freshness and crispiness deteriorate while crumb firmness and rigidity increase. Over the past few years, the bakery industry has exploited the advantages of freezing technology.[9,10] It is well recognized that temperature affects the performance of dough and yeast during preparation.[10] Frozen bakery products are expected to be characterized by quick preparation time and affordable price. They look and taste as if they were freshly and homemade.[5]

In frozen dough preparation, when prolonged frozen storage intervenes between dough formation and bread baking, many factors contribute to a deterioration of the products and adversely influence dough behaviour during freezing and thawing, resulting in the loss of consumer acceptability for bakery products.[5,6,11] In the technology of frozen dough, the main problem is damage to the gluten network due to crystallization and recrystallization of water, which results in loss of bread quality.[12,13] It has been shown that the influence of fibre characteristics on yeast activity and bread quality during 30 days freezing was beneficial.[14] The possibility of mathematical interpretation of commercial fibres on yeast dough during frozen storage is of particular interest both for those involved in frozen dough preparation and in thawing and baking and could positively contribute to a better quality of the final products. There are not many reports on the effects of different fibres incorporated into frozen yeast dough.

Objective of this paper is to present an analysis of the influence of three commercial fibres (fibrex, inulin HPX and GR) at a level of 5 % on dough rheology and the quality of bread during the freezing process. Regarding the mathematical analysis, this information is required either for the successful incorporation of different fibres types and/or an analysis of the effects of fibres on frozen dough to enable the production of consumer-acceptable, fibre-enriched bakery products.

EXPERIMENTAL

Material

For commercial bread production, white flour from a local industrial mill (moisture, ash and protein contents were 13.5, 0.45 and 11.2 % d.d., respectively), salt and compressed yeast were used. Fibrex with a particle size of less than 150 μm was a commercial product originnating from sugar-beet and produced by Denisco Sugar AB; while Inulin HPX and inulin GR fine, white powders characterized by an average degree of polymerization of more than 10 sugar units and 2 to 5 sugar units, respectively, were commercial products made from the root of Jerusalem artichoke and produced by “Orafti Active Food Ingredients”, Belgium.

Dough preparation

Dough samples were prepared in a Farinograph bowl at a temperature of 30 °C according to the following dough formula: flour (100–95 %), fibres (fibrex, inulin HPX or inulin GR) (0–5 %), salt (2 %) and yeast (2.5 %). Water was added according to the Farinograph absorption, *i.e.*, to 500 BU: no fibres (60.4 %), fibrex 5 and 10 % (68.0 %), inulin HPX 5 % (56.6 %) and inulin GR 5 and 10 % (52.3 %). Round shaped dough, weighing 150 g, with or without 5 % of different fibres, was placed in a freezing chamber (Koma, Koeltechnishe Industrie, B.V., The Netherlands) at a temperature of –18 °C. After freezing, the samples were packed in PVC bags and stored at –18 °C for 0, 1, 30 and 60 days. After the required freezing period, dough pieces were kept for 2 h at ambient temperature and then placed in a maturograph fermentation chamber at 30±1 °C.

Dough characteristics

The rheological properties of the frozen and non-frozen dough during fermentation were determined in a Maturograf (Brabender, Duisburg, Germany). The procedure is not standardized, usually it is adjusted to bread making procedures.[15] The constituents and preparation of the dough for Maturograf determination were the same as those described for dough preparation. The Maturograph measures the behaviour of yeast dough during the final proofing under constant conditions, (temperature 30±1°C and relative humidity 80–85 %). After thawing (2 h), a dough piece was placed in the dough container under a stamp weighing 150 g. Depending on the dough's gas production, gas retention and elasticity characteristics, the pressure stamp is raised progressively to certain levels giving information about fermentation and dough handling.

Baking test

AACC Baking test (method 10-09.01) was applied to eliminate as much as possible the human element introduced by the operator. Dough or a dough piece after thawing was moulded by hand. The dough loaf was placed seam down in a greased tall baking form pan (length, 10.5 cm, width, 6.0 cm, bottom length, 9.3 cm). The end of proof was determined according to the Maturograph data. The dough constituents were the same as those used for dough preparation. The bread was baked for approximately 15 min in a Chopin laboratory oven at 260 °C, until the mass of baked bread ranged between 135 and 137 g. The quality of the bread was scored 24 h after baking. Bread volume and crumb quality was evaluated by five trained panellists. The bread volume was determined by the seed displacement method. Crumb grain is defined as the cell structure exposed when a loaf of bread is sliced. The best score is characterized by relatively large cells with thin walls (score 2.5), whereas a close grain consisting of small cells with thick walls has the worst score (0). Crumb elasticity is determined entirely by the sense of touch. The fingers are pressed lightly against the cut surface of a loaf and scored, the best being 4.5 and the worst 0. Crumb quality number is the sum of the scores for crumb grain and crumb elasticity, the maximum grade is 7 and minimum 0.[15]

Statistical analysis

All samples were prepared and analyzed in total 6 times and the average result is reported.

The results concerning dough (proofing time and stability) and bread quality (volume and crumb quality) were statistically tested by analysis of multivariance Manova and discriminative tested. ANOVA functions and Roy test with 0.05 significance level were used as the univariant statistical procedures to assess significant differences among the means.[16]

RESULTS AND DISCUSSION

Mathematical analysis of effect of fibres on behaviour of frozen dough at final proof

It has been claimed that freezing adversely affects the protein matrix and yeast viability.[6,7] Good dough handling is beneficial in the bread making process, positively contributing to an improved gas-retention capacity. Therefore, dough behaviour at the final proof is presented by the proof duration and proofing stability, (Table I). The mean value and standard deviation show that the duration of the final proof depends on the sample in respect to the type, *i.e.*, on the type of fibres and the length of storage at low temperatures. Keeping dough with inulin HPX under frozen conditions for a longer period, from 30 to 60 days, leads to a decrease in the duration of the final proof. According to the statistical data, the sample with inulin HPX differed significantly from the other samples. The final proof of the dough with inulin HPX and GR was shorter than that with fibrex (Table I, Figs. 1 and 2). These data may indicate that inulin either HPX or GR positively contribute to preserving the yeast fermentative activity during freezing, contrary to fibrex. The longest final proof time of the dough with fibrex can be negatively connected with the great ability of absorbing water from fibrex (68 %), resulting in the inability of the gluten to take water and forcing the baker to add more water to the dough with fibrex.

TABLE I. Effect of fibres on dough properties during freezing

Time, days	Final proofing time, min				Proofing stability, min			
	Mean value	Confidence interval		p[a]	Mean value	Confidence interval		p[a]
0 % Fibres								
0	82±1.5[a]	80.75	83.91	0.833	15±2.4[a]	12.8	17.9	0.956
1	110±4.6	105.2	114.8	0.996	5±2.4[a]	2.79	7.88	0.956
30	128±2.8[a]	125.0	131.0	0.996	2±1.5	0.750	3.91	0.833
60	68±20	46.55	89.45	0.996	7±2.1[a]	4.80	9.20	0.988
5 % Fibrex								
0	82±3.7[a]	78.76	86.57	0.626	7±2.3[a]	5.21	10.1	0.998
1	127±3.2[a]	124.3	131.0	0.959	2±1.3	0.670	3.33	0.518
30	132±10[a]	121.4	143.2	0.943	5±2.8	2.11	7.89	0.976
60	133±9.5[a]	123.0	143.0	0.518	3±1.1[a]	1.85	4.15	0.573
5 % Inulin HPX								
0	81±3.4	78.05	85.28	1.00	4±1.0	3.58	5.75	0.272
1	112±4.1	108.3	117.0	0.964	8±5.4[a]	2.37	13.6	0.968
30	98±1.5	96.75	99.91	0.833	1±1.1	–0.150	2.15	0.573
60	45±6.5	38.13	51.87	0.996	6±1.5	4.75	7.91	0.833
5 % Inulin GR								
0	85±3.2[a]	82.30	89.03	0.959	9±2.9[a]	6.58	12.8	0.946
1	115±3.4[a]	112.0	119.3	1.00	5±3.0[a]	1.69	7.98	0.750
30	121±1.6	119.6	123.0	0.682	1±1.6	–0.380	3.05	0.682
60	67±1.7	65.24	68.76	0.754	9±3.7[a]	5.82	13.5	0.993

[a]p-Test of conclusion

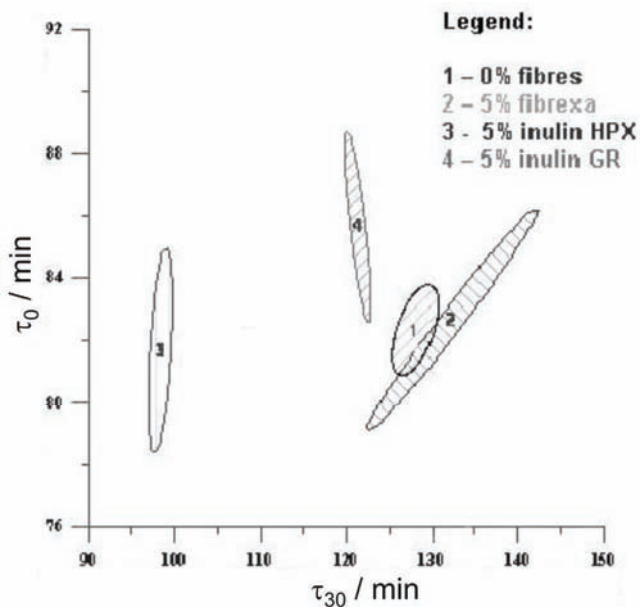

Fig. 1. Trust interval of the final proof of dough with fibres frozen for 0 day (τ_0) and 30 days (τ_{30}).

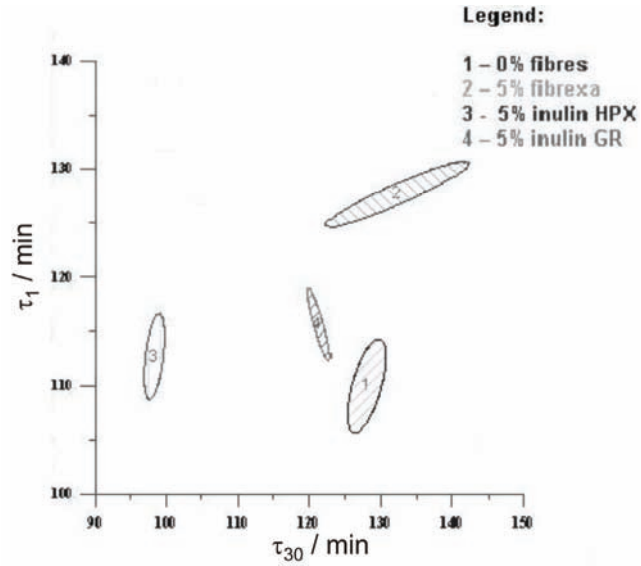

Fig. 2. Trust interval of the final proof of dough with fibres frozen for 1 day (τ_1) and 30 days (τ_{30}).

The influence of different fibres on the behaviour of dough at the final proof fermentation was analyzed by the multivariant procedure and discriminative analysis (Tables II and III).[16] The Manova test showed that there was a significant difference in the effect of different fibres on the dough properties during frozen

storage (0, 1, 30 and 60 days) since $p = 0.000$, and the alternative hypothesis that there was a significant difference in the effect of the fibre type on the observed parameters during freezing was confirmed by the Roy test, since $p < 1$ (Table II). In non-frozen dough, the fibres do not have a significant influence on the final proof since $p > 1$, while the fibres have a far greater influence on the dough properties during freezing for 1, 30 and 60 days since $p < 1$ (Table II). The discrimination coefficient indicates that the greatest influence of fibres on the final proof and proofing stability was after 30 days (6.250) and after 0 days (6.158), respectively (Table IV).

TABLE II. Statistical analysis of the effects of fibres on the final fermentation on freezing of dough with fibres (F – Fisher test, p – confidence of the test)

Test	τ / days	Final proofing time, min		Proofing stability, min	
		F	p	F	p
Manova	4	20.0	0.0	10.6	0.0
Roy test	0	1.97	0.15	23.0	0.0
	1	24.3	0.0	3.21	0.04
	30	45.5	0.0	5.74	0.005
	60	62.6	0.0	8.46	0.001

TABLE III. Discriminative analysis of the effects of fibres on the final proof of frozen dough with fibres (Fisher test; $p = 0.0$ (confidence of the test))

τ / days	Final proofing time, min	Proofing stability, min
4	25.1	11.4

TABLE IV. Discriminative analysis of the effects of fibres on the final proof of frozen dough with fibres

τ / days	Final proofing time, min	Proofing stability, min
0	4.77	6.16
1	3.88	3.07
30	6.25	1.39
60	3.19	2.24

Based on the overall statistical calculation of discriminative analysis it can be stated that fibrex and inulin HPX affect the final proof after 1 day. The largest homogeneity is 100 % (Table V) indicating that the influence of these fibres is constant and uniform and depends on the fibre characteristics, *i.e.*, on their interaction with the gluten network. On the contrary, inulin GR showed different characteristics.

The discriminative analyses the presented date proved that fibres affect the final proof mostly at the beginning of freezing. Later, some interactions between the fibres and other dough constituents, such as ice crystals and yeast cells, also contributed to the quality of frozen dough during freezing.

TABLE V. Characteristics and contribution of the fibre characteristics to the final proof after freezing of the dough (how many samples differ from related value)

	Final proofing time, min					Proofing stability, min				
τ / days	0 % Fibres	5 % Fibrex	5 % Inulin HPX	5 % Inulin GR	Contribution %	0 % Fibres	5 % Fibrex	5 % Inulin HPX	5 % Inulin GR	Contribution %
0	Lower	Higher	The lowest	The highest	26.5	The highest	Lower	The lowest	Higher	47.6
1	The lowest	The highest	Lower	Higher	21.5	Higher	The lowest	The highest	Lower	25.3
30	Higher	The highest	The lowest	Lower	34.7	Higher	The highest	The lowest	Lower	2.00
60	Higher	The highest	The lowest	Lower	17.4	Higher	The lowest	Lower	The highest	25.1
Homogeneity %	100	100	100	66.7	–	100	100	83.3	66.7	–

Statistical analysis from Table I prove that the type of the fibres and the length of freezing have an influence on the dough characteristics and that the dough with fibrex had the shortest proof stability during freezing for 1, 30, 60 days, particularly concerning both types of inulin. The greatest influence of fibres on the stability of fermentation was after 0 days of frozen storage (Table IV), because the fibres were not well incorporated into the gluten structure and had a negative effect on the gluten matrix, which was also confirmed by the fibre contribution, which was 47 %, Table V. The dough with inulin HPX and GR had homogeneities of 83.3 and 66.7 %, respectively, which are not stable proofing stabilities (Table V).

Mathematical analysis of the effect of fibres on the quality of bread made of frozen dough

The effect dough freezing on bread quality was assessed through the bread volume and crumb quality, Table VI. The mean value and standard deviation showed that the bread volume depended on the type of the sample, *i.e.*, on the type of incorporated fibre and the length of the low temperature storage.

The effect of the different fibres on the baking properties of bread made from frozen dough was analyzed by the multivariate procedure and discriminative analysis (Tables VII and VIII).[16] Differences in the effect of the fibres on the behaviour of dough after freezing (0, 1, 30 and 60 days) were examined by the Manova procedure. The Manova test (Table VII) showed that there was a significant difference between the effects of the studied fibres since $p = 0.0$. The alternative hypothesis that there is a significant difference in effect of fibres on observed parameter during frozen storage is tested by the Roy test. It was shown that during 1 and 30 days of freezing, the fibres did not have a significant in-

fluence on the bread quality since $p > 1$, while the fibres had a far greater influence on the bread volume and bread crumb quality after frozen storage for 30 and 60 days since $p < 1$ (Table VII). The discrimination coefficient proved that the greatest influence of the fibres on bread volume and breadcrumb quality (15.488 and 3.638) can be expected with non-frozen dough (Table IX), due to their above-mentioned adverse the effect on the gluten network.

TABLE VI. Effect of fibres on the baking properties of bread after freezing (p – test of conclusion)

τ / days	Bread volume, ml				Bread crumb quality[a]		
	Mean value	Confidence region		p	Mean value	Confidence region	
			0 % Fibres				
0	392±15.5[a]	376.2	408.8	0.996	6.4±0.2	6.11	6.59
1	340±35.2[a]	303.7	377.6	0.999	6.4±0.4	5.92	6.80
30	297±19.9[a]	276.6	318.4	0.996	5.2±1.3	3.92	6.58
60	287±15.8[a]	270.9	304.1	0.996	4.6±0.3	4.31	4.99
			5 % Fibrex				
0	257±39.1	216.5	298.7	0.996	5.2±1.3	3.93	6.57
1	292±32.9	258.0	327.0	0.996	5.7±0.9	4.75	6.65
30	245±15.8	228.4	261.6	0.996	5.3±1.0	4.20	6.40
60	277±43.5	231.8	323.2	0.953	4.9±1.0	3.92	6.04
			5 % Inulin HPX				
0	407±5.2[a]	401.6	412.4	0.996	6.9±0.1	6.83	7.00
1	363±4.5[a]	359.1	368.5	0.883	6.9±0.1	6.79	7.01
30	312±6.4[a]	305.5	319.1	0.996	6.3±0.5[a]	5.78	6.82
60	256±6.7[a]	249.7	263.8	0.998	6.6±0.3[a]	6.27	6.93
			5% Inulin GR				
0	366±4.0[a]	362.5	370.9	0.996	4.5±0.1	4.35	4.65
1	325±3.9	320.9	329.1	0.996	5.1±0.7	4.36	5.84
30	280±5.6	274.1	285.9	0.996	5.0±1.0[a]	3.98	6.10
60	233±4.2	228.6	237.4	0.943	2.9±0.5	2.42	3.38

[a]Bread crumb quality; maximum 7.0, minimum 0

TABLE VII. Statistical analysis of the effects of fibres on the properties of bread made from frozen dough (F – Fisher test, p – confidence of the test)

Method	Bread volume, ml			Bread crumb quality[a]		
	τ / days	F	p	τ / days	F	p
Manova	4	12.395	0.000	4	5.867	0.000
Anova	0	60.488	0.000	0 day	21.000	0.000
	1	9.106	0.001	1 day	1.481	0.249
	30	28.013	0.000	30 day	0.875	0.470
	60	6.336	0.003	60 day	11.173	0.000

[a]Maximum 7.0, minimum 0

TABLE VIII. Discriminative analysis of the effect of fibres on the properties of bread made from frozen dough (Fisher test, $p = 0.0$ (confidence of the test))

τ / days	Bread volume, ml	Bread crumb quality[a]
4	26.5	6.83

[a]Bread crumb quality; maximum 7.0, minimum 0

TABLE IX. Difference in the influence of the fibre types on the bread properties

τ / days	Bread volume, ml	Bread crumb quality[a]
0	15.5	3.64
1	0.641	0.271
30	8.18	1.36
60	8.23	1.12

[a]Bread crumb quality; maximum 7.0, minimum 0

The dough with incorporated inulin HPX had the greatest volume and differed significantly from other samples (Table VI and X) during the first 30 days of freezing, Figs. 3 and 4. The adverse influence of fibrex on the gluten structure found by Wang *et al.*[3] was confirmed in this study as the lowest bread volume was registered when dough containing these fibres was kept at low temperatures for the first 30 days of frozen storage. However, after 60 days, the beneficial effect of fibrex on the yeast activity positively contributed to the bread volume. As it was stated concerning the final proof data, inulin HPX was better incorporated into the gluten matrix, thus contributing the best to the bread volume as opposed to other types of fibres, with which dominating influence on the bread volume was the length of frozen storage. Dough with incorporated inulin GR had the lowest volume after 60 days of frozen storage (Table VI and X), as these fibres act as an inclusion element thus contributing to structure deterioration and poor volume.[18]

In period of 60 days of frozen storage, inulin HPX also positively contributed to the bread volume and crumb quality (Tables VI and X). The bread was evaluated with excellent grades, 6.3 to 6.9 out of a maximum of 7. Dough containing fibrex was evaluated as having the same quality regardless of the duration of the freezing period. Concerning fibrex and inulin HPX, the crumb quality remained constant regardless of the duration of frozen storage, contrary to samples without fibres or with inulin GR fibres. Bread with inulin GR was graded as good and attributed with the highest homogeneity. The protective effects of fibrex and inulin HPX against the adverse influence of low temperatures on dough was proved by the relatively uniform breadcrumb scores, particularly the high scores for inulin HPX was proved by the highest homogeneity (Table X). The greatest fibre contribution was registered by the bread volume and crumb quality numbers of 47.9 and 56.9 %, respectively, with non-frozen dough (Table X).

TABLE X. Characteristics and effects of the fibre characteristics on the baking properties of bread made from frozen dough (how many samples differ from related value)

	Bread volume, ml					Bread crumb quality[a]				
τ / days	0 % Fibres	5 % Fibrex	5 % Inulin HPX	5 % Inulin GR	Contri-bution %	0 % Fibres	5 % Fibrex	5 % Inulin HPX	5 % Inulin GR	Contri-bution %
0	Higher	The lowest	The highest	Lower	47.9	–	–	–	Good	56.9
1	Higher	The lowest	The highest	Lower	10.8	–	–	–	–	4.24
30	Higher	The lowest	The highest	Lower	17.4	Good	Good	Excel-lent	Good	21.3
60	The highest	Higher	Lower	The lowest	23.9	–	–	Excel-lent	–	17.5
Homo-geneity %	100	100	100	100	–	83.3	66.7	100	100	–

[a]Maximum 7.0, minimum 0

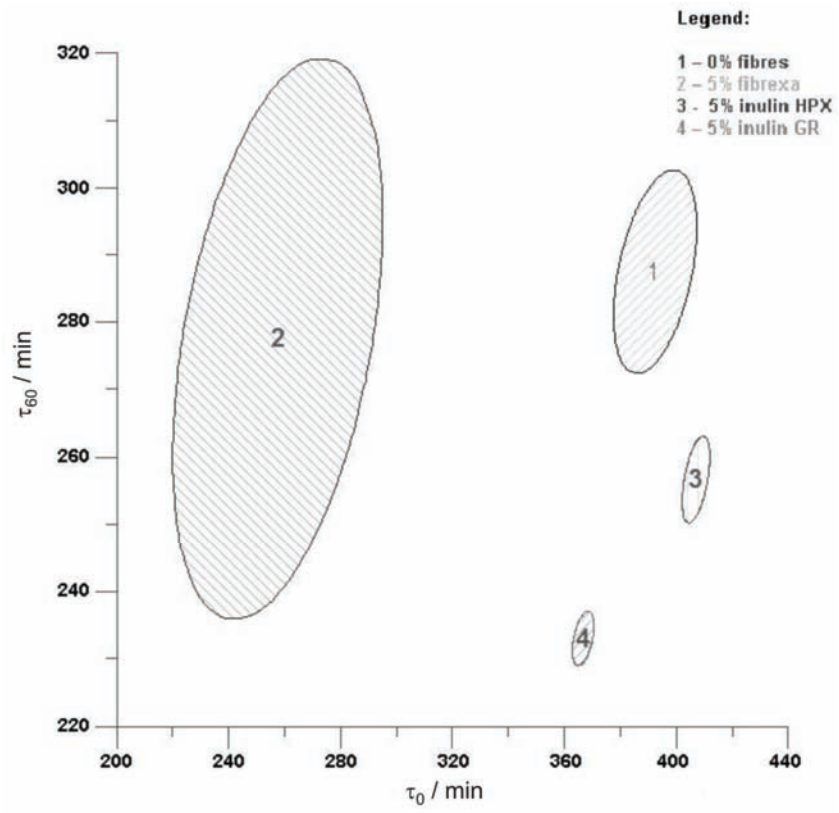

Fig. 3. Trust interval of bread volume with fibres after 0 (τ_0) and 60 (τ_{60}) days of frozen storage.

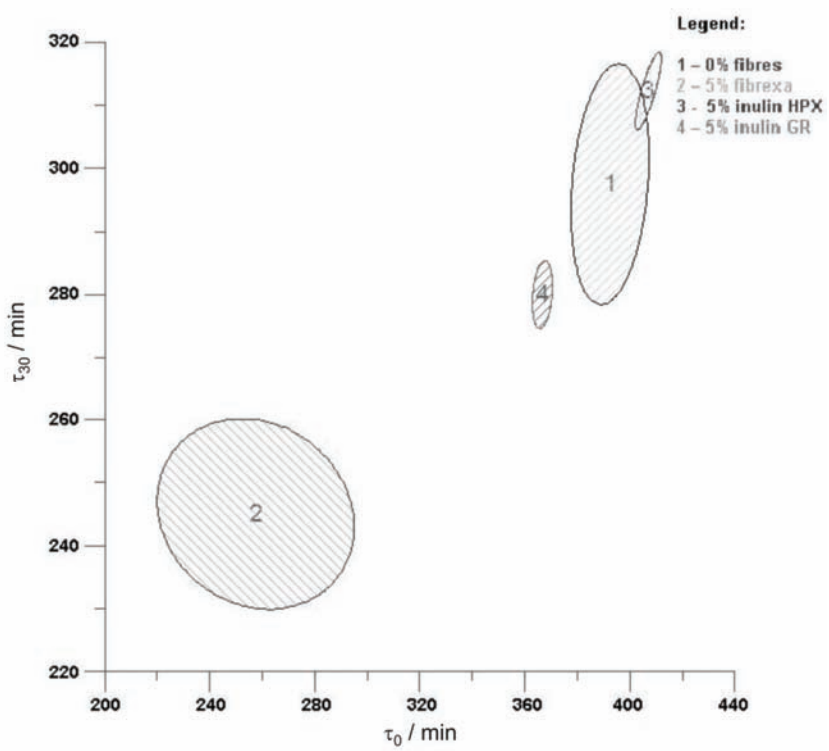

Fig. 4. Trust interval of bread volume with fibres after 0 (τ_0) and 30 (τ_{30}) days of frozen storage.

This indicates to the positive effects of HPX fibres on decreasing the negative effects of freezing. Inulin HPX was incorporated the best into the gluten matrix; hence, the resulting bread had the largest volume (Table VI). The volumes of the other breads with different types of fibres depended on the length of frozen storage, because ice crystals interfere with the gluten structure, which consequently decreases the volume of the bread (Table VI).

CONCLUSIONS

Statistical interpretation of the data proved that the fibre type and storage period influence the characteristics of dough and bread; at the beginning, the fibre characteristics exhibit a dominating adverse effect on the gluten network, but later, their interactions with other dough constituents positively contribute to dough and bread quality.

Multivariate and discriminative analyses indicated that there was a significant difference between the dough rheology without fibres and dough with three types of fibres (fibrex, inulin HPX and GR).

The discrimination coefficient proved that the highest effect of fibres was on the final proof after 30 days of freezing (6.250) and on the proofing stability of non-frozen (fresh) dough (6.16), while the effect of the fibres on the bread volume and crumb quality were the greatest in non-frozen (fresh) dough (15.5 and 3.64, respectively).

The statistical date proved that the long chains of inulin HPX were incurporate well into the gluten matrix and probably protected the yeast cells from the ice formed during freezing for 1, 30 and 60 days; hence, bread with the largest volume was obtained. The protective role of inulin HPX can be seen in the well--preserved quality of the final product after 60 days of frozen storage of the dough and the quality was the same as bread made of non-frozen dough without fibres.

The inulin GR fibres were incorporated into the gluten structure contributing to a deterioration of the gluten structure, which resulted in a diminution of the properties of the frozen dough, which in turn had an adverse effect on the bread volume and crumb quality.

The results from all sample highlighted the complex role of fibres in frozen dough.

Acknowledgement. These results are part of a project supported by the Ministry of Science and Technological Development of the Republic of Serbia, TR 20068.

ИЗВОД

УТИЦАЈА ВЛАКАНА НА ОСОБИНЕ ЗАМРЗНУТОГ ТЕСТА И КВАЛИТЕТ ХЛЕБА

ЈЕЛЕНА ФИЛИПОВИЋ[1], НАДА ФИЛИПОВИЋ[2] и ВЛАДИМИР ФИЛИПОВИЋ[3]

[1]Институт за прехрамбене технологије, Бул. цара Лазара 1, 21000 Нови Сад, [2]Технолошки факултет, Универзитет у Новом Саду, Бул цара Лазара 1, 21000 Нови Сад и [3]Млинпек Завод, Бул. Ослобођења 66б, Нови Сад

У високоразвијеним земљама запажен је смањени дневни унос прехрамбених влакана које позитивно утичу на људско здравље. Циљ овог истраживања је анализа утицаја 5 % различитих врста влакана (Fibrex, комерцијални производ из влакна шећерне репе и инулин HPX велике и инулин GR мале молекулске масе пореклом из артичоке) на квалитет теста, при чему су праћене реолошке особине замрзнутог теста и квалитет хлеба са влакнима. Реолошке особине теста са влакнима праћене су на Брабендеровом матурограму, а хлеб је печен по стандардној AACC методи. Тесто је замрзавано на –18 °C и чувано 60 дана. Реолошке особине теста са влакнима (дужина завршне ферментације и стабилитет ферментације) и квалитет хлеба са влакнима (запремина и вредносни број средине) су статисички тестирани мултиваријаном методом Manova и дискриминативном анализом, при чему је доказано да постоји значајна разлика између теста без влакана и теста са различитом врстом влакана. Коефицијент дискриминације је показао да је највећи утицај влакана на завршну ферментацију је после 30 дана чувања (6,25) а на стабилитет ферментације (6,16) и квалитет хлеба (запремина хлеба 15,5 и вредносни број средине 3,64) код незамрзнутог теста.

(Примљено 25. маја, ревидирано 26. августа 2009)

REFERENCES

1. H. Goesaert, K. Brijs, W. S. Veraverbeke, C. M. Courtin, K. Gebruers, J. A. Delcour, *Trends Food Sci. Tech.* **16** (2005) 12
2. A. Sangnark, A. Noomhorm, *Lebensmittel-Wissenschaft und Technologie* **37** (2004) 697
3. J. Wang, C. M. Rosell, C. B. Barber, *Food Chem.* **79** (2002) 221
4. A. Angioloni, C. Collar**,** *Food Hydrocolloids* **23** (2009) 742
5. P. Ribotta, A. León, M. C. Añón, *J. Agr. Food Chem.* **49** (2001) 913
6. P. D. Ribotta, A. E. León, M. C. Añón, *Food Res. Int.* **36** (2003) 357
7. C. S. Brennan, C. M. Tudorica, *Int. J. Food Sci. Tech.* **43** (2008) 215
8. Y. Pomeranz, *Chemical composition of kernel structures in wheat: chemistry and technology*, Vol. 97, AACC, St. Paul, MN, 1988
9. M. Bhattachary, T. M. Langstaff, W. A. Berzonsky, *Food Res. Int.* **36** (2003) 365
10. Y. Jinhee, L. William, J. Johnson, *J. Food. Sci.* **74** (2009) 278
11. Y. Phimolsirilpol, U. Siripatrawan, V. Tulyatham, D. J Cleland, *J. Food Eng.* **84** (2008) 48
12. R. Sharadayt, K. Khan, *Cereal Chem.* **80** (2003) 764
13. S. Natio, S. Fukami, Y. Mizokami, N. Ishida, H. Takano, M. Koizumi. *Cereal Chem.* **81** (2004) 80
14. J. Filipović, S. Popov, N. Filipović**,** *CI&CEQ* **14** (2008) 257
15. G. Kaluđerski, N. Filipović, *Methods of testing the quality of grain, flour and finished products*, Faculty of Technology, Novi Sad, 1998 (in Serbian)
16. T. W. Anderson, *An introduction to multivariate statistical analysis*, 2nd ed., John Wiley & Sons, San Francisco, CA, 1984
17. R. Wang, W. Zhou, H.-H. Yu, W.-F. Chow, *J. Sci. Food Agr.* **86** (2006) 85
18. A. Nelson, *High-fiber ingredients*, AACC, St. Paul, MN, 2001, p.p. 29–44.

Journal of the Serbian Chemical Society
JSCS@tmf.bg.ac.rs • www.shd.org.rs/JSCS
J. Serb. Chem. Soc. *75* (2) 209–215 (2010)
JSCS–3953
UDC 582.912.42+582.937.4:665.5+581.19
Original scientific paper

Chemical composition of *Rhododendron aureum* (gold rosebay) essential oil from Pribaikal'e (Russian Federation)

DANIIL N. OLENNIKOV[1]*, LUBOV' V. DUDAREVA[2], SEMION N. OSIPENKO[3] and TAT'YANA A. PENZINA[4]

[1]*Laboratory of Medical and Biological Research, Department of Biologically Active Substances, Institute of General and Experimental Biology, Siberian Division, Russian Academy of Sciences, Sakh'yanovoi st., 6, 670047, Ulan-Ude,* [2]*Laboratory of Physico-chemical Research Methods, Siberian Institute of Plant Physiology and Biochemistry, Siberian Division, Russian Academy of Sciences, Lermontova st., 132, 664033, Irkutsk-33,* [3]*Laboratory of Plant Physiological Genetics, Siberian Institute of Plant Physiology and Biochemistry, Siberian Division, Russian Academy of Sciences, Lermontova st., 132, 664033, Irkutsk-33 and* [4]*Greenhouse group, Siberian Institute of Plant Physiology and Biochemistry, Siberian Division, Russian Academy of Sciences, Lermontova st., 132, 664033, Irkutsk-33, Russian Federation*

(Received 3 June, revised 21 July 2009)

Abstract: The essential oils from five samples of leaves of *Rhododendron aureum* from the Irkutsk region, Pribaikal'e, Russian Federation, were isolated by hydrodistillation and analyzed by a combination of GC and GC/MS. Compounds representing 70.5–78.3 % of the oils were identified. Twenty-seven compounds were identified according to their chromatographic retention indices and mass spectra. The major components of the oils were calarene (10.4––66.4 %), β-bourbonene (0.5–27.4 %), α-selinene (2.1–8.0 %) and kaur-16-ene (2.0–6.3 %). It was found that the chemical composition of *Rh. aureum* essential oil depends on the altitude of the growing plants.

Keywords: *Rhododendron aureum*; gold rosebay; essential oil; calarene.

INTRODUCTION

Rhododendron is a genus from the Ericaceae family which includes about eight hundred species of evergreen, half-deciduous and deciduous shrubs and trees. Rhododendrons are distributed mainly in the temperate zone of the northern hemisphere, with the greatest diversity of species occurring in southern China, the Himalayas, Japan, Southeast Asia and North America.[1] A resent feasibility study revealed several opportunities for the commercialization of *Rhododendron* as mulch, biofuel, charcoal, foliage, a source of phytochemicals and wood for turnery.[2]

* Corresponding author. E-mail: oldaniil@rambler.ru
doi: 10.2298/JSC1002209O

The leaves of *Rhododendron* species contain essential oils, the volatile compounds of which have been widely studied by different scientists. The following presents information about the dominant components and their contents in the essential oils from some *Rhododendron* species: *Rh. adamsii* – *trans*-nerolidol (18.2––29.5 %) and *β*-farnesene (6.9–17.1 %); *Rh. anthopogon* – *α*-pinene (37.4 %) and *β*-pinene (16.0 %); *Rh. aureum* – hexanoic acid (10.0 %) and carvacrol (7.8 %); *Rh. calophytum* – 3,7,11,15-tetramethyl-2-hexadecen-1-ol (5.68 %) and 1,3,5-trimethylbenzene (5.53 %); *Rh. dauricum* – *β*-caryophyllene (28.3 %) and *α*-humulene (15.0 %); *Rh. ledebouri* – *β*-myrcene (13.3 %) and bornyl acetate (11.8 %); *Rh. sichotense* – *α*-pinene (44.3 %) and *β*-pinene (13.1 %); *Rh. sutchuenense* –– caryophyllene (12.5 %) and guaiol (8.8 %); *Rh. simsii* – phytol (15.2 %) and 3,7-dimethyl-1,6-octadien-3-ol (12.6 %); *Rh. mucronulatum* – *α*-humulene (28.8 %) and *β*-caryophyllene (14.6 %); *Rh. naamkwanense* – [*Z*,*Z*,*Z*]-9,12,15-octadecatrienoic acid (45.3 %) and phytol (8.6 %).[3–8] Tasdemis *et al*. analyzed the volatile components of hexane- and CH_2Cl_2-extracts from five *Rhododendron* species growing in Turkey.[9] They found that the dominate compounds in the hexane-extract of *Rh. ponticum* leaves were 5,15-rosadiene (42.8 %) and 2-ethylhexanol (13.3 %) and in the CH_2Cl_2-extract, 1-butanol (17.0 %) and *γ*-butyrolactone (13.5 %); in the hexane-extract of *Rh. luteum* leaves, ethyl acetate (13.3 %) and 6-methyl-5-heptene-2-one (11.1 %) were dominant and in the CH_2Cl_2--extract, 1-butanol (58.7 %) and benzyl alcohol (17.1 %); in the hexane-extract from *Rh.*×*sochadzeae* leaves, 6-methyl-5-heptene-2-one (11.9 %) and calarene (7.1 %) were dominant while, in the CH_2Cl_2-extract, phenethyl alcohol (100 %); in the hexane-extract of *Rh. ungernii* leaves, 6-methyl-5-heptene-2-one (29.4 %) and 2-ethylhexanol (24.4 %) dominated while in the CH_2Cl_2-extract, 2-(2--ethoxyethoxy)ethanol (12.8 %) and phenethyl alcohol (11.5 %); in the hexane--extract of *Rh. smirnovii* leaves, 6-methyl-5-heptene-2-one (21.7 %) and viridiflorol (15.4 %) were dominant. The total content of identified compounds was 75.3–100 % in the hexane-extracts and 60.1–100 % in the CH_2Cl_2-extracts.

Gold rosebay, kashkara (*Rhododendron aureum* Georgi) is a small evergreen shrub of the Ericaceae family with a dark-brown bark, stems procumbent usually crooked and lifted at 20–100 cm from the ground branches; the blossom period is May–June and fruiting in July–August. It grows on stony slopes and rocks in the mountainous regions of eastern Siberia and the Far East, reaching the Western Sayan and the Abakan Range, mainly in the alpine zone.[10] The harvesting season of rhododendron is in August–September. In Russia, mass harvesting occurs in the Pribaikal'e (Irkutsk region) and Zabaikal'e (Buryatia and Chita region).

In Tibetan medicine, *Rh. aureum* is used under the names *shu-mkhan* or *da-li* for the treatment of rheumatism and for cardiovascular and diuretic means.[11,12] Experimentally, it was found that *Rh. aureum* drugs have pronounced effects on the heart in patients with cardiovascular insufficiency, reducing shortness of breath,

palpitations, edema and venous pressure, and increasing the speed of blood flow and diuresis. *Rh. aureum* extracts have bactericidal effects against pathogenic microflora, especially streptococcus and staphylococcus, due to the presence of phenols and essential oil.[13]

Chemical studies on *Rh. aureum* found the presence of: diterpenes (andromedotoxin), triterpenes (campanulin, simmiarol, uvaol, oleanolic acid), simple phenols (rhododendrol, rhododendrin, hydroquinone, arbutine, 1-*O*-*β*-glucopyranosyl-5-methoxy-3-hydroxy-benzene, 5-methoxy-1,3-dihydroxybenzene) and flavonoids (quercetin, hyperin, avicularin, polystachoside).[14–17] Earlier research on the essential oil from Zabaikal'e *Rh. aureum* samples has already been realized[6] but not the study of the essential oil from Pribaikal'e samples.

This paper reports the results of an analysis of the essential oil of *Rh. aureum* growing in the Irkutsk region of Pribaikal'e.

EXPERIMENTAL

Plant material

The plant materials of *Rh. aureum* leaves were collected from different locations on Pribaikal'e (Irkutsk region, Russia), in August 2008 (Table I). The samples were gathered after the flowering period. A voucher specimen is kept at the Siberian Institute of Plants Physiology and Biochemistry, Siberian Division, Russian Academy of Sciences.

TABLE I. Characteristics of the *Rh. aureum* samples

Sample No.	Locality	Altitude, m a.s.l.	Collected date	Essential oil content / %
RA-1	Village Rechka Vydrinnaia	460	23 VIII 2008	0.25
RA-2	Village Sliudianka	1172	16 VIII 2008	0.20
RA-3	Village Sliudianka	1350	16 VIII 2008	0.15
RA-4	Village Sliudianka	1402	16 VIII 2008	0.14
RA-5	Village Sliudianka	1452	16 VIII 2008	0.09

Isolation of the essential oil

Fresh leaves (200 g) were subjected to hydrodistillation in a Clevenger-type apparatus for 150 min, which gave the essential oil. The amounts of essential oil extracted from the different samples are given in Table I.

Gas chromatography

The GC analysis was performed on an Agilent 6890N series gas chromatograph fitted with a HP-5MS fused capillary column (30 m×0.25 mm, film thickness 0.50 μm, 5 % diphenyl- and 95 % dimethylpolysiloxane stationary phase). The oil solutions (0.20 μl) in hexane (≈ 1 %) were injected in the split mode (1:20). The carrier gas was helium at a flow of 1.0 ml min^{-1}. The column temperature was programmed from 150–250 °C at 2.0 °C min^{-1}; the injector temperature was 250 °C and the detector (FID) temperature was 300 °C.

Gas-chromatography/mass spectroscopy

The GC/MS analysis was performed on the same gas chromatograph but instead of the FID detector, it was coupled to an Agilent Technologies 5973 N mass selective/quadrupole

detector. The same column and chromatographic conditions as above were employed. The ion source temperature was 230 °C. The EIMS spectra (70 eV) were obtained in the scan mode in the *m*/*z* range 41–450.

Component identification and quantification

Identification of compounds was realized by comparison of the peak retention times with those of analytical standards of available terpenoids and by comparison of the mass spectra with those found in the literature,[18] the mass spectrometry data bank (NIST 05) and a computer search of the Wiley library. For quantification purposes, the relative percent peak areas registered using the FID were used.

RESULTS AND DISCUSSION

The chemical compositions of the essential oils of *Rh. aureum* leaves are presented in Table II. In the samples of essential oils, forty components were detected, of which twenty-seven were identified. The identified components accounted for 70.5–78.3 % of the total oils. The content of hydrocarbons was 60.5–78.2 % and of oxygenated terpenes 0–11.6 %; the dominant constituents were sesquiterpene compounds.

TABLE II. Chemical compositions (area, %) of the essential oils from *Rh. aureum* leaves from Pribaical'e

No.	Compound	RA-1	RA-2	RA-3	RA-4	RA-5
1	*cyclo*-Sativene	–	–	–	0.1	0.8
2	*α*-Ylangene	0.6	0.4	0.5	0.7	6.0
3	*α*-Copaene	0.4	0.1	2.0	1.2	10.3
4	*α*-Bourbonene	0.7	–	–	–	–
5	*β*-Bourbonene	4.1	0.5	12.9	7.8	27.4
6	Aristolene	0.5	1.3	0.6	0.9	–
7	n.i.[a] ($C_{15}H_{24}$)	2.1	–	3.3	–	–
8	Calarene	34.4	66.4	26.2	41.3	10.4
9	*cis*-Calamene	0.6	–	–	–	0.2
10	n.i ($C_{15}H_{24}$)	–	8.2	–	3.4	–
11	*trans*-*α*-Bergamotene	0.1	–	–	–	0.6
12	n.i. ($C_{15}H_{24}$)	2.0	–	–	–	–
13	*α*-Humulene	0.3	–	–	–	0.3
14	Aromadendrene	11.1	–	0.5	7.1	0.8
15	*α*-Amorphene	0.2	0.3			0.4
16	Germacrene D	0.1		1.6	0.5	1.7
17	*β*-Selinene	1.6	1.0	1.6	1.5	0.3
18	*α*-Selinene	8.0	3.5	3.8	4.9	2.1
19	Isoledene	0.3	–	–	–	–
20	n.i. ($C_{15}H_{24}$)	2.4	–	–	–	–
21	*α*-Muurolene	–	–	–	0.4	–
22	*γ*-Cadinene	1.1	0.9	2.8	0.9	1.9
23	*δ*-Cadinene	0.1	0.5	1.1	0.3	1.2
24	*β*-Cadinene	1.2	1.2	0.7	1.2	2.9
25	*α*-Cadinene	–	–	–	0.2	0.4

TABLE II. Continued

No.	Compound	RA-1	RA-2	RA-3	RA-4	RA-5
26	α-Calacorene	0.4	0.2	–	0.3	0.4
27	n.i. ($C_{15}H_{26}O$)	2.7	–	–	0.4	–
28	Spathulenol	–	–	11.6	–	–
29	Caryophyllene oxide	0.3	–	–	0.3	–
30	n.i. ($C_{15}H_{26}O$)	1.9	–	–	3.0	–
31	n.i. ($C_{15}H_{24}O$)	–	2.2	–	–	–
32	τ-Muurolol	—	–	–	0.5	–
33	α-Cadinol	–	–	–	0.2	–
34	n.i. ($C_{20}H_{24}$)	–	–	–	0.9	–
35	n.i. ($C_{15}H_{24}O$)	–	–	–	14.1	–
36	n.i. ($C_{15}H_{26}O$)	2.7	3.1	–	–	–
37	n.i. ($C_{15}H_{24}O$)	4.8	3.0	11.7	1.3	16.7
38	n.i. ($C_{20}H_{32}O$)	8.9	5.2	12.8	3.8	11.7
39	n.i. ($C_{20}H_{32}O$)	2.0	–	–	–	–
40	Kaur-16-ene	4.4	2.0	6.3	2.8	3.5
Total identified compd.		70.5	78.3	72.2	73.1	71.6
Total unidentified compd.		29.5	21.7	27.8	26.9	28.4

[a]Not identified

The essential oils from the different samples of *Rh. aureum* leaves were characterized by a high level of variability. In the essential oil of sample RA-1, the major compounds were calarene (34.4 %), aromadendrene (11.1 %), α-selinene (8.0 %), kaur-16-ene (4.4 %) and β-bourbonene (4.1 %); in sample RA-2, they were calarene (66.4 %), α-selinene (3.5 %) and kaur-16-ene (2.0 %); in sample RA-3, they were calarene (26.2 %), β-bourbonene (12.9 %), spathulenol (11.6 %) and kaur-16-ene (6.3 %); in sample RA-4, they were calarene (41.3 %), β-bourbonene (7.8 %), aromadendrene (7.1 %) and α-selinene (4.9 %); in sample RA-5, they were β-bourbonene (27.4 %), calarene (10.3 %), α-copaene (10.3 %) and ylangene (6.0 %).

A comparative study of altitude and the composition of the essential oils revealed an important feature, *i.e.*, with changing altitude the terpene synthesis also changed. In samples RA-1–RA-4, the aristolane derivative calarene was dominant but in sample RA-5, the prevailing compound was β-bourbonene, which represents a group of bourbonane derivatives. The content of essential oil was inversely related to the value of the altitude, *i.e.*, with increasing altitude, the oil content decreased from 0.25 to 0.09 % (Table I). There was also a change in the appearance of the essential oils. The essential oils from samples RA-1–RA-4 were solid, poorly-colored substances with a weak odor, while the oil from sample RA-5 was a green liquid with a strong specific smell. The reason for this is likely to be the change in environmental conditions and the occurrence of stress factors affecting the plants on a cellular level, which led to profound changes in the terpene biogenesis of the plants.

Previously, a study of *Rh. aureum* essential oil was conducted on specimens growing in the Tunkin Valley (Zabaikal'e, Buryatia, Russian Federation). It was found that in October samples of *Rh. aureum*, the essential oil was dominated by the compounds calarene (5.6 %), *α*-terpineol (1.2 %) and *β*-selinene (0.7 %) and in the November samples by hexanoic acid (10.0 %), carvacrol (7.8 %) and *α*-pinene (5.4 %).[6] These data show that despite the geographical proximity to Zabaikal'e, the *Rh. aureum* growing in Pribaikal'e refers to another chemotype.

И З В О Д

ХЕМИЈСКИ САСТАВ ЕТАРСКОГ УЉА БИЉКЕ *Rhododendron aureum* ИЗ ПРИБАЈКАЛСКЕ ОБЛАСТИ (РУСКА ФЕДЕРАЦИЈА)

DANIIL N. OLENNIKOV[1], LUBOV' V. DUDAREVA[2], SEMION N. OSIPENKO[3] и TAT'YANA A. PENZINA[4]

[1]Laboratory of Medical and Biological Research, Department of Biologically Active Substances, Institute of General and Experimental Biology, Siberian Division, Russian Academy of Sciences, Sakh'yanovoi st., 6, 670047, Ulan-Ude, [2]Laboratory of Physicochemical Research Methods, Siberian Institute of Plant Physiology and Biochemistry, Siberian Division, Russian Academy of Sciences, Lermontova st., 132, 664033, Irkutsk-33, [3]Laboratory of Plant Physiological Genetics, Siberian Institute of Plant Physiology and Biochemistry, Siberian Division, Russian Academy of Sciences, Lermontova st., 132, 664033, Irkutsk-33 и [4]Greenhouse group, Siberian Institute of Plant Physiology and Biochemistry, Siberian Division, Russian Academy of Sciences, Lermontova st., 132, 664033, Irkutsk-33, Russian Federation

Дестилацијом воденом паром је изоловано етарско уље из пет узорака лишћа биљке *Rhododendron aureum*, која расте у области Иркутска, Прибајкал, Руска федерација. Уље је анализирано методама GC и GC/MS. Идентификована су једињења која чине 70,5–78,2 % укупног садржаја уља. Идентификовано је 27 једињења на основу њихових хроматографских ретенционих времена и масених спектара. Главни састојци уља су каларен (10,3–66,4 %), *β*-бурбонен (0,5–27,4 %), *α*-селинен (2,1–8,0 %) и каур-16-ен (2,0–6,3 %). Хемијски састав етарског уља *Rh. aureum* зависи од надморске висине на којој биљка расте.

(Примљено 3. јуна, ревидирано 21. јула 2009)

REFERENCES

1. J. Cullen, *Notes Roy. Bot. Gard. Edinburgh* **39** (1980) 113
2. J. Wong, E. Youde, B. Dickinson, M. Hale, *Report of the Rhododendron feasibility study* School Agric. Forest Sci., Univ. Wales, Bangor, 2002, p. 73
3. M. V. Belousov, E. V. Basova, M. S. Usubov, T. P. Berezovskaya, L. M. Pokrovskii, A. V. Tkachev, *Chem. Plant Raw Mater.* **4** (2000) 45 (in Russian)
4. M. Yonzon, J. L. Dong, T. Yokochi, Y. Kawano, T. Nakahara, *J. Essent. Oil Res*. **17** (2005) 107
5. C. X. Zhao, Y. Z. Liang, X. N. Li, H. Z. Fang, *Acta Pharm. Sin.* **40** (2005) 854 (in Chinese)
6. A. D. Rogachev, V. V. Fomenko, O. I. Sal'nikova, L. M. Pokrovskii, N. F. Salakhutdinov, *Chem. Nat. Comp.* **42** (2006) 426
7. G.-H. Tian, C.-F. Liu, X. Wang, *J. Guangxi Norm. Univ.* **23** (2007) 39 (in Chinese)
8. X.-L. Fu, Y. Lin, P. Zhuang, J. Bai, F. Chen, *Lishizhen Medic. Mater. Med. Res*. **19** (2008) 93

9. D. Tasdemir, B. Demirci, F. Demirci, A. A. Donmez, K. H. C. Baser, P. Ruedi, *Z. Naturforsch.* **52c** (2003) 797
10. *Dikorastuschie poleznye rasteniya Rossii*, SPKhPhA, St. Petersburg, 2001, p. 663 (in Russian)
11. T. A. Aseeva, K. F. Blinova, G. P. Yakovlev, *Lekarstvennye rasteniya tibetskoi meditsiny*, Nauka, Novosibirsk, 1985, p. 154 (in Rusian)
12. *Tibetskaia meditsina u buryat*, RAN, Novosibirsk, 2008, p. 323 (in Rusian)
13. *Rastitel'nye resursy SSSR. Semeistva Paeoniaceae-Thymelaeaceae*, Nauka, Leningrad, 1986, p. 336 (in Russian)
14. G. A. Fokina, N. B. Belova, *Chem. Nat. Comp.* **9** (1970) 827
15. Z. Jin, R. Chen, T. Shang, X. Liang, *Acta Pharm. Sin.* **16** (1981) 869 (in Chinese)
16. G. G. Zapesochnaya, A. I. Ban'kovskii, *Chem. Nat. Comp.* **1** (1965) 262
17. A. G. Gorshkov, I. A. Murashkina, A. L. Vereshagin, A. I. Syrchina, T. P. Zyubr, A. A. Semenov, *Pharm. Chem. J.* **34** (2000) 658
18. R. P. Adams, *Identification of essential oil components by gas chromatography/mass spectroscopy*, Allured Publ. Corp., Carol Stream, IL, 1995, p. 467.

Journal of the Serbian Chemical Society
JSCS@tmf.bg.ac.rs • www.shd.org.rs/JSCS

J. Serb. Chem. Soc. *75* (2) 217–228 (2010)
JSCS–3954

UDC 547.415.584+542.913:57–188:543.42
Original scientific paper

Template synthesis and characterization of biologically active transition metal complexes comprising 14-membered tetraazamacrocyclic ligand

DHARMPAL SINGH[1]*, KRISHAN KUMAR[1], RAMESH KUMAR[1] and JITENDER SINGH[2]

[1]*Department of Chemistry, National Institute of Technology, Kurukshetra- 136 119 and*
[2]*D. M. Division, National Dairy Research Institute, Karnal-132 001, India*

(Received 7 March, revised 7 May 2009)

Abstract: A novel series of complexes of the type $[M(C_{28}H_{24}N_4)X_2]$, where M = Co(II), Ni(II), Cu(II), Zn(II) and Cd(II), X = Cl^-, NO_3^-, CH_3COO^- and ($C_{28}H_{24}N_4$) corresponds to the tetradentate macrocyclic ligand, were synthesized by template condensation of 1,8-diaminonaphthalene and diacetyl in the presence of divalent metal salts in methanolic medium. The complexes were characterized by elemental analyses, conductance and magnetic measurements, as well as by UV/Vis, NMR, IR and MS spectroscopy. The low values of the molar conductance indicate non-electrolyte type of complexes. Based on these spectral data, a distorted octahedral geometry may be proposed for all of these complexes. All the synthesized macrocyclic complexes were tested for *in vitro* antibacterial activity against some pathogenic bacterial strains, *viz Bacillus cereus*, *Salmonella typhi*, *Escherichia coli* and *Staphylococcus aureus*. The *MIC* values shown by the complexes against these bacterial strains were compared with the *MIC* shown by the standard antibiotics linezolid and cefaclor.

Keywords: antibacterial activity; diaminonaphthalene; macrocyclic complexes; spectroscopic studies.

INTRODUCTION

The design and study of well-arranged metal-containing macrocycles is an interesting field of chemistry.[1] Some synthetic macrocyclic complexes (*e.g.*, Cu--complex) have been investigated for accelerating the photodegradation of hazardous pollutants.[2]

In situ one-pot template condensation reactions lie at the heart of macrocyclic chemistry.[3,4] Therefore, template reactions have been widely used for the synthesis of macrocyclic complexes, in which transition metal ions are generally used as the template agent.[5] There is continued interest in the synthesis of macro-

* Corresponding author. E-mail: dpsinghchem@yahoo.co.in
doi: 10.2298/JSC1002217S

cyclic complexes because of their potential application in fundamental and applied sciences.[6,7] Synthetic macrocyclic complexes mimic some naturally occurring macrocycles because of their resemblance with many natural macrocycles, such as metalloproteins and metalloenzymes.[8] Macrocyclic nickel complexes find use in DNA recognition and oxidation.[9] Macrocyclic copper complexes find use in DNA binding and cleavage[10] and copper containing proteins have been identified.[11] Macrocyclic metal complexes of lanthanides, *e.g.*, Gd^{3+} are used as MRI contrast agents.[12] The macrocyclic metal chelating agent, DOTA, is useful for detecting tumour lesions.[13] The chemistry of macrocyclic complexes is also important due to their use as dyes and pigments,[14] as well as NMR shift reagents.[15] Some macrocyclic complexes have received special attention because of their mixed soft–hard donor character and versatile coordination behaviour[16] and because of their pharmacological properties, *i.e.*, toxicity against bacterial and fungal growth.[17]

Prompted by these facts, in the present paper, the synthesis and characterization of cobalt(II), nickel(II), copper(II), zinc(II), and cadmium(II) macrocyclic complexes derived from 1,8-diaminonaphthalene and diacetyl (2,3-butanedione) are discussed. The complexes were characterized using various physico-chemical techniques, such as IR, NMR, elemental analyses, magnetic susceptibility and conductivity measurements. All the synthesized macrocyclic complexes were tested for *in vitro* antibacterial activity against some bacterial strains using spot-on-lawn on Muller Hinton Agar. Four test pathogenic bacterial strains, *viz. Bacillus cereus* (MTCC 1272), *Salmonella typhi* (MTCC 733), *Escherichia coli* (MTCC 739) and *Staphylococcus aureus* (MTCC 1144) were considered for the determination of the *MIC* (minimum inhibitory concentration) values of the synthesized complexes. The *MIC* values exhibited by the complexes against these bacterial strains were compared with the *MIC* values shown by the standard antibiotics linezolid and cefaclor.

EXPERIMENTAL

Materials

All the chemicals and solvent used in this study were of AnalaR grade. 1,8-Diaminonaphthalene and diacetyl were procured from Acros, the metal salts were purchased from s.d.-fine, Merck, Ranbaxy and were used as received.

Isolation of complexes

All the complexes were synthesized by the template method, *i.e.*, by condensation of 1,8-diaminonaphthalene and diacetyl in the presence of the respective divalent metal salts. To a stirred hot methanolic solution (≈ 50 cm^3) of 1,8-diaminonaphthalene (10 mmol) was added a divalent cobalt, nickel, copper, zinc or cadmium salt (5 mmol) dissolved in the minimum quantity of MeOH (≈ 20 cm^3). The resulting solution was refluxed for 0.5 h, after which diacetyl (10 mmol) was added to the refluxing mixture and the refluxing was continued for 8–10 h. The mixture was concentrated to half its volume and kept in a desiccator overnight. On

overnight cooling, a dark coloured precipitate formed which was filtered, washed with methanol, acetone and diethyl ether, and dried *in vacuo*. The obtained yield was ≈ 60–75 %. The complexes were soluble in DMF and DMSO. They were found to be thermally stable up to ≈ 260–280 °C, after which decomposition occurred.

The template condensation of 1,8-diaminonaphthalene and diacetyl in the presence of divalent metal salts, in the molar ratio 2:2:1, is shown in Scheme 1.

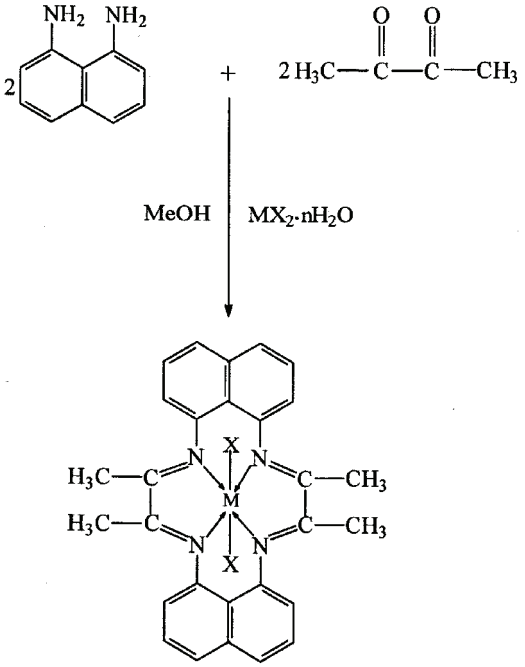

Scheme 1. Synthesis of the macrocyclic complexes, where M = Co(II), Ni(II), Cu(II), Zn(II), Cd(II); X = Cl^-, NO_3^-, CH_3COO^-; *n* = 2, 3, 4, 6.

Analytical and physical measurements

Microanalyses for C, H, and N were performed using an elemental analyzer (Perkin Elmer 2400) at the SAIF, Punjab University, Chandigarh. The magnetic susceptibility measurements were performed at SAIF, IIT Roorkee using a Vibrating Sample Magnetometer (Model PAR 155). The metal contents in the complexes were determined by a literature method.[18] The IR spectra were recorded on a FT-IR spectrophotometer (Perkin Elmer) in the range 4000–200 cm^{-1} using Nujol Mull. The ^{1}H-NMR spectra (at room temperature, in DMSO-d_6) were recorded on a Bruker AVANCE II 400 NMR spectrometer (400 MHz) at the SAIF, Punjab University, Chandigarh. The electronic spectra (in DMSO) were recorded on a Cary 14 spectrophotometer at room temperature. The FAB (Fast atom bombardment) mass spectra (at room temperature) were recorded on a TOF MS ES+ mass spectrometer. The conductivity was measured using a digital conductivity meter (HPG system, G-3001). The melting points were determined in capillaries using an electrical melting point apparatus.

In vitro *antibacterial activity*

All synthesized macrocyclic complexes were tested for *in vitro* antibacterial activity against some bacterial strains using spot-on-lawn on Muller Hinton Agar.[19]

Four test pathogenic bacterial strains, *viz Bacillus cereus* (MTCC 1272), *Salmonella typhi* (MTCC 733), *Escherichia coli* (MTCC 739) and *Staphylococcus aureus* (MTCC 1144) were considered for the determination of the *MIC* (minimum inhibitory concentration) of selected complexes.

The test pathogens were subcultured aerobically using Brain Heart Infusion Agar (HiMedia, Mumbai, India) at 37 °C for 24 h. Working cultures were stored at 4 °C in Brain Heart Infusion (BHI) broth while stock cultures were maintained at –70 °C in BHI broth containing 15 % (v/v) glycerol (Qualigens, Mumbai, India). The organism was grown overnight in 10 ml BHI broth, centrifuged at 5000 *g* for 10 min and the pellet was suspended in 10 ml of phosphate buffer saline (PBS, pH 7.2). The optical density at 545 nm (OD-545) was adjusted to obtain 10^8 Cfu/ml, followed by plating serial dilution onto plate count agar (HiMedia, Mumbai, India).

The minimum inhibitory concentration (*MIC*) is the lowest concentration of an antimicrobial agent that prevents the development of viable growth after overnight incubation. The antimicrobial activity of the compounds was evaluated using spot-on-lawn on Muller Hinton Agar (MHA, HiMedia, Mumbai, India). Soft agar was prepared by adding 0.75 % agar in Muller Hinton Broth. The soft agar was inoculated with 1 % of 10^8 Cfu/ml of the test pathogen and 10 ml was overlaid on MHA. From a 1000X solution of the compound (1 mg/ml of DMSO) 1, 2, 4, 8, 16, 32, 64 and 128X solutions were prepared. Dilutions of standard antibiotics (linezolid and cefaclor) were also prepared in the same manner. 5µl of the appropriate dilution was spotted onto the soft agar and incubated at 37 °C for 24 h. The zones of inhibition of the compounds were considered after subtraction of the inhibition zone of DMSO. The negative control (with no compound) was also observed.

RESULTS AND DISCUSSION

Chemistry

The analytical data show the suggested formula for the macrocyclic complexes as $[M(C_{28}H_{24}N_4)X_2]$, where M = Co(II), Ni(II), Cu(II), Zn(II) and Cd(II), and X = Cl^- NO_3^- CH_3COO^- and ($C_{28}H_{24}N_4$) corresponds to the tetradentate macrocyclic ligand. The tests for anions were positive only after decomposing the complexes with conc. HNO_3, indicating their presence inside the coordination sphere. The low molar conductance values (10–17 Ω^{-1} cm^2 mol^{-1}) of the complexes determined in DMSO indicate their non-electrolyte nature.[20] Various attempts to obtain a single crystal suitable for X-ray crystallography, such as crystallization using mixtures of solvents and low temperature crystallization, were unsuccessful in order. However, the analytical, spectroscopic and magnetic data enabled the possible structure of the synthesized complexes to be predicted. All complexes gave satisfactory results of elemental analyses, as shown in Table I.

IR spectra

It was noted that a pair of bands were present in the spectrum of 1,8-diaminonaphthalene at 3350 and 3390 cm^{-1} corresponding to $\nu(NH_2)$, which were absent in the infrared spectra of all the complexes. Furthermore, no strong absorption band was observed near 1716 cm^{-1}, indicating the absence of the C=O

TABLE I. Analytical data of the synthesised divalent cobalt, nickel, copper, zinc and cadmium complexes derived from 1,8-diaminonaphthalene and diacetyl

Complex	Molecular weight	Found (Calcd.), %				Colour
		M	C	H	N	
$[Co(C_{28}H_{24}N_4)Cl_2]$ (**1**)	546	10.68 (10.79)	61.44 (61.53)	4.36 (4.39)	10.09 (10.26)	Black
$[Co(C_{28}H_{24}N_4)(NO_3)_2]$ (**2**)	599	9.79 (9.83)	56.00 (56.09)	3.93 (4.00)	13.96 (14.02)	Black
$[Co(C_{28}H_{24}N_4)(OAc)_2]$ (**3**)	593	9.90 (9.93)	64.59 (64.75)	4.96 (5.06)	9.37 (9.44)	Black
$[Ni(C_{28}H_{24}N_4)Cl_2]$ (**4**)	545	10.63 (10.76)	61.58 (61.65)	4.40 (4.40)	10.08 (10.27)	Grey
$[Ni(C_{28}H_{24}N_4)(NO_3)_2]$ (**5**)	598	9.70 (9.81)	56.09 (56.18)	3.91 (4.01)	14.01 (14.04)	Reddish brown
$[Ni(C_{28}H_{24}N_4)(OAc)_2]$ (**6**)	592	9.86 (9.91)	64.83 (64.86)	5.00 (5.07)	9.29 (9.45)	Dark grey
$[Cu(C_{28}H_{24}N_4)Cl_2]$ (**7**)	550	11.43 (11.55)	61.03 (61.09)	4.29 (4.36)	10.04 (10.18)	Black
$[Cu(C_{28}H_{24}N_4)(NO_3)_2]$ (**8**)	603	10.39 (10.53)	55.61 (55.72)	3.86 (3.98)	13.87 (13.93)	Black
$[Cu(C_{28}H_{24}N_4)(OAc)_2]$ (**9**)	597	10.63 (10.64)	64.22 (64.32)	4.99 (5.02)	9.20 (9.38)	Dark grey
$[Zn(C_{28}H_{24}N_4)(OAc)_2]$ (**10**)	599	10.85 (10.91)	64.03 (64.10)	4.97 (5.01)	9.19 (9.34)	Black
$[Cd(C_{28}H_{24}N_4)(OAc)_2]$ (**11**)	646	17.31 (17.40)	59.34 (59.44)	4.50 (4.64)	8.59 (8.67)	Black

group of the diacetyl moiety. The disappearance of these bands and appearance of a new strong absorption band near 1590–1629 cm^{-1} confirms the condensation of the carbonyl group of diacetyl and the amino group of diaminonaphthalene, and the formation of the macrocyclic Schiff's base,[21] as these bands may be assigned to ν(C=N) stretching vibrations.[22,23] The lower value of ν(C=N) may be explained based on a drift of the lone pair density of the azomethine nitrogen towards the metal atom,[24,25] indicating that coordination occurred through the nitrogen of the C=N groups. The medium intensity bands present in the region 2830–2950 cm^{-1} may be assigned to ν(C–H) stretching vibrations of the methyl group of the diacetyl moiety.[26] The various absorption bands in the region of 1400–1588 cm^{-1} may be assigned to ν(C=C) aromatic stretching vibrations of the naphthalene ring.[27,28] The bands in the region 740–785 cm^{-1} may be assigned to ν(C–H) out of plane bending of the aromatic ring.[29,30] The presence of the absorption bands at 1408–1440, 1290–1320 and 1010–1030 cm^{-1} in the IR spectra of all the nitrato complexes suggest that both the nitrate groups are coordinated to the central metal ion in a unidentate fashion.[31] The IR spectra of all the acetate complexes show an absorption band in the region 1650–1680 cm^{-1}

that is assigned to the $\nu(COO^-)_{as}$ asymmetric stretching vibrations of the acetate ion and another in the region 1258–1290 cm^{-1} that can be assigned to the $\nu(COO^-)_s$ symmetric stretching vibration of the acetate ion. The difference between ν_{as} and ν_s, which was around 390–370 cm^{-1}, *i.e.*, greater than 144 cm^{-1}, indicates the unidentate coordination of the acetate group with the central metal ion.[32]

The far infrared spectra show bands in the region 420–450 cm^{-1} corresponding to ν(M–N) vibrations.[33–35] The presence of bands in all complexes in the region 420–450 cm^{-1}, originating from (M–N) azomethine vibrational modes, identify coordination of the azomethine nitrogen.[36] The bands present in the range 300–320 cm^{-1} may be assigned to ν(M–Cl) vibration.[33–35] The bands present in the region 220–250 cm^{-1} in all nitrato complexes are related to ν(M–O) stretching vibration.[33,34]

^{1}H-NMR spectra

The ^{1}H-NMR spectrum of the zinc(II) complex shows multiplets at 6.65––7.32 ppm, corresponding to the aromatic ring protons (12H) of the naphthalene moiety[37]. The singlet at 2.12 ppm may be assigned to the methyl protons (12H) of diacetyl.[38]

Mass spectra

The FAB mass spectra of the Co(II), Ni(II), Cu(II), Zn(II) and Cd(II) macrocyclic complexes were recorded using an NBA (nitrobenzyl alcohol) matrix. The peaks at 136, 137, 154, 284 and 307 are due to the matrix. All the spectra exhibited parent peaks due to molecular ions $[M]^+$ and $[M+2]^+$. The proposed molecular formula of these complexes were confirmed by comparing their molecular formula weights with the *m*/*z* values. The molecular ion $[M]^+$ and $[M+2]^+$ peaks obtained for the various complexes are given in Table II. The data are in good agreement with the proposed molecular formula for these complexes, *i.e.*, $[M(C_{28}H_{24}N_4)X_2]$. This confirms the formation of the macrocyclic frame. In addition to the molecular ion peaks, the spectra exhibited other peaks assignable to various fragments arising from the thermal cleavage of the complexes (Table II). The peak intensities give an idea of the stability of the fragments.

Magnetic measurements and electronic spectra

Cobalt complexes. The magnetic moment of the cobalt complexes was measured at room temperature and lay in the range of 4.90–4.99 μ_B, which corresponds to three unpaired electrons. The electronic spectra of the cobalt(II) complexes recorded in DMSO exhibits three absorption peaks in the region 1227.0––1077.6 nm (ν_1), 740.7–643.1 nm (ν_2) and 540.5–487.8 nm (ν_3). The spectra resemble those of complexes reported to be octahedral.[39] Thus, assuming the effective symmetry to be D_{4h}, the various bands may be assigned to the transitions: $^4T_{1g} \rightarrow {}^4T_{2g}(F)$ (ν_1); $^4T_{1g} \rightarrow {}^4A_{2g}(F)$ (ν_2) and $^4T_{1g} \rightarrow {}^4T_{1g}(P)$ (ν_3), respectively.

TABLE II. FAB mass spectral data of the synthesised divalent cobalt, nickel, copper, zinc and cadmium complexes derived from 1,8-diaminonaphthalene and diacetyl

Complex	Molecular ion peak $[M]^+$ and $[M+2]^+$ at *m/z*	Important peaks due to complex fragmentation
$[Co(C_{28}H_{24}N_4)Cl_2]$ (**1**)	$[M]^+ = 545.6(^{35}Cl)$, $[M+2]^+ = 547.6(^{37}Cl)$	$[Co(C_{28}H_{24}N_4)Cl]^+ = 510.1$, $[Co(C_{28}H_{24}N_4)–H]^+ = 473.6$, $[C_{28}H_{24}N_4]^+ = 414.6$, $[(C_{24}H_{12}N_4)–H]^+ = 353.6$
$[Co(C_{28}H_{24}N_4)(NO_3)_2]$ (**2**)	$[M]^+ = 598.6$	$[Co(C_{28}H_{24}N_4)(NO_3)]^+ = 536.6$, $[Co(C_{28}H_{24}N_4)–H]^+ = 473.6$, $[C_{28}H_{24}N_4]^+ = 414.6$, $[(C_{24}H_{12}N_4)–H]^+ = 353.6$
$[Co(C_{28}H_{24}N_4)(OAc)_2]$ (**3**)	$[M]^+ = 592.9$	$[Co(C_{28}H_{24}N_4)(OAc)]^+ = 533.9$, $[Co(C_{28}H_{24}N_4)–H]^+ = 473.9$, $[C_{28}H_{24}N_4]^+ = 414.9$, $[(C_{24}H_{12}N_4)–H]^+ = 353.9$
$[Ni(C_{28}H_{24}N_4)Cl_2]$ (**4**)	$[M]^+ = 544.4$ (^{35}Cl), $[M+2]^+ = 546.4(^{37}Cl)$	$[Ni(C_{28}H_{24}N_4)Cl]^+ = 508.9$, $[Ni(C_{28}H_{24}N_4)]^+ = 473.4$, $[(C_{28}H_{24}N_4)]^+ = 414.7$, $[C_{24}H_{12}N_4–H]^+ = 353.7$
$[Ni(C_{28}H_{24}N_4)(NO_3)_2]$ (**5**)	$[M]^+ = 597.5$	$[Ni(C_{28}H_{24}N_4)(NO_3)]^+ = 535.5$, $[Ni(C_{28}H_{24}N_4)]^+ = 473.5$, $[C_{28}H_{24}N_4]^+ = 414.8$, $[(C_{24}H_{12}N_4)–H]^+ = 353.8$
$[Ni(C_{28}H_{24}N_4)(OAc)_2]$ (**6**)	$[M]^+ = 590.9$	$[Ni(C_{28}H_{24}N_4)(OAc)]^+ = 531.9$, $[Ni(C_{28}H_{24}N_4)]^+ = 472.9$, $[C_{28}H_{24}N_4]^+ = 414.2$, $[(C_{24}H_{12}N_4)–H]^+ = 353.2$
$[Cu(C_{28}H_{24}N_4)Cl_2]$ (**7**)	$[M]^+ = 548.6$ (^{35}Cl), $[M+2]^+ = 550.6$ (^{37}Cl)	$[Cu(C_{28}H_{24}N_4)Cl]^+ = 513.1$, $[Cu(C_{28}H_{24}N_4)]^+ = 477.6$, $[C_{28}H_{24}N_4]^+ = 414.1$, $[(C_{24}H_{12}N_4)–H]^+ = 353.1$
$[Cu(C_{28}H_{24}N_4)(NO_3)_2]$ (**8**)	$[M]^+ = 602.6$	$[Cu(C_{28}H_{24}N_4)(NO_3)]^+ = 540.6$, $[Cu(C_{28}H_{24}N_4)]^+ = 477.6$, $[C_{28}H_{24}N_4]^+ = 414.0$, $[(C_{24}H_{12}N_4)–H]^+ = 353.0$
$[Cu(C_{28}H_{24}N_4)(OAc)_2]$ (**9**)	$[M]^+ = 595.5$	$[Cu(C_{28}H_{24}N_4)(OAc)]^+ = 536.5$, $[Cu(C_{28}H_{24}N_4)]^+ = 477.5$, $[C_{28}H_{24}N_4]^+ = 413.9$, $[(C_{24}H_{12}N_4)–H]^+ = 352.9$
$[Zn(C_{28}H_{24}N_4)(OAc)_2]$ (**10**)	$[M]^+ = 598.7$	$[Zn(C_{28}H_{24}N_4)(OAc)]^+ = 539.7$, $[Zn(C_{28}H_{24}N_4)–H]^+ = 479.7$, $[C_{28}H_{24}N_4]^+ = 414.3$, $[(C_{24}H_{12}N_4)–H]^+ = 353.3$
$[Cd(C_{28}H_{24}N_4)(OAc)_2]$ (**11**)	$[M]^+ = 645.5$	$[Cd(C_{28}H_{24}N_4)(OAc)]^+ = 586.5$, $[Cd(C_{28}H_{24}N_4)]^+ = 527.5$, $[(C_{28}H_{24}N_4)–H]^+ = 414.1$, $[(C_{28}H_{24}N_4)–H]^+ = 353.1$

It appears that the symmetry of these complexes is not idealized octahedral (O_h), but is D_{4h}. The assignment of the first spin-allowed band seems plausible since the first band appears approximately at half the energy of the visible band.[40]

Nickel complexes. The magnetic moment of the nickel complexes at room temperature was observed in the range 2.94–3.10 μ_B. These values are in tune with a high spin configuration and show the presence of an octahedral environment around the Ni(II) ion in all the complexes. The spectra of Ni(II) complexes recorded in DMSO solution exhibited a well discernable band with a shoulder on the low energy side. The other two bands generally observed in the region 606.1––581.4 nm (ν_2), and 359.7–353.4 nm (ν_3) were assigned to $^3A_{2g} \rightarrow {}^3T_{1g}(F)$ (ν_2) and $^3A_{2g} \rightarrow {}^3T_{1g}(P)$ (ν_3), respectively. The first two bands result from the splitting of one band, ν_1, and are in the ranges ≈ 1036.3–980.4 and 843.9–809.7 nm, which can be assigned to $^3B_{1g} \rightarrow {}^3E_g$ and $^3B_{1g} \rightarrow {}^3B_{2g}$, respectively, assuming the effective symmetry to be D_{4h} (component of $^3T_{2g}$ in O_h symmetry).[39] The intense, higher energy bands at 289.5 nm may be due to a π–π* transition of the (C=N) group. Various bands do not follow any regular pattern and seem to be anion independent. The spectra are consistent with the distorted octahedral nature of these complexes.

Copper complexes. The magnetic moment of copper complexes is in the range 1.76–1.80 μ_B. The electronic spectra of the Cu(II) complexes exhibited bands in the region 563.4–512.8 nm, with a shoulder on the low energy side at ≈ 689.7––625.0 nm, which showed that these complexes are distorted octahedral.[38,39] Assuming tetragonal distortion in the molecule, the d-orbital energy level sequence for these complexes may be: $x^2–y^2 > z^2 > xy > xz > yz$ and the shoulder can be assigned to: $z^2 \rightarrow x^2–y^2$ ($^2B_{1g} \rightarrow {}^2B_{2g}$) and the broad band contains both the $xy \rightarrow x^2–y^2$ ($^2B_{1g} \rightarrow {}^2E_g$) and $xy, yz \rightarrow x^2–y^2$ ($^2B_{1g} \rightarrow {}^2A_{2g}$) transitions.[41] The band separation of the spectra of the complexes is of the order 4000 nm, which is consistent with proposed geometry of the complexes.[41] Therefore, it may be concluded that all the complexes formed by macrocycles with Cu(II) metal are distorted octahedral.

Biological results and discussion

The *MIC* (minimum inhibitory concentration) shown by the complexes against the studied bacterial strains was compared with the MIC exhibited by the standard antibiotics linezolid and cefaclor in Table III. Complex **6**, $[Ni(C_{28}H_{24}N_4)(OAc)_2]$, showed a minimum inhibitory concentration ranging from 8–64 μg/ml. The complex also showed a minimum inhibitory concentration of 16 μg/ml against the bacterial strain *Escherichia coli*, which is equal to the *MIC* shown by the standard antibiotic linezolid against the same bacterial strain. The *MIC* of complex **10**, $[Zn(C_{28}H_{24}N_4)(OAc)_2]$, against *E. coli* was found to be 16 μg/ml, which is equal to the minimum inhibitory concentration shown by the standard antibiotic

linezolid against the same bacterial strain. For complexes **1**, **3**, **4**, **7** and **9** from Table I, a minimum inhibitory concentration of 32 μg/ml was registered against the bacterial strain *Salmonella typhi*, which is equal to *MIC* shown by the standard antibiotic linezolid against the same bacterial strain (Table III). In the whole series, based on the *MIC*, complex **6**, $[Ni(C_{28}H_{24}N_4)(OAc)_2]$, was found to be the most effective complex as it showed a *MIC* of 8 μg/ml against the bacterial strain *Staphylococcus aureus*. Complexes **4**, $[Ni(C_{28}H_{24}N_4)Cl_2]$, and **7**, $[Cu(C_{28}H_{24}N_4)Cl_2]$, showed an *MIC* of 32 μg/ml against the bacterial strain *Bacillus cereus* (Table III). Complexes **3**, **5** and **8** exhibited an *MIC* of 32 μg/ml against the bacterial strain *S. aureus.* Complexes **1**, **2**, **3** and **4** showed an *MIC* of 32 μg/ml against the bacterial strain *E. coli* (Table III).

TABLE III. Minimum inhibitory concentration (*MIC*) shown by complexes against the test bacteria using the agar dilution assay

Complex	*MIC* / μg ml^{-1}			
	Bacillus cereus	*Staphylococcus aureus*	*Escherichia coli*	*Salmonella typhi*
$[Co(C_{28}H_{24}N_4)Cl_2]$ (**1**)	64	64	32	32
$[Co(C_{28}H_{24}N_4)(NO_3)_2]$ (**2**)	64	>128	32	>128
$[Co(C_{28}H_{24}N_4)(OAc)_2]$ (**3**)	16	32	32	32
$[Ni(C_{28}H_{24}N_4)Cl_2]$ (**4**)	32	64	32	32
$[Ni(C_{28}H_{24}N_4)(NO_3)_2]$ (**5**)	64	32	>128	>128
$[Ni(C_{28}H_{24}N_4)(OAc)_2]$ (**6**)	16	8	16	64
$[Cu(C_{28}H_{24}N_4)Cl_2]$ (**7**)	32	128	128	32
$[Cu(C_{28}H_{24}N_4)(NO_3)_2]$ (**8**)	>128	32	64	64
$[Cu(C_{28}H_{24}N_4)(OAc)_2]$ (**9**)	128	64	64	32
$[Zn(C_{28}H_{24}N_4)(OAc)_2]$ (**10**)	128	16	16	64
Cefaclor[1]	8	2	8	16
Linezolid[1]	4	4	16	32

[1]Standard antibiotics

Bearing in mind the rising problems of antimicrobial resistance, these chemical compounds may be used for the formulation of novel chemotherapeutic agents. Further investigation will be necessary to identify the active component.

CONCLUSIONS

Based on various studies, such as elemental analyses, conductance measurements and magnetic susceptibilities, as well as IR, NMR, electronic and mass spectral studies, a distorted octahedral geometry may be proposed for all these complexes. The proposed structure is shown in Fig. 1.

It has been suggested that chelation/coordination reduces the polarity of the metal ion, mainly because of the partial sharing of its positive charge with a donor group within the whole chelate ring system.[42] This process of chelation thus increases the lipophilic nature of the central metal atom, which in turn, favours

its permeation through the lipoid layer of the membrane, thus causing the metal complex to cross the bacterial membrane more effectively thereby increasing the activity of the complexes. In addition to this, many other factors, such as solubility, dipole moment and conductivity as well as the influence of the metal ion, may be possible reasons for the remarkable antibacterial activities of these complexes.[43]

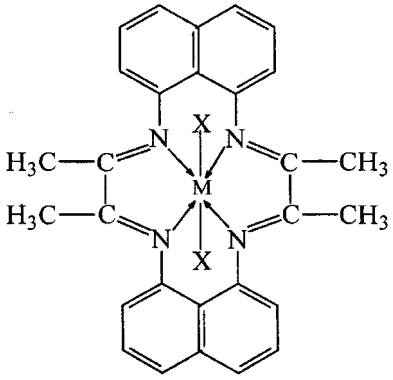

Fig. 1. Proposed structure of the complexes (M = Co(II), Ni(II), Cu(II), Zn(II), Cd(II) and X = Cl^-, NO_3^-, CH_3COO^-).

ABBREVIATIONS

MIC – Minimum inhibitory concentration
MTCC – Microbial type culture collection
MHA – Muller hinton agar
CFU – Colony forming unit
μ_B – Bohr magneton
DMF – *N*,*N*-Dimethylformamide
DMSO – Dimethyl sulphoxide
BHI – Brain heart infusion
DOTA – 1,4,7,10-Tetraazacyclododecane-1,4,7,10-tetraacetic acid
NMR – Nuclear magnetic resonance
MRI – Magnetic resonance imaging
IR – Infrared

Acknowledgements. D. P. Singh thanks the University Grants Commission, New Delhi, for financial support in the form of a Major Research Project [MRP-F.No.32-196/2006(SR)] and Krishan Kumar for the award of project fellowship under the above project. Thanks are also due to the authorities of N.I.T., Kurukshetra, for providing necessary research facilities.

ИЗВОД

ТЕМПЛАТНА СИНТЕЗА И КАРАКТЕРИЗАЦИЈА БИОЛОШКИ АКТИВНИХ КОМПЛЕКСА ПРЕЛАЗНИХ МЕТАЛА КОЈИ САДРЖЕ ЧЕТРНАЕСТОЧЛАНЕ ТЕТРААЗАМАКРОЦИКЛИЧНЕ ЛИГАНДЕ

DHARMPAL SINGH[1], KRISHAN KUMAR[1], RAMESH KUMAR[1] и JITENDER SINGH[2]

[1]*Department of Chemistry, National Institute of Technology, Kurukshetra- 136 119 и*
[2]*D. M. Division, National Dairy Research Institute, Karnal-132 001, India*

Темплатном кондензацијом 1,8-диаминонафталена и диацетила у присуству двовалентних металних соли у метанолу синтетисана је нова серија комплекса типа $[M(C_{28}H_{24}N_4)X_2]$, где је M = Co(II), Ni(II), Cu(II), Zn(II) и Cd(II); X = Cl^-, NO_3^-, CH_3COO^-, а ($C_{28}H_{24}N_4$) одговара тетрадентатном макроцикличном лиганду. Комплекси су окарактерисани елементалном анализом, мерењем проводљивости и магнетним мерењима, UV/Vis, NMR, IR и MS спектроскопијом. Мала вредност моларне проводљивости указује на комплекс типа неелектролита. На основу спектралних података предложена је дисторгована октаедарска геометрија за све комплексе. Сви макроциклични комплекси су тестирани на *in vitro* антибактеријску активност према сојевима неких патогених бактерија, тј. *Bacillus cereus*, *Salmonella typhi*, *Escherichia coli* и *Staphylococcus aureus*. *MIC* комплекса према овим бактеријским сојевима упоређене су са *MIC* стандардних антибиотика линезолид и цефаклор.

(Примљено 7. марта, ревидирано 7. маја 2009)

REFERENCES

1. S. Chandra, L. K. Gupta, S. Agrawal, *Transition Met. Chem.* **32** (2007) 240
2. A. I. Hanafy, A .B. K. T. Maki, M. M. Mostafa, *Transition Met. Chem.* **32** (2007) 960
3. N. F. Curtis, *Coord. Chem. Rev*. **3** (1968) 3
4. M. S. Niasari, M. Bazarganipour, M. R. Ganjali, P. Norouzi, *Transition Met. Chem.* **32** (2007) 9
5. M. S. Niasari, F. Davar, *Inorg. Chem. Commun*. **9** (2006) 175
6. D. S. Kumar, V. Alexander, *Polyhedron* **18** (1999) 1561
7. S. Ilhan, H. Temel, R. Ziyadanogullari, M. Sekerci, *Transition Met. Chem.* **32** (2007) 584
8. M. Shakir, S. Khatoon, S. Parveen, Y. Azim, *Transition Met. Chem.* **32** (2007) 42
9. J. G. Muller, X. Chen, A. C. Dadiz, S. E. Rokita, C. J. Burrows, *Pure Appl. Chem.* **65** (1993) 545
10. J. Liu, T. B. Lu, H. Deng, L. N. Ji, L. H. Qu, H. Zhou, *Transition Met. Chem.* **28** (2003) 116
11. P. Akilan, M. Thirumavalavan, M. Kandaswamy, *Polyhedron* **22** (2003) 3483
12. D. P. Singh, R. Kumar, V. Malik, P. Tyagi, *J. Enzyme Inhib. Med. Chem.* **22** (2007) 177
13. C. Kosmos, D. Snook, C. S. Gooden, N. S. Courtenay Luck, M. J. McCalla, C. F. Meares, A. A. Epenetos, *Cancer Res.* **52** (1992) 904
14. J. Seto, S. Tamura, N. Asai, N. Kishii, Y. Kijima, N. Matsuzawa, *Pure Appl. Chem.* **68** (1996) 1429
15. W. Dong, R. Yang, L. Yan, *Indian J. Chem.* **40A** (2001) 202
16. S. Chandra, R. Gupta, N. Gupta, S. S. Bawa, *Transition Met. Chem.* **31** (2006) 147
17. S. Chandra, L. K. Gupta, S. Agrawal, *Transition Met. Chem.* **32** (2007) 558
18. A. I. Vogel, *A text book of quantitative chemical analysis*, 5th ed., Longman, London, 1989

19. D. P. Singh, R. Kumar, J. Singh, *Eur. J. Med. Chem.* **44** (2009) 1731
20. W. J. Geary, *Coord. Chem. Rev*. **7** (1971) 81
21. D. P. Singh, R. Kumar, P. Tyagi, *Transition Met. Chem*. **31** (2006) 970
22. Z. A. Siddiqi, M. Khan, M. Khalid, S. Kumar, *Trans. Met. Chem.* **32** (2007) 927
23. D. P. Singh, N. Shishodia, B. P. Yadav, V. B. Rana, *Polyhedron* **16** (1997) 2229
24. S. Chandra, S. D. Sharma, *Transition Met. Chem*. **27** (2002) 732
25. C. Lodeiro, R. Basitida, E. Bertolo, A. Macias, R. Rodriguez, *Transition Met. Chem*. **28** (2003) 388
26. R. Singh, P. Kumar, R. Shyam, V. Malik, S. Arya, *J. Indian Chem. Soc.* **83** (2006) 616
27. R. N. Prasad, M. Mathur, A. Upadhayay, *J. Indian Chem. Soc*. **84** (2007) 1202
28. J. Costamagna, G. Ferraudi, M. Villagran, E. Wolcan, *J. Chem. Soc. Dalton Trans.* (2000) 2631
29. S. Chandra, L. K. Gupta, *J. Indian Chem. Soc*. **82** (2005) 454
30. D. P. Singh, N. Shishodia, B. P. Yadav, V. B. Rana, *J. Indian Chem. Soc.* **81** (2004) 287
31. S. Chandra, L. K. Gupta, *Spectrochim. Acta A* **60** (2004) 2767
32. K. Nakamoto, *Infrared and Raman spectra of inorganic and coordination compounds*, Wiley Interscience Publication, New York, 1978
33. M. Shakir, O. S. M. Nasman, S. P. Varkey, *Polyhedron* **15** (1996) 309
34. M. Shakir, K. S. Islam, A. K. Mohamed, M. Shagufa, S. S. Hasan, *Transition Met. Chem.* **24** (1999) 577
35. S. Chandra, R. Kumar, *Transition Met. Chem*. **29** (2004) 269
36. V. B. Rana, D. P. Singh, P. Singh, M. P. Teotia, *Transition Met. Chem.* **7** (1982) 174
37. H. Jiang, H. Sun, S. Zhang, R. Hua, Y. Xu, S. Jin, H. Gong, L. Li, *J. Inclusion Phenom. Macrocylic Chem.* **58** (2007) 133
38. V. K. Sharma, S. Srivastva, *Turk. J. Chem.* **30** (2006) 755
39. a) V. B. Rana, P. Singh, D. P. Singh, M. P. Teotia, *Transition Met. Chem.* **6** (1981) 36; b) V. B. Rana, P. Singh, D. P. Singh, *Polyhedron* **1** (1982) 377
40. A. B. P. Lever, *Inorganic electronic spectroscopy*, Elsevier, Amsterdam, 1968
41. A. B. P. Lever, E. Mantovani, *Inorg. Chem.* **10** (1971) 817
42. Z. H. Chohan, H. Pervez, A. Rauf, K. M. Khan, C. T. Supuran, *J. Enzyme Inhib. Med. Chem*. **19** (2004) 417
43. Z. H. Chohan, A. Scozzafava, C. T. Supuran, *J. Enzyme Inhib. Med. Chem.* **17** (2002) 261.

Journal of the Serbian Chemical Society
JSCS@tmf.bg.ac.rs • www.shd.org.rs/JSCS

J. Serb. Chem. Soc. 75 (2) 229–242 (2010)
JSCS–3955

UDC 546.562'732'742'472+542.913+547.85+547.656+633.71–32
Original scientific paper

Synthesis and structural studies of complexes of Cu, Co, Ni and Zn with isonicotinic acid hydrazide and isonicotinic acid (1-naphthylmethylene)hydrazide

ANGELA KRIZA[1], LUCICA VIORICA ABABEI[2]*, NICOLETA CIOATERA[3], ILEANA RĂU[4] and NICOLAE STĂNICĂ[5]

[1]*University of Bucharest, Chemistry Faculty, 23, Dumbrava Rosie Street, Bucharest,* [2]*The House of Teaching Staff Giurgiu, 8, Nicholae Droc Barcian Street, Giurgiu,* [3]*University of Craiova, Chemistry Faculty, 107 I, Calea Bucuresti Street, Craiova,* [4]*Polytechnic Institute of Bucharest, Faculty of Applied Chemistry and Materials Science, 1, Polizu Steet, 011061 Bucharest and* [5]*Romanian Academy, Chemistry-Physics Institute, 202 Independence Avenue, 77208 Bucharest, Romania*

(Received 15 April, revised 11 September 2009)

Abstract: Eight new complexes of Cu(II), Co(II), Ni(II) and Zn(II) with isonicotinic acid hydrazide (isoniazid, (INH)) and isonicotinic acid (1-naphthylmethylene)hydrazide (INNMH), having the formula of the type $[M(INH)(ac)_2]$ or $[M(INNMH)(ac)_2]$ (M = Co(II), Ni(II) and Zn(II)) and $[Cu(INH)(ac)_2]_2$, $[Cu(INNMH)(ac)_2]_2$, were synthesized and characterized. All complexes were characterized based on elemental analyses, and IR, UV–VIS–NIR and EPR spectroscopy, as well as by thermal analysis and determination of their molar conductivity and magnetic moments. The structure of INNMH was established by single crystal X-ray analysis. In all complexes, both ligands were coordinated to the metal *via* N and O. The complexes of Cu (II) were dimeric, with four bridges between acetate ions and Cu(II).

Keywords: isoniazid; isonicotinic acid (1-naphthylmethylene)hydrazide; template synthesis; X-ray study; transition metal complexes.

INTRODUCTION

Isonicotinic acid hydrazide (isoniazid, INH) is a known tuberculostatic agent. It forms metal chelates with many bivalent ions. These complexes have been used in the determination of the structure of isoniazid.[1,2]

Numerous research papers have described the bactericide and fungicide properties of various mixed ligand complexes of metal ions with isoniazid and hydrazone derivatives.[3,4]

* Corresponding author. E-mail: lucica_32@yahoo.com
doi: 10.2298/JSC1002229K

Hydrazones play an important role in inorganic chemistry, as they easily form stable complexes with most transition metal ions. The development of the field of bioinorganic chemistry has increased the interest in hydrazone complexes, since it was recognized that many of these complexes may serve as models for biologically important species.[5–9] In context to previous research,[10,11] a number of complexes of transition metals with isonicotinoylhydrazone ligands were obtained and characterized.

In the present paper, the synthesis and characterization of eight new complexes of Cu(II), Co(II), Ni(II) and Zn(II) acetate with isoniazid (INH) and isonicotinic acid (1-naphthylmethylene)hydrazide (INNMH) are reported. The structural formula of isoniazid is shown in Fig. 1a and a molecular drawing and the atom labeling scheme of isonicotinic acid (1-naphthylmethylene)hydrazide are shown in Fig. 1b.

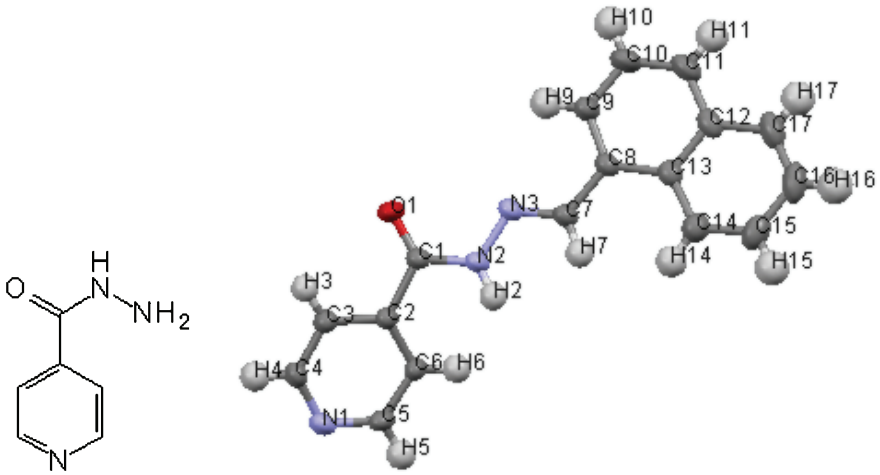

(a) (b)

Fig. 1. a) The structural formula for isoniazid, INH, and b) the crystal structure of isonicotinic acid (1-naphthylmethylene)hydrazide, INNMH.

EXPERIMENTAL

Isonicotinic acid (1-naphthylmethylene)hydrazide, INNMH, was obtained by refluxing a mixture of isoniazid and 1-naphthaldehyde (1:1 molar ratio) on a water bath for 5 h. Methanol (30 ml) was used as the solvent. After cooling, a brilliant yellowish white precipitate formed, which was filtered, washed with methanol and dried under vacuum over $CaCl_2$. Single crystals were separated from the solid and subjected to a single crystal X-ray study whereby their crystal structure was determined.

Synthesis of the complexes

To a methanolic solution (30 ml) of the required metal acetate with crystal water (0.001 mol) was added a methanolic solution of isoniazid (INH) in a 1:1 molar ratio. The resulting precipitates **1**–**4** were filtered, washed with methanol and dried under vacuum over $CaCl_2$.

For the complexes with the hydrazone, isoniazid (0.0020 mol in 30 ml of methanol) was added to a methanolic solution of 1-naphthaldehyde (0.0020 mol in 30 ml methanol). The mixture was stirred at 50 °C for 30 min, cooled to room temperature and to this was added under stirring, a methanolic solution of Cu(II), Co(II), Ni(II) or Zn(II) acetate (0.0010 mol in 15 ml methanol). Immediately, the metallic complexes precipitated. The solid products **5**–**8** were filtered, washed with methanol and dried under vacuum over anhydrous $CaCl_2$.

Instrumentation

The elemental analyses (C, H, N) were realized with an elemental combustion system CHNS-O, using a Costech device, type ECS 4010, and the metal contents were determined by gravimetric methods.[12]

The IR spectra (4000–400 cm^{-1}) were recorded in KBr pellets using a Bio-Rad FTS-135 spectrometer. The UV–VIS–NIR electronic spectra (200–2200 nm) were recorded by diffuse reflection using a Jasco V 670 UV–VIS–NIR spectrophotometer.

The magnetic susceptibility of the complexes was determined at room temperature, using the Faraday method. The electronic paramagnetic resonance (EPR) spectra of the Cu complexes were recorded at room temperature on a Jeol JESS FA 100 spectrometer, with a 100 Hz field modulation.

The thermal analyses were performed with a Perkin Elmer Diamond instrument at a heating of 5 °C/min under a dynamic air atmosphere (150 ml/min). All complexes were investigated in the temperature range 20–800 °C, with the exception of the cobalt complexes, which were investigated up to 960 °C.

Single-crystal X-ray diffraction was used for crystal structure determination of isonicotinic acid (1-naphthylmethylene)hydrazide. The XRD data were collected at room temperature on a Stoe IPDS II diffractometer operating with an Mo Kα (λ = 0.71073 Å) X-ray tube with a graphite monochromator. Data collection and cell refinement were realized using Stoe X-AREA.[13] The structures were solved by direct methods and refined with anisotropic displacement parameters based on F^2, using SHELXS-97[14] and SHELXL-97[15] crystallographic software packages.

RESULTS AND DISCUSSION

By the reaction of Co(II), Ni(II) and Zn(II) acetate with INH, complexes of the type $[M(INH)(ac)_2]\cdot xH_2O$ (x = 3, M = Co and x = 2, M = Ni and Zn; INH = = isoniazid) were obtained and by the reaction of Cu(II) acetate with INH in 1:1 molar ratio, the dimer $[Cu(INH)(ac)_2]_2\cdot 3H_2O$ was obtained. The complexes were insoluble or slightly soluble in usual organic solvents (methanol, ethanol, DMF, acetone, diethyl ether and chloroform).

The structure of INNMH (isonicotinic acid (1-naphthylmethylene)hydrazide) was determined in a single crystal X-ray diffraction study. Details of crystal structure determination are summarized in Table I, and the bond lengths and angles in Table II.

The complexes with INNMH were obtained by template synthesis. The compounds were soluble in DMF and insoluble in other common (methanol, ethanol, acetone, diethyl ether and chloroform.) organic solvents. Molar conductivity measurements in DMF showed that they were non-electrolytes.

TABLE I. Crystallographic data, details of data collection and structure refinement parameters for INNMA

Chemical formula	$C_{17}H_{13}N_3O_1$
M / g mol^{-1}	275.30
T / K	293(2)
λ / Å	0.71073
Crystal system	Monoclinic
Space group	P21/n
a / Å	9.1732(9)
b / Å	11.342(1)
c / Å	13.161(1)
α / °	90.00
β / °	99.400(7)
γ / °	90.00
V / Å^3	1350.9(2)
Z	4
ρ /g cm^{-3}	1.354
F (000)	576
R_{int}	0.0421
Reflections collected	5171
Unique reflections	3440
Goodness-of-fit on F^2	1.073

TABLE II. Bond distances and angles for INNMH

C1–O1 1.2158(2)	C13–C14 1.418(2)	C13–C8–C7 120.70(1)
C1–N2 1.3567(2)	C14–C15 1.368(3)	C8–C9–C10 121.83(2)
C1–C2 1.5071(2)	C15–C16 1.400(3)	C11–C10–C9 119.95(2)
C2–C6 1.383(2)	C16–C17 1.352(3)	C10–C11–C12 121.04(2)
C2–C3 1.386(2)	N2–N3 1.3781(16)	C11–C12–C17 121.43(2)
C3–C4 1.384(2)	O1–C1–N2 124.00(13)	C11–C12–C13 119.72(2)
C4 –N1 1.333(2)	O1–C1–C2 120.83(1)	C17–C12–C13 118.83(2)
C5–N1 1.338(2)	N2–C1–C2 115.16(1)	C14–C13–C12 118.01(1)
C5–C6 1.388(2)	C6–C2–C3 118.18(1)	C14–C13–C8 123.86(1)
C7–N3 1.2680(2)	C6–C2–C1 123.25(1)	C12–C13–C8 118.12(1)
C7–C8 1.4693(2)	C3–C2–C1 118.36(1)	C15–C14–C13 120.81(2)
C8–C9 1.375(2)	C4–C3–C2 118.74(1)	C14–C15–C16 120.97(2)
C8–C13 1.434(2)	N1–C4–C3 123.97(1)	C17–C16–C15 120.03(2)
C9–C10 1.402(2)	N1–C5–C6 123.57(1)	C16–C17–C12 121.28(2)
C10–C11 1.354(3)	C2–C6–C5 118.86(1)	C4–N1–C5 116.69(1)
C11–C12 1.408(3)	N3–C7–C8 121.11(1)	C1–N2–N3 118.50(1)
C12–C17 1.422(2)	C9–C8–C13 119.25(1)	C7–N3–N2 115.72(1)
C12–C13 1.429(2)	C9–C8–C7 119.92(1)	

Results of the elemental analyses of the obtained complexes are listed below (ac = $C_2H_3O_2^-$).

[Cu(INH)(ac)$_2$]$_2$·3H$_2$O (***1***). Anal. Calcd. for $Cu_2C_{20}H_{32}N_6O_{13}$: C, 34.711; H, 4.665; N, 12.157; Cu, 18.382. Found: C, 34.989; H, 4.873; N, 12.449; Cu, 18.618.

[Co(INH)(ac)$_2$]·3H$_2$O (***2***). Anal. Calcd. for $CoC_{10}H_{19}N_3O_8$: C, 34.246; H, 4.894; N, 12.005; Co, 16.832. Found: C, 34.011; H, 4.678; N, 12.120; Co, 16.630.

[Ni(INH)(ac)$_2$]·2H$_2$O (***3***). Anal. Calcd. for $NiC_{10}H_{17}N_3O_7$: C, 31.427; H, 4.487; N, 10.999; Ni, 15.370. Found: C, 31.771; H, 4.621; N, 11.100; Ni, 15.600.

[Zn(INH)(ac)$_2$]·2H$_2$O (***4***). Anal. Calcd. for $ZnC_{10}H_{17}N_3O_7$: C, 30.559; H, 5.390; N, 10.703; Zn, 16.652. Found: C, 30.711; H, 5.604; N, 10.912; Zn, 16.705.

[Cu(INNMH)(ac)$_2$]$_2$·4H$_2$O (***5***). Anal. Calcd. for $Cu_2C_{42}H_{44}N_6O_{16}$: C, 51.192; H, 4.607; N, 8.538; Cu, 12.909. Found: Cu, C, 51.316; H, 4.982; N, 8.611; 12.800.

[Co(INNMH)(ac)$_2$]·4H$_2$O (***6***). Anal. Calcd. for $CoC_{21}H_{26}N_3O_9$: C, 46.650; H, 5.038; N, 7.780; Co, 10.909. Found: C, 46.510; H, 5.103; N, 7.610; Co, 10.872.

[Ni(INNMH)(ac)$_2$]·2H$_2$O (***7***). Anal. Calcd. for $NiC_{21}H_{22}N_3O_7$: C, 51.649; H, 4.751; N, 8.614; Ni, 12.029. Found: C, 51.712; H, 4.842; N, 8.702; Ni, 12.200.

[Zn(INNMH)(ac)$_2$]·2H$_2$O (***8***). Anal. Calcd. for $ZnC_{21}H_{22}N_3O_7$: C, 50.949; H, 4.687; N, 8.497; Zn, 13.220. Found: C, 50.732; H, 4.502; N, 8.378; Zn, 13.310.

Some physical properties (color, melting point, molar conductivity) of the complexes are given in Table III.

TABLE III. Selected physical and chemical properties of the complexes **1**–**8** (INH = isoniazid; INNMH = isonicotinic (1-naphthylmethylene)hydrazide; ac = CH_3COO^-)

Complex	Color	Melting point, °C	Λ_M[a] / cm^2 mol^{-1}	μ_{eff} / μ_B
[Cu(INH)(ac)$_2$]$_2$·3H$_2$O (**1**)	Green	277	–	2.180
[Co(INH)(ac)$_2$]·3H$_2$O (**2**)	Brown	280[b]	–	4.32
[Ni(INH)(ac)$_2$]·2H$_2$O (**3**)	Green	299[b]	–	3.386
[Zn(INH)(ac)$_2$]·2H$_2$O (**4**)	Yellowish	263	–	Diamagnitic
[Cu(INNMH)(ac)$_2$]$_2$·4H$_2$O (**5**)	Green	193	9.04	2.39
[Co(INNMH)(ac)$_2$]·4H$_2$O (**6**)	Brown	233	8.88	5.02
[Ni(INNMH)(ac)$_2$]·2H$_2$O (**7**)	Grey	317	8.85	2.801
[Zn(INNMH)(ac)$_2$]·2H$_2$O (**8**)	Yellowish	206	8.44	Diamagnetic

[a]10^{-3} M Solution in DMF; [b]carbonization

IR spectra

The main bands in the IR spectra of INH and its metal complexes **1**–**4** are presented in Table IV and the bands in the IR spectra of INHNA and its metal complexes **5**–**8** are given in Table V.

In the IR spectrum of isoniazid, very intense bands appeared at 3302, 3112, 1667 and 1555 cm^{-1}, which were assigned to the vibration frequencies $\nu(NH_{as})$ and $\nu(NH_{sym})$ and to amide-I and amide-II-groups. The average intensity band at 887 cm^{-1} was assigned to the N–N vibration frequency.[16]

TABLE IV. Selected infrared frequencies (cm^{-1}) of isoniazid (INH) and its complexes **1**–**4** (ac = CH_3COO^-)

Complex	ν(OH)	ν(N–H)	ν(C=O) Amide I	ν Amide II	ν(N–N)	ν(COO)		
						ν_{as}	ν_{sym}	$\Delta\nu$
INH	–	3302 3112	1667	1555	887	–	–	–
$[Cu(INH)(ac)_2]_2\cdot 3H_2O$ (**1**)	3429	–	1627	1499	837	1561	1418	143
$[Co(INH)(ac)_2]\cdot 3H_2O$ (**2**)	3363	3245	1650	1549	832	1596	1416	180
$[Ni(INH)(ac)_2]\cdot 2H_2O$ (**3**)	3380	3257	1660	1550	857	1580	1416	164
$[Zn(INH)(ac)_2]\cdot 2H_2O$ (**4**)	3421	3211	1634	1547	855	1580	1408	172

TABLE V. Selected infrared frequencies (cm^{-1}) of isonicotinic acid (1-naphthylmethylene)-hydrazide (INNMH) and complexes **5**–**8** (ac = CH_3COO^-)

Complex	ν(OH)	ν(N–H)	ν(C=O) Amide I	ν(C=N) Azomethine	ν(COO)		
					ν_{as}	ν_{sym}	$\Delta\nu$
INNMH	–	3175 3011	1675	1552	–	–	–
$[Cu(INNMH)(ac)_2]_2\cdot 4H_2O$ (**5**)	3416	–	1623	1521	1557	1419	138
$[Co(INNMH)(ac)_2]\cdot 4H_2O$ (**6**)	3416	3196 3047	1654	1516	1598	1419	179
$[Ni(INNMH)(ac)_2]\cdot 2H_2O$ (**7**)	3416	3201 3057	1649	1516	1577	1419	158
$[Zn(IHNMH)(ac)_2]\cdot 2H_2O$ (**8**)	3416	3180 3052	1654	1506	1593	1398	195

In the complexes **1**–**4**, the band corresponding to the amide-I group is shifted towards lower values by $\Delta\nu$ between 7 and 40 cm^{-1}, which indicates the involvement of the carbonyl group in the coordination.[17] The ν(N–H) vibration frequencies are strongly displaced in all complexes. The movement of the band 3302 cm^{-1} to lower wave numbers suggests the involvement of the amino nitrogen in the coordination to the metal ions. This conclusion is supported by the movement of the ν(N–N) frequency vibration towards lower values in the complexes.

The spectrum of complexes show bands which could be assigned to both bridging and chelating binding coordination mode of the acetate anion.[18] A correlation between the infrared antisymmetric and symmetric absorption frequencies of the carboxylate group and the type of carboxylate group has been developed. The acetate ion in aqueous solution is characterized by bands at 1578 and 1411 cm^{-1}, which are commonly assigned to the antisymmetric (ν_{as}) and the

symmetric (ν_{sym}) stretching vibrations of the carboxylate group. These frequencies and, in particular, their difference, $\Delta\nu = \nu_{as} - \nu_{sym}$, have been used as empirical indicators of coordination modes of the acetate group. According to Deacon and Phillips,[18] a difference larger than 200 cm^{-1} indicates a monodentate coordination, whereas a difference smaller than 150 cm^{-1} indicates a bridging coordination mode. Moreover, it is accepted that a values of $\Delta\nu$ smaller than 200 cm^{-1} can indicate a bidentate coordination mode. In complexes **1**–**4**, the frequencies of the vibration ν_{as}(COO) appears in the range 1561–1596 cm^{-1}, while those characteristic of the ν_{sym}(COO), ranged from 1408 to 1418 cm^{-1}. For complex **1**, a value of $\Delta\nu$ <150 cm^{-1}, which is indicative of a bridge in the coordination of the acetate group.[18] However, for the complexes **2**–**4**, $\Delta\nu$ is >150 cm^{-1}, which leads to the conclusion that the acetate group is a chelating binding ligand in these complexes.

Bands in the region 3363–3429 cm^{-1} in the IR spectra of the complexes suggests the presence of crystallization water.[19] In the region 400–500 cm^{-1}, there are bands that can be attributed to modes of vibration ν(M–N) and ν(M–O). All this data supports the idea that in the metal complexes, the isoniazid was coordinated through the amino nitrogen and the carbonyl oxygen.

In the IR spectrum of INNMH, intense bands appear at 1675 and 1552 cm^{-1}, which were assigned to the vibrations ν(C=O amide I) and ν(C=N azomethine).

For the complexes **5**–**8**, the band corresponding to amide I was shifted by 21–53 cm^{-1} toward lower frequencies, which indicates the involvement of carbonyl group in coordination.[17] In addition, a shift towards lower values by 31–46 cm^{-1} was observed for the bands characteristic of the azomethine group of metal complexes with INHNA. This suggests involvement of the azomethine nitrogen in the coordination with the metal ions.[17] The ν_{as}(COO) vibration band appeared in the domain 1557–1598 cm^{-1} in the spectra of the complexes **5**–**8**, while those characteristic of the ν_{sym}(COO) appeared in the 1398–1419 cm^{-1} range. For complex **5**, $\Delta\nu$ was <150 cm^{-1}, suggesting that the acetate group is coordinated in a bridge. In complexes **6**–**8**, $\Delta\nu$ was >150 cm^{-1} which leads to the conclusion that the acetate group in these complexes was in a chelating binding mode.[18]

The IR spectral data showed that isonicotinic acid (1-naphthylmethylene)-hydrazide was coordinated to the metal ions through the azomethine nitrogen and the carbonyl oxygen.

Magnetic properties

The magnetic moments calculated for complexes **1** and **5** (at room temperature) of 2.18 and 2.39 μ_B, respectively, reasonably correspond to octahedral geometry of the Cu(II) complexes.[20]

For the Co (II) complexes **2** and **6**, the magnetic moments were 4.32 and 5.02 μ_B, respectively, indicating a high-spin character, excluding the oxidation to

Co(III). These values are within the range (4.3–5.7 μ_B) corresponding to an octahedral geometry for the Co(II) ion.[20]

For the Ni(II) complexes **3** and **7**, the values for the magnetic moments were 3.38 and 2.80 μ_B, respectively. These values are within the range (2.8–3.5 μ_B) found for paramagnetic complexes of Ni(II) with octahedral geometry.[20]

The Zn(II) complexes **4** and **8** were diamagnetic, as expected for complexes of metal ions with a d^{10} configuration.

Electronic spectra

The data of the electronic spectra of the ligands and those of complexes **1**–**8** are given in Table VI. The spectrum of isoniazid presented two bands in the UV interval at 42372 and 37037 cm^{-1}, assigned to $\pi \rightarrow \pi^*$ and $n \rightarrow \pi^*$ transitions, respectively, and that of INNMH also exhibited two bands at 39682 and 30864 cm^{-1}, assigned to the same transitions, $\pi \rightarrow \pi^*$ and $n \rightarrow \pi^*$, respectively.

TABLE VI. Electronic spectral data and geometries for the ligands and their complexes

Complex	ν / cm^{-1}	Assignments	Geometry	$10Dq$ / cm^{-1}	B	β
INH	42372	$\pi \rightarrow \pi^*$	–	–	–	–
	37037	$n \rightarrow \pi^*$				
$[Cu(INH)(ac)_2]_2 \cdot 3H_2O$ (**1**)	34482	$\pi \rightarrow \pi^*$	Octahedral	–	–	–
	29411	$n \rightarrow \pi^*$				
	13404	$xy \rightarrow x^2-y^2$				
	11467	$z^2 \rightarrow x^2-y^2$				
$[Co(INH)(ac)_2] \cdot 3H_2O$ (**2**)	40983	$\pi \rightarrow \pi^*$	Octahedral	2188	592	0.609
	36764	$n \rightarrow \pi^*$				
	24390	$^4T_{1g} \rightarrow {}^4T_{1g}(P)$				
	11037	$^4T_{1g}(F) \rightarrow {}^4A_{2g}$				
	8849	$^4T_{1g} \rightarrow {}^4T_{2g}$				
$[Ni(INH)(ac)_2] \cdot 2H_2O$ (**3**)	40000	$\pi \rightarrow \pi^*$	Octahedral	9225	893.2	0.867
	33745	$n \rightarrow \pi^*$				
	25641	$^3A_{2g} \rightarrow {}^3T_{1g}(P)$				
	15432	$^3A_{2g} \rightarrow {}^3T_{1g}$				
	9225	$^3A_{2g} \rightarrow {}^3T_{2g}$				
$[Zn(INH)(ac)_2] \cdot 2H_2O$ (**4**)	39062	$\pi \rightarrow \pi^*$	Octahedral	–	–	–
	34246	$n \rightarrow \pi^*$				
INHNA	39682	$\pi \rightarrow \pi^*$	–	–	–	–
	30864	$n \rightarrow \pi^*$				
$[Cu(INNMH)(ac)_2]_2 \cdot 4H_2O$ (**5**)	39062	$\pi \rightarrow \pi^*$	Octahedral	–	–	–
	28409	$n \rightarrow \pi^*$				
	14204	$xy \rightarrow x^2-y^2$				
	7246	$z^2 \rightarrow x^2-y^2$				
$[Co(INNMH)(ac)_2] \cdot 4H_2O$ (**6**)	45045	$\pi \rightarrow \pi^*$	Octahedral	–	–	–
	28409	$n \rightarrow \pi^*$				
	17667	$^4T_{1g} \rightarrow {}^4T_{1g}(P)$				
	10000	$^4T_{1g} \rightarrow {}^4T_{2g}$				

TABLE VI. Continued

Complex	ν / cm^{-1}	Assignments	Geometry	10Dq / cm^{-1}	B	β
[Ni(INNMH)(ac)$_2$]·2H$_2$O (**7**)	37593	$\pi \rightarrow \pi^*$	Octahedral	10309	1014	0.984
	28901	$^3A_{2g} \rightarrow {}^3T_{1g}(P)$				
	17241	$^3A_{2g} \rightarrow {}^3T_{1g}$				
	10309	$^3A_{2g} \rightarrow {}^3T_{2g}$				
[Zn(INNMH)(ac)$_2$]·2H$_2$O (**8**)	31250	$n \rightarrow \pi^*$	Octahedral	–	–	–

The electronic spectrum of complex **1** had two bands at 13404 and 11467 cm^{-1}, which can be attributed to the transitions $xy \rightarrow x^2–y^2$ and $z^2 \rightarrow x^2–y^2$, characteristic for a Cu(II) ion in an octahedral environment. The electronic spectrum of complex **5** showed a broad band at 14204 cm^{-1} attributed to the transition $xy \rightarrow x^2–y^2$, also corresponding to an octahedral Cu(II) ion.[21]

The electronic spectrum of the complex **2** displayed three bands at 24390, 11037 and 8849 cm^{-1}, attributed to the d–d transitions: $^4T_{1g} \rightarrow {}^4T_{1g}(P)$, $^4T_{1g}(F) \rightarrow$ $\rightarrow {}^4A_{2g}$, and $^4T_{1g} \rightarrow {}^4T_{2g}$, respectively The electronic spectrum of complex **6** displayed two bands at 17667 cm^{-1} and 10000 cm^{-1}. These transitions are consistent with the characteristic octahedral geometry.[21]

Both electronic spectra of the Ni(II) complexes, **3** and **7**, exhibited three bands at: 25641, 15432 and 9225 cm^{-1}, and 28901, 17241 and 10309 cm^{-1}, respectively, attributed to the transitions $^3A_{2g} \rightarrow {}^3T_{1g}(P)$, $^3A_{2g} \rightarrow {}^3T_{1g}$ and $^3A_{2g} \rightarrow$ $\rightarrow {}^3T_{2g}$, respectively, which are characteristic of an octahedral geometry.[21]

The values for the parameters 10Dq, B and β for the Co and Ni complexes were calculated using formulas of Konig[22] and they are presented in Table VI.

In the spectra of the Zn(II) complexes **4** and **8**, as expected, there were only the bands characterizing the ligand, but displaced to lower values compared with the corresponding bands in the spectrum of the free ligand, which proves the coordination of the ligands to the metal ion.

EPR spectra

The EPR spectra of the Cu(II) complexes **1** and **5** (Figs. 2a and 2b, respectively), measured at room temperature using polycrystalline powders, were analyzed. Complex **1** exhibited no signal, while for complex **5**, the "g" parameter had only one value ($g_{isotropic}$ = 2.1). These values and the spectral rate indicate that both Cu(II) complexes could be dimeric.

Thermogravimetric analysis

The results of the thermal analysis of complexes **1–8** are given in Table VII.

The TG curves of these complexes indicated the presence of water molecules outside the coordination and the final products were the corresponding metal oxides. The decomposition occurred in three stages, represented generally as follows:

$$[M(L)(ac)_2]_x \cdot yH_2O \rightarrow x[M(L)(ac)_2] \rightarrow xMO \quad (1)$$

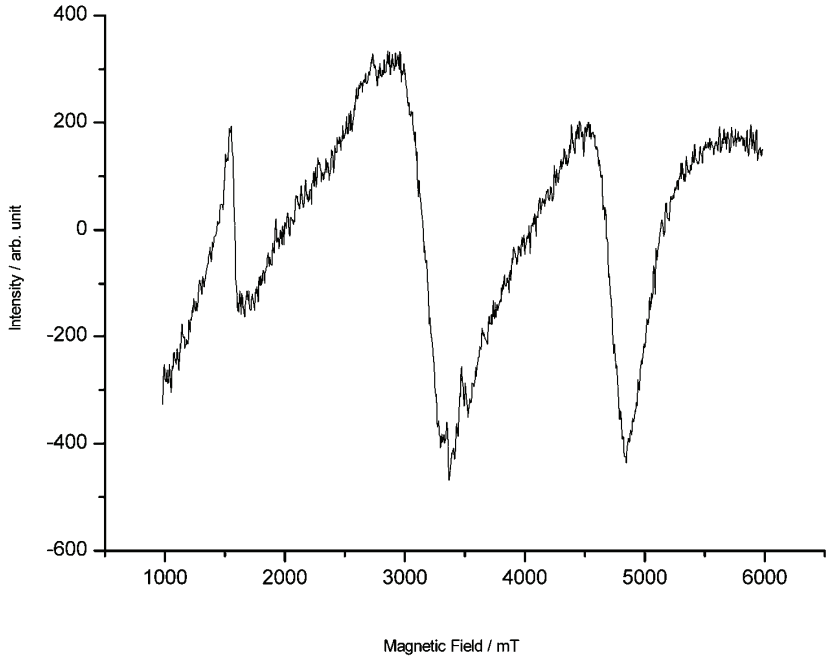

(a)

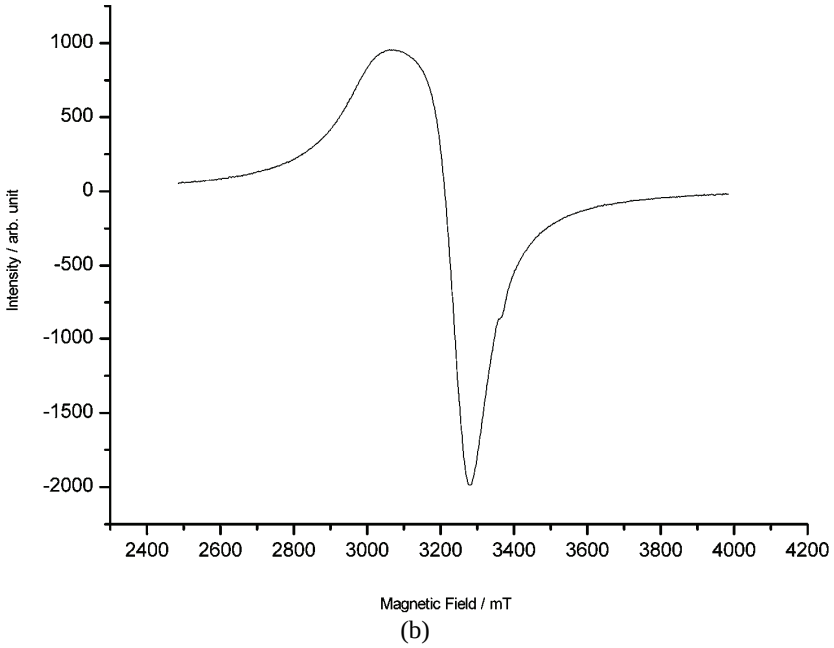

(b)

Fig. 2. The room temperature EPR spectra for complex **1** (a) and **5** (b).

where L = INH or INNMH; M = Co, x = 1, y = 3 for INH and y = 4 for INNMA; M = Ni or Zn, x = 1, y = 2 in for both ligands; M = Cu, x = 2, y = 3 for INH and y = 4 for INNMA.

The mass losses were accompanied by exothermic effects.

TABLE VII. Thermal data for the complexes **1**–**8**

Complex	Decomp. temp. °C	Lost fragment	Weight loss, %	
			Experimental	Theoretical
$[Cu(INH)(ac)_2]_2 \cdot 3H_2O$ (**1**)	19–119	$3H_2O$	8.619	8.019
	119–800	2INH, $2CO_2$	52.389	53.78
	>800	residue 2CuO	32.054	31.406
$[Co(INH)(ac)_2] \cdot 3H_2O$ (**2**)	25–113	$3H_2O$	15.767	14.67
	113–928	INH, $2CO_2$	60.384	61.125
	>928	residue CoO	23.849	20.350
$[Ni(INH)(ac)_2] \cdot 2H_2O$ (**3**)	20–103	$2H_2O$	10.238	10.685
	103–400	INH, $2CO_2$	63.968	63.942
	400–800	residue NiO	21.223	24.009
$[Zn(INH)(ac)_2] \cdot 2H_2O$ (**4**)	18–227	$2H_2O$	11.605	10.10
	227–360	$2CO_2$	31.039	30.83
	360–472	INH	38.864	38.45
	472–800	residue ZnO	23.74	22.82
$[Cu(INNMH)(ac)_2]_2 \cdot 4H_2O$ (**5**)	20–201	$4H_2O$	8.52	7.267
	201-280	INNMH	29.519	28.046
	280–807	INNMH	27.982	28.046
	>807	residue 2CuO	32.106	33.764
$[Co(INNMH)(ac)_2] \cdot 4H_2O$ (**6**)	51–202	$4H_2O$	10.38	11.155
	202–407	INNMH, $2CO_2$	75.705	74.97
	407–943	residue CoO	13.91	15.34
$[Ni(INNMH)(ac)_2] \cdot 2H_2O$ (**7**)	20–110	$2H_2O$	9.323	7.378
	110–800	INNMH, $2CO_2$	74.224	75.0014
	>800	residue NiO	15.978	15.711
$[Zn(INNMH)(ac)_2] \cdot 2H_2O$ (**8**)	18-–272	$2H_2O$	6.595	7.281
	272–513	INHNA, $3CO_2$	80.659	82.875
	513–800	Residue ZnO	12.746	13.44

CONCLUSIONS

Eight new complexes of Cu(II), Co(II), Ni(II) and Zn(II) with isoniazid (INH) and isonicotinic acid (1-naphthylmethylene)hydrazide (INNMA) ligands were synthesized and characterized. Based on all results obtained by elemental analysis, IR, electronic and EPR spectroscopy, magnetic measurements and thermogravimmetric analysis, the structural formulae presented in Figs. 3a–d are proposed for complexes **1**–**8**.

The structure of the INNMH was established in a single crystal X-ray study. Both ligands act as a bidentate through the oxygen and nitrogen in the Co(II), Ni(II) and Zn(II) complexes. The Cu(II) complexes are dimeric, with four brid-

ges between the acetate ions and Cu(II). The number of water molecules of crystallization was determined by differential thermal analysis.

Supplementary material. Crystallographic data for the structure in this article have been deposited with the Cambridge Crystallographic Data Centre, CCDC number: CCDC 727344. This data can be obtained free of charge at http://www.ccdc.cam.ac.uk/deposit (or from the Cambridge Crystallographic Data Centre, 12, Union Road, Cambridge, CB2 1EZ, UK; Tel: (44) 1223 762910; Fax: (44) 1223 336033; E-mail: deposit@ccdc.cam.ac.uk).

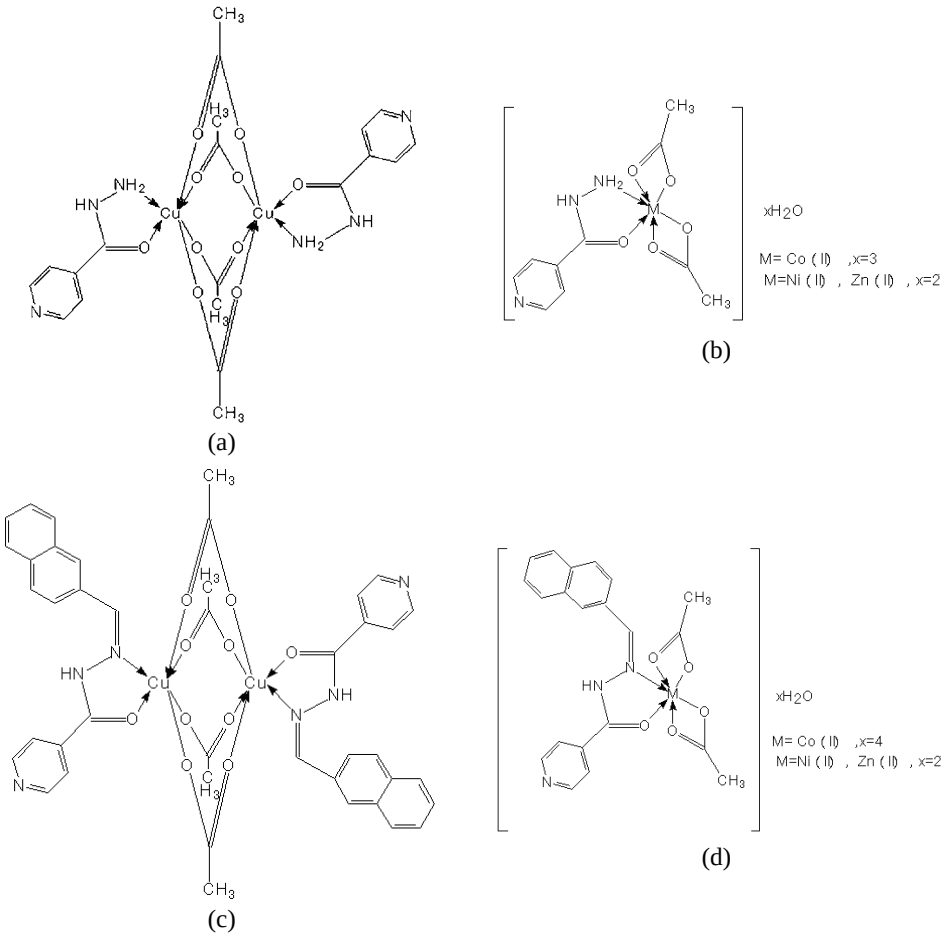

Fig. 3. The structural formula proposed for the a) $[Cu(INH)(ac)_2]_2$ complex, b) $[M(INH)(ac)_2]$ type of complexes, M = Co(II), Ni(II) or Zn(II), c) $[Cu(INNMH)(ac)_2]_2$ complex and d) $M(INNMH)(ac)_2]$ type of complexes, M = Co(II), Ni(II) or Zn(II).

ИЗВОД

СИНТЕЗА И СТРУКТУРНО ПРОУЧАВАЊЕ КОМПЛЕКСА Cu, Co, Ni И Zn СА ХИДРАЗИДОМ ИЗОНИКОТИНСКЕ КИСЕЛИНЕ И (1-НАФТИЛМЕТИЛЕН)ХИДРОЗИДОМ ИЗОНИКОТИНСКЕ КИСЕЛИНЕ

ANGELA KRIZA[1], LUCICA VIORICA ABABEI[2], NICOLETA CIOATERA[3], ILEANA RĂU[4] И NICOLAE STĂNICĂ[5]

[1]University of Bucharest, Chemistry Faculty, 23, Dumbrava Rosie Street, Bucharest, [2]The House of Teaching Staff Giurgiu, 8, Nicholae Droc Barcian Street, Giurgiu, [3]University of Craiova, Chemistry Faculty, 107 I, Calea Bucuresti Street, Craiova, [4]Polytechnic Institute of Bucharest, Faculty of Applied Chemistry and Materials Science, 1, Polizu Steet, 011061 Bucharest and [5]Romanian Academy, Chemistry-Physics Institute, 202 Independence Avenue, 77208 Bucharest, Romania

Добијено је и окарактерисано осам нових комплекса Cu(II), Co(II), Ni(II) и Zn(II) са изонијазидом (INH) и (1-нафтилметилен)хидразидом изоникотинске киселине (INNMH) опште формуле $[M(INH)(ac)_2]$, $[M(INNMH)(ac)_2]$ (M = Co(II), Ni(II) и Zn(II)), односно $[Cu(INH)(ac)_2]_2$, $[Cu(INNMH)(ac)_2]_2$. Сви комплекси су окарактерисани елементалном анализом, IR, UV–VIS–NIR и EPR спектроскопијом, као и термичком анализом, одређивањем моларне проводљивости и магнетних момената. Структура INNMH хидразона је утврђена рендгенском структурном анализом на моно-кристалу. Оба лиганда се координују за метал преко N,O у свим комплкесима. Комплекси Cu(II) су димерни, са четири ацетато јона који премошћују Cu(II).

(Примљено 15. априла, ревидирано 11. септембра 2009)

REFERENCES

1. S. Zommer, T. Lipiec, *Acta Pol. Pharm.* **20** (1963) 229
2. J. W. Munson, K. A. Connors, *J. Pharm. Sci.* **61** (1972) 211
3. K. K. Narang, P. Vinod, *Synth. React. Inorg. Met-Org. Chem.* **2** (1996) 191
4. R. N. Pandey, S. Sarita, *Orient. J. Chem.* **11** (1994) 145
5. A. M. Donia, S. A. Amer, M. M. Ayad, *Thermochim. Acta* **137** (1989) 189
6. P. P. T. Sah, S. A. Peoples, *J. Am. Pharm. Assoc.* **43** (1954) 513
7. E. M. Bavin, D. J. Drain, M. Seiler, D. E. Seymour, *J. Pharm. Pharmacol*. **4** (1954) 844
8. P. H. Buu-Hoi, D. Xuong, H. Nam, F. Binon, R. Royer, *J. Chem. Soc*. (1953) 1358
9. Z. H. Chohan, S. K. A. Sheazi, *Synth. React. Inorg. Met.-Org. Chem.* **29** (1999) 105
10. A. Kriza, L. Mitu, N. Stănică, *Rev. Chim. Bucharest* **2** (2005) 137
11. L. Mitu, A. Kriza, *Asian J. Chem.* **19** (2007) 658
12. A. I. Vogel, *A text book of quantitative inorganic analysis*, 2nd ed., Longmans, London, UK, 1961
13. Stoe & Cie, X-AREA, version 1.18, Stoe & Cie, Darmstadt, Germany, 2002
14. G. M. Sheldrick, *SHELXS-97, A program for the solution of crystal structures*, University of Gottingen, Germany, 1997
15. G. M. Sheldrick, *SHELXL-97, A program for the solution of crystal structures*, University of Gottingen, Gottingen, Germany, 1997
16. A. Kriza, C. Pîrnău, N. Popa, *Rev. Chim. Bucharest* **52** (2001) 346 (in Romanian)
17. K. Nakamoto, *Infrared spectra of inorganic and coordination compounds*, 2nd ed., Wiley-Interscience, New York, USA, 1970
18. G. B. Deacon, R. J. Philips, *Coord. Chem. Rev.* **23** (1980) 227

19. B. Singh, K. K. Narang, R. Srivastava, *Synth. React. Inorg. Met.-Org. Chem.* **32** (2002) 1577
20. R. K Agarwal, D. Sharma, L. Shing, H. Agarwal, *Bioinorg. Chem. Appl*. **2006** (2006) 29238
21. A. B. P Lever, *Inorganic electronic spectroscopy*, Elsevier, Amsterdam, 1984
22. E. Konig, *Structure Bonding* **9** (1971) 175.

Journal of the Serbian Chemical Society
JSCS@tmf.bg.ac.rs • www.shd.org.rs/JSCS

J. Serb. Chem. Soc. *75* (2) 243–248 (2010)
JSCS–3956

UDC 547.587.51–3+541.124.7+
519.687+543.554
Original scientific paper

Computer programs for calculating pK_a: a comparative study for 3-(3-(2-nitrophenyl)prop-2-enoyl)-2*H*-1-benzopyran-2-one

SELMA ŠPIRTOVIĆ-HALILOVIĆ* and DAVORKA ZAVRŠNIK

Department of Pharmaceutical Chemistry, Faculty of Pharmacy, University of Sarajevo, Čekaluša 90, Sarajevo, Bosnia and Herzegovina

(Received 1 July, revised 20 August 2009)

Abstract: Coumarin-based compounds containing a chalcone moiety exhibit antimicrobial activity. These substances are potential drugs and it is important to determine their pK_a values. However, they are almost insoluble in water. The dissociation constant was experimentally determined by potentiometric titration for 3-[3-(2-nitrophenyl)prop-2-enoyl]-2*H*-1-benzopyran-2-one because this compound shows good activity and solubility. A number of different computer programs for the calculation of the dissociation constant of chemical compounds have been developed. The pK_a value of the target compound was calculated using three different computer programs, *i.e.*, the ACD/pK_a, CSpKaPredictor and ADME/ToxWEB programs, which are based on different theoretical approaches. The analysis demonstrated good agreement between the experimentally observed pK_a value of 3-[3-(2-nitrophenyl)prop-2-enoyl]-2*H*-1-benzopyran-2-one and the value calculated using the computer program CSpKa.

Keywords: coumarin-based compounds; dissociation constant; computer programs; potentiometric titration.

INTRODUCTION

The presence of a reactive *α,β*-unsaturated keto function in chalcones was found to be responsible for their antimicrobial activity. The properties of this keto function may be altered depending on the type and position of substituents on the aromatic rings.[1]

From 3-acetyl-4-hydroxy-2*H*-1-benzopyran-2-one using an appropriate aromatic aldehyde with pyridine and piperidine as catalysts, two of chalcones were synthesized. The course of the reaction is presented in a previous work.[2]

Bearing in mind the potential of these compounds to be employed as drugs, it is important to investigate their dissociation constant (pK_a). Knowledge of the acid dissociation constant of a molecule is a critical step toward understanding its structure and reactivity.[3]

* Corresponding author. E-mail: selmaspirtovic@yahoo.com
doi: 10.2298/JSC1002243S

The acid–base ionization/dissociation constant, pK_a, is a measure of the tendency of a molecule or ion to keep a proton (H^+) at its ionization center(s) and is related to the ionization ability of chemical species. The pK_a value is the core property of an electrolyte that defines chemical and biological behavior. In biological terms, the pK_a is important in determining whether a molecule will be taken up by aqueous tissue components or lipid membranes and is related to log *P* (the partition coefficient).

The widespread application of pK_a in chemistry and drug design explains the need for quick procedures to quantify the acid dissociation constant. As experimental measurements are time consuming and difficult, computational methods are very valuable tools for calculation of pK_a for large sets of compounds, particularly at the screening stage. A number of different computer programs for prediction have recently been developed.[4]

In this study, three computer programs, based on different theoretical approaches for predicting pK_a values, were compared with experimental data.

The aim of this work was to correlate the experimentally determined and calculated pK_a values for 3-[3-(2-nitrophenyl)prop-2-enoyl]-2*H*-1-benzopyran-2-one using three different computer programs.

EXPERIMENTAL

*Potentiometric determination of p*K$_a$

The pK_a value for 3-[3-(2-nitrophenyl)prop-2-enoyl]-2*H*-1-benzopyran-2-one was evaluated by potentiometric titration with a 0.005 M solution NaOH. From the stock solution (0.090 g 3-[3-(2-nitrophenyl)prop-2-enoyl]-2*H*-1-benzopyran-2-one in 8.25 g DMSO), solutions with different H_2O contents were made:

– 6.45 % H_2O (1.0 mL stock solution of 3-[3-(2-nitrophenyl)prop-2-enoyl]-2*H*-1-benzopyran-2-one, 12.6 g DMSO and 0.94 g H_2O);

– 7.83 % H_2O (1.0 mL stock solution of 3-[3-(2-nitrophenyl)prop-2-enoyl]-2*H*-1-benzopyran-2-one, 12.4 g DMSO and 1.14 g H_2O);

– 31.2 % H_2O (1.0 mL stock solution of 3-[3-(2-nitrophenyl)prop-2-enoyl]-2*H*-1-benzopyran-2-one, 9.0 g DMSO and 4.53 g H_2O);

– 40.0 % H_2O (1.0 mL primary solution of 3-[3-(2-nitrophenyl)prop-2-enoyl]-2*H*-1-benzopyran-2-one, 7.72 g DMSO and 5. 81 g H_2O).

The substance was dissolved in the organic solvent (DMSO) and diluted with water to avoid precipitation. This is followed by four titrations of the system water/DMSO, with different DMSO contents.

The solution was then titrated with 0.25 mL aliquots of a 0.005 M NaOH solution, under constant stirring using a magnetic mixer; the pH was measured after each added aliquot. The procedure was repeated until the pH value of the titrated solution reached and kept a constant value with further addition of aliquots. The dissociation constant of the tested coumarin derivative, with a given content of the solvent DMSO/H_2O was read from the potentiometric curve, using the semi-neutralization point where pH = pK_a.Through extrapolation of the results for pK_a at different DMSO contents, the pK_a value of the tested substance in pure aqueous medium was obtained.[5,6]

The program CurveExpert 1.3. was used for statistical analysis of the data and regression analysis.

Calculation methods

A number of different computer programs for the calculation dissociation constants of chemical compounds have been developed. The quality of these programs was evaluated by how well the computed pK_a values agreed with the experimentally determined pK_a value for the investigated compound. In this work, the SMILES (Simplified Molecular Input Line Entry System) notation created by the structure drawing program CambridgeSoft's ChemDrawPro was used as the chemical structure input.

ACD/pKa is a program which quickly and accurately predicts the acid–base ionization constant of a wide range of organic compounds. It uses Hammett equations derived from a library of highly curated compounds to predict an aqueous pK_a value. In addition, two reference databases are available that offer quick look-ups of published data: one contains > 31000 experimental pK_a values for approximately 16000 compounds in aqueous solutions; the other provides experimental data for more than 2000 molecules in non-aqueous solvents. This software is used by the majority of pharmaceutical and API companies worldwide and has been tested on a wide variety of chemical classes.[7-9]

The CSpKaPredictor program selects descriptors and searches for the optimal relation between pK_a values obtained through experiment and pK_a values obtained using the SpKa predictor. The program uses 519 topological and "E-state" descriptors that determine the electron availability for non-covalent, inert-molecular interactions in each atom.[10] 158 of the 519 descriptors are new molecular descriptors developed at ChemSilico. In order to validate the prediction results, cross-validations between the experimentally obtained pK_a values and the values predicted using the CSpKa predictor were performed.

ADME/ToxWEB consults powerful ADME and Tox prediction on-line systems from the Pharma Algorithms Company. ADME/ToxWEB is a scalable version of ADME Boxes and Tox Boxes designed to fit into departmental and corporate collaborative networks. ADME/ /ToxWEB has the flexible modular architecture of ADME and Tox Boxes while also offering powerful interface customization possibilities and direct programmatic access to its modules. With this prediction system, users can predict all the following: toxicity, acute toxicity (mouse and rat); genotoxicity, health effects (blood, liver, lungs); ADME, overall oral bioavailability, pK_a values, log *D* values, substrate and inhibitor specificity, solubility in pure water and in buffer, active transport properties, absorption, physicochemical properties, *etc*.

RESULTS AND DISCUSSION

Given that the derivates are almost insoluble in water, the dissociation constant was determined by the conventional method adjusted to the tested compound. The values of pK_a for 3-[3-(2-nitrophenyl)prop-2-enoyl]-2*H*-1-benzopyran-2-one in the system DMSO:H_2O were established through potentiometric titration by determining the pH values at the point of semi-neutralization, where pH = pK_a. The potentiometric titrations of 3-[3-(2-nitrophenyl)prop-2-enoyl]-2*H*--1-benzopyran-2-one with NaOH in the system DMSO:H_2O were performed in triplicate. The changes of the pH during the titration of 3-[3-(2-nitrophenyl)prop--2-enoyl]-2*H*-1-benzopyran-2-one in the DMSO:H_2O system having different contents of water are shown in Table I.

The titration curves for 3-[3-(2-nitrophenyl)prop-2-enoyl]-2*H*-1-benzopyran--2-one with NaOH in systems having different ratios of DMSO:H_2O are shown in Figs. 1a–1d.

TABLE I. Changes of pH during the titration of 3-[3-(2-nitrophenyl)prop-2-enoyl]-2*H*-1-benzopyran-2-one in DMSO:H_2O systems having different contents of water

V(NaOH) / mL	6.45 % H_2O	7.83 % H_2O	31.1 % H_2O	40.0 % H_2O
0	4.22	4.18	4.36	4.47
0.25	4.39	4.19	4.39	4.54
0.50	4.49	4.23	4.51	4.62
0.75	4.57	4.35	4.56	4.79
1.00	4.65	4.44	4.66	4.84
1.25	4.70	4.56	4.85	5.01
1.50	4.80	4.66	5.04	5.23
1.75	4.89	4.76	5.26	5.41
2.00	4.99	4.92	5.93	6.32
2.25	5.14	5.10	6.93	7.48
2.50	5.40	5.55	7.59	7.94
2.75	6.10	7.88	8.17	8.64
3.00	8.28	9.41	9.59	9.99
3.25	9.50	14.13	11.35	12.02
3.50	14.14	14.31	12.20	12.14
3.75	14.23	14.49	12.51	12.48
4.00	14.28	14.58	12.63	12.53
4.25	14.35	14.61	12.70	12.54
4.50	14.36	14.63	12.72	12.55
4.75	14.38	14.63	12.74	15.55
5.00	14.38	14.63	12.75	12.55
5.25	14.38	14.63	12.75	12.55

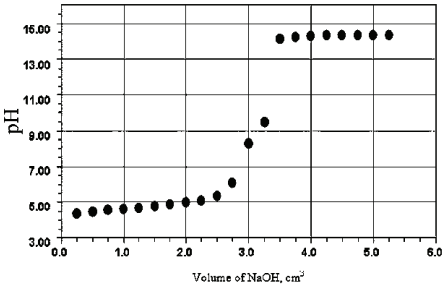

(a)

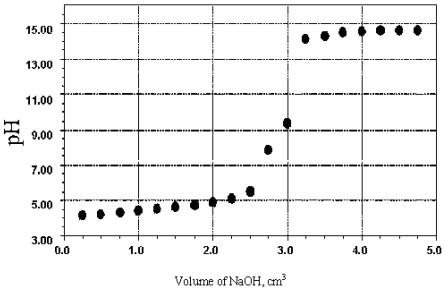

(b)

Fig. 1. Titration curves of 3-[3-(2-nitrophenyl)-prop-2-enoyl]-2*H*-1-benzopyran-2-one with NaOH in systems having a different ratio of solvents. a) H_2O:DMSO = 6.4:93.6 and b) H_2O:DMSO = = 7.8:92.2.

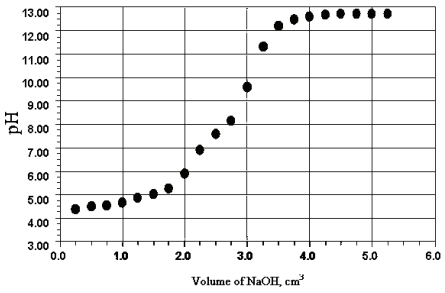

(c)

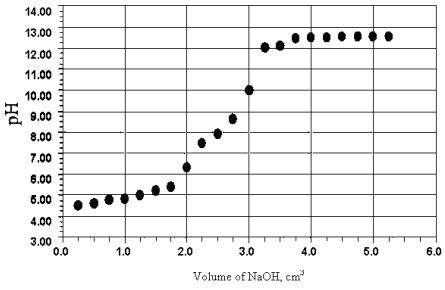

(d)

Fig. 1 continued. Titration curves of 3-[3-(2-nitrophenyl)prop-2-enoyl]-2*H*-1-benzopyran-2-one with NaOH in systems having a different ratio of solvents. c) H_2O:DMSO = 31.1:68.9 and d) H_2O:DMSO = 40.0:60.0.

Through extrapolation of the results for pK_a at different DMSO contents (60.0–93.6 %), Fig. 2, the theoretic pK_a value of the tested substance in pure aqueous water medium (DMSO, 0 %), p$K_a \approx 6.0$, was obtained.

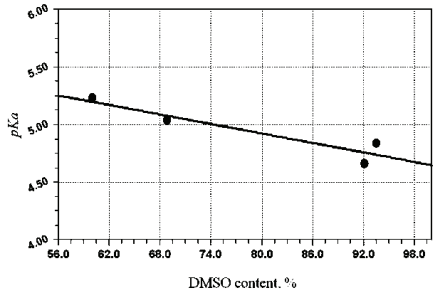

Fig. 2. Plot of the pK_a value obtained at different DMSO contents (60.0–93.6 %) *vs.* the content of DMSO. By extrapolation to zero content of DMSO, the pK_a value of the tested substance in pure aqueous medium, p$K_a \approx 6.0$, is obtained.

All the computer programs showed themselves to be relatively simple. The best correlation between the experimentally determined and the calculated pK_a values was found for the CSpKa program, ΔpK_a (log pK_a(exp) – log pK_a(cal)) = 0.56.

CONCLUSIONS

Three calculation methods, based on different theoretical approaches, were studied and the calculated pK_a values for 3-[3-(2-nitrophenyl)prop-2-enoyl]-2*H*--1-benzopyran-2-one were correlated with the experimentally determined pK_a values. The analysis showed that the agreement between the experimentally ob-

served pK_a value and the value calculated by the CSpKa program was the best. To obtain a reliable picture on the applicability of the calculation methods in pK_a studies of this kind of coumarin compounds, a larger number of substances with varying pK_a values should be studied.

И З В О Д

КОМПЈУТЕРСКИ ПРОГРАМИ ЗА РАЧУНАЊЕ pK_a: КОМПАРАТИВНА СТУДИЈА 3-[3-(2-НИТРОФЕНИЛ)ПРОП-2-ЕНОИЛ]-2*H*-1-БЕНЗОПИРАН-2-ОНА

SELMA ŠPIRTOVIĆ-HALILOVIĆ и DAVORKA ZAVRŠNIK

Department of Pharmaceutical Chemistry, Faculty of Pharmacy, University of Sarajevo, Čekaluša 90, Sarajevo, Bosnia and Herzegovina

Једињења кумаринског типа, са халконском групом у својој структури, показала су антимикробну активност. Ове супстанце су потенцијални лекови, па им је важно одредити pK_a вредности. Вредност pK_a за 3-[3-(2-нитрофенил)проп-2-еноил]-2*H*-1-бензопиран-2-он експериментално је одређена потенциометријском титрацијом и израчуната уз употребу три различита компјутерска програма. Ова супстанца је скоро нерастворна у води, па је њена константа дисоцијације одређена уз употребу конвенционалне методе. Развијен је већи број различитих компјутерских програма за рачунање константе дисоцијације хемијских једињења. У нашем раду коришћена су три компјутерска програма базирана на различитим теоријским приступима: ACD/pK_a програм, CSpKaPredictor и ADME/ToxWEB програм. У нашем испитивању утврђено је најбоље слагање између експериментално добијене pK_a вредности за 3-[3-(2-нитрофенил)проп-2-еноил]-2*H*-1-бензопиран-2-он и вредности добијене компјутерским програмом CSpKaPredictor.

(Примљено 1. јула, ревидирано 20. августа 2009)

REFERENCES

1. Y. R. Prasad, P. R. Kumar, D. J. Smiles, P. A. Babu, *ARKIVOC* **11** (2008) 266
2. D. Završnik, F. Bašić, F. Bečić, E. Bečić, S. Jažić, *Period. Biol.* **105** (2003) 137
3. S. G. Tajc, B. S. Tolbert, R. Basavappa, B. L. Miller, *J. Am. Chem. Soc.* **126** (2004) 10508
4. M. Kelen, N. Sanli, *J. Braz. Chem. Soc.* **20** (2009) 67
5. L. Z. Benet, J. E. Goyan, *J. Pharm. Sci.* **56** (1967) 665
6. A. Avdeef, J. E. A. Comer, S. J. Thomson, *Anal. Chem.* **65** (1993) 42
7. P. Ertl, Quant. Struct. Act. Relat. **16** (1997) 377
8. R. F. Rekker, A. M. Laak, R. Mannhold, *Quant. Struct. Act. Relat.* **12** (1993) 152
9. B. Slater, A. McCormack, A. Avdeef, J. E. Comer, *Pharm. Sci.* **83** (1994) 1280
10. L. H. Hall, L. B. Kier, *J. Mol. Graph. Model.* **20** (2001) 4.

Journal of the Serbian Chemical Society
JSCS@tmf.bg.ac.rs • www.shd.org.rs/JSCS

J. Serb. Chem. Soc. *75* (2) 249–258 (2010)
JSCS–3957

UDC 546.262.3–3+542.913:549.641:531.3+544.4
Original scientific paper

A kinetic study of CO oxidation over the perovskite-like oxide $LaSrNiO_4$

KEJUN WANG* and PING ZHONG

College of Chemistry and Life Sciences, Gannan Normal University, Ganzhou 341000, China

(Received 27 October 2008, revised 3 September 2009)

Abstract: The effect of reactant/product concentrations, reaction temperature and contact time on CO oxidation was investigated, using the perovskite-like oxide $LaSrNiO_4$ as the catalyst. It was found that the reaction order of CO (reactant), as well as that of CO_2 (product), is negative, the reaction orders for CO and CO_2 being –0.32 and –0.51, respectively. However, the reaction order for O_2 is positive, having a value of 0.62. The negative reaction order of CO and CO_2 might be due to their competitive adsorption with O_2, preventing the proceeding of oxygen dissociation (the rate-determining step of the reaction). The activation energy (E_a) of the reaction was calculated to be 49.3 kJ mol^{-1}; this small activation energy suggests that $LaSrNiO_4$ is a potential candidate for the CO oxidation reaction. The optimum weight hourly space velocity (WHSV) of the reaction was found to be 0.6 g s cm^{-3}. The reaction conditions in the present case were (0.5–1 % CO + 0.5–2 % O_2 + 0–2 % CO_2), with He as the balance gas.

Keywords: CO oxidation; perovskite-like oxide; $LaSrNiO_4$; kinetics; mechanism.

INTRODUCTION

Carbon oxide is one of the gases that are toxic and unwanted in the environment. The oxidation of CO is not only of interest to eliminate this poisonous compound from exhaust, but also can act as a test reaction for surface structure–activity correlation studies.[1] Many catalysts[2–10] have been investigated and used for the CO oxidation reaction. Among them, noble metal catalysts (*e.g.*, Au) can show full CO conversion even at ambient reaction temperature, but they are susceptible to sintering and are expensive, and furthermore, their activity is lowered with increasing reaction time.[7] Comparatively, perovskite-type catalysts show full CO conversion at relatively high temperatures (> 300 °C), but they have a long catalyst life and their activity can be retained irrespective of the reaction time.[1]

* Corresponding author. E-mail: wangkejun@sina.com
doi: 10.2298/JSC1002249W

Perovskite-type oxides (ABO_3) are one kind of excellent catalysts for oxidetion reactions; they have attract much attention in catalysis since the work of Libby[11] and Voorhoeve *et al.*[2] To date, many studies[1–6,12–17] have focused on the catalytic properties of perovskite-type oxides (ABO_3) in CO oxidation reaction, but little on perovskite-like oxides (A_2BO_4), consisting of alternating layers of perovskite (ABO_3) and rock-salt (AO), which also show high activity in oxidetion reactions.[18–23] In fact, the perovskite-like oxides (A_2BO_4) possess better properties than perovskite-type oxides (ABO_3) to some extent, such as: thermal stability,[24] ion exchangeability,[25] and so on. Thus, investigating the catalytic properties of perovskite-like oxides (A_2BO_4) in CO oxidation is of interest.

In the present study, the effects of reactant/product concentration, reaction temperature and contact time (*W*/*F*) on the activity of $LaSrNiO_4$ for CO oxidation were investigated. By changing the concentration of CO, O_2 and CO_2 in the feed gas, the reaction order and the kinetics of CO oxidation are discussed and deduced. The activation energy of the reaction was also calculated, in order to illustrate the usability of this system in practice.

EXPERIMENTAL

Materials

$La(NO_3)_3{\cdot}6H_2O$, A.R., Beijing Chemical Works, $Sr(NO_3)_3{\cdot}2H_2O$, C.P., Tianjin No.3 Chemical Reagent Factory, $Ni(NO_3)_2{\cdot}6H_2O$, A.R., Beijing No. 57601 Chemical Works and CO/H_2/He, H.R., Dalian Guangming Special Type Gas Co., Ltd., were employed.

Instrumentation

X-Ray diffractometer: type D/MAX-IIB, Rigaku; gas chromatograph: type 103, Shanghai Analyze Apparatus Company; temperature programmed desorption (TPD) and temperature programmed reduction (TPR): a self-made setup equipped with a thermal conductivity detector (TCD) were used.

Preparation method

The sample of $LaSrNiO_4$ was prepared by the citric acid combustion method as follows:[25,26] stoichiometric amounts of La^{3+}, Sr^{2+} and Ni^{2+} nitrates were first dissolved in deionized water, then a solution of citric acid 100 % in excess of the cations was added. The resulting solution was evaporated to dryness and subsequently, the precursors were thermal decomposed, calcined at 500 °C for 2 h, and finally pelletized and calcined in air at 900 °C for 5 h.

Characterization

The characterization of the crystal structure and the physico–chemical properties of $LaSrNiO_4$, such as XRD, O_2-TPD and H_2-TPR, were previously described in detail[25,26] and will not be repeated herein.

Activity test

The activities of CO oxidation over $LaSrNiO_4$ were performed in a single-pass flow micro-reactor made of quartz with an internal diameter of 6 mm. The reactants (0.5–1 % CO + 0.5–2 % O_2 + 0–2 % CO_2, balanced with helium) were passed through 0.2 g of catalyst at a rate of 10–30 mL/min in the temperature range of 250–325 °C. The gas compositions were analyzed before and after the reaction by an online gas chromatograph equipped with mole-

cular sieve 5A column and thermal conductivity detector (TCD). Here, the change of CO concentration was used as the means to evaluate the activity, *i.e.*, $X_{[CO]} = ([CO]_{in} - [CO]_{out})/[CO]_{in}$, where $[CO]_{in}$ and $[CO]_{out}$ are the concentration of CO measured before and after the reaction, respectively. Before the data were obtained, reactions were maintained for a period of ≈0.5 h at each temperature to ensure steady-state conditions.

RESULTS AND DISCUSSION

Effect of O_2 partial pressure

The effect of the O_2 partial pressure on the activity of CO oxidation is shown in Fig. 1. The CO conversion increased almost linearly with the O_2 partial pressure, indicating that O_2 partial pressure has large and positive effect on the CO oxidation reaction. With increasing O_2 partial pressure, the dissociation rate of O_2 molecule increases, as reported elsewhere.[27] As a result, a greater number of oxygen atoms are incumbent on the catalyst surface, giving more opportunities for CO molecular contact and reaction, and thus improving the CO conversion.

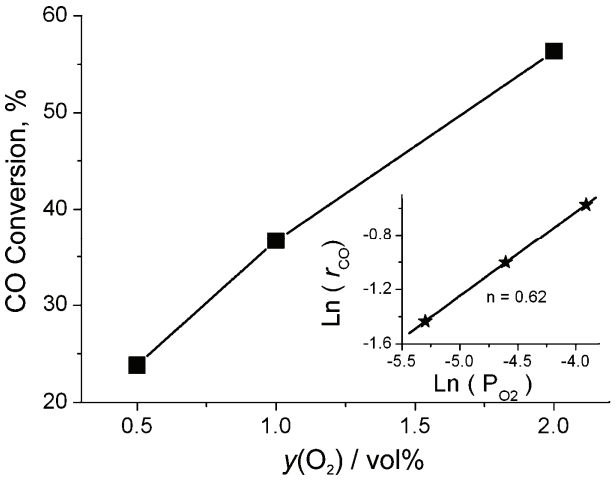

Fig. 1. Effect of oxygen partial pressure on CO conversion and the ln (r_{CO}) – ln (p_{O_2}) plot (inset) over $LaSrNiO_4$. Feed gas: 1% CO/He + 0.5–2 % O_2/He; W/F = 0.6 g s cm^{-3}, t = 300 °C.

The kinetic calculation in this study refer to the work reported by Teraoka *et al.*,[28] in which the subject was also a kinetic study of a catalytic reaction (*i.e.*, NO decomposition) over perovskite-type oxides. Thus, to determine the reaction order of O_2 in the CO oxidation reaction, it was assumed that the kinetics of CO oxidation ($2CO + O_2 \rightarrow 2CO_2$) obeys the power rate law:

$$r_{CO} = k[CO]^m[O_2]^n[CO_2]^p$$

where k is the rate constant; [CO], $[O_2]$ and $[CO_2]$ are the concentrations of CO, O_2 and CO_2 in the feed gas, respectively; m, n and p are the apparent reaction order for CO, O_2 and CO_2, respectively. When determining the reaction order of the reactant (*i.e.*, O_2), the ln r – ln $[O_2]$ values were plotted. The O_2 concentra-

tion was varied in the feed while maintaining the total flow rate constant. In the same way, the reaction order for CO and CO_2 can also be determined.

The ln r – ln [O_2] plot is also shown in Fig. 1 (inset). The plot gave a straight line with a slope of 0.62, indicating the reaction order with respect to O_2 is positive with a value of 0.62. This is different from that reported by Zhang-Steenwinkel *et al.*, who observed that O_2 is near-zero order when the CO/O_2 ratio is stoichiometric.[13]

Effect of CO partial pressure

The effect of the CO partial pressure on the activity of CO oxidation is shown in Fig. 2. It was found that the CO conversion decreased with increasing CO partial pressure and the reaction order with respect to CO was calculated to be –0.32. This is also different from the results reported by Zhang-Steenwinkel *et al.*,[13] who found that the reaction rates were facilitated by the CO partial pressure with a first reaction order. The decrease of the CO conversion found in the present study could be explained by the fact that with increasing CO partial pressure, the CO/O_2 ratio increases, which means a decrease of the O_2 partial pressure; hence, the chance for O_2 adsorption and dissociation decreases, resulting in a decrease of the CO conversion. This is in accordance with the above result, *i.e.*, a decrease of the O_2 partial pressure (which means an increase of the CO/O_2 ratio) leads to a decrease in the CO conversion. However, it should be emphasized that the total amount of CO oxidized increases with increasing CO partial pressure. For example, at 0.5 vol. % CO partial pressure, the CO conversion was 69.86 vol. %; while at 1 vol. % CO partial pressure the CO conversion was 56.33 vol. %. Thus, the total amount of CO oxidized at 0.5 vol. % CO partial pressure was (0.5×69.86) vol. %, which is lower than that at 1 vol. % CO partial pressure

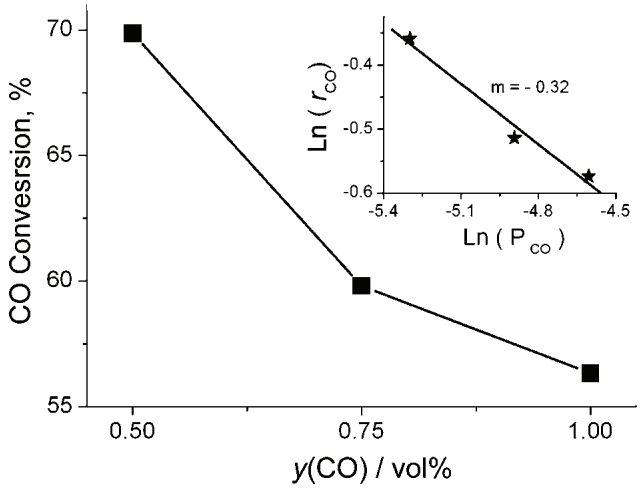

Fig. 2. Effect of CO partial pressure on CO conversion and the ln (r_{CO}) – ln (p_{CO}) plot (inset) over $LaSrNiO_4$. Feed gas: 0.5–1 % CO/He + + 2 % O_2/He; W/F = = 0.6 g s cm^{-3}, t = 300 °C.

((1×56.33) vol. %). In all, this result indicates that the CO reaction order calculated is negative in the present case (m = – 0.32, see inset in Fig. 2).

Effect of CO_2 partial pressure

It was reported that CO_2 desorption is the rate-determining step in CO oxidation,[13] which certifies the importance of the CO_2 partial pressure to the reaction rate. Hence, it was considered worthwhile to investigate the influence of CO_2 on the reaction. The change of CO conversion with CO_2 partial pressure is shown in Fig. 3 (here, the CO_2 partial pressure includes the CO_2 added in the feed gas and that produced by CO oxidation. For example, when adding 1 % CO_2 to the feed gas, the CO conversion was 60.76 % (≈0.61), then, the CO_2 partial pressure was considered to be 1.61 %). It can be seen that the CO conversion decreased progressively with increasing CO_2 partial pressure, showing the inhibitory action of CO_2 due to the difficulty of CO_2 desorption from the active sites, which decreases the chance for O_2 dissociation and hence for CO oxidation. Based on the activity data, the CO_2 reaction order in the reaction, p, was calculated to be –0.51 (see inset in Fig. 3). This certifies that the CO_2 partial pressure has indeed a large negative effect on the CO oxidation reaction.

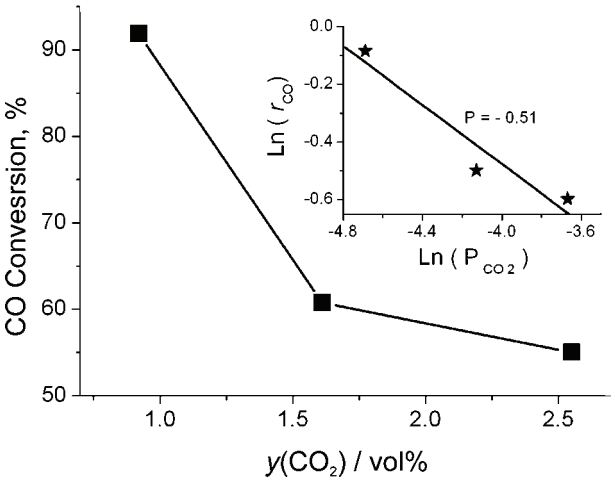

Fig. 3. Effect of CO_2 partial pressure on CO conversion and the ln (r_{CO}) – ln(p_{CO_2}) plots (inset) over $LaSrNiO_4$. Feed gas: 1% CO/He + 2 % O_2/He + 0–2 % CO_2/He; W/F = 0.6 g s cm^{-3} t = 300 °C.

Effect of reaction temperature

The plot of CO convention *vs*. reaction temperature is shown in Fig. 4. The CO conversion increase slightly at low temperatures (t < 275 °C), then a substantial increase was observed at t > 275 °C, indicating that CO oxidation over perovskite type oxides mainly occurred at high temperatures (t > 275 °C). This is similar to the results reported by Ciambelli *et al.*[1] The reason might be that above this temperature (275 °C), the oxygen that was chemically adsorbed on the catalyst surface was activated,[29] leading to the creation of oxygen vacancies and,

hence, improving the activity, since oxygen vacancies are a crucial parameter of the oxidation reaction.

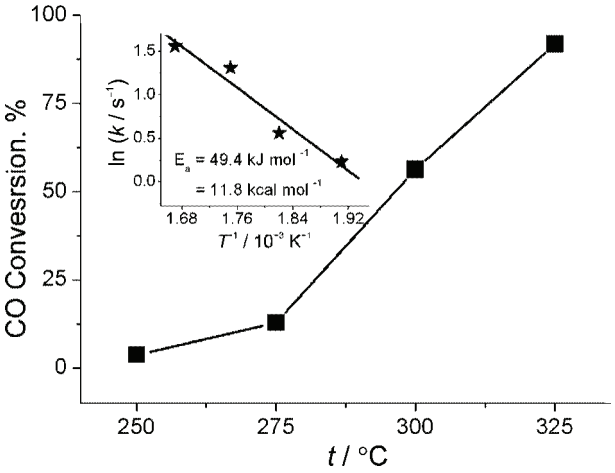

Fig. 4. Effect of reaction temperature on CO conversion and the ln k – $1/T$ plot over $LaSrNiO_4$. Feed gas: 1 % CO/He + 2 % O_2/He; W/F = 0.6 g s cm^{-3}.

On the other hand, according to the reaction order of CO, O_2 and CO_2 calculated above, the kinetics of CO oxidation could be written as:

$$-r_{CO} = k\,[CO]^{-0.32}[O_2]^{0.62}[CO_2]^{-0.51}$$

Therefore, the k value at different temperatures could be deduced. By plotting the function of ln k *vs.* $1/T$ (see inset in Fig. 4), the activation energy (E_a) is deduced. The calculated E_a value is 11.8 kcal mol^{-1}, which is far lower than that of $LaAl_{0.985}Fe_{0.015}O_3$ (18.1 kcal mol^{-1}) – the lowest activation energy for CO oxidation in the $LaAl_{1-x}Fe_xO_3$ system, as reported by Ciambelli *et al.*,[1] indicating that $LaSrNiO_4$ is a more suitable catalyst for CO oxidation.

Effect of contact time (W/F)

The effect of contact time (W/F, W = catalyst weight (g); F = flow rate of the reactant (mL/min)) on the CO oxidation reaction is shown in Fig. 5. An abrupt increase in CO conversion was observed from W/F = 0.4 to 0.6 g s cm^{-3} and then remained almost constant from W/F = 0.6 to 1.2 g s cm^{-3}. At a low contact time (W/F = 0.4 g s cm^{-3}), the CO cannot be oxidized sufficiently before elution due to the high flow rate. In other words, the catalyst is overloaded and the active sites cannot be regenerated in time for CO oxidation under this condition. As a result, only a low conversion of CO was observed. With increasing contact time or decreasing flow rate (W/F = 0.6 g s cm^{-3}), the amount of active sites used for CO oxidation could be regenerated in time, which thus leads to the abrupt increase in the CO conversion. However, only a minor increase in the CO conversion was observed when the contact time was increased further (from 0.6 to 1.2 g s cm^{-3}), which might mean that the catalyst had reached its maximal capa-

bility for CO oxidation at W/F = 0.6 g s cm^{-3}. That is to say, the optimum contact time for CO oxidation is 0.6 g s cm^{-3} under the present conditions.

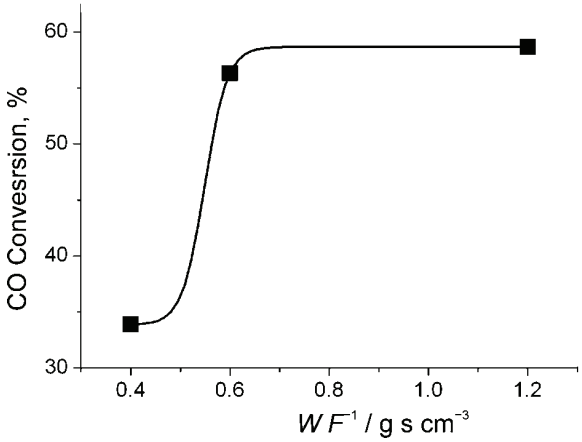

Fig. 5. Effect of contact time (W/F) on CO conversion over $LaSrNiO_4$. Feed gas: 1 % CO/He + 2 % O_2/He, t = 300 °C.

Reaction mechanisms based on the kinetic analysis

The reaction steps for CO oxidation from the literatures[13] could be described as follows:

$$O_2 + 2s \underset{k_{-1}}{\overset{k_1}{\rightleftharpoons}} 2O_s \qquad K_1 = \frac{k_1}{k_{-1}} \; ; \qquad K_{-1} = \frac{k_{-1}}{k_1}$$

$$CO + s \underset{k_{-2}}{\overset{k_2}{\rightleftharpoons}} CO_s \qquad K_2 = \frac{k_2}{k_{-2}} \; ; \qquad K_{-2} = \frac{k_{-2}}{k_2}$$

$$CO_s + O_s \underset{k_{-3}}{\overset{k_3}{\rightleftharpoons}} CO_{2s} + s \qquad K_3 = \frac{k_3}{k_{-3}} \; ; \qquad K_{-3} = \frac{k_{-3}}{k_3}$$

$$CO_{2s} \underset{k_{-4}}{\overset{k_4}{\rightleftharpoons}} CO_2 + s \qquad K_4 = \frac{k_4}{k_{-4}} \; ; \qquad K_{-4} = \frac{k_{-4}}{k_4}$$

Here, "s" is a surface active site. To determine the kinetics of CO oxidation, each step has been assumed to be the rate-determining step; accordingly, the following four equations could be deduced:

Case 1. The dissociation of oxygen is the rate-determining step:

$$-r = \frac{Nk_1 p_{O_2}}{(1 + \frac{k_{-3}k_{-4}}{k_2}\frac{p_{CO_2}}{p_{CO}} + k_2 p_{CO} + k_{-4} p_{CO_2})^2} \qquad \text{(R1)}$$

Case 2. The adsorption of CO is the rate-determining step:

$$-r = \frac{Nk_2 p_{CO}}{1 + k_1^{1/2} p_{O_2}^{1/2} \frac{k_{-3}k_{-4}}{k_1^{1/2}} \frac{p_{CO_2}}{p_{O_2}^{1/2}} + k_{-4} p_{CO_2}} \quad \text{(R2)}$$

Case 3. The formation of CO_{2s} is the rate-determining step:

$$-r = \frac{Nk_3 k_1^{1/2} k_2 p_{CO} p_{O_2}^{1/2}}{1 + k_1^{1/2} p_{O_2}^{1/2} + k_2 p_{CO} + k_{-4} p_{CO_2}} \quad \text{(R3)}$$

Case 4. The desorption of CO_2 is the rate-determining step:

$$-r = \frac{Nk_4 k_1^{1/2} k_2 k_3 p_{CO} p_{O_2}^{1/2}}{1 + k_1^{1/2} p_{O_2}^{1/2} + k_2 p_{CO} + k_1^{1/2} k_2 k_3 p_{CO} p_{O_2}^{1/2}} \quad \text{(R4)}$$

Of all these cases, only the rate equation (R1) shows a negative reaction order for CO, which was the case in the present study. Hence, oxygen dissociation is considered to be the rate-determining step and Eq. (R1) is the expression of rate equation. The apparent reaction order for CO in Eq. (R1) is between –2 and 2, which contains the value (–0.32) found in this study. The apparent reaction order for O_2 is 1, which is higher than that found in this work (0.62). The reason might be ascribed to the competitive adsorption of CO (reactant) and CO_2 (product) with O_2 for the active sites, thus decreasing the opportunity for oxygen adsorption and hence the reaction order. The apparent reaction order for CO_2 is –0.51, which is within the range appearing in Eq. (R1) (–2–0). In addition, the low value of CO_2 reaction order, –2, in Eq. (R1) suggests that, in some cases, CO_2 desorption could predominate in the reaction and become the rate-determining step.

Altogether, the present study suggests that the dissociation of oxygen is the rate-determining step of CO oxidation. Therefore, it is possible that $LaSrNiO_4$ shows an efficient activity for CO oxidation since it contains large numbers of oxygen vacancies,[26] which were reported to be very active sites for oxygen dissociation.[27] This might also be part of the reasons why noble metals can show high activity for CO oxidation even at low temperatures, since they are efficient materials for promoting oxygen dissociation at low temperatures.

CONCLUSIONS

CO oxidation on the compound oxide $LaSrNiO_4$ was investigated. Based on the CO conversion found under different conditions, the reaction order of CO, O_2 and CO_2 were determined. It was found that the reaction orders of CO and CO_2 are negative, while that of O_2 is positive with the value of 0.62, suggesting that oxygen dissociation is the rate-determining step of the reaction. The kinetics of

CO oxidation was discussed assuming each elementary step to be the rate-determining step. The activation energy of the reaction is very small (11.8 kcal mol^{-1}), which suggests that $LaSrNiO_4$ maybe a potential candidate for CO oxidation. The optimum contact time of the reaction found in the present case is 0.6 g s cm^{-3}.

Acknowledgements. This work was financially supported by the program for New Century Excellent Talents in Universities (NCET-06-0577) and the National Natural Science Foundation of China (NNSFC-20861001). The authors are greatly thankful for the sample ($LaSrNiO_4$) from and the discussion with Dr. J. Zhu in the Changchun Institute of Applied Chemistry, CAS.

И З В О Д

КИНЕТИКА ОКСИДАЦИЈЕ УГЉЕНИК(II)-ОКИДА НА ОКСИДИМА СЛИЧНИМ ПЕРОВСКИТУ $LaSrNiO_4$

KEJUN WANG и PING ZHONG

College of Chemistry and Life Science, Gannan Normal University, Ganzhou 341000, China

Испитан је утицај концентрације реактанта/производа реакције, реакционе температуре и времена контакта (*W*/*F*) на кинетику каталитичке оксидације CO на оксидима сличним перовскиту $LaSrNiO_4$. Утврђен је негативан парцијални ред реакције како у односу на реактант CO (–0,32) тако и у односу на производ реакције CO_2 (–0,51), док је ред реакције у односу на O_2 позитиван, 0,62. Негативни ред реакције у односу на CO и CO_2 потиче вероватно од њихове компететивне адсорпције са O_2, која је спори ступањ реакције. Вредност израчуната за енергију активације (E_a) је 49,3 kJ mol^{-1} и указује на то да $LaSrNiO_4$ може бити потенцијални катализатор за оксидацију CO. Оптимално време контакта за реакцију је 0,6 g s cm^{-3}. Састав реакционе смеше у хелијуму као носећем гасу је био: 0.5–1 vol % CO + + 0.5–2 vol % O_2 + 0–2 vol % CO_2.

(Примљено 27. октобра 2008, ревидирано 3. септембра 2009)

REFERENCES

1. P. Ciambelli, S. Cimino, G. Lasorella, L. Lisi, S. De Rossi, M. Faticanti, G. Minelli, P. Porta, *Appl. Catal. B* **37** (2002) 231
2. R. J. H. Voorhoeve, J. P. Remeika, P. E. Freeland, B. T. Matthias, *Science* **177** (1972) 353
3. H. Falcón, M. J. Martinez-Lope, J. A. Alonso, J. L. G. Fierro, *Appl. Catal. B* **26** (2000) 131
4. a) G. Parravano, *J. Am. Chem. Soc.* **75** (1953) 1452; b) G. Parravano, *J. Am. Chem. Soc.* **75** (1953) 1497
5. Y. Zhang-Steenwinkel, J. Beckers, A. Bliek, *Appl. Catal. A* **235** (2002) 79
6. J. J. Zhu, Z. Zhao, D. H. Xiao, J. Li, X. G. Yang, Y. Wu, *Ind. Eng. Chem. Res.* **44** (2005) 4227
7. H. L. Lian, M. J. Jia, W. C. Pan, Y. Li, W. X. Zhang, D. Z. Jiang, *Catal. Commun.* **6** (2005) 47
8. S. C. Yan, W. T. Chuang, A. Chaudhari, S. L. Lee, *Appl. Surf. Sci.* **252** (2005) 784
9. M. Manzoli, R. Di Monte, F. Boccuzzi, S. Coluccia, J. Kašpar, *Appl. Catal. B* **61** (2005) 192
10. P. Bera, K. C. Patil, M. S. Hegde, *Phys. Chem. Chem. Phys.* **2** (2000) 3715
11. W. F. Libby, *Science* **171** (1971) 499
12. Y. Teraoka, H. Nii, S. Kagawa, K. Jansson, M. Nygren, *Appl. Catal. A* **194**–**195** (2000) 35

13. Y. Zhang-Steenwinkel, L. M. Van der Zande, H. L. Castricum, A. Bliek, *Appl. Catal. B* **54** (2004) 93, and references therein
14. P. K. Gallagher, D. W. Johnson, J. P. Remeika, F. Schrey, L. E. Trimble, E. M. Vogel, R. J. H. Voorhoeve, *Mater. Res. Bull.* **10** (1975) 529
15. S. Cimino, L. Lisi, S. De Rossi, M. Faticanti, P. Porta, *Appl. Catal. B* **43** (2003) 397
16. S. Colonna, S. De Rossi, M. Faticanti, I. Pettiti, P. Porta, *J. Mol. Catal. A* **187** (2002) 269
17. H. Falcón, M. J. Martínez-Lope, J. A. Alonso, J. L. G. Fierro, *Solid State Ionics* **131** (2000) 237
18. J. J. Zhu, Z. Zhao, D. H. Xiao, J. Li, X. G. Yang, Y. Wu, *Z. Phys. Chem.* **219** (2005) 807
19. A. K. Ladavos, P. J. Pomonis, *Appl. Catal. B* **1** (1992) 101
20. T. Nitadori, M. Muramatsu, M. Misono, *Chem. Mater.* **1** (1989) 215
21. X. M. Yang, L. T. Luo, H. Zhong, *Appl. Catal. A* **272** (2004) 299
22. A. K. Ladavos, P. J. Pomonis, *Appl. Catal. A* **165** (1997) 73
23. R. J. H. Voorhoeve, L. E. Trimble, C. P. Khattak, *Mater. Res. Bull.* **9** (1974) 655
24. Z. Zhao, X. G. Yang, Y. Wu, *Appl. Catal. B* **8** (1996) 281
25. J. J. Zhu, D. H. Xiao, J. Li, X. G. Yang, Y. Wu, *J. Mol. Catal. A* **234** (2005) 99
26. J. J. Zhu, Z. Zhao, D. H. Xiao, J. Li, X. G. Yang, Y. Wu, *Electrochem. Commun.* **7** (2005) 58
27. Y. Wu, T. Yu, B. S. Dou, C. X. Wang, X. F. Xie, Z. L. Yu, S. R. Fan, L. C. Wang, *J. Catal.* **120** (1989) 88
28. Y. Teraoka, T. Harada, S. Kagawa, *J. Chem. Soc., Faraday Trans.* **94** (1998) 1887
29. N. Yamazoe, Y. Teraoka, T. Seiyama, *Chem. Lett.* (1981) 1767.

Journal of the Serbian Chemical Society
JSCS@tmf.bg.ac.rs • www.shd.org.rs/JSCS
J. Serb. Chem. Soc. 75 (2) 259–269 (2010) UDC 538.913:667.284:532.14:66.081.2+535.33
JSCS–R3958 *Original scientific paper*

DFT Studies on the electronic structures of indoline dyes for dye-sensitized solar cells

JIE XU*, GUIJIE LIANG, LUOXIN WANG, WEILIN XU, WEIGANG CUI, HUI ZHANG and ZENGCHANG LI

Key Lab of Green Processing & Functional Textiles of New Textile Materials, Ministry of Education, Wuhan University of Science & Engineering, 430073, Wuhan, Hubei, China

(Received 5 January, revised 3 September 2009)

Abstract: A series of indoline dyes with promising efficiency for dye-sensitized solar cells (DSSCs) were studied using the density functional theory at the B3LYP/6-31g (*d*) level. The ground-state geometries, electronic structures and absorption spectra of these dyes are reported. The calculated results indicate that the energy levels of the HOMOs and LUMOs of these dyes are advantageous for electron injection. Their intense and broad absorption bands as well as favorable excited-state energy levels are key factor for their outstanding efficiencies in DSSCs.

Keywords: density functional theory; indoline dyes; dye-sensitized solar cells; electronic structures.

INTRODUCTION

Due to the increasingly serious energy-demanding and environmental-concerning nature of conventional energy systems, new systems based on renewable sources have drawn more and more attention. Over the past years, significant emphasis has been put on the development and understanding of light-driven charge separation in molecular systems as methods of converting and storing solar energy. Dye-sensitized solar cells (DSSCs) have attracted widespread interest for the conversion of sunlight into electricity because of their high efficiency and low cost.[1–4]

Generally, transition metal coordination compounds (ruthenium polypyridyl complexes) are used as effective sensitizers, due to their intense charge-transfer absorption over the whole visible range and highly efficient metal-to-ligand charge transfer.[5] However, Ru polypyridyl complexes contain a heavy metal, which is undesirable from the environmental point of view.[6] Moreover, the synthesis processes of such complexes are complicated and costly. In addition to Ru com-

* Corresponding author. E-mail: xujie0@ustc.edu
doi: 10.2298/JSC1002259X

plexes, pure organic dyes as sensitizers are also under intensive investigation due to their high molar extinction coefficients, flexible structural modifications and low costs,[7] and some of them have reached good efficiency.[8–11] Indoline dyes have been reported as high-efficient sensitizers for DSSCs because of their strong and intense absorption bands in the visible region.[9,12,13]

An accepted model for a DSSC is as follows: a sensitizing dye molecule absorbs visible or near infrared light and injects an electron into a semiconductor from its excited state(s).[14] Once the electron is transferred into, for example, solid TiO_2, it proceeds through the semiconductor to an external circuit. Subsequently, the oxidized sensitizer receives an electron from an electron donor, such as an iodide ion, present in the electrolyte. Therefore, the performance of DSSC strongly depends on the following factors: 1) the absorption efficiency of the sensitizing dye for the solar light spectrum; 2) electron transfer, probably from the excited state of the sensitizing dye to TiO_2 (efficiency of the charge separation); and 3) probability of the electron transfer from the electron donor to the oxidized dye.[3] All these factors are closely associated with the structure of the ground and excited electronic states of the sensitizing dye. From this point of view, it is imperative to investigate the electronic structures of both the ground and excited states of the sensitizing dye molecule for an understanding of the mechanism of the charge separation and the electron transfer, which are the key processes in this type of solar cells. In order to design and synthesize more efficient sensitizing dyes, it is also necessary to understand the electronic structures of the existing efficient sensitizing dyes.

The density functional theory (DFT) has emerged as a reliable standard tool for the theoretical treatment of structures as well as electronic and absorption spectra. Its time-dependent extension, called time-dependent DFT (TD-DFT), can give reliable values for the valence excitation energies with standard exchange-correlation functionals. The computational cost of a TD-DFT calculation is comparative to that of a Hartree–Fock based single excitation theory, such as, configuration interaction singles (CIS) or the time-dependent Hartree–Fock (TD--HF) method, and maintains a uniform accuracy for open-shell and closed-shell systems. In recent years, TD-DFT has been extensively used to study the structures and absorption spectra of sensitizing dyes for DSSCs. Ru complexes have been widely investigated by TD-DFT calculations.[4,15–22] TD-DFT calculations have also been applied to the study of some pure organic dyes which act as sensitizers in DSSCs.[23–26] Zhang *et al.*[25] employed DFT and TD-DFT calculations to study the absorption spectra and electronic structures of a series of coumarin dyes. However, there have been relatively few attempts to investigate the electronic structures of indoline dyes.

In this study, a series of indoline dyes (shown in Fig. 1) were examined using DFT and TD-DFT. The ground-state geometries, electronic structures and

UV–Vis absorption spectra were obtained. The theoretical calculation studies provide an in-depth understanding concerning molecular structures and physical properties, which is helpful for the interpretation and prediction of optical absorption spectra of this series of indoline dyes at a molecular level.

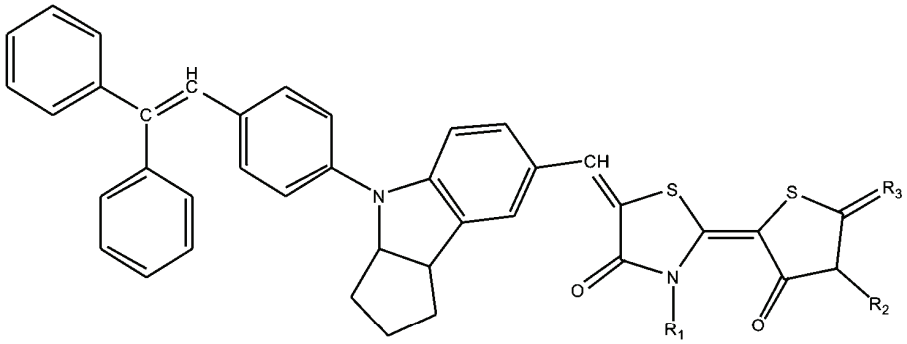

Indoline Dye	R_1	R_2	R_3
1	—CH_2COOH	—CH_2CH_3	=S
2	—CH_2COOH	—CH_2COOH	=S
3	—CH_2CH_2COOH	—CH_2CH_3	=S
4	—CH_2COOH	—CH_2CH_3	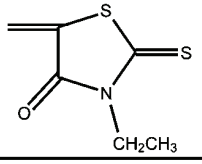

Fig. 1. Chemical structures of the indoline dyes D102, D131 and D149.

COMPUTATIONAL METHOD

All the calculations were performed using the Gaussian 03 program package.[27] The ground-state geometries were fully optimized without any symmetry constrains at the DFT level of theory with the Becke[29] three parameters hybrid functional and the Lee, Yang and Parr correlational functional B3LYP[29] sing a standard 6-31g (d) basis set on all atoms. The excitation energies and oscillator strengths for the lowest 30 singlet-singlet transitions at the optimized geometry in the ground state were obtained in TDFT calculations using the same basis set as for the ground state. According to the calculated results, the UV–Vis absorption spectra were simulated by a Gaussian convolution with a full width at half-maximum of 0.4 eV (3200 cm^{-1}).[4] Solvation effects were introduced by the SCRF method, *via* the conductor polarizable continuum model (CPCM)[30,31] implemented in the Gaussian program, for both geometry optimizations and the TD-DFT calculations.

RESULTS AND DISCUSSION

Molecular structures

The framework of the indoline dyes in this study is formed by a phenylethenyl group, an indoline ring and two or three rhodanine rings. The optimized

ground-state geometries of the four indoline dyes are shown in Fig. 2. The physical separation of the electron-donating (ED) and electron accepting groups (EA) for these dyes are quite similar (11.33±0.01 Å) although their substituent groups

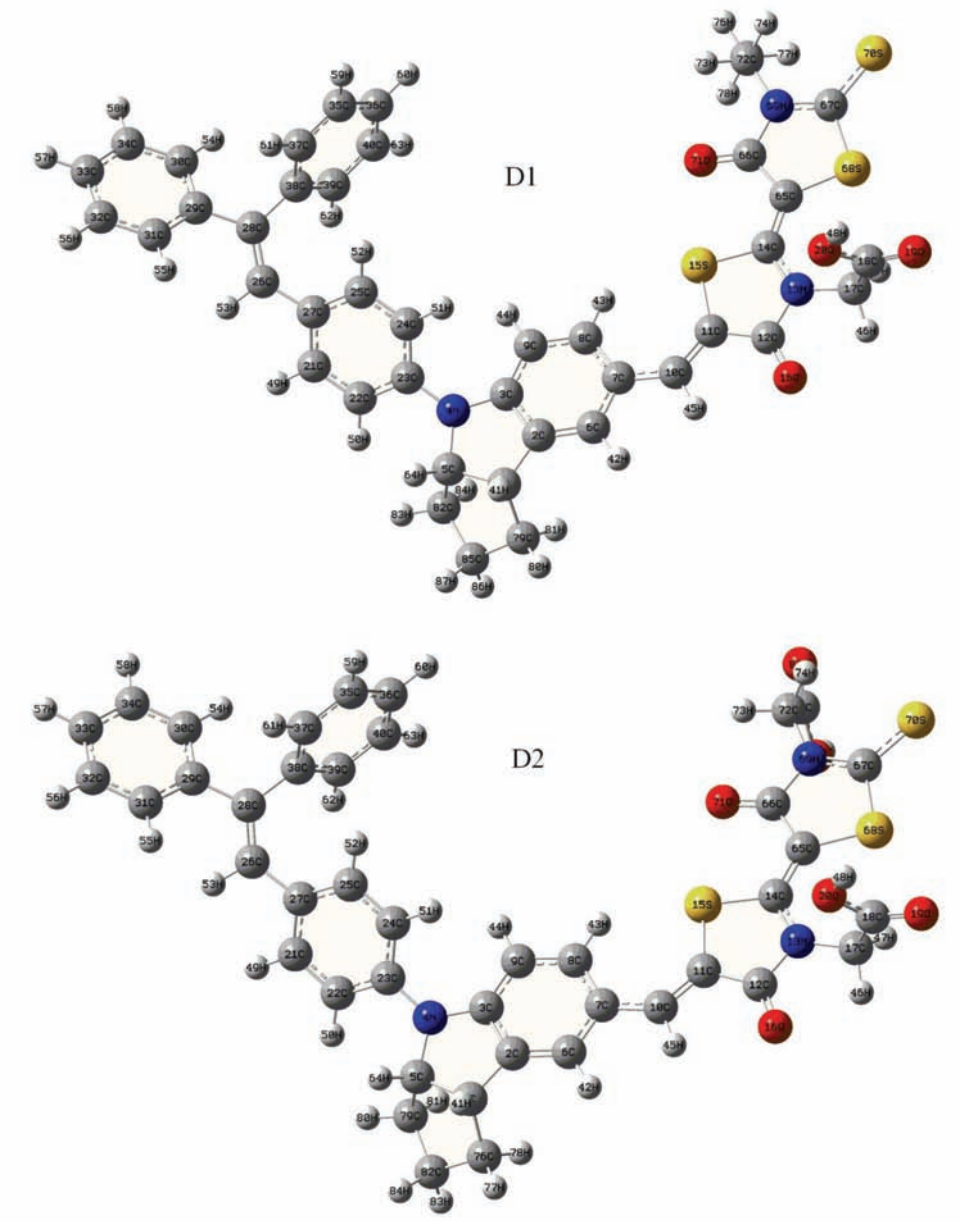

Fig. 2. Optimized ground-state geometries of the indoline dyes. (Continued on next page).

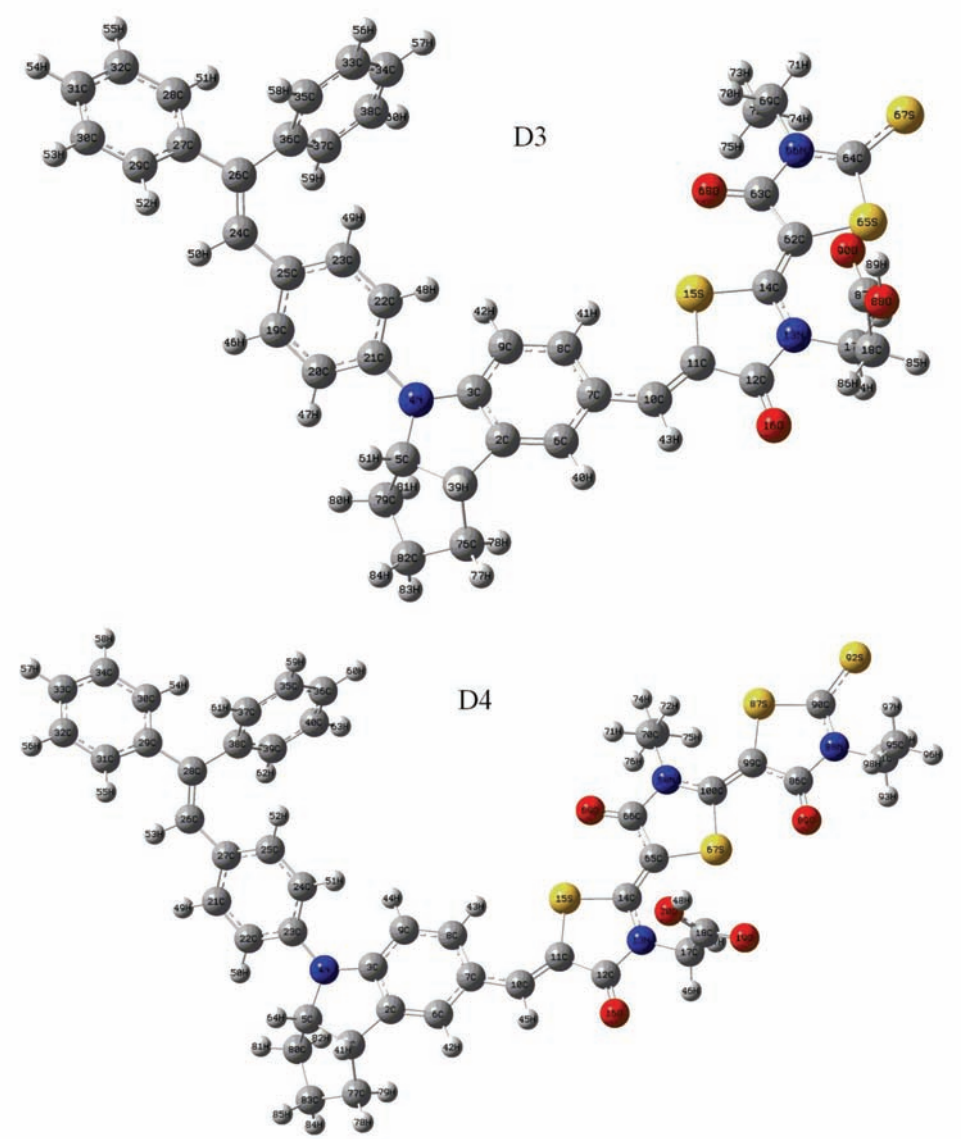

Fig. 2. Optimized ground-state geometries of the indoline dyes. (Continued).

differ from each other. The C10-C11 bond lengths for these dyes are 1.364–1.365 Å, exhibiting a delocalized π-bond character. The dihedral angles of the C–C and C=C bonds at the methine bridge between the indoline and rhodanine rings (∠C8–C7–C10–C11) for D1, D2, D3 and D4 are 3.50, –0.22, 3.88 and 1.59°, respectively. In comparison to D1, the rhodanine rings are distorted by 3.72° in response to the orientation of the second carboxyl group for D2 and by 1.91° in res-

ponse to an increased rhodanine ring for D4, but very slightly in response to the increased methylene for D3. The N13-C17 bond for D1 (1.456 Å) are shorter than that for D3 (1.476 Å), indicating that the increased methylene in carboxyl group would be disadvantageous to the electron injection through the anchoring carboxyl group in DSSCs. The dipole moments for D1, D2, D3 and D4 are 14.562, 15.697, 13.035 and 15.227 D, respectively.

Electronic structures

The molecular orbitals involved in the analyzed transitions were examined by the DFT method. The vertical excitation energy and oscillator strength along with the main excitation configuration are listed in Table I. The major electronic absorption bands are assigned to those excitations with significant oscillator strengths. The electronic structures of these dyes are quite similar although their substituent groups are distinct from one another. The HOMO and LUMO orbitals of D1 are shown in Fig. 3 as a representation. The electron distribution of the HOMO orbital is delocalized over the π-system with the highest electron density centered on the central nitrogen atom. It is noticed that the LUMO orbital have larger compositions of the terminal carboxyl group compared with the HOMO orbital. Therefore, the HOMO–LUMO excitation induced by light irradiation could shift the electron distribution from the middle of the molecule to the anchoring moieties, thus favoring electron injection from dye to TiO_2. The absolute energies of the HOMOs are –4.95, –4.98, –4.93, and –4.93 eV, while the absolute energies of the LUMOs are –2.56, –2.59, –2.50, and –2.56 eV for D1, D2, D3, and D4, respectively. The calculated energies of D1 herein are quite consistent

TABLE I. Excitation energy (E and calculated λ), oscillator strength (f) and main configuration of indoline dyes (H = HOMO, L = LUMO, L+1 = LUMO+1, *etc*.)

Dye	E / eV	λ / nm	f	Configuration	Assignment
D1	2.12	585.7	0.913	H → L (+89 %)	π → π*
	2.82	439.3	0.546	H–1 → L (+75 %); H → L+1 (+16 %)	
	2.95	420.0	0.386	H → L+1 (+73 %); H-1 → L (+16 %)	
	3.26	380.2	0.549	H–2 → L (+68 %); H → L+2 (+19 %)	
D2	2.33	532.8	1.024	H → L (+86 %)	π → π*
	3.10	399.6	0.281	H–1 → L (+91 %)	
	3.48	356.3	0.202	H → L+1 (+81 %); H → L+2 (+7 %)	
D3	2.13	581.1	0.944	H → L (+89 %)	π → π*
	2.83	437.5	0.520	H–1 → L (+76 %); H → L+1 (+15 %)	
	2.98	415.5	0.433	H → L+1 (+74 %); H–1 → L (+14 %)	
	3.25	381.1	0.522	H–2 → L (+66 %); H → L+2 (+23 %)	
D4	2.08	596.7	1.103	H → L (+90 %)	π → π*
	2.65	467.7	0.701	H–1 → L (+58 %); H → L+1 (+34 %)	
	2.76	449.5	0.405	H → L+1 (+58 %); H–1 → L (+31 %)	
	3.07	403.3	0.163	H–2 → L (+86 %)	
	3.25	381.2	0.353	H → L+2 (+72 %); H–1 → L+1 (+18 %)	

with the experimental data (cited as D149, HOMO: –4.901 eV, LUMO: –2.873 eV).[32] For comparison, the HOMO level for N719 (calculated at the DFT level of theory in a water environment) is –5.3 eV with the LUMO at –2.7 eV.[33] The HOMO (conduction band) energy level of TiO_2 calculated for a $Ti_{38}O_{76}$ cluster exposing the anatase (101) surface[34] is located at –6.55 eV, and the corresponding LUMO at –2.77 eV.

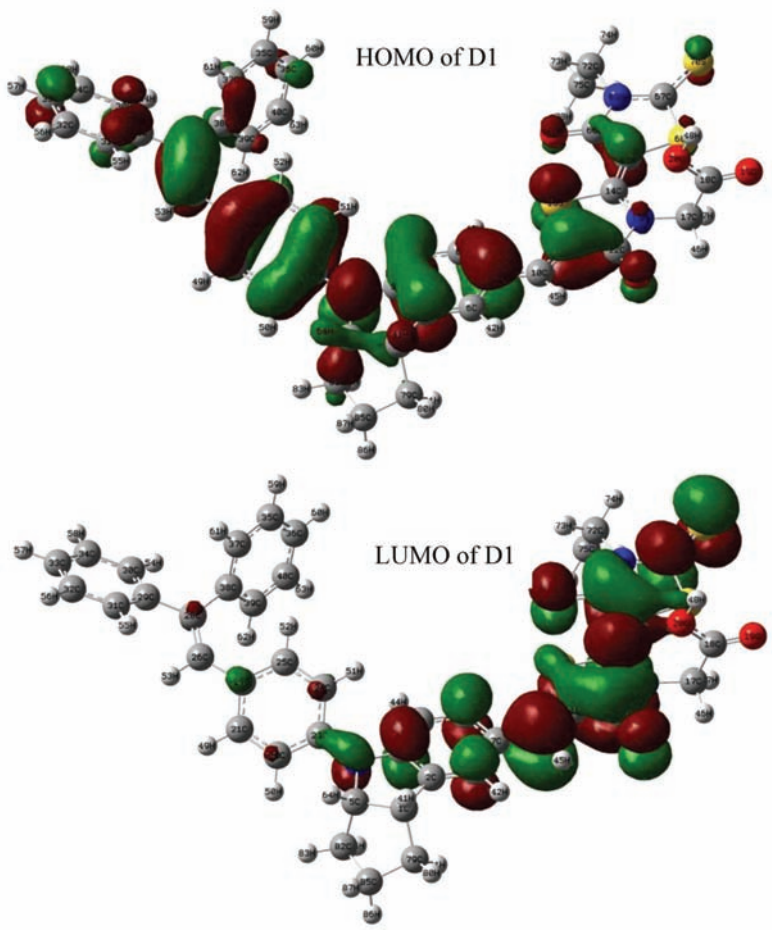

Fig. 3. HOMO and LUMO of the indoline dyes computed on the ground-stated geometries.

The HOMO and LUMO levels of a dye used in a DSSC must match with the conduction-band-edge energy level (E_{cb}) of the TiO_2 and the redox potential of electrolyte for an efficient charge separation and dye regeneration. The HOMO level has to be sufficiently more positive than the redox potential (0.40 V *vs.* NHE for I^-/I_3^-) and the LUMO of the dye has to be sufficiently more negative

than the E_{cb} of TiO_2. Usually, an energy gap of more than 0.2 V between the LUMO level of the dye and the E_{cb} of TiO_2 (–0.50 V *vs*. NHE) is necessary for an effective electron injection from the excited dye to the conduction band of TiO_2.[24] The energy levels of the excited state of the four dyes are depicted in Fig. 4. The HOMO levels are more positive than the redox potential of I^-/I_3^- (0.40 V *vs*. NHE), meaning that the resultant dye^+ can be deoxidized by I^- in the electrolyte. The LUMO levels are sufficiently more negative than the E_{cb} (–0.5 V *vs*. NHE) to inject electrons from the dyes. The relatively large energy gaps between the LUMO and the E_{cb} values could improve the voltage and, consequently, the total efficiency.

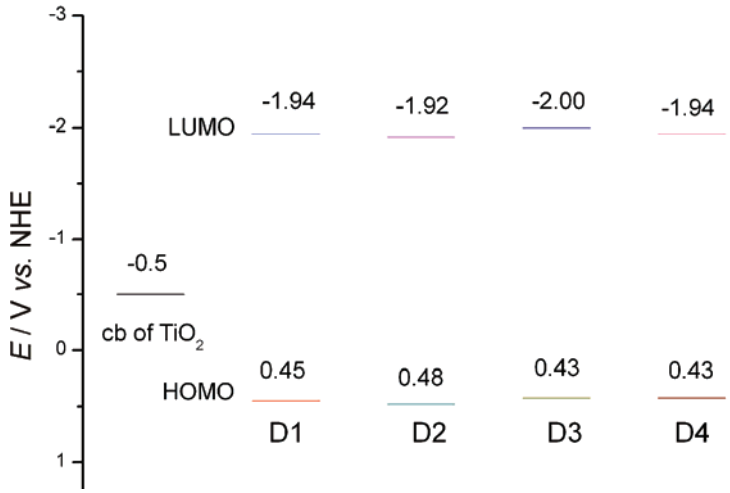

Fig. 4. Energy level diagram of the conduction bands of TiO_2, and the ground state and single excited states of the indoline dyes.

UV–Vis absorption spectra

The simulated absorption spectra of the four indoline dyes in solutions are shown in Fig. 5. The first optically allowed electronic transition of D1, D2, D3 and D4 are predicted to populate the HOMO → LUMO transitions at 585.7, 532.8, 581.1 and 596.7 nm, respectively. The observed experimental λ_{max} values are at 526, 531, and 532 nm for D1, D2 and D3 (D4 has a slightly red-shifted absorption spectrum peak, but the λ_{max} value is not valuable).[9] It seems that the calculated results did not reproduce the corresponding experimental spectra very well. The inclusion of the solvent is important to calculate spectra in good agreement with the experiment. However, the experimental data[9] were obtained in *tert*-butyl alcohol/acetonitrile (1/1); while the present calculation was carried out with only the solvation effect of acetonitrile.

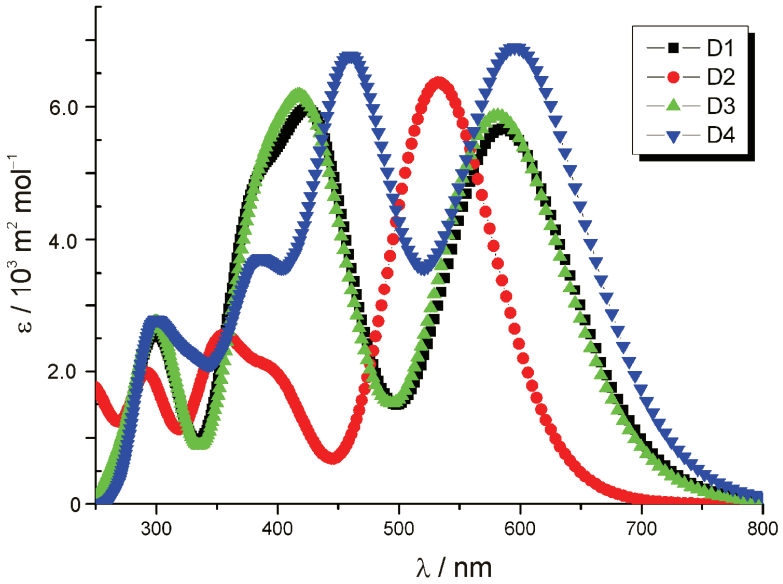

Fig. 5. Simulated absorption spectra of the indoline dyes.

CONCLUSIONS

In this paper, the ground-state geometries and electronic structures of four indoline dyes in acetonitrile were investigated by DFT calculations. The high absorption coefficients of these dyes in visible region make them very suitable for efficient light harvesting. The absolute energies of the HOMOs are –4.95, –4.98, –4.93, and –4.93 eV, while the absolute energies of the LUMOs are –2.56, –2.59, –2.50, and –2.56 eV for D1, D2, D3, and D4, respectively, indicating that electron transfer from the excited dyes to the TiO_2 conduction band is available.

Acknowledgements. This work was supported by the Foundation of Wuhan University of Science & Engineering (No. 20073208), the Natural Science Foundation of Hubei Province (No. 2007ABA075 and 2008CDB261), and the Key Project of Science and Technology Research of Ministry of Education (No.208089). The authors gratefully wish to express their thanks to the reviewers for critically reviewing the manuscript and making important suggestions.

ИЗВОД

DFT ИСПИТИВАЊА ЕЛЕКТРОНСКЕ СТРУКТУРЕ ИНДОЛНИХ БОЈА СОЛАРНЕ ЋЕЛИЈЕ ОСЕТЉИВЕ НА БОЈУ

JIE XU, GUIJIE LIANG, LUOXIN WANG, WEILIN XU, WEIGANG CUI, HUI ZHANG и ZENGCHANG LI

Key Lab of Green Processing & Functional Textiles of New Textile Materials, Ministry of Education, Wuhan University of Science & Engineering, 430073, Wuhan, Hubei, China

Серија индолних боја које имају обећавајућу ефикасност за соларне ћелије осетљиве на боју испитивана је помоћу теорије функционала густине на B3LYP/6-31g (d) нивоу. При-

казани су геометрије основних стања, електронске структуре и апсорпциони спектри ових боја. Резултати израчунавања указују на то да су HOMO и LUMO енергетски нивои ових боја погодни за пријем електрона. Нихове интензивне и широке апсорпционе траке, као и фаворизовани енеггетски нивои ексцитованог стања су кључни фактори за њихову изузетну ефикасност у DSSC.

(Примљено 5. јануара, ревидирано 3. септембра 2009)

REFERENCES

1. B. O'Regan, M. Grätzel, *Nature* **353** (1991) 737
2. M. K. Nazeeruddin, A. Kay, I. Rodicio, R. Humpbry-Baker, E. Miiller, P. Liska, N. Vlachopoulos, M. Grätzel, *J. Am. Chem. Soc.* **115** (1993) 6382
3. M. K. Nazeeruddin, P. Péchy, T. Renouard, S. M. Zakeeruddin, R. Humphry-Baker, P. Comte, P. Liska, L. Cevey, E. Costa, V. Shklover, L. Spiccia, G. B. Deacon, C. A. Bignozzi, M. Grätzel, *J. Am. Chem. Soc.* **123** (2001) 1613
4. M. K. Nazeeruddin, F. D. Angelis, S. Fantacci, A. Selloni, G. Viscardi, P. Liska, S. Ito, B. Takeru, M. Grätzel, *J. Am. Chem. Soc.* **127** (2005) 16835
5. S. Hao, J. Wu, Y. Huang, J. Lin, *Sol. Energy* **80** (2006) 209
6. Y. Amao, T. Komori, *Biosensors Bioelectron.* **19** (2004) 843
7. R. Mosurkal, J.-A. He, K. Yang, L. A. Samuelson, J. Kumar, *J. Photochem. Photobiol. A: Chem.* **168** (2004) 191
8. K. Hara, M. Kurashige, Y. Dan-oh, C. Kasada, A. Shinpo, S. Suga, K. Sayama, H. Arakawa, *New J. Chem.* **27** (2003) 783
9. T. Horiuchi, H. Miura, K. Sumioka, S. Uchida, *J. Am. Chem. Soc.* **126** (2004) 12218
10. T. Kitamura, M. Ikeda, K. Shigaki, T. Inoue, N. A. Anderson, X. Ai, T. Lian, S. Yanagida, *Chem. Mater.* **16** (2004) 1806
11. K. Hara, T. Sato, R. Katoh, A. Furube, T. Yoshihara, M. Murai, M. Kurashige, S. Ito, A. Shinpo, S. Suga, H. Arakawa, *Adv. Funct. Mater.* **15** (2005) 246
12. T. Horiuchi, H. Miura, S. Uchida, *Chem. Comm.* (2003) 3036
13. T. Horiuchi, H. Miura, S. Uchida, *J. Photochem. Photobiol. A: Chem.* **164** (2004) 29
14. F. Aiga, T. Tada, *J. Mol. Struct.* **658** (2003) 25
15. C. Barolo, M. K. Nazeeruddin, S. Fantacci, D. Di Censo, P. Comte, P. Liska, G. Viscardi, P. Quagliotto, F. De Angelis, S. Ito, M. Gratzel, *Inorg. Chem.* **45** (2006) 4642
16. N. Onozawa-Komatsuzaki, O. Kitao, M. Yanagida, Y. Himeda, H. Sugihara, K. Kasuga, *New J. Chem.* **30** (2006) 689
17. J. E. Monat, J. H. Rodriguez, J. K. McCusker, *J. Phys. Chem. A* **106** (2002) 7399
18. S. Fantacci, F. De Angelis, A. Selloni, *J. Am. Chem. Soc.* **125** (2003) 4381
19. F. D. Angelis, S. Fantacci, A. Selloni, *Chem. Phys. Lett.* **389** (2004) 204
20. F. D. Angelis, S. Fantacci, A. Selloni, M. K. Nazeeruddin, *Chem. Phys. Lett.* **415** (2005) 115
21. X. Zhang, J.-J. Zhang, Y.-Y. Xia, *J. Photochem. Photobiol. A: Chem.* **185** (2007) 283
22. Y. Xu, W.-K. Chen, M.-J. Cao, S.-H. Liu, J.-Q. Li, A. I. Philippopoulos, P. Falaras, *Chem. Phys.* **330** (2006) 204
23. Y. Kurashige, T. Nakajima, S. Kurashige, K. Hirao, Y. Nishikitani, *J. Phys. Chem. A* **111** (2007) 5544
24. K. Hara, T. Sato, R. Katoh, A. Furube, Y. Ohga, A. Shinpo, S. Suga, K. Sayama, H. Sugihara, H. Arakawa, *J. Phys. Chem. B* **107** (2003) 597

25. X. Zhang, J.-J. Zhang, Y.-Y. Xia, *J. Photochem. Photobiol. A: Chem.* **194** (2008) 167
26. Z. Liu, THEOCHEM (J. Mol. Struct.) **862** (2008) 44
27. M. J. Frisch, G. W. Trucks, H. B. Schlegel, G. E. Scuseria, M. A. Robb, J. R. Cheeseman, J. A. Montgomery Jr., T. Vreven, K. N. Kudin, J. C. Burant, J. M. Millam, S. S. Iyengar, J. Tomasi, V. Barone, B. Mennucci, M. Cossi, G. Scalmani, N. Rega, G. A. Petersson, H. Nakatsuji, M. Hada, M. Ehara, K. Toyota, R. Fukuda, J. Hasegawa, M. Ishida, Y. Nakajima, Y. Honda, O. Kitao, H. Nakai, M. Klene, X. Li, I. E. Knox, H. P. Hratchian, J. B. Cross, V. Bakken, C. Adamo, J. Jaramillo, R. Gomperts, R. E. Stratmann, O. Yazyev, A. J. Austin, R. Cammi, C. Pomelli, J. W. Ochterski, P. Y. Ayala, K. Morokuma, G. A. Voth, P. Salvador, J. J. Dannenberg, V. G. Zakrzewski, S. Dapprich, A. D. Daniels, M. C. Strain, O. Farkas, D. K. Malick, A. D. Rabuck, K. Raghavachari, J. B. Foresman, J. V. Ortiz, Q. Cui, A. G. Baboul, S. Clifford, J. Cioslowski, B. B. Stefanov, G. Liu, A. Liashenko, P. Piskorz, I. Komaromi, R. L. Martin, D. J. Fox, T. Keith, M. A. Al-Laham, C. Y. Peng, A. Nanayakkara, M. Challacombe, P. M. W. Gill, B. Johnson, W. Chen, M. W. Wong, C. Gonzalez, J. A. Pople, *Gaussian 03*, Gaussian Inc., Wallingford, CT, 2004.
28. A. D. Becke, *J. Chem. Phys.* **98** (1993) 5648
29. C. Lee, W. Yang, R. G. Parr, *Phys. Rev. B* **37** (1988) 785
30. M. Cossi, V. Barone, R. Cammi, J. Tomasi, *Chem. Phys. Lett.* **255** (1996) 327
31. V. Barone, M. Cossi, *J. Phys. Chem. A* **102** (1998) 1995
32. R. Jose, A. Kumar, V. Thavasi, S. Ramakrishna, *Nanotechnology* **19** (2008) 424004
33. T. J. Meyer, G. J. Meyer, B. W. Pfennig, J. R. Schoonover, C. J. Timpson, J. F. Wall, C. Kobusch, X. Chen, B. M. Peek, C. G. Wall, W. Ou, B. W. Erickson, C. A. Bignozzit, *Inorg. Chem.* **33** (1994) 3952
34. F. D. Angelis, A. Tilocca, A. Selloni, *J. Am. Chem. Soc.* **126** (2004) 15024.

Journal of the Serbian Chemical Society
JSCS@tmf.bg.ac.rs • www.shd.org.rs/JSCS

J. Serb. Chem. Soc. *75* (2) 271–282 (2010)
JSCS–3959

UDC 66.017–039.26.004.12:544.018.2
Original scientific paper

Preparation and characterization of a new carbonaceous material for electrochemical systems

ZI JI LIN[1,2], XUE BU HU[1,2], YONG JIAN HUAI[1,2] and ZHENG HUA DENG[1,2]*

[1]*Chengdu Institute of Organic Chemistry, Chinese Academy of Sciences, Chengdu, Sichuan 610041, and Graduate School of Chinese Academy of Sciences, Beijing, 100039 and* [2]*Zhongke Laifang Power Science & Technology Co., Ltd., Chengdu, Sichuan 610041, P.R. China*

(Received 19 February, revised 4 June 2009)

Abstract: A new carbonaceous material was successfully prepared by the pyrolysis of scrap tire rubber at 600 °C under a nitrogen atmosphere. The physical characteristics of the prepared carbonaceous material were studied by scanning electron microscopy (SEM), X-ray powder diffraction (XRD) and X-ray photoelectron spectroscopy (XPS). It was proved that the carbonaceous material had a disordered structure and spherical morphology with an average particle size about 100 nm. The prepared carbonaceous material was also used as electrodes in electrochemical systems to examine its electrochemical performances. It was demonstrated that it delivered a lithium insertion capacity of 658 mA h g^{-1} during the first cycle with a coulombic efficiency of 68 %. Cyclic voltammograms test results showed that a redox reaction occurred during the cycles. The chemical diffusion coefficient based on the impedance diagram was about 10^{-10} cm^2 s^{-1}. The pyrolytic carbonaceous material derived from scrap tire rubber is therefore considered to be a potential anode material in lithium secondary batteries or capacitors. Furthermore, it is advantageous for environmental protection.

Keywords: pyrolytic carbon; scrap tire rubber; carbonaceous materials; electrochemical performance; coulombic efficiency; chemical diffusion coefficient.

INTRODUCTION

The lithium-ion battery has developed rapidly in the past decades due to its advantages of high electromotive force and high energy density. In today's commercial lithium-ion batteries, carbonaceous materials are widely used as the anodes. As compared with lithium metal, carbonaceous anodes reduce the formation of lithium dendrites on the surface of the anodes during the cycling process, which effectively enhances the safety and prolongs the cycle of lithium-ion batteries. In general, carbonaceous materials are classified into two groups: highly

* Corresponding author. E-mail: zhdeng@cioc.ac.cn
doi: 10.2298/JSC10020271L

graphitized carbons and slightly graphitized carbons of disordered structures. Graphitic carbons are the dominant anode material in today's lithium-ion technology because of their good characteristics of a relatively flat potential and stable structure upon cycling. However, the formation of graphitic carbons usually requires high reaction temperatures and their reversible capacities which, normally below 372 mA h g^{-1}, are limited compared with lithium metal.

Low-crystalline carbons, also named disordered carbons, have received considerable interest because of their appealing features, such as higher specific capacities of lithium insertion; good cycling performances; structural characteristics controllable by changing the organic precursors, heat-treatment temperature and soaking time.[1,2] Disordered carbons synthesized by the pyrolysis of organic precursors can accommodate much larger amounts of lithium than graphitic carbons, because disordered carbons contain predominantly planar hexagonal networks but lack extended graphitic crystallite ordering. Moreover, the short-sized graphite layers in disordered carbons are relatively facile for the insertion of lithium ions compared with graphitic carbons.[3]

Scrap tires are usually considered as waste materials. Owing to their flexible nature and resistance to degradation, under-grounding tires would occupy large volumes of land and tires tend to cause destabilization of compacted landfill sites. Scrap tires would also lead to significant fire hazards and generate high levels of pollution to the air, soil and waters. In fact, scrap tires may represent a source of many valuable products. According to recent management strategies that focus on valuable resources recycling and environmental protection, pyrolysis is regarded as one of the most promising techniques in terms of the recovery of valuable products from scrap tire rubber.[4]

Disordered carbons prepared by the pyrolysis of condensed aromatics[5,6] and a multitude of natural precursors[7–11] have been reported. These disordered carbons showed high initial insertion specific capacities and good electrochemical performance but low initial coulombic efficiencies. In this paper, the results of the structural characteristics and electrochemical performance of carbonaceous material pyrolyzed from scrap tire rubber are reported. The as-prepared carbonaceous material in the present study was designated as TRC. To evaluate the electrochemical properties of TRC, the widely used commercial powdered graphite carbons (abbreviated as CGP and F-0), activated carbon (abbreviated as AC) were used for comparative purposes.

EXPERIMENTAL

Preparation of the carbonaceous material

The scrap tire rubber employed in this work was in powdered form of particle size about 0.3 mm. A tube furnace was used to produce the carbonaceous material. Before pyrolysis, the rubber powder was washed with anhydrous ethanol. Subsequently, the above rubber precursor was heated at 600 °C for 2 h in flowing nitrogen at a heating rate of 2 °C min^{-1}. After natural

cooling to room temperature, the residual solid sample was mixed with a 1.0 M acetic acid solution in a 250 mL screw cap glass bottle to leach the inorganic elements to a minimum. The mixture was milled by magnetic force for 24 h and then end-over-end shaken for 6 h at room temperature. Afterwards, the mixture was filtered through a low-ash filter paper and then washed with distilled water until the pH value of the filtrate was neutral.

Analytical and testing instruments

SEM Images were obtained with a Hitachi X-650B microscope. The XRD data was collected between the scattering angles (2θ) 0 and 90° using a Rigaku D/Max 2550 powder diffractometer equipped with Cu-Kα radiation source (λ = 0.15418 nm). The XPS was collected on a VG Escalab MK II instrument.

Assembly of cells and performance evaluation

The electrochemical properties of various carbonaceous materials were evaluated with a lithium metal foil as the counter electrode. The working electrode was prepared by mixing TRC (or CGP, F-0 and AC), acetylene black and an aqueous binder LA132 (from Indigo, China) at a weight ratio of 87:5:8, in an appropriate amount of distilled water to make slurry. After mixing well, the slurry was pasted onto a 12 μm copper foil and dried at 120 °C to give the electrodes. All electrodes were cut into disks with a diameter of 14.5 mm (thus the area of 1.65 cm^2), pressed, dried at 90 °C under vacuum for 4 h, and weighed to determine the active mass of carbon.

All the operations on the cells assembly were realized in an argon-filled dry glove box. The electrolyte was 1.0 M $LiPF_6$ dissolved in a mixture of ethylene carbonate (EC), dimethyl carbonate (DMC) and ethylene methyl carbonate (EMC) with a volume ratio of 1:1:1. A porous Celgard 2400 polypropylene membrane was used as the separator. The constant current charge–discharge and room temperature cycling performance of the cells were tested on a Neware battery tester (China) and cyclic voltammograms (CVs) were measured using an Arbin Instrument (USA). Electrochemical impedance spectra (EIS) were investigated by a Solartron 1260/1287 (UK) impedance analyzer in the frequency range of 10^{-1}–10^6 Hz.

RESULTS AND DISCUSSION

SEM Characterization of the carbonaceous materials

The SEM microphotographs of CGP, F-0, AC and TRC are shown in Fig. 1. The carbonaceous materials showed different morphologies. The SEM image of TRC revealed a spherical morphology and the TRC spheres were comparatively smooth with an average particle size of *ca*. 100 nm. According to Aurbach,[12] carbonaceous materials with a smoother surface give a better lithium-ion in-sertion/desertion performance. This is because a smooth surface is advantageous for the formation of an effective passivation layer. In addition, carbon spheres are thought to be beneficial for obtaining an improved performance because of their high pack density, low surface-to-volume ratio, good structural stability, *etc*.[13] Therefore, this morphological feature of the TRC material derived from the pyrolysis of scrap tire rubber is expected to be favorable for good cycling stability.

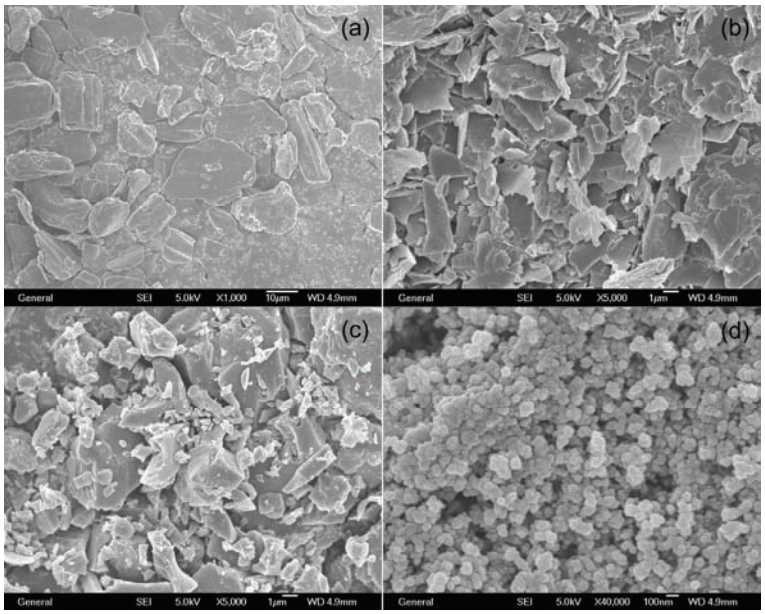

Fig. 1. SEM Images of a) CGP, b) F-0, c) AC and d) TRC.

XRD Characterization

The XRD patterns of CGP, F-0, AC and TRC are presented in Fig. 2. As Sandí *et al.*[14] indicated, CGP and F-0 show a highly graphitized carbon structure, while AC and TRC display disordered carbon systems. The diffraction peak of (100) at around 43° indicates the presence of planar hexagonal cluster structures, while the broad reflection of (002) at around 24° indicates stacking of the graphite sheets in TRC, as shown in Fig. 2d. The d_{002} of TRC is about 3.65 Å, which is a little larger than that of pure graphite carbon, as revealed in Figs. 2a and 2b. The larger interlayer distance of TRC is facile for the insertion and desertion of lithium ions and the retention the structural stability of TRC during cycles.

As indicated by Liu *et al.*,[15] the empirical parameter *R* can be used to estimate the concentration of nonparallel single layers of carbon in carbonaceous materials pyrolyzed at low temperatures. In the present study, the *R* value of TRC was found to be about 3.10. As shown in Figs. 2c and 2d, the *R* value of AC was higher than that of TRC, indicating more graphitized carbon single layers in TRC. The amount of the precursor loaded for pyrolysis is considered to be a condition for a large value of *R*. The reason is that large sample (more than 10 g precursor) when heat-treated can generate a higher partial vapor pressure of volatile organic products which may be able to redeposit in a process similar to the chemical vapor deposition (CVD) action. The capacity of a sample is correlated with

the value of *R* that lies on the fraction of the single layers. Samples with lower *R* values have more single layers and generally give a larger reversible specific capacity. For all single layers $R = 1$,[15] as shown in Figs. 2a and 2b. Therefore, the single-layer fraction in TRC is small, which is one of the possible reasons that TRC has a relatively lower reversible specific capacity.

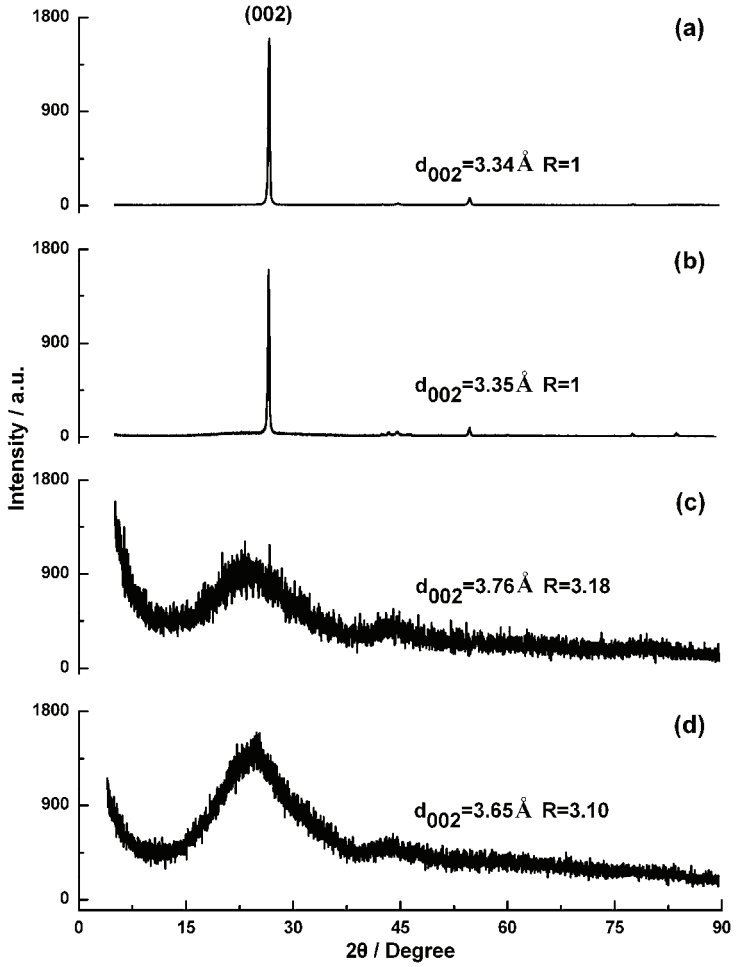

Fig. 2. XRD Patterns of a) CGP, b) F-0, c) AC and d) TRC.

XPS Measurements

The X-ray photoelectron binding energy spectrum of C_{1s} in TRC is given in Fig. 3. The spectrum shows that the TRC mainly consists of four kinds of carbon, including elemental carbon (C–C), phenol or ether (C–O), carbonyl (C=O) and carboxyl (COOH), which correspond to binding energies at 284.8, 286.2, 287.9

and 289.6 eV, respectively. Surface functional groups such as C–O, C=O and COOH were mainly formed during the pyrolysis process. As Ogihara *et al*. discussed,[3] these surface functional groups would cause a loss of reversible capacity because of their potential reactions with lithium.

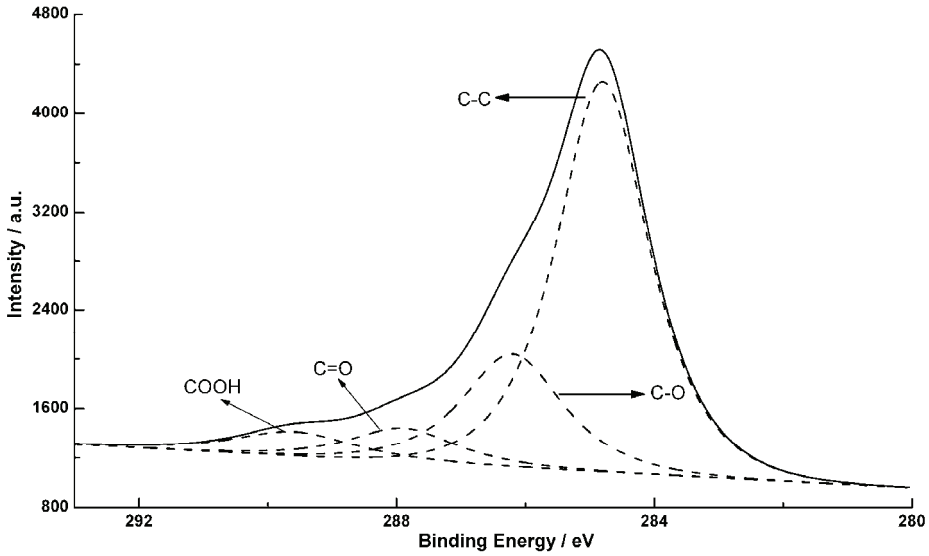

Fig. 3. X-Ray photoelectron binding energy spectrum of C1s in TRC.

Cyclic voltammetry

The CVs of CGP, F-0, AC and TRC are shown in Fig. 4 (1). The scan rate for all the electrodes was 0.2 mV s^{-1}. As can be seen from Fig. 4 (1), the four carbonaceous materials showed different electrochemical behaviors. The charge –discharge curves of CGP, F-0, AC and TRC, as shown in Fig. 4 (2), also display their different electrochemical properties. The CGP and F-0 electrodes exhibited the same oxidation-reduction behavior, *i.e*., Li-ion insertion–extraction, in the electrodes. The AC electrode exhibited no redox peaks, which is due to the process of electrostatic adsorbing–desorbing of PF_6^- in AC. The TRC electrode exhibited two reduction peaks in the potential regions of 1.4–0.4 V and 0.4–0 V. The currents (*i*) at 1.4–0.4 V varied almost linearly with the scan rate (*v*), especially at the potentials of 0.6 and 0.4 V, as shown in Fig. 5. This result demonstrates a surface reaction behavior,[16] which is consistent with those of Ogihara.[3] In the potential region 1.4–0.4 V, a solid-electrolyte interface (SEI) film formed. The SEI films were mainly produced by the electrochemical reduction of solvent species at 1.2 V, the emphraxis of EC-solvated lithium on the carbonyl edges (C_{edge}=O), and the reaction of lithium ions with C_{edge}=O to give the reversible redox reaction C_{edge}=O/C_{edge}–OLi.[17] Consequently, the high capacity in the po-

tential region of 1.4–0.4 V is the result of the electrochemically reversible redox of C_{edge}=O/C_{edge}–OLi, which is cyclable and occurs only on the electrode surface. In the potential region of 0.4–0 V, as suggested by other authors,[18–20] this is regarded as lithium ion insertion into the graphite layers (C_6Li) and/or electrochemical deposition of metallic lithium clusters (Li^0). Simultaneously, a LiF resistive film is formed irreversibly at around 0.2 V.[17]

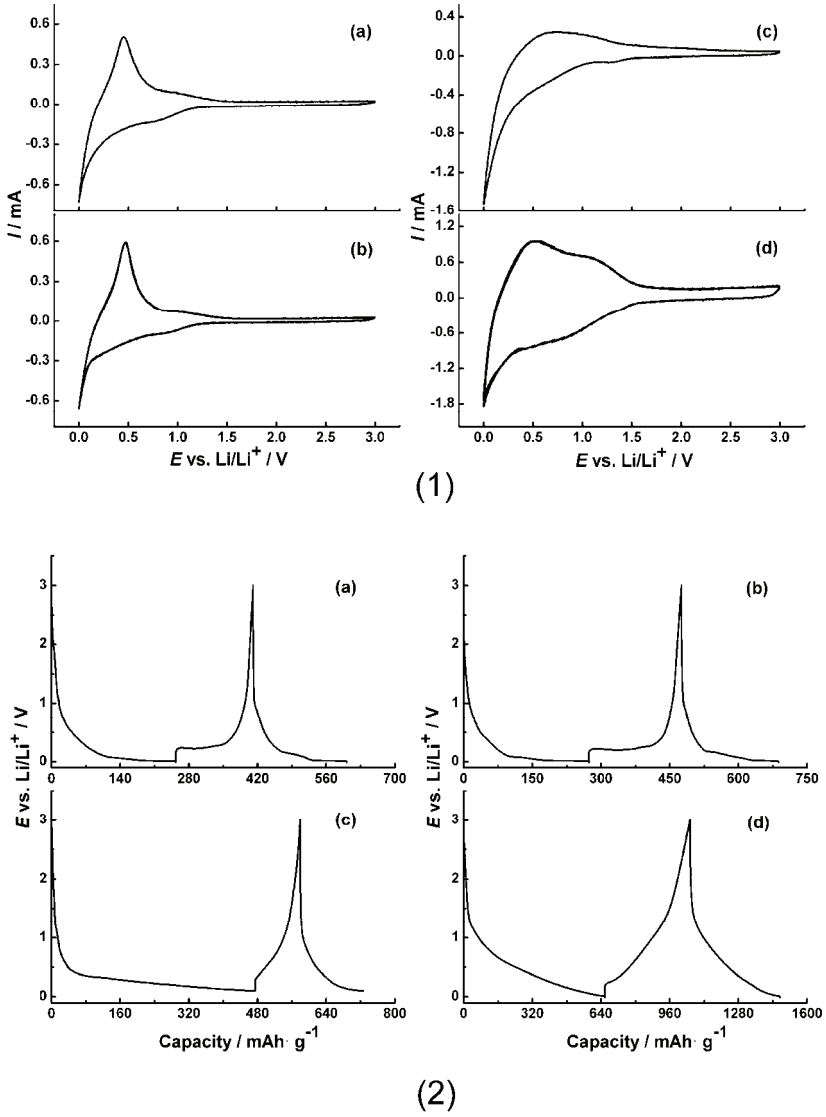

Fig. 4. 1) Cyclic voltammograms and 2) charge–discharge curves of a) CGP, b) F-0, c) AC and d) TRC.

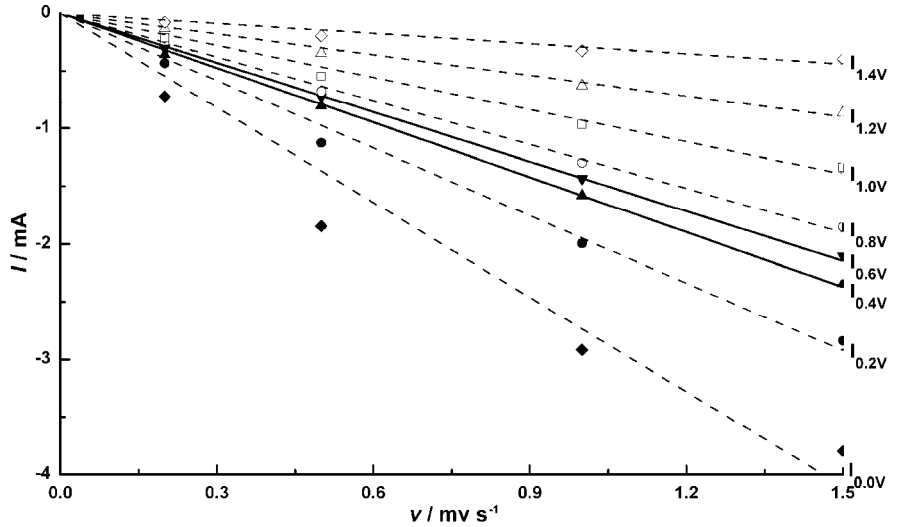

Fig. 5. Scan rate (v) dependence of the current (i) for TRC at potentials of 1.4, 1.2, 1.0, 0.8, 0.6, 0.4, 0.2 and 0.0 V.

Cycling properties

The variations of the charge and discharge capacities with cycle number, together with the coulombic efficiency, for TRC are shown in Fig. 6. The cells were cycled between 0 and 3 V *vs.* Li/Li^+ at a current density of 0.45 mA cm^{-2}. A

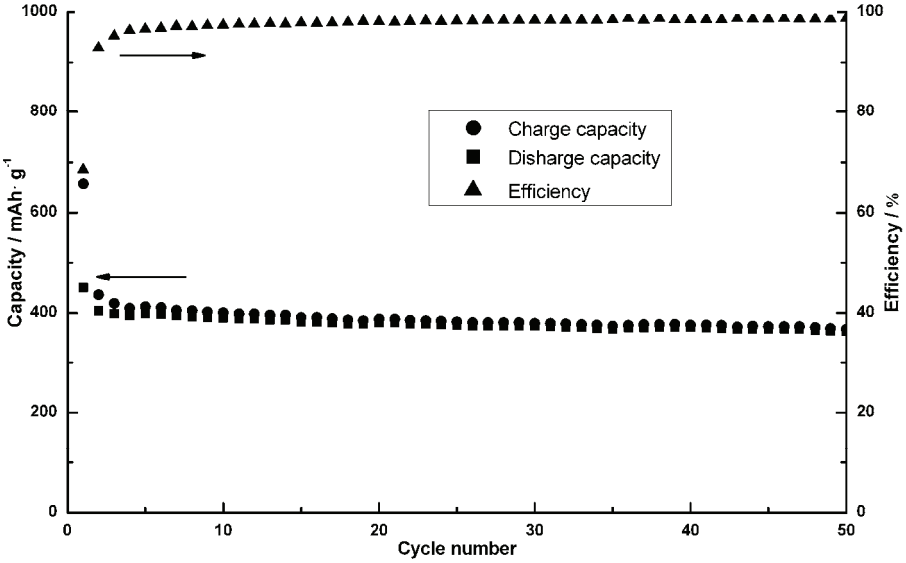

Fig. 6. Variation of the charge and discharge capacities with cycle numbers, together with the coulombic efficiency for TRC.

capacity of 658 mA h g^{-1} was obtained during the initial discharge with a coulombic efficiency of 68 %. The initial coulombic efficiency was much higher than that of many other carbonaceous materials obtained by pyrolysis.[7,10,11,21,22] The TRC electrode exhibited a rapid capacity fading in the first two cycles, although the irreversible capacities gradually decreased in the subsequent cycles. A sufficient passivation layer was not formed because of the structural characteristics of TRC and electrochemical parameters, such as large surface area, abundant functional groups, and/or large current density are thought to be the reasons. The low coulombic efficiencies of the first two cycles are considered to be caused by the fact that the applied current was consumed not only when lithium ions were inserted into the TRC during the discharge process, but also by other side reactions, such as solvent decomposition. After the 2nd cycle, the fading of both the charge and discharge capacities become slow and the coulombic efficiency reaches up to 95 %, which were because highly passivated surface films formed, the effect of side reactions abated and the structure of TRC became much more stable with cycling.

Impedance measurements

The impedance diagrams obtained for cells with a TRC electrode before cycling and after four cycles are shown in Fig. 7. The semicircles in the medium frequency region correspond to the process of insertion of lithium ions. The semicircle in the high frequency region for the cell after four cycles is considered to correspond to the formation of an SEI film on the electrode surface. The diagram

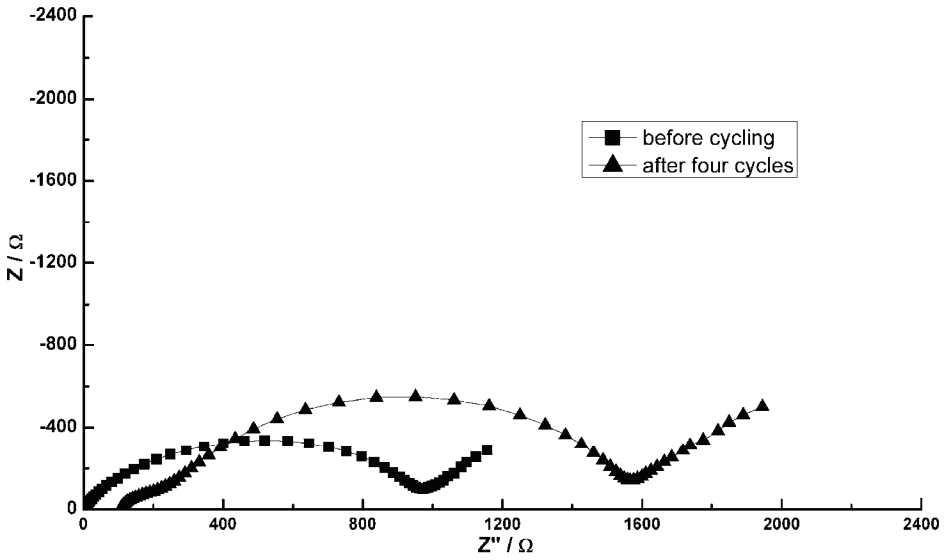

Fig. 7. Impedance diagram of the TRC electrode system before cycling and after four cycles.

also demonstrates that the impedance of the cell greatly increased upon cycling. This would be caused by the micro-exfoliation of the carbon particles during the repeated insertion-desertion process. As indicated by Levi *et al.*,[23] the micro-exfoliation would result in an increase of the surface area electrode and lead to a continuous reduction of the solvent species. As a result, the electrode becomes more covered by solution-reduced products and exfoliated carbon; hence the impedance of the cell increases. The chemical diffusion coefficient of lithium was calculated from the straight line of the impedance spectrum[24] shown in Fig. 7. This value corresponds to 2.0×10^{-10} cm^2 s^{-1}, which is larger than the value obtained by Sandí *et al.*[14]

CONCLUSIONS

Scrap tire rubber was proved to be a suitable precursor for the production of carbonaceous electroactive materials for lithium-ion batteries. The prepared sample showed a disordered structure and spherical morphology with a relatively smooth surface and comparatively uniform particle size distribution. The higher chemical diffusion coefficient of lithium indicated the rapid transfer of lithium ions during cycling. As suggested by Aurbach *et al.*,[25] the structural characteristics of carbonaceous materials have an important influence on the voltage profile, reversibility and the final stoichiometry of the lithium-inserted carbon. The electrochemical performances of TRC were largely determined by its surface morphology and structural characteristics. A structure with a certain degree of crystallization and a certain number of pores is necessary for TRC to give a high capacity because the cavities in the TRC may be favorable for a greater accommodation of lithium ions. The disordered pyrolytic carbon TRC derived from scrap tire rubber showed a first-cycle coulombic efficiency of more than 65 %, which is much higher than other carbonaceous materials of the same family obtained from other precursors, although it exhibited a relatively low reversible capacity.

More importantly, not only the electrode materials could be obtained from scrap tire rubber by pyrolysis, but also the serious “black pollution” by scrap tires would be effectively solved by this method, which is thus advantageous for environmental protection.

ИЗВОД

СИНТЕЗА И КАРАКТЕРИЗАЦИЈА НОВОГ УГЉЕНИЧНОГ МАТЕРИЈАЛА ЗА УПОТРЕБУ У ЕЛЕКТРОХЕМИЈСКИМ СИСТЕМИМА

ZI JI LIN[1,2], XUE BU HU[1,2], YONG JIAN HUAI[1,2] и ZHENG HUA DENG[1,2]

[1]*Chengdu Instutute of Organuc Chemustry, Chunese Academy of Scuences, Chengdu, Suchuan 610041, and Graduate School of Chunese Academy of Scuences, Beujung, 100039 и* [2]*Zhongke Laufang Power Scuence & Technology Co., Ltd, Chengdu, Suchuan 610041, P.R. China*

Синтетисан је нови угљенични материјал пиролизом отпадака аутомобилских гума на 600 °C у атмосфери азота. Физичке карактеристике угљеничног материјала су испитиване

скенирајућом електронском микроскопијом (SEM), дифракцијом X-зрака (XRD) и фотоелектронском спектроскопијом X-зрака (XPS). Показано је да материјал има неуређену структуру и сферну морфологију са просечном величином честица од око 100 nm. Синтетисани угљенични материјал је коришћен и као електрода у електрохемијским системима да би се испитале његове електрохемијске карактеристике. Резултати су показали да је капацитет интеркалације литијума 658 mAh/g током првог циклуса уз кулоновску ефикасност од 68 %. Цикличном волтаметријом је показано да се током циклуса одиграва редокс реакција. На основу импедансних мерења одређен је коефицијент дифузије литијума од око 10^{-10} cm^2/s. На основу ових резултата може се рећи да би се угљенични материјал добијен пиролизом отпадака аутомоблиских гума могао користити као анодни материјал у литијумским батеријама, што би истовремено био и допринос очувању животне средине.

(Примљено 19. фебруара, ревидирано 4. јуна 2009)

REFERENCES

1. T. Zheng, Y. Liu, E. W. Fuller, S. Tseng, U. von Sacken, J. R. Dahn, *J. Electrochem. Soc.* **142** (1995) 2581
2. S. Yata, H. Kinoshita, M. Komori, N. Ando, T. Kashiwamura, T. Harada, K. Tanaka, T. Yamabe, *Synth. Met.* **62** (1994) 153
3. N. Ogihara, Y. Igarashi, A. Kamakura, K. Naoi, Y. Kusachi, K. Utsugi, *Electrochim. Acta* **52** (2006) 1713
4. F. Chen, J. Qian, *Waste Manage.* **23** (2003) 463
5. K. Sato, M. Noguchi, A. Demachi, N. Oki, M. Endo, *Science* **264** (1994) 556
6. A. Mabuchi, K. Tokumitsu, H. Fujimoto, T. Kasuh, *J. Electrochem. Soc.* **142** (1995) 1041
7. G. T. K. Fey, D. C. Lee, Y. Y. Lin, T. P. Kumar, *Synth. Met.* **139** (2003) 71
8. Y. Ohzawa, M. Mitani, J. Li, T. Nakajima, *Mater. Sci. Eng., B* **113** (2004) 91
9. G. T. K. Fey, Y. C. Kao, *Mater. Chem. Phys.* **73** (2002) 37
10. A. M. Stephan, T. P. Kumar, R. Ramesh, S. Thomas, S. K. Jeong, K. S. Nahm, *Mater. Sci. Eng. A* **430** (2006) 132
11. Y. J. Hwang, S. K. Jeong, J. S. Shin, K. S. Nahm, A. M. Stephan, *J. Alloys Comp*. **448** (2008) 141
12. D. Aurbach, H. Teller, E. Levi, *J. Electrochem. Soc*. **149** (2002) A1255
13. M. Yoshio, H. Wang, Y. Lee, K. Fukuda, *Electrochim. Acta* **48** (2003)791
14. G. Sandí, R. E. Winans, K. A. Carrado, *J. Electrochem. Soc.* **143** (1996) L95
15. Y. Liu, J. S. Xue, T. Zheng, J. R. Dahn, *Carbon* **34** (1996) 193
16. L. M. Doubova, S. Daolio, A. D. Battisti, *J. Electroanal. Chem*. **532** (2002) 25
17. K. Naoi, N. Ogihara, Y. Igarashi, A. Kamakura, Y. Kusachi, K. Utsugi, *J. Electrochem. Soc*. **152** (2005) A1047
18. F. Chevallier, M. Letellier, M. Morcrette, J. M. Tarascon, E. Frackowiak, J. N. Rouzaud, F. Béguin, *Electrochem. Solid-State Lett*. **6** (2003) A225
19. K. Guérin, M. Ménétrier, A. Février-Bouvier, S. Flandrois, B. Simon, P. Biensan, *Solid State Ionics* **127** (2000) 187
20. I. Mochida, C. H. Ku, Y. Korai, *Carbon* **39** (2001) 399
21. Y. J. Hwang, S. K. Jeong, K. S. Nahm, J. S. Shin, A. M. Stephan, *J. Phys. Chem. Solids* **68** (2007) 182
22. I. Watanabe, T. Doi, J. Yamaki, Y. Y. Lin, G. T. K. Fey, *J. Power Sources* **176** (2008) 347
23. M. D. Levi, E. Levi, D. Aurbach, *J. Electroanal. Chem.* **421** (1997) 89

24. C. Ho, I. D. Raistrick, R. A. Huggins, *J. Electrochem. Soc*. **127** (1980) 343
25. D. A. Aurbach, Y. Ein-Elin, *J. Electrochem. Soc*. **142** (1995) 1746.

Journal of the Serbian Chemical Society
JSCS@tmf.bg.ac.rs • www.shd.org.rs/JSCS

J. Serb. Chem. Soc. *75* (2) 283–293 (2010)
JSCS–3960

UDC 547.42/.43+547.427.3:544–971
Original scientific paper

Derived thermodynamic properties of alcohol + cyclohexylamine mixtures

IVONA R. RADOVIĆ[#], MIRJANA LJ. KIJEVČANIN[*#], ALEKSANDAR Ž. TASIĆ, BOJAN D. DJORDJEVIĆ[#] and SLOBODAN P. ŠERBANOVIĆ[#]

Faculty of Technology and Metallurgy, University of Belgrade, Karnegijeva 4, P. O. Box 35-03, 11120 Belgrade, Serbia

(Received 2 April, revised 19 August 2009)

Abstract: Thermal expansion coefficients, α, excess thermal expansion coefficients, α^{E}, isothermal coefficients of pressure excess molar enthalpy, $(\partial H^{E}/\partial p)_{T,x}$, partial molar volumes, $\overline{V}_i$, partial molar volumes at infinite dilution, $\overline{V}_i^{\infty}$, partial excess molar volumes, $\overline{V}_i^{E}$, and partial excess molar volumes at infinite dilution, $\overline{V}_i^{E,\infty}$, were calculated using experimental densities and excess molar volumes, V^{E}, data. All calculations are performed for the binary systems of cyclohexylamine with 1-propanol or 1-butanol or 2-butanol or 2-methyl-2-propanol. The Redlich–Kister polynomial and the reduced excess molar volume approach were used in the evaluation of these properties. In addition, the aim of this investigation was to provide a set of various volumetric data in order to asses the influence of temperature, chain length and position of hydroxyl group in the alcohol molecule on the molecular interactions in the examined binary mixtures.

Keywords: binary mixtures; densities; volumetric properties; alcohols; cyclohexylamine.

INTRODUCTION

Knowledge of derived thermodynamics properties such as partial molar volumes, excess partial molar volumes, thermal expansion coefficients, excess thermal expansion and isothermal coefficient of pressure excess molar enthalpy is of practical interest and importance in the investigation of specific interactions of complex liquid mixtures, such as mixtures containing alcohols.[1]

In last few years, considerable work has been performed in order to better understand the molecular structures of solutions with strong interactions.

The densities of binary mixtures of cyclohexylamine with 1-propanol or 1-butanol or 2-butanol or 2-methyl-2-propanol or 1-pentanol were already experi-

* Corresponding author. E-mail: mirjana@tmf.bg.ac.rs
# Serbian Chemical Society member.
doi: 10.2298/JSC1002283R

mentally determined and details of this research were given previously.[2,3] In this paper, the results of density measurements and calculated data of excess molar volumes were used for additional analyses.

In this work, the aforementioned thermodynamic derived properties for binary systems of cyclohexylamine with 1-propanol or 1-butanol or 2-butanol or 2-methyl-2-propanol or 1-pentanol were evaluated using the Redlich–Kister Equation and the reduced excess molar volume approach.

The derived properties were used to assess the influence of temperature, chain length and position of the hydroxyl group in the alcohol molecule on molecular interactions in the examined binary mixtures.

RESULTS AND DISCUSSION

The excess molar volumes, V^E, of the binary mixtures were calculated from density data by applying Eq. (1):

$$V^E = (x_1M_1 + x_2M_2)/\rho - x_1M_1/\rho_1 - x_2M_2/\rho_2 \quad (1)$$

where x_1, x_2, M_1 and M_2 are the mole fraction and molar mass of components 1 and 2, while ρ, ρ_1 and ρ_2 stand for the measured densities of the mixture, and the pure components 1 and 2, respectively.

The obtained V^E values were fitted to a modified Redlich–Kister (RK) polynomial:[4]

$$V^E = x_1x_2 \sum_{p=0}^{m} B_p (x_1 - x_2)^p \quad (2)$$

where B_p denotes a temperature dependent parameter:

$$B_p = \sum_{q=0}^{k} B_{pq} T^q \quad (3)$$

where T stands for the absolute temperature.

The results were also explained using the reduced excess molar volume, $V^E/x_1(1 - x_1)$, which has a better physical significance and is more sensitive than V^E to interactions which occur in dilute regions:

$$V^E/x_1(1-x_1) = \sum_{n=0}^{l} A_n x^n \quad (4)$$

where the optimal number of parameters A_n was 3. The values of the adjustable parameters of Eq. (4), B_{pq} and A_n, were given previously.[2]

The thermal expansion coefficient, α, for a pure component and for a mixture can be computed using the expression:

$$\alpha = (\partial \ln \rho / \partial T)_{p,x} \quad (5)$$

which takes into account the temperature dependence of the density. The expression relating the molar volume of a mixture and its excess molar volume, in accordance to Eq. (1), is:

$$V = \sum_{i=1}^{N} x_i V_i^{\circ} + V^{\mathrm{E}} \tag{6}$$

where V_i° is the molar volume of pure component i and N is the number of components in a mixture. Differentiation of Eq. (6) and dividing by V leads to:[5]

$$\alpha = V^{-1}((\partial V^{E}/\partial T)_{p,x_i} + \sum_{i=1}^{N} \alpha_i x_i V_i^{\circ}) \tag{7}$$

where α and α_i are the thermal expansion coefficients of the mixture and the pure component, respectively. Comparison of the α values with literature data[6–8] of pure components at selected temperatures showed very good agreement up to 7×10^{-3} K^{-1}.

The excess thermal expansion coefficient, α^{E}, is calculated as:

$$\alpha^{\mathrm{E}} = \alpha - \sum_{i=1}^{N} \phi_i \alpha_i \tag{8}$$

where ϕ_i is the volume fraction of component i:

$$\phi_i = x_i V_i^{\circ} / \sum_{i=1}^{N} x_i V_i^{\circ} \tag{9}$$

In addition, the isothermal coefficient of the pressure excess molar enthalpy, $(\partial H^{\mathrm{E}}/\partial p)_{T,x}$, can be derived from volumetric measurements using the following expression:

$$(\partial H^{\mathrm{E}}/\partial p)_{T,x} = V^{\mathrm{E}} - T(\partial V^{\mathrm{E}}/\partial T)_{p,x} \tag{10}$$

Values of α, α_i and $(\partial H^{\mathrm{E}}/\partial p)_{T,x}$ for the examined binary mixtures over the entire studied temperature range are summarized in Table I (supplementary material, electronic version only at http://www.shd.org.rs/jscs/) and are graphically represented in Fig. 1 for 303.15 K. For all liquids, α increases with increasing temperature and decreases with the chain length of the 1-alcohols. The values of α for 2-butanol and 2-methyl-2-propanol are higher than those of the 1-alcohols for the same temperature. Fig 1a shows that for 1-alcohol molecules, the value of α for the mixtures slightly decreases with mole fraction of the alcohols. However, the branched alcohols behave in a rather different way, particularly for the system with 2-methyl-2-propanol where α sharply increases as the concentration of 2-methyl-2-propanol increases. For the system with 2-butanol, α is nearly constant with slight sigmoid shape. As can be seen from Fig 1b, all the excess thermal expansion coefficient, α^{E}, curves for the systems 1-alcohol + cyclohexylamine have sigmoid shape with small values which slightly increase with increasing temperature.

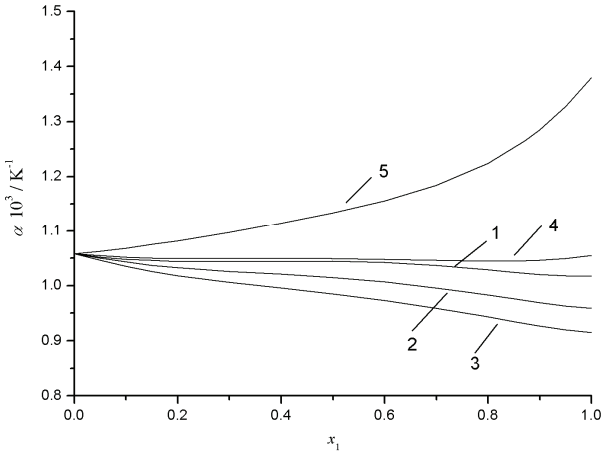

(a)

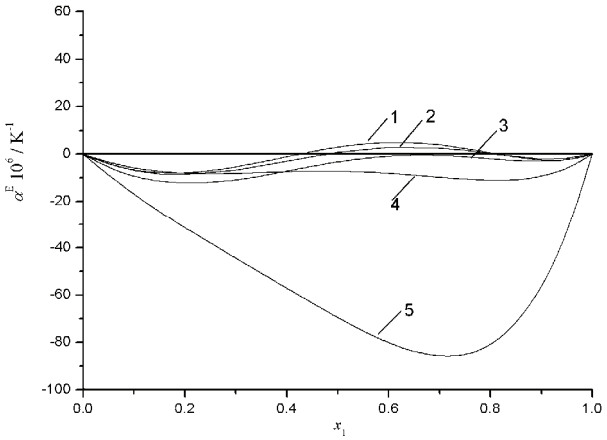

(b)

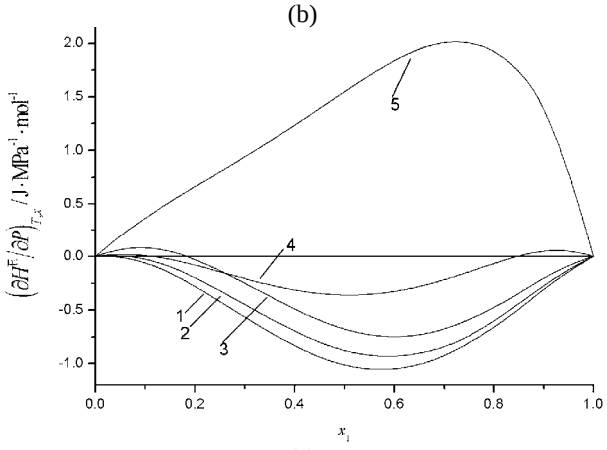

(c)

Fig. 1. Plots of a) the thermal expansion coefficient, α, b) excess thermal expansion coefficient, α^E and c) isothermal coefficient of pressure excess molar enthalpy, $(\partial H^E/\partial p)_{T,x}$, at 303.15 K for the systems: 1--propanol (1) + cyclohexylamine (2), line 1; 1-butanol (1) + cyclohexylamine (2), line 2; 1--pentanol (1) + cyclohexylamine (2), line 3; 2-butanol (1) + cyclohexylamine (2), line 4; 2--methyl-2-propanol (1) + cyclohexylamine (2), line 5.

As can be observed from Fig 1c, for all systems except for the system with 2-methyl-2-propanol, the isothermal coefficient of pressure excess molar enthalpy, $(\partial H^{\mathrm{E}}/\partial p)_{T,x}$, become more negative with increasing temperature. For the system 2-methyl-2-propanol + cyclohexylamine, this quantity is positive and rises with increasing temperature.

Furthermore, the partial molar volumes, $\bar{V}_1$, and $\bar{V}_2$, of components 1 and 2, can be calculated using the equations:

$$\bar{V}_1 = V^{\mathrm{E}} + V_1^{\circ} + (1-x_1)(\partial V^{\mathrm{E}}/\partial x_1)_{p,T} \tag{11}$$

$$\bar{V}_2 = V^{\mathrm{E}} + V_2^{\circ} - x_1(\partial V^{\mathrm{E}}/\partial x_1)_{p,T} \tag{12}$$

Differentiation of Eq. (2) with respect to x_1, leads to the following equations for the partial molar volumes:

$$\bar{V}_1 = V_1^{\circ} + (1-x_1)^2\left(\sum_{p=0}^{m} B_p(2x_1-1)^p + x_1\sum_{p=1}^{m} 2pB_p(2x_1-1)^{p-1}\right) \tag{13}$$

$$\bar{V}_2 = V_2^{\circ} + (1-x_2)^2\left(\sum_{p=0}^{m} B_p(2x_1-1)^p - x_2\sum_{p=1}^{m} 2pB_p(2x_1-1)^{p-1}\right) \tag{14}$$

In Eqs. (13) and (14), B_p is the temperature dependent parameter defined by Eq. (3).

Table I (supplementary material, electronic version only at http://www.shd.org.rs/jscs/) also presents the partial molar volumes, $\bar{V}_i$, for both components in the investigated mixtures, calculated by Eqs. (13) and (14) using the RK parameters listed previously.[2]

Plots of the partial molar volumes, $\bar{V}_1$ and $\bar{V}_2$, and partial excess molar volumes, $\bar{V}_1^{\mathrm{E}}$ and $\bar{V}_2^{\mathrm{E}}$, are presented in Figs. 2 a–d, respectively. From Figs. 2a and 2b, it is clear that the influence of temperature on the partial molar volume $\bar{V}_1$ and $\bar{V}_2$ for all mixtures is low and that a slightly increasing trend appears when the temperature is increased. Figures 2c and 2d show that for all systems, the partial excess molar volumes, $\bar{V}_1^{\mathrm{E}}$ and $\bar{V}_2^{\mathrm{E}}$, over the whole concentration range are negative, indicating that the interactions of unlike molecules is stronger than those of like molecules.

A great part of investigations of volumetric behavior is related to the derived volumetric properties, $\bar{V}_i^{\infty}$ and $\bar{V}_i^{\mathrm{E},\infty}$. Setting $x_1 = 0$ and $x_1 = 1$ leads to the equations for the partial molar volumes at infinite dilution, $\bar{V}_1^{\infty}$ and $\bar{V}_2^{\infty}$:

$$\bar{V}_1^{\infty} = V_1^{\circ} + \sum_{p=0}^{m} B_p(-1)^p \tag{15}$$

$$\bar{V}_2^{\infty} = V_2^{\circ} + \sum_{p=0}^{m} B_p \tag{16}$$

In this work, the partial excess molar volumes, $\bar{V}_1^{\mathrm{E}}$ and $\bar{V}_2^{\mathrm{E}}$, were calculated from the equations:

$$\bar{V}_1^{\mathrm{E}} = \bar{V}_1 - V_1^{\circ} \tag{17}$$

$$\bar{V}_2^{\mathrm{E}} = \bar{V}_2 - V_2^{\circ} \tag{18}$$

where $\bar{V}_1$ and $\bar{V}_2$ are the partial molar volumes calculated from Eqs. (13) and (14), respectively. The results for $\bar{V}_i^{\mathrm{E}}$ are also given in Table I (supplementary material, electronic version only at http://www.shd.org.rs/jscs/).

Using the values of $\bar{V}_1^{\infty}$, and $\bar{V}_2^{\infty}$ obtained from Eqs. (15) and (16), the partial excess molar volumes at infinite dilution, $\bar{V}_1^{\mathrm{E},\infty}$, and $\bar{V}_2^{\mathrm{E},\infty}$, were calculated by the following equations:[9]

$$\bar{V}_1^{\mathrm{E},\infty} = \bar{V}_1 - V_1^{\circ} \tag{19}$$

$$\bar{V}_2^{\mathrm{E},\infty} = \bar{V}_2 - V_2^{\circ} \tag{20}$$

The partial excess molar volumes at infinite dilution, $\bar{V}_1^{\mathrm{E},\infty}$ and $\bar{V}_2^{\mathrm{E},\infty}$, are of fundamental importance since they provide insight into the solute–solvent interactions independent of the composition effect, while in the limit of infinite dilution, the solute–solute interactions disappear. Bearing in mind that the RK Equation and its derivatives do not always provide the best representation of these properties, two other alternatives through the reduced excess molar volumes[10] and apparent molar volumes[9,11] were also included in this study.

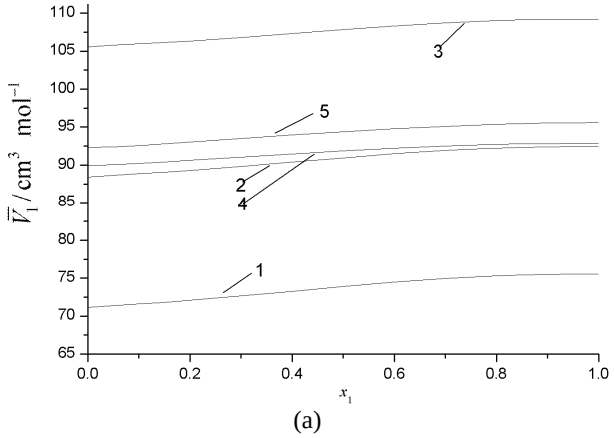

(a)

Fig. 2. Plots of partial molar volumes, a) $\bar{V}_1$ and b) $\bar{V}_2$, and partial excess molar volumes. c) $\bar{V}_1^{\mathrm{E}}$ and d) $\bar{V}_2^{\mathrm{E}}$ at 303.15 K for the systems: 1-propanol (1) + cyclohexylamine (2), line 1; 1-butanol (1) + cyclohexylamine (2), line 2; 1-pentanol (1) + cyclohexylamine (2), line 3; 2-butanol (1) + cyclohexylamine (2), line 4; 2-methyl-2-propanol (1) + cyclohexylamine (2), line 5.

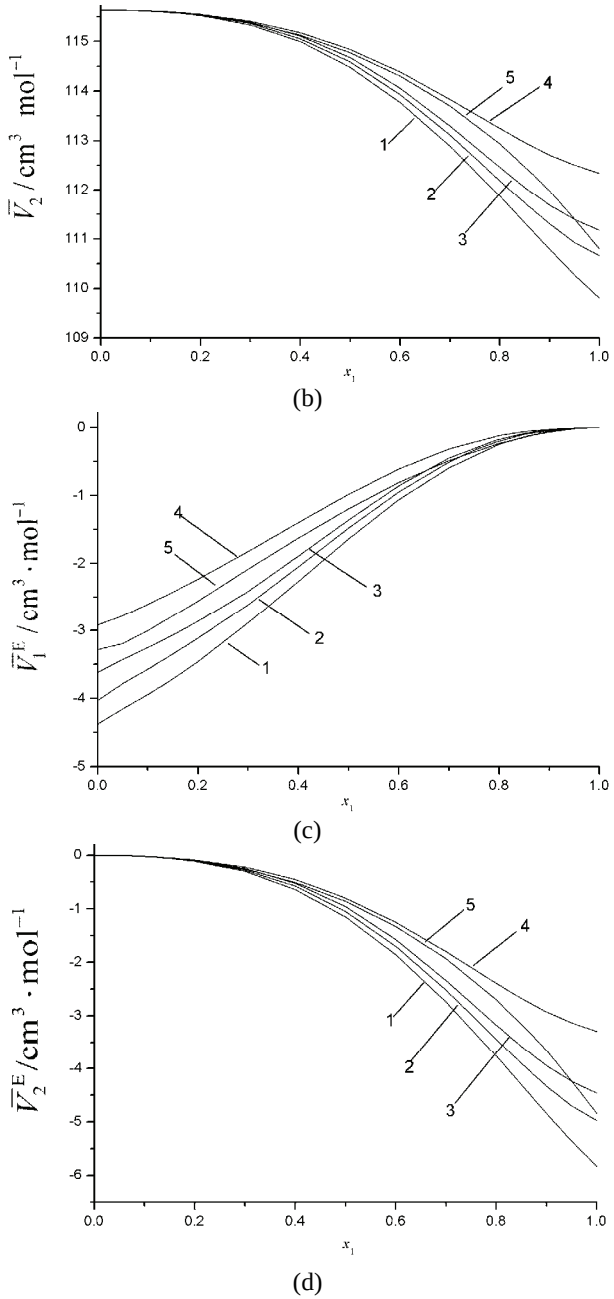

Fig. 2 continued. Plots of partial molar volumes, a) $\bar{V}_1$ and b) $\bar{V}_2$, and partial excess molar volumes. c) $\bar{V}_1^E$ and d) $\bar{V}_2^E$ at 303.15 K for the systems: 1-propanol (1) + cyclohexylamine (2), line 1; 1-butanol (1) + + cyclohexylamine (2), line 2; 1-pentanol (1) + cyclohexylamine (2), line 3; 2-butanol (1) + cyclohexylamine (2), line 4; 2-methyl-2-propanol (1) + cyclohexylamine (2), line 5.

First, the values of the partial excess molar volumes at infinite dilution, $\bar{V}_1^{E,\infty}$ and $\bar{V}_2^{E,\infty}$, were calculated by the RK Equation using the following equations:

$$\bar{V}_1^{\mathrm{E},\infty} = \sum_{p=0}^{m} B_p (-1)^p \tag{21}$$

$$\bar{V}_2^{\mathrm{E},\infty} = \sum_{p=0}^{m} B_p \tag{22}$$

Table I (supplementary material, electronic version only at http://www.shd.org.rs/jscs/) also contains the partial molar volumes at infinite dilutions, $\bar{V}_i^{\infty}$ and $\bar{V}_i^{\mathrm{E},\infty}$, for components 1 and 2 evaluated using the RK parameters.

Analytical extrapolation of Eq. (4) for the reduced excess molar volumes to $x_1 = 0$ gives $\bar{V}_1^{\mathrm{E},\infty}$, while extrapolation to $x_1 = 1$ leads to $\bar{V}_2^{\mathrm{E},\infty}$.

The apparent molar volumes of components 1 and 2 can be expressed as:

$$V_{\phi_1} = V_1^{\circ} + (V^{\mathrm{E}} / x_1) \tag{23}$$

$$V_{\phi_2} = V_2^{\circ} + (V^{\mathrm{E}} / x_2) \tag{24}$$

Graphical or analytical extrapolation of V_{ϕ_1} to $x_1 = 0$ and V_{ϕ_2} to $x_1 = 1$ leads to the values of the limiting apparent molar volumes, which are also called the partial molar volumes at infinite dilution, $\bar{V}_1^{\infty}$ and $\bar{V}_2^{\infty}$. The values $\bar{V}_{\phi_1}^{\mathrm{E},\infty}$ and $\bar{V}_{\phi_2}^{\mathrm{E},\infty}$ were calculated using Eqs. (19) and (20).

The results of $\bar{V}_1^{\mathrm{E},\infty}$ and $\bar{V}_2^{\mathrm{E},\infty}$ obtained from the reduced excess molar volumes extrapolation of Eq. (4) are given in Table II (supplementary material, electronic version only at http://www.shd.org.rs/jscs/). Similar results were obtained using the extrapolation of the apparent molar volume and the RK alternatives.

As can be seen from Table II (supplementary material, electronic version only at http://www.shd.org.rs/jscs/) and Fig. 3, the trends of both partial volumes, $\bar{V}_i^{\mathrm{E},\infty}$ and $\bar{V}_i^{\infty}$, at infinite dilution are the same, and increase with increasing chain length of the 1-alcohols.

The partial molar volumes at infinite dilution, $\bar{V}_1^{\infty}$ and $\bar{V}_2^{\infty}$, are lower than the molar volume of the pure liquids for all the investigated systems. The difference between the molar volumes of 1-propanol, as the lowest alcohol, and cyclohexylamine in their pure state was the highest, but after mixing $\bar{V}_1^{\infty}$ had the lowest value, comparing with the other 1-alcohols. The value of $\bar{V}_1^{\infty}$ increases with increasing number of C atoms in the 1-alcohols, since the difference in the molar volumes of both components is significantly lower.

This phenomenon indicates that after the mixing process, the molar volumes of both components in the mixture are smaller than the molar volumes in their pure liquid state, showing compression in volume,[2] which indicates a better packing efficiency in the mixture than in the pure state.

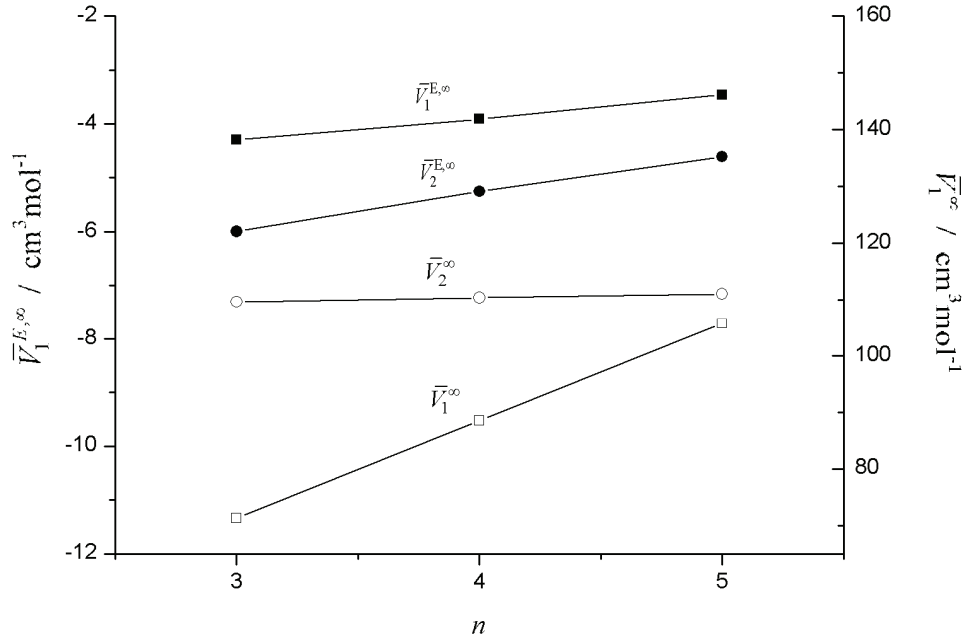

Fig. 3. Influence of increasing the number of C atoms in 1-alcohol + cyclohexylamine systems on $\bar{V}_1^{E,\infty}$ (■), $\bar{V}_1^{\infty}$ (□), $\bar{V}_2^{E,\infty}$ (●) and $\bar{V}_2^{\infty}$ (○), at 303.15 K. The symbols refer to experimental points.

Figure 3 also shows that for all systems with 1-alcohols, the $\bar{V}_1^{E,\infty}$ and $\bar{V}_2^{E,\infty}$ values are negative, increasing with increasing length of the 1-alcohols, indicating that the interactions of unlike molecules are stronger than those of like molecules, according to the previously given explanations. This also means that intermolecular hydrogen bonds are not broken in dilute regions.

The values of both properties $\bar{V}_i^{E,\infty}$ and $\bar{V}_i^{\infty}$ for the mixtures with 2-butanol and 2-methyl-2-propanol are in accordance with the explanations already given previously.

Finally, from Table II (supplementary material, electronic version only at http://www.shd.org.rs/jscs/) and Fig. 4, it is clear that the influence of temperature on $\bar{V}_i^{E,\infty}$ and $\bar{V}_i^{\infty}$ for all mixtures is low, with a slightly increasing trend with increasing temperature, because of the larger expansion capability of the molecules in the pure state compared to in the mixture in the infinite dilution regions.

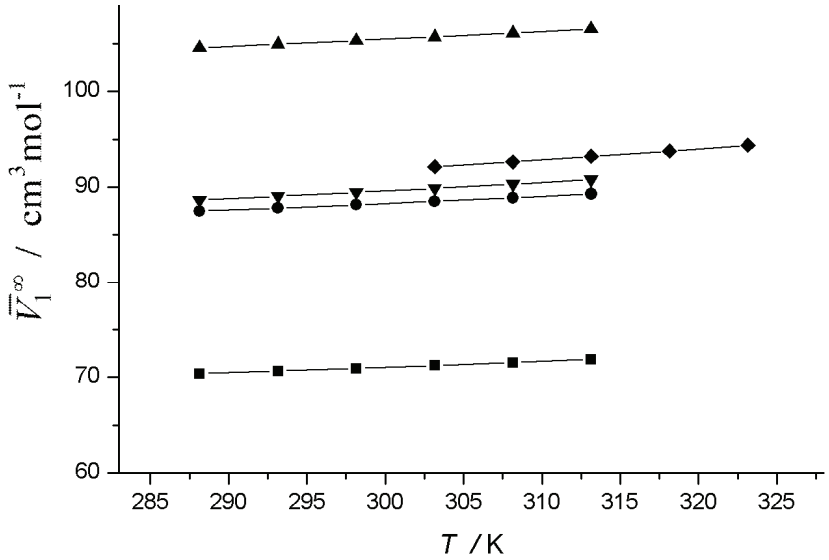

Fig. 4. Influence of temperature on $\bar{V}_1^{\infty}$ for the systems: 1-propanol (1) + cyclohexylamine (2) (■); 1-butanol (1) + cyclohexylamine (2)[2] (●); 1-pentanol (1) + cyclohexylamine (2) (▲), 2-butanol (1) + cyclohexylamine (2) (▼) and 2-methyl-2-propanol (1) + cyclohexylamine (2) (◆). The symbols refer to experimental points.

CONCLUSIONS

The aim of this work was to include thermodynamically derived properties in the analysis of the complex behavior of liquid mixtures.

For this reason, the thermal expansion coefficient, α, the excess thermal expansion coefficient, α^{E}, the isothermal coefficient of the pressure excess molar volumes, $(\partial H^{\mathrm{E}}/\partial p)_{T,x}$, the partial molar volumes, $\bar{V}_i$, the partial molar volumes at infinite dilution, $\bar{V}_i^{\infty}$, the partial excess molar volumes, $\bar{V}_i^{\mathrm{E}}$ and the partial excess molar volumes at infinite dilution, $\bar{V}_i^{\mathrm{E},\infty}$, were calculated using experimental densities and excess molar volumes, V^{E}, data of binary mixtures of cyclohexylamine with 1-propanol, or 1-butanol, or 2-butanol, or 2-methyl-2-propanol. The Redlich-Kister polynomial and the reduced excess molar volume approach were used in the determination of these properties. In this way, the influence of temperature, chain length and position of the hydroxyl group in the alcohol molecule on the molecular interactions in mixtures, including the infinite dilute region, was examined.

Acknowledgement. The authors gratefully acknowledge the financial support received from the Research Fund of the Ministry of Science and Technological Development of the Republic of Serbia and the Faculty of Technology and Metallurgy, University of Belgrade (project No 142064).

И З В О Д

ИЗВЕДЕНЕ ТЕРМОДИНАМИЧКЕ ОСОБИНЕ СМЕША АЛКОХОЛ + ЦИКЛОХЕКСИЛАМИН

ИВОНА Р. РАДОВИЋ, МИРЈАНА Љ. КИЈЕВЧАНИН, АЛЕКСАНДАР Ж. ТАСИЋ, БОЈАН Д. ЂОРЂЕВИЋ и СЛОБОДАН П. ШЕРБАНОВИЋ

Технолошко-металуршки факултет, Универзитет у Београду, Карнегијева 4, 11120 Београд

Термички коефицијент експанзије, α, допунски термички коефицијент, α^{E}, изотермски коефицијент притиска допунске моларне енталпије, $(\partial H^{E}/\partial p)_{T,x}$, парцијалне моларне запремине, $\overline{V}_i$, парцијалне моларне запремине при бесконачном разблажењу, $\overline{V}_i^{\infty}$, парцијалне допунске моларне запремине, $\overline{V}_i^{E}$, и парцијалне допунске моларне запремине при бесконачном разблажењу, $\overline{V}_i^{E,\infty}$, су израчунате из експерименталних података за густине и података за допунске моларне запремине V^{E}. Сви прорачуни су извршени на бинарним смешама циклохексиламина са 1-пропанолом, или 1-бутанолом, или 2-бутанолом, или 2-метил-2-пропанолом. Полином Redlich–Kister-a и приступ редуковане допунске моларне запремине су коришћени у израчунавању ових особина. При томе, циљ овог истраживања је био да се одреди сет различитих волуметријских података да би се проценио утицај температуре, дужине ланца и положаја хидроксилне групе у молекулу алкохола на молекулске интеракције у испитиваним бинарним смешама.

(Примљено 2. априла, ревидирано 19. августа 2009)

REFERENCES

1. B. D. Djordjević, I. R. Radović, M. Lj. Kijevčanin, A. Ž. Tasić, S. P. Šerbanović, *J. Serb. Chem. Soc.* **74** (2009) 477
2. I. R. Radović, M. Lj. Kijevčanin, A. Ž. Tasić, B. D. Djordjević, S. P. Šerbanović, *J. Serb. Chem. Soc.* **74** (2009) 1303
3. M. Lj. Kijevčanin, I. R. Radović, S. P. Šerbanović, A. Ž. Tasić, B. D. Djordjević, *Thermochim. Acta* **496** (2009) 71
4. O. Redlich, A. Kister, *Ind. Eng. Chem.* 40 (1948) 345
5. C. González, M. Iglesias, J. Lanz, J. M. Resa, *Thermochim. Acta* **328** (1999) 277
6. J. A. Riddick, W. B. Bunger, T. K. Sakano, *Physical Properties and Methods of Purification, vol. II, Organic Solvents*, John Wiley & Sons, New York, 1986
7. I. Gascón, M. C. López, C. Lafuente, F. M. Royo, P. Cea, *Thermochim. Acta* **423** (2004) 49
8. A. Villares, S. Martín, M. Haro, B. Giner, H. Artigas, *J. Chem. Thermodyn.* **36** (2004) 1027
9. B. Hawrylak, K. Gracie, R. Palepu, *J. Solution Chem.* **27** (1998) 17
10. G. Perron, L. Couture, J. E. Desnoyers, *J. Solution Chem.* **21** (1992) 433
11. R. B. Tôrres, A. C. M. Marchiore, P. L. O. Volpe, *J. Chem. Thermodyn.* **38** (2006) 526.

Journal of the Serbian Chemical Society
JSCS@tmf.bg.ac.rs • www.shd.org.rs/JSCS

J. Serb. Chem. Soc. 75 (2) I–XI (2010)
JSCS–3960SM

Supplementary material

SUPPLEMENTARY MATERIAL (ELECTRONIC VERSION ONLY) TO

Derived thermodynamic properties of alcohol + cyclohexylamine mixtures

J. *Serb. Chem. Soc.* **75** (2) (2010) 283–293

IVONA R. RADOVIĆ[#], MIRJANA LJ. KIJEVČANIN*[#], ALEKSANDAR Ž. TASIĆ, BOJAN D. DJORDJEVIĆ[#] and SLOBODAN P. ŠERBANOVIĆ[#]

Faculty of Technology and Metallurgy, University of Belgrade, Karnegijeva 4, P. O. Box 35-03, 11120 Belgrade, Serbia

(Received 2 April, revised 19 August 2009)

Table I. Partial molar volumes, $\bar{V}_i$, partial excess molar volumes, $\bar{V}_i^E$, thermal expansion coefficients, α, excess thermal expansion coefficients, α^E, and isothermal coefficients of pressure excess molar enthalpy, $(\partial H^E/\partial P)_{T,x}$, for alcohol (1) + cyclohexylamine (2) binary mixtures at different temperatures (288.15 to 323.15) K and atmospheric pressure

x_1	α / 10^{-3} K^{-1}	α^E / 10^{-6} K^{-1}	$(\partial H^E/\partial p)_{T,x}$ / J·MPa^{-1}·mol^{-1}	$\bar{V}_1$ / cm^3·mol^{-1}	$\bar{V}_2$ / cm^3·mol^{-1}	$\bar{V}_1^E$ / cm^3·mol^{-1}	$\bar{V}_2^E$ / cm^3·mol^{-1}
1-Propanol (1) + cyclohexylamine (2)							
T = 288.15 K							
0.0000	1.041	0	0	70.303[b]	113.827	–4.1012[d]	0
0.0509	1.034	–5.77	0.0439	70.458	113.823	–3.9462	–0.0032
0.1017	1.029	–9.73	0.0265	70.610	113.811	–3.7939	–0.0160
0.1486	1.025	–11.89	–0.0338	70.784	113.786	–3.6201	–0.0411
0.1992	1.023	–12.85	–0.1351	71.006	113.739	–3.3985	–0.0880
0.3007	1.021	–11.51	–0.4031	71.541	113.558	–2.8633	–0.2691
0.4009	1.021	–7.78	–0.6734	72.148	113.227	–2.2563	–0.5999
0.4998	1.021	–3.75	–0.8650	72.766	112.718	–1.6382	–1.1090
0.6002	1.020	–1.48	–0.9235	73.350	112.002	–1.0543	–1.8250
0.7000	1.015	–1.7	–0.8197	73.830	111.108	–0.5740	–2.7183
0.7997	1.008	–3.89	–0.5725	74.170	110.093	–0.2345	–3.7336
0.8500	1.005	–4.95	–0.4137	74.282	109.566	–0.1224	–4.2603
0.8998	1.002	–5.23	–0.2526	74.355	109.059	–0.0496	–4.7673
0.9502	1.001	–3.91	–0.1054	74.394	108.585	–0.0107	–5.2419
1.0000	1.001	0	0	74.404	108.193[c]	0	–5.6334[e]
T = 293.15 K							
0.0000	1.047	0	0	70.576	114.423	–4.1970	0
0.0509	1.040	–5.23	0.0288	70.757	114.419	–4.0168	–0.0038
0.1017	1.035	–8.73	–0.0011	70.929	114.405	–3.8447	–0.0182

* Corresponding author. E-mail: mirjana@tmf.bg.ac.rs
[#] Serbian Chemical Society member.

TABLE I. Continued

x_1	α 10^{-3} K^{-1}	α^E 10^{-6} K^{-1}	$(\partial H^E/\partial p)_{T,x}$ J·MPa^{-1}·mol^{-1}	$\bar{V}_1$ cm^3·mol^{-1}	$\bar{V}_2$ cm^3·mol^{-1}	$\bar{V}_1^E$ cm^3·mol^{-1}	$\bar{V}_2^E$ cm^3·mol^{-1}
1-Propanol (1) + cyclohexylamine (2)							
T = 293.15 K							
0.1486	1.032	–10.53	–0.0709	71.117	114.378	–3.6560	–0.0454
0.1992	1.030	–11.17	–0.1803	71.352	114.328	–3.4218	–0.0950
0.3007	1.029	–9.42	–0.4582	71.902	114.142	–2.8709	–0.2812
0.4009	1.029	–5.51	–0.7315	72.515	113.808	–2.2579	–0.6151
0.4998	1.029	–1.5	–0.9211	73.134	113.299	–1.6397	–1.1242
0.6002	1.027	0.63	–0.9739	73.715	112.586	–1.0579	–1.8376
0.7000	1.022	0.16	–0.8619	74.194	111.695	–0.5791	–2.7281
0.7997	1.015	–2.4	–0.6041	74.534	110.678	–0.2390	–3.7456
0.8500	1.011	–3.72	–0.4390	74.648	110.145	–0.1257	–4.2779
0.8998	1.008	–4.32	–0.2708	74.722	109.628	–0.0515	–4.7950
0.9502	1.006	–3.40	–0.1152	74.762	109.137	–0.0113	–5.2865
1.0000	1.006	0	0	74.773	108.721	0	–5.7025
T = 298.15 K							
0.0000	1.052	0	0	70.295	115.026	–4.2873	0
0.0509	1.046	–4.70	0.0135	71.066	115.021	–4.0826	–0.0044
0.1017	1.041	–7.74	–0.0292	71.257	115.005	–3.8915	–0.0204
0.1486	1.039	–9.19	–0.1086	71.460	114.976	–3.6887	–0.0496
0.1992	1.037	–9.52	–0.2262	71.706	114.924	–3.4426	–0.1017
0.3007	1.036	–7.35	–0.5142	72.272	114.733	–2.8769	–0.2926
0.4009	1.036	–3.28	–0.7906	72.890	114.396	–2.2585	–0.6293
1-Propanol (1) + cyclohexylamine (2)							
T = 298.15 K							
0.4998	1.037	0.73	–0.9781	73.508	113.888	–1.6406	–1.1381
0.6002	1.034	2.71	–1.0252	74.087	113.177	–1.0611	–1.8485
0.7000	1.029	1.99	–0.9047	74.564	112.290	–0.5840	–2.7360
0.7997	1.021	–0.94	–0.6362	74.905	111.270	–0.2434	–3.7555
0.8500	1.017	–2.51	–0.4647	75.019	110.733	–0.1290	–4.2931
0.8998	1.014	–3.42	–0.2893	75.095	110.206	–0.0534	–4.8201
0.9502	1.011	–2.9	–0.1252	75.137	109.698	–0.0119	–5.3279
1.0000	1.011	0	0	74.582	109.258	0	–5.7679
T = 308.15 K							
0.0000	1.063	0	0	71.468	116.248	–4.4513	0
0.0509	1.058	–3.66	–0.0180	71.719	116.243	–4.2003	–0.0055
0.1017	1.054	–5.81	–0.0869	71.945	116.224	–3.9735	–0.0244
0.1486	1.052	–6.57	–0.1860	72.175	116.191	–3.7441	–0.0574
0.1992	1.051	–6.29	–0.3203	72.443	116.134	–3.4760	–0.1141
0.3007	1.051	–3.31	–0.6290	73.035	115.935	–2.8837	–0.3136
0.4009	1.052	1.1	–0.9118	73.662	115.594	–2.2567	–0.6547
0.4998	1.052	5.09	–1.0951	74.278	115.087	–1.6404	–1.1620
0.6002	1.049	6.79	–1.1303	74.852	114.383	–1.0665	–1.8656
0.7000	1.044	5.59	–0.9926	75.326	113.502	–0.5931	–2.7462
0.7997	1.035	1.94	–0.7022	75.667	112.480	–0.2517	–3.7686

TABLE I. Continued

x_1	α 10^{-3} K^{-1}	α^E 10^{-6} K^{-1}	$(\partial H^E/\partial p)_{T,x}$ J·MPa^{-1}·mol^{-1}	$\bar{V}_1$ cm^3·mol^{-1}	$\bar{V}_2$ cm^3·mol^{-1}	$\bar{V}_1^E$ cm^3·mol^{-1}	$\bar{V}_2^E$ cm^3·mol^{-1}
1-Propanol (1) + cyclohexylamine (2)							
T = 308.15 K							
0.8500	1.031	–0.12	–0.5175	75.784	111.932	–0.1353	–4.3163
0.8998	1.026	–1.64	–0.3272	75.862	111.386	–0.0570	–4.8623
0.9502	1.023	–1.91	–0.1456	75.906	110.847	–0.0131	–5.4016
1.0000	1.022	0	0	75.919	110.361	0	–5.8876
T = 313.15 K							
0.0000	1.069	0	0	71.790	116.869	–4.5251	0
0.0509	1.064	–3.15	–0.0341	72.063	116.863	–4.2521	–0.0060
0.1017	1.061	–4.86	–0.1164	72.307	116.843	–4.0086	–0.0263
0.1486	1.059	–5.28	–0.2257	72.548	116.808	–3.7670	–0.0610
0.1992	1.058	–4.7	–0.3685	72.826	116.749	–3.4887	–0.1198
0.3007	1.058	–1.32	–0.6879	73.431	116.545	–2.8845	–0.3232
0.4009	1.059	3.25	–0.9739	74.061	116.202	–2.2542	–0.6660
0.4998	1.060	7.22	–1.1550	74.676	115.695	–1.6395	–1.1719
0.6002	1.057	8.78	–1.1841	75.247	114.995	–1.0686	–1.8718
0.7000	1.051	7.34	–1.0376	75.718	114.118	–0.5973	–2.7486
0.7997	1.042	3.35	–0.7359	76.059	113.094	–0.2557	–3.7720
0.8500	1.037	1.04	–0.5445	76.177	112.541	–0.1383	–4.3243
0.8998	1.032	–0.79	–0.3466	76.256	111.986	–0.0588	–4.8793
0.9502	1.029	–1.44	–0.1561	76.302	111.431	–0.0136	–5.4337
1.0000	1.027	0	0	76.315	110.927	0	–5.9419
1-Butanol (1) + cyclohexylamine (2)[a]							
T = 288.15 K							
0.0000	1.041	0	0	87.398	113.827	–3.7317	0
0.0499	1.030	–6.75	0.0930	87.553	113.823	–3.5771	–0.0035
0.1019	1.022	–10.8	0.0899	87.707	113.810	–3.4224	–0.0164
0.1499	1.017	–12.31	0.0217	87.871	113.787	–3.2591	–0.0400
0.1997	1.013	–12.25	–0.0930	88.064	113.745	–3.0652	–0.0814
0.2995	1.007	–9.39	–0.3822	88.529	113.588	–2.6007	–0.2382
0.4000	1.002	–5.25	–0.6546	89.076	113.291	–2.0534	–0.5354
0.4994	0.996	–2.02	–0.8266	89.647	112.822	–1.4830	–1.0043
0.6006	0.988	–0.59	–0.8621	90.193	112.152	–0.9366	–1.6744
0.6977	0.978	–1.1	–0.7602	90.626	111.350	–0.5032	–2.4768
0.7497	0.972	–1.63	–0.6585	90.807	110.879	–0.3231	–2.9480
0.7984	0.966	–2.39	–0.5410	90.938	110.430	–0.1919	–3.3968
0.8500	0.960	–2.76	–0.4008	91.037	109.968	–0.0931	–3.8585
0.8993	0.954	–2.77	–0.2608	91.095	109.565	–0.0350	–4.2611
0.9508	0.949	–1.74	–0.1193	91.123	109.218	–0.0063	–4.6085
1.0000	0.945	0	0	91.130	109.003	0	–4.8234
T = 293.15 K							
0.0000	1.047	0	0	87.715	114.423	–3.8425	0
0.0499	1.037	–5.86	0.0666	87.906	114.419	–3.6514	–0.0044
0.1019	1.029	–9.53	0.0532	88.088	114.404	–3.4692	–0.0195

TABLE I. Continued

x_1	α 10^{-3} K^{-1}	α^E 10^{-6} K^{-1}	$(\partial H^E/\partial p)_{T,x}$ J·MPa^{-1}·mol^{-1}	$\bar{V}_1$ cm^3·mol^{-1}	$\bar{V}_2$ cm^3·mol^{-1}	$\bar{V}_1^E$ cm^3·mol^{-1}	$\bar{V}_2^E$ cm^3·mol^{-1}
1-Butanol (1) + cyclohexylamine (2)[a]							
T = 293.15 K							
0.1499	1.024	–10.99	–0.0152	88.270	114.378	–3.2878	–0.0457
0.1997	1.020	–11.04	–0.1253	88.476	114.333	–3.0809	–0.0897
0.2995	1.014	–8.51	–0.4034	88.954	114.172	–2.6034	–0.2507
0.4000	1.009	–4.49	–0.6725	89.504	113.874	–2.0533	–0.5493
0.4994	1.003	–1.08	–0.8500	90.073	113.406	–1.4845	–1.0169
0.6006	0.995	0.62	–0.8933	90.617	112.739	–0.9401	–1.6845
0.6977	0.984	0.16	–0.7925	91.050	111.937	–0.5073	–2.4858
0.7497	0.978	–0.49	–0.6871	91.231	111.465	–0.3269	–2.9580
0.7984	0.972	–1.48	–0.5630	91.362	111.014	–0.1950	–3.4092
0.8500	0.965	–2.18	–0.4139	91.462	110.548	–0.0952	–3.8756
0.8993	0.959	–2.53	–0.2653	91.521	110.138	–0.0361	–4.2851
0.9508	0.954	–1.75	–0.1178	91.551	109.781	–0.0066	–4.6427
1.0000	0.950	0	0	91.557	109.553	0	–4.8702
T = 298.15 K							
0.0000	1.052	0	0	88.050	115.026	–3.9406	0
0.0499	1.043	–4.99	0.0397	88.271	115.021	–3.7196	–0.0051
0.1019	1.036	–8.27	0.0158	88.476	115.004	–3.5141	–0.0221
0.1499	1.030	–9.68	–0.0528	88.674	114.975	–3.3167	–0.0506
0.1997	1.026	–9.85	–0.1582	88.893	114.929	–3.0977	–0.0972
0.2995	1.019	–7.65	–0.4249	89.384	114.763	–2.6067	–0.2625
0.4000	1.014	–3.75	–0.6906	89.938	114.463	–2.0527	–0.5630
0.4994	1.008	–0.18	–0.8738	90.506	113.996	–1.4848	–1.0298
0.6006	1.000	1.8	–0.9251	91.048	113.331	–0.9427	–1.6947
0.6977	0.990	1.4	–0.8255	91.479	112.532	–0.5111	–2.4937
0.7497	0.983	0.62	–0.7161	91.660	112.060	–0.3306	–2.9661
0.7984	0.977	–0.6	–0.5854	91.792	111.607	–0.1983	–3.4190
0.8500	0.970	–1.63	–0.4272	91.893	111.136	–0.0975	–3.8898
0.8993	0.964	–2.3	–0.2698	91.953	110.719	–0.0374	–4.3065
0.9508	0.958	–1.78	–0.1162	91.983	110.350	–0.0070	–4.6759
1.0000	0.954	0	0	91.990	110.106	0	–4.9194
T = 308.15 K							
0.0000	1.063	0	0	88.781	116.248	–4.0982	0
0.0499	1.056	–3.28	–0.0154	89.041	116.242	–3.8379	–0.0061
0.1019	1.049	–5.81	–0.0609	89.281	116.223	–3.5985	–0.0258
0.1499	1.044	–7.13	–0.1298	89.504	116.190	–3.3750	–0.0581
0.1997	1.039	–7.51	–0.2256	89.745	116.139	–3.1344	–0.1092
0.2995	1.032	–5.96	–0.4691	90.264	115.965	–2.6153	–0.2836
0.4000	1.026	–2.29	–0.7279	90.829	115.659	–2.0501	–0.5900
0.4994	1.020	1.62	–0.9227	91.397	115.192	–1.4822	–1.0565
0.6006	1.013	4.12	–0.9902	91.934	114.533	–0.9450	–1.7152
0.6977	1.002	3.84	–0.8930	92.361	113.742	–0.5177	–2.5065
0.7497	0.995	2.81	–0.7755	92.541	113.272	–0.3380	–2.9768

TABLE I. Continued

x_1	α 10^{-3} K^{-1}	α^E 10^{-6} K^{-1}	$(\partial H^E/\partial p)_{T,x}$ J·MPa^{-1}·mol^{-1}	$\bar{V}_1$ cm^3·mol^{-1}	$\bar{V}_2$ cm^3·mol^{-1}	$\bar{V}_1^E$ cm^3·mol^{-1}	$\bar{V}_2^E$ cm^3·mol^{-1}
1-Butanol (1) + cyclohexylamine (2)[a]							
T = 308.15 K							
0.7984	0.988	1.14	–0.6313	92.674	112.817	–0.2052	–3.4312
0.8500	0.981	–0.53	–0.4545	92.776	112.339	–0.1030	–3.9094
0.8993	0.973	–1.85	–0.2790	92.838	111.907	–0.0407	–4.3418
0.9508	0.967	–1.83	–0.1129	92.871	111.509	–0.0080	–4.7396
1.0000	0.963	0	0	92.879	111.223	0	–5.0250
T = 313.15 K							
0.0000	1.069	0	0	89.178	116.869	–4.1578	0
0.0499	1.063	–2.44	–0.0437	89.448	116.863	–3.8879	–0.0063
0.1019	1.056	–4.61	–0.1002	89.698	116.842	–3.6379	–0.0269
0.1499	1.051	–5.87	–0.1693	89.931	116.809	–3.4044	–0.0606
0.1997	1.046	–6.37	–0.2602	90.182	116.755	–3.1543	–0.1138
0.2995	1.038	–5.13	–0.4918	90.715	116.576	–2.6206	–0.2930
0.4000	1.032	–1.57	–0.7469	91.288	116.266	–2.0480	–0.6031
0.4994	1.027	2.5	–0.9477	91.857	115.799	–1.4792	–1.0703
0.6006	1.019	5.27	–1.0236	92.391	115.144	–0.9448	–1.7255
0.6977	1.009	5.04	–0.9276	92.815	114.358	–0.5205	–2.5113
0.7497	1.002	3.9	–0.8060	92.994	113.890	–0.3417	–2.9793
0.7984	0.994	2	–0.6549	93.127	113.436	–0.2090	–3.4334
0.8500	0.986	0	–0.4685	93.230	112.954	–0.1061	–3.9149
0.8993	0.979	–1.63	–0.2837	93.293	112.514	–0.0426	–4.3556
0.9508	0.972	–1.84	–0.1113	93.327	112.099	–0.0086	–4.7701
1.0000	0.968	0	0	93.336	111.788	0	–5.0814
1-Pentanol (1) + cyclohexylamine (2)							
T = 288.15 K							
0.0000	1.041	0	0	104.434	113.827	–3.2902	0
0.0506	1.027	–7.79	0.1404	104.539	113.824	–3.1855	–0.0025
0.1001	1.015	–12.78	0.1912	104.644	113.815	–3.0809	–0.0111
0.1500	1.006	–15.45	0.1704	104.772	113.797	–2.9528	–0.0296
0.2002	0.998	–16.21	0.0921	104.929	113.763	–2.7959	–0.0631
0.2997	0.987	–13.82	–0.1696	105.326	113.629	–2.3984	–0.1980
0.3995	0.979	–8.61	–0.4705	105.819	113.361	–1.9054	–0.4659
0.5004	0.970	–3.65	–0.7025	106.360	112.915	–1.3643	–0.9116
0.6003	0.959	–1.1	–0.7812	106.870	112.289	–0.8543	–1.5380
0.6998	0.944	–1.57	–0.6790	107.288	111.513	–0.4370	–2.3131
0.7962	0.928	–3.99	–0.4365	107.562	110.705	–0.1631	–3.1216
0.8500	0.919	–5.21	–0.2727	107.653	110.283	–0.0719	–3.5437
0.8995	0.912	–5.44	–0.1321	107.701	109.952	–0.0239	–3.8751
0.9501	0.906	–4.04	–0.0280	107.721	109.707	–0.0034	–4.1196
1.0000	0.903	0	0	107.725	109.578	0	–4.2484
T = 293.15 K							
0.0000	1.047	0	0	104.799	114.423	–3.4079	0
0.0506	1.033	–7.03	0.1185	104.936	114.420	–3.2708	–0.0033

TABLE I. Continued

x_1	α 10^{-3} K^{-1}	α^E 10^{-6} K^{-1}	$(\partial H^E/\partial p)_{T,x}$ J·MPa^{-1}·mol^{-1}	$\bar{V}_1$ cm^3·mol^{-1}	$\bar{V}_2$ cm^3·mol^{-1}	$\bar{V}_1^E$ cm^3·mol^{-1}	$\bar{V}_2^E$ cm^3·mol^{-1}
1-Pentanol (1) + cyclohexylamine (2)							
T = 293.15 K							
0.1001	1.022	–11.6	0.1575	105.067	114.409	–3.1401	–0.0140
0.1500	1.013	–14.09	0.1322	105.216	114.388	–2.9911	–0.0355
0.2002	1.005	–14.86	0.0550	105.389	114.351	–2.8181	–0.0724
0.2997	0.994	–12.82	–0.1946	105.806	114.210	–2.4011	–0.2136
0.3995	0.985	–8.14	–0.4799	106.305	113.938	–1.9016	–0.4849
0.5004	0.975	–3.55	–0.7012	106.845	113.494	–1.3619	–0.9292
0.6003	0.964	–1.05	–0.7792	107.351	112.873	–0.8562	–1.5502
0.6998	0.949	–1.26	–0.6855	107.765	112.104	–0.4423	–2.3192
0.7962	0.934	–3.31	–0.4550	108.039	111.296	–0.1685	–3.1276
0.8500	0.925	–4.39	–0.2957	108.131	110.867	–0.0760	–3.5559
0.8995	0.917	–4.64	–0.1551	108.181	110.524	–0.0264	–3.8994
0.9501	0.911	–3.48	–0.0442	108.203	110.258	–0.0042	–4.1650
1.0000	0.907	0	0	108.207	110.097	0	–4.3266
T = 298.15 K							
0.0000	1.052	0	0	105.180	115.026	–3.5162	0
0.0506	1.039	–6.29	0.0962	105.346	115.022	–3.3503	–0.0040
0.1001	1.028	–10.44	0.1231	105.500	115.009	–3.1964	–0.0166
0.1500	1.019	–12.75	0.0933	105.668	114.985	–3.0284	–0.0408
0.2002	1.012	–13.52	0.0172	105.856	114.945	–2.8405	–0.0809
0.2997	1.000	–11.85	–0.2200	106.291	114.798	–2.4052	–0.2280
0.3995	0.990	–7.68	–0.4895	106.797	114.523	–1.8990	–0.5026
0.5004	0.980	–3.46	–0.7000	107.336	114.079	–1.3600	–0.9463
0.6003	0.968	–1.01	–0.7772	107.838	113.463	–0.8579	–1.5629
0.6998	0.954	–0.96	–0.6922	108.249	112.699	–0.4468	–2.3266
0.7962	0.938	–2.63	–0.4738	108.523	111.891	–0.1732	–3.1349
0.8500	0.930	–3.58	–0.3190	108.617	111.457	–0.0796	–3.5685
0.8995	0.922	–3.85	–0.1785	108.668	111.103	–0.0285	–3.9225
0.9501	0.916	–2.92	–0.0608	108.691	110.819	–0.0048	–4.2066
1.0000	0.911	0	0	108.696	110.629	0	–4.3972
T = 308.15 K							
0.0000	1.063	0	0	105.994	116.248	–3.7048	0
0.0506	1.051	–4.84	0.0506	106.207	116.243	–3.4920	–0.0052
0.1001	1.041	–8.16	0.0527	106.399	116.228	–3.2998	–0.0209
0.1500	1.032	–10.11	0.0135	106.599	116.199	–3.0997	–0.0496
0.2002	1.025	–10.9	–0.0602	106.812	116.153	–2.8861	–0.0951
0.2997	1.012	–9.94	–0.2722	107.281	115.995	–2.4178	–0.2530
0.3995	1.001	–6.77	–0.5091	107.801	115.714	–1.8978	–0.5348
0.5004	0.990	–3.27	–0.6975	108.341	115.269	–1.3578	–0.9790
0.6003	0.978	–0.93	–0.7730	108.838	114.659	–0.8604	–1.5896
0.6998	0.964	–0.36	–0.7059	109.245	113.903	–0.4538	–2.3453
0.7962	0.948	–1.3	–0.5123	109.518	113.096	–0.1806	–3.1530
0.8500	0.940	–1.99	–0.3669	109.613	112.654	–0.0853	–3.5946

TABLE I. Continued

x_1	α 10^{-3} K^{-1}	α^E 10^{-6} K^{-1}	$(\partial H^E/\partial p)_{T,x}$ J·MPa^{-1}·mol^{-1}	$\bar{V}_1$ cm^3·mol^{-1}	$\bar{V}_2$ cm^3·mol^{-1}	$\bar{V}_1^E$ cm^3·mol^{-1}	$\bar{V}_2^E$ cm^3·mol^{-1}
1-Pentanol (1) + cyclohexylamine (2)							
T = 308.15 K							
0.8995	0.932	–2.28	–0.2264	109.667	112.284	–0.0319	–3.9649
0.9501	0.925	–1.82	–0.0948	109.693	111.970	–0.0059	–4.2781
1.0000	0.919	0	0	109.699	111.733	0	–4.5155
T = 313.15 K							
0.0000	1.069	0	0	106.427	116.869	–3.7850	0
0.0506	1.058	–4.13	0.0272	106.657	116.864	–3.5543	–0.0056
0.1001	1.048	–7.04	0.0166	106.865	116.847	–3.3469	–0.0226
0.1500	1.039	–8.82	–0.0274	107.078	116.816	–3.1338	–0.0532
0.2002	1.032	–9.61	–0.0999	107.302	116.768	–2.9094	–0.1010
0.2997	1.018	–9	–0.2990	107.785	116.606	–2.4263	–0.2637
0.3995	1.006	–6.32	–0.5191	108.313	116.320	–1.8992	–0.5491
0.5004	0.995	–3.19	–0.6962	108.854	115.875	–1.3575	–0.9946
0.6003	0.983	–0.88	–0.7708	109.350	115.265	–0.8613	–1.6038
0.6998	0.969	–0.07	–0.7129	109.756	114.513	–0.4561	–2.3567
0.7962	0.954	–0.65	–0.5320	110.029	113.705	–0.1832	–3.1638
0.8500	0.945	–1.21	–0.3914	110.124	113.261	–0.0873	–3.6081
0.8995	0.937	–1.51	–0.2509	110.179	112.885	–0.0331	–3.9842
0.9501	0.929	–1.29	–0.1122	110.205	112.561	–0.0063	–4.3081
1.0000	0.923	0	0	110.212	112.306	0	–4.5631
2-Butanol (1) + cyclohexylamine (2)							
T = 288.15 K							
0.0000	1.041	0	0	88.673	113.827	–2.7586	0
0.0495	1.039	–2.31	–0.0177	88.773	113.823	–2.6582	–0.0034
0.1011	1.037	–3.88	–0.0625	88.921	113.811	–2.5102	–0.0156
0.1505	1.036	–4.6	–0.1253	89.076	113.789	–2.3551	–0.0380
0.1995	1.036	–4.68	–0.2013	89.244	113.753	–2.1871	–0.0738
0.3004	1.037	–3.34	–0.3765	89.631	113.622	–1.8003	–0.2042
0.3996	1.039	–1.12	–0.5335	90.046	113.398	–1.3858	–0.4290
0.4974	1.041	0.77	–0.6323	90.454	113.064	–0.9778	–0.7622
0.5997	1.042	1.8	–0.6446	90.838	112.597	–0.5937	–1.2298
0.7000	1.041	1.25	–0.5546	91.134	112.047	–0.2972	–1.7794
0.7999	1.039	–0.37	–0.3789	91.327	111.474	–0.1048	–2.3522
0.8488	1.038	–1.19	–0.2745	91.382	111.216	–0.0495	–2.6106
0.8997	1.038	–1.63	–0.1652	91.415	110.987	–0.0161	–2.8400
0.9498	1.038	–1.38	–0.0692	91.429	110.823	–0.0024	–3.0037
1.0000	1.039	0	0	91.431	110.718	0	–3.1081
T = 293.15 K							
0.0000	1.047	0	0	89.082	114.423	–2.8071	0
0.0495	1.044	–2.67	–0.0045	89.194	114.420	–2.6957	–0.0037
0.1011	1.042	–4.55	–0.0382	89.352	114.407	–2.5373	–0.0167
0.1505	1.041	–5.52	–0.0924	89.515	114.383	–2.3741	–0.0403
0.1995	1.041	–5.84	–0.1609	89.690	114.346	–2.1999	–0.0774

TABLE I. Continued

x_1	α 10^{-3} K^{-1}	α^E 10^{-6} K^{-1}	$(\partial H^E/\partial p)_{T,x}$ J·MPa^{-1}·mol^{-1}	$\bar{V}_1$ cm^3·mol^{-1}	$\bar{V}_2$ cm^3·mol^{-1}	$\bar{V}_1^E$ cm^3·mol^{-1}	$\bar{V}_2^E$ cm^3·mol^{-1}
2-Butanol (1) + cyclohexylamine (2)							
T = 293.15 K							
0.3004	1.041	–4.97	–0.3221	90.084	114.213	–1.8052	–0.2104
0.3996	1.043	–3.29	–0.4646	90.502	113.987	–1.3878	–0.4367
0.4974	1.044	–1.97	–0.5481	90.910	113.653	–0.9799	–0.7698
0.5997	1.044	–1.54	–0.5452	91.293	113.187	–0.5968	–1.2361
0.7000	1.043	–2.48	–0.4462	91.589	112.639	–0.3010	–1.7846
0.7999	1.041	–4	–0.2756	91.782	112.063	–0.1078	–2.3598
0.8488	1.040	–4.46	–0.1823	91.838	111.801	–0.0517	–2.6220
0.8997	1.040	–4.23	–0.0928	91.872	111.565	–0.0174	–2.8584
0.9498	1.041	–2.91	–0.0267	91.887	111.391	–0.0028	–3.0327
1.0000	1.044	0	0	91.890	111.269	0	–3.1539
T = 298.15 K							
0.0000	1.052	0	0	89.500	115.026	–2.8609	0
0.0495	1.049	–3.02	0.0090	89.624	115.022	–2.7375	–0.0040
0.1011	1.047	–5.21	–0.0136	89.793	115.008	–2.5678	–0.0179
0.1505	1.045	–6.43	–0.0589	89.965	114.983	–2.3961	–0.0427
0.1995	1.045	–6.98	–0.1199	90.146	114.945	–2.2155	–0.0812
0.3004	1.045	–6.59	–0.2667	90.548	114.809	–1.8128	–0.2168
0.3996	1.046	–5.42	–0.3946	90.969	114.581	–1.3926	–0.4445
0.4974	1.046	–4.68	–0.4624	91.376	114.248	–0.9847	–0.7775
0.5997	1.046	–4.83	–0.4441	91.759	113.783	–0.6026	–1.2427
0.7000	1.044	–6.16	–0.3359	92.054	113.234	–0.3067	–1.7913
0.7999	1.042	–7.58	–0.1706	92.249	112.654	–0.1121	–2.3713
0.8488	1.042	–7.69	–0.0886	92.306	112.386	–0.0547	–2.6394
0.8997	1.043	–6.78	–0.0192	92.342	112.140	–0.0190	–2.8855
0.9498	1.045	–4.43	0.0166	92.358	111.952	–0.0033	–3.0742
1.0000	1.049	0	0	92.361	111.809	0	–3.2167
T = 308.15 K							
0.0000	1.063	0	0	90.366	116.248	–2.9837	0
0.0495	1.059	–3.72	0.0367	90.516	116.244	–2.8332	–0.0048
0.1011	1.056	–6.51	0.0370	90.711	116.228	–2.6389	–0.0207
0.1505	1.054	–8.22	0.0097	90.901	116.200	–2.4489	–0.0481
0.1995	1.053	–9.22	–0.0356	91.095	116.159	–2.2546	–0.0894
0.3004	1.052	–9.74	–0.1530	91.514	116.018	–1.8357	–0.2302
0.3996	1.052	–9.57	–0.2509	91.939	115.788	–1.4105	–0.4605
0.4974	1.052	–9.95	–0.2867	92.347	115.455	–1.0030	–0.7931
0.5997	1.050	–11.24	–0.2367	92.728	114.991	–0.6219	–1.2570
0.7000	1.048	–13.32	–0.1098	93.025	114.440	–0.3244	–1.8089
0.7999	1.046	–14.55	0.0448	93.225	113.842	–0.1243	–2.4063
0.8488	1.047	–13.98	0.1038	93.286	113.556	–0.0632	–2.6921
0.8997	1.049	–11.78	0.1318	93.326	113.282	–0.0235	–2.9660
0.9498	1.053	–7.39	0.1054	93.345	113.054	–0.0046	–3.1942
1.0000	1.060	0	0	93.350	112.855	0	–3.3935

TABLE I. Continued

x_1	α 10^{-3} K^{-1}	α^E 10^{-6} K^{-1}	$(\partial H^E/\partial p)_{T,x}$ J·MPa^{-1}·mol^{-1}	$\bar{V}_1$ cm^3·mol^{-1}	$\bar{V}_2$ cm^3·mol^{-1}	$\bar{V}_1^E$ cm^3·mol^{-1}	$\bar{V}_2^E$ cm^3·mol^{-1}
2-Butanol (1) + cyclohexylamine (2)							
T = 313.15 K							
0.0000	1.069	0	0	90.817	116.869	–3.0529	0
0.0495	1.065	–4.06	0.0508	90.982	116.864	–2.8873	–0.0052
0.1011	1.062	–7.14	0.0629	91.190	116.847	–2.6795	–0.0221
0.1505	1.060	–9.09	0.0449	91.390	116.818	–2.4797	–0.0510
0.1995	1.058	–10.31	0.0075	91.591	116.775	–2.2782	–0.0938
0.3004	1.057	–11.27	–0.0948	92.019	116.632	–1.8510	–0.2372
0.3996	1.056	–11.58	–0.1773	92.446	116.400	–1.4235	–0.4687
0.4974	1.055	–12.5	–0.1966	92.853	116.068	–1.0163	–0.8011
0.5997	1.053	–14.35	–0.1304	93.234	115.604	–0.6355	–1.2648
0.7000	1.050	–16.8	0.0061	93.533	115.049	–0.3364	–1.8199
0.7999	1.049	–17.94	0.1551	93.737	114.439	–0.1322	–2.4298
0.8488	1.050	–17.04	0.2023	93.801	114.142	–0.0686	–2.7274
0.8997	1.052	–14.2	0.2092	93.843	113.850	–0.0264	–3.0194
0.9498	1.057	–8.83	0.1508	93.864	113.596	–0.0055	–3.2728
1.0000	1.066	0	0	93.870	113.362	0	–3.5075
2-Methyl-2-propanol (1) + cyclohexylamine (2)							
T = 308.15 K							
0.0000	1.063	0	0	92.833	116.248	–3.4054	0
0.0508	1.068	–8.5	0.1874	92.939	116.244	–3.3006	–0.0050
0.1002	1.074	–16.19	0.3500	93.142	116.227	–3.0978	–0.0217
0.1502	1.081	–23.51	0.5020	93.364	116.195	–2.8758	–0.0536
0.2001	1.088	–30.53	0.6477	93.596	116.145	–2.6437	–0.1030
0.3005	1.105	–43.97	0.9423	94.074	115.985	–2.1654	–0.2637
0.3991	1.122	–56.84	1.2505	94.534	115.736	–1.7051	–0.5123
0.4996	1.141	–69.35	1.5772	94.974	115.377	–1.2659	–0.8719
0.5998	1.164	–79.42	1.8698	95.368	114.893	–0.8714	–1.3551
0.6997	1.194	–84.09	2.0368	95.708	114.261	–0.5320	–1.9872
0.7999	1.235	–78.08	1.9322	95.981	113.437	–0.2585	–2.8114
0.8712	1.277	–62.86	1.5790	96.125	112.704	–0.1149	–3.5445
0.8992	1.296	–53.77	1.3533	96.167	112.376	–0.0724	–3.8723
0.9504	1.339	–30.83	0.7831	96.221	111.710	–0.0185	–4.5385
1.0000	1.389	0	0	96.239	111.019	0	–5.2294
T = 313.15 K							
0.0000	1.069	0	0	93.386	116.869	–3.5203	0
0.0508	1.075	–7.99	0.1727	93.499	116.864	–3.4088	–0.0052
0.1002	1.082	–15.39	0.3290	93.708	116.847	–3.1991	–0.0225
0.1502	1.089	–22.61	0.4814	93.936	116.814	–2.9717	–0.0551
0.2001	1.096	–29.68	0.6325	94.172	116.764	–2.7355	–0.1054
0.3005	1.112	–43.48	0.9463	94.656	116.601	–2.2512	–0.2681
0.3991	1.129	–56.7	1.2727	95.122	116.349	–1.7854	–0.5197
0.4996	1.149	–69.25	1.6055	95.569	115.983	–1.3381	–0.8860
0.5998	1.173	–78.78	1.8853	95.976	115.485	–0.9314	–1.3844

TABLE I. Continued

x_1	α 10^{-3} K^{-1}	α^E 10^{-6} K^{-1}	$(\partial H^E/\partial p)_{T,x}$ J·MPa^{-1}·mol^{-1}	$\bar{V}_1$ cm^3·mol^{-1}	$\bar{V}_2$ cm^3·mol^{-1}	$\bar{V}_1^E$ cm^3·mol^{-1}	$\bar{V}_2^E$ cm^3·mol^{-1}
2-Methyl-2-propanol (1) + cyclohexylamine (2)							
T = 313.15 K							
0.6997	1.204	–82.44	2.0224	96.332	114.822	–0.5757	–2.0474
0.7999	1.247	–75.4	1.8839	96.624	113.940	–0.2834	–2.9293
0.8712	1.289	–59.98	1.5188	96.780	113.142	–0.1270	–3.7275
0.8992	1.309	–51.07	1.2948	96.827	112.781	–0.0804	–4.0879
0.9504	1.350	–29.01	0.7420	96.887	112.043	–0.0207	–4.8261
1.0000	1.399	0	0	96.907	111.266	0	–5.6027
T = 318.15 K							
0.0000	1.075	0	0	93.966	117.497	–3.6291	0
0.0508	1.081	–7.48	0.1578	94.082	117.492	–3.5137	–0.0054
0.1002	1.088	–14.6	0.3077	94.297	117.474	–3.2992	–0.0230
0.1502	1.095	–21.72	0.4604	94.528	117.441	–3.0681	–0.0562
0.2001	1.103	–28.85	0.6170	94.767	117.390	–2.8290	–0.1071
0.3005	1.119	–43	0.9504	95.256	117.225	–2.3395	–0.2715
0.3991	1.137	–56.57	1.2953	95.729	116.970	–1.8674	–0.5266
0.4996	1.157	–69.12	1.6343	96.186	116.596	–1.4105	–0.9009
0.5998	1.182	–78.13	1.9011	96.606	116.081	–0.9903	–1.4161
0.6997	1.214	–80.78	2.0078	96.979	115.386	–0.6175	–2.1114
0.7999	1.259	–72.74	1.8349	97.290	114.447	–0.3065	–3.0501
0.8712	1.301	–57.12	1.4576	97.458	113.587	–0.1382	–3.9098
0.8992	1.321	–48.39	1.2353	97.508	113.196	–0.0876	–4.3005
0.9504	1.362	–27.22	0.7002	97.573	112.393	–0.0226	–5.1044
1.0000	1.409	0	0	97.595	111.539	0	–5.9579
T = 323.15 K							
0.0000	1.081	0	0	94.572	118.130	–3.7317	0
0.0508	1.087	–6.98	0.1426	94.689	118.125	–3.6153	–0.0054
0.1002	1.095	–13.83	0.2861	94.906	118.107	–3.3982	–0.0233
0.1502	1.103	–20.85	0.4391	95.139	118.074	–3.1651	–0.0568
0.2001	1.110	–28.02	0.6013	95.380	118.022	–2.9242	–0.1081
0.3005	1.127	–42.52	0.9545	95.874	117.856	–2.4302	–0.2740
0.3991	1.144	–56.42	1.3182	96.353	117.597	–1.9511	–0.5329
0.4996	1.165	–68.99	1.6636	96.821	117.214	–1.4832	–0.9164
0.5998	1.191	–77.47	1.9171	97.256	116.680	–1.0479	–1.4502
0.6997	1.225	–79.14	1.9930	97.647	115.951	–0.6573	–2.1791
0.7999	1.271	–70.12	1.7851	97.976	114.957	–0.3280	–3.1736
0.8712	1.314	–54.31	1.3955	98.156	114.039	–0.1483	–4.0915
0.8992	1.333	–45.77	1.1749	98.210	113.620	–0.0941	–4.5100
0.9504	1.374	–25.46	0.6578	98.280	112.757	–0.0243	–5.3735
1.0000	1.419	0	0	98.304	111.835	0	–6.2949

[a]Calculations for system 1-butanol + cyclohexylamine are based on literature experimental data[3]; [b]partial molar volume at infinite dilution $\bar{V}_1^{\infty}$ at $x_1 = 0$; [c]partial molar volume at infinite dilution $\bar{V}_2^{\infty}$ at $x_1 = 1$; [d]partial excess molar volume at infinite dilution $\bar{V}_1^{E,\infty}$ at $x_1 = 0$; [e]partial excess molar volume at infinite dilution $\bar{V}_2^{E,\infty}$ at $x_1 = 1$

TABLE II. Molar volumes, V_1° and V_2°, partial molar volumes at infinite dilution, $\bar{V}_1^\infty$ and $\bar{V}_2^\infty$, and partial excess molar volumes at infinite dilution, $\bar{V}_1^{E,\infty}$ and $\bar{V}_2^{E,\infty}$

T / K	V_1° / cm^3·mol^{-1}	V_2° / cm^3·mol^{-1}	$\bar{V}_1^\infty$ / cm^3·mol^{-1}	$\bar{V}_2^\infty$ / cm^3·mol^{-1}	$\bar{V}_1^{E,\infty}$ / cm^3·mol^{-1}	$\bar{V}_2^{E,\infty}$ / cm^3·mol^{-1}
1-Propanol (1) + cyclohexylamine (2)						
288.15	74.404	113.827	70.388	107.992	–4.0167	–5.8346
293.15	74.773	114.423	70.662	108.534	–4.1111	–5.8894
298.15	75.148	115.026	70.946	109.083	–4.2023	–5.9428
303.15	75.530	115.634	71.241	109.638	–4.2896	–5.9959
308.15	75.919	116.248	71.555	110.206	–4.3637	–6.0421
313.15	76.315	116.869	71.886	110.800	–4.4289	–6.0689
1-Butanol(1) + cyclohexylamine (2)						
288.15	91.130	113.827	87.493	108.706	–3.6363	–5.1205
293.15	91.557	114.423	87.820	109.244	–3.7373	–5.1794
298.15	91.990	115.026	88.166	109.811	–3.8246	–5.2152
303.15	92.431	115.634	88.519	110.380	–3.9118	–5.2538
308.15	92.879	116.248	88.890	110.959	–3.9889	–5.2896
313.15	93.336	116.869	89.281	111.544	–4.0544	–5.3251
1-Pentanol (1) + cyclohexylamine (2)						
288.15	107.7247	113.827	104.588	109.374	–3.1369	–4.4529
293.15	108.2070	114.423	104.961	109.918	–3.2460	–4.5056
298.15	108.6963	115.026	105.338	110.466	–3.3586	–4.5601
303.15	109.1931	115.634	105.730	111.024	–3.4627	–4.6106
308.15	109.6986	116.248	106.145	111.589	–3.5537	–4.6595
313.15	110.2117	116.869	106.576	112.182	–3.6354	–4.6873
2-Butanol (1) + cyclohexylamine (2)						
288.15	91.431	113.827	88.651	110.572	–2.7800	–3.2544
293.15	91.890	114.423	89.067	111.125	–2.8223	–3.2985
298.15	92.361	115.026	89.471	111.672	–2.8903	–3.3541
303.15	92.847	115.634	89.889	112.209	–2.9587	–3.4249
308.15	93.350	116.248	90.327	112.736	–3.0222	–3.5120
313.15	93.870	116.869	90.786	113.252	–3.0831	–3.6169
2-Methyl-2-propanol (1) + cyclohexylamine (2)						
303.15	95.591	115.634	92.137	110.729	–3.4535	–4.9046
308.15	96.239	116.248	92.663	110.969	–3.5752	–5.2791
313.15	96.907	116.869	93.215	111.220	–3.6922	–5.6494
318.15	97.595	117.497	93.790	111.494	–3.8057	–6.0032
323.15	98.304	118.130	94.395	111.795	–3.9089	–6.3352

Journal of the Serbian Chemical Society
JSCS@tmf.bg.ac.rs • www.shd.org.rs/JSCS

J. Serb. Chem. Soc. 75 (2) 295 (2010)

Errata (printed version only)

Issue No. 1 (2010), Vol. **75**:
page 145:
– Line 21 from the bottom should be deleted.
page 146:
– The lines before line 1 from the top should be inserted as follows: "Branko Drakulić, *Institute of Chemistry, Technology and Metallurgy, Center of Chemistry, Belgrade, Serbia*"
page 152:
– Lines 20 and 21 from the top should read: "Alessandro Pedretti, *Dipartimento di Scienze Farmaceutiche "Pietro Pratesi", Universita degli Studi di Milano, Italy*"